

Alma Mater Studiorum – Università di Bologna

DOTTORATO DI RICERCA IN

CHIMICA

Ciclo **XXIX**

Settore Concorsuale di afferenza: **03/C1**

Settore Scientifico disciplinare: **CHIM/06**

TITOLO TESI

**Design and synthesis of new molecular tools for the detection of
compounds used for the preservation of artworks
and substances of environmental concern**

Presentata da: **Stella Beglaryan**

Coordinatore Dottorato

Prof. Aldo Roda

Relatore

Prof. Emilio Tagliavini

Correlatore

Prof.ssa Paola Galletti

Esame finale anno 2017



ALMA MATER STUDIORUM
UNIVERSITÀ DI BOLOGNA

L'Ordine del Giorno è il seguente:

...
2. Approvazione delle presentazioni dei Dottorandi del 29° Ciclo e dei prorogati del 28° Ciclo
...

...

2. Approvazione delle presentazioni delle tesi dei dottorandi del 29° Ciclo e dei prorogati del 28° Ciclo

Il Coordinatore fa presente al Collegio dei docenti che i dottorandi, iscritti all'ultimo anno di corso, hanno presentato, nei termini previsti, le dissertazioni finali scritte.

Il Collegio è chiamato a redigere, per ciascuno di essi, la "presentazione" da allegare alla tesi finale.

Si invitano, a tal fine, i componenti del Collegio, che prevalentemente hanno guidato le attività di ricerca dei dottorandi, a voler illustrare i contenuti delle predette tesi ed i risultati conseguiti.

Dopo ampia discussione, sentiti anche i dottorandi in merito alle ricerche svolte, oggetto della dissertazione scritta, il Collegio dei Docenti decide unanime di approvare le "presentazioni" di seguito riportate le quali illustrano l'attività scientifico-formativa svolta durante il corso, mettendone in luce gli aspetti positivi o, eventualmente, negativi.

...

7) *Dott. Stella Beglaryan*

Supervisore: Prof. Emilio

Tagliavini Co-supervisore: Prof.

Paola Galletti Curriculum:

Scienze Chimiche Indirizzo:

Chimica Organica

Titolo della tesi: Design and synthesis of new molecular tools for the detection of compounds used for the preservation of artworks and substances of environmental concern.

Il Coordinatore
Prof. Aldo Roda

Il Segretario
Prof. Massimo Guardigli



ALMA MATER STUDIORUM
UNIVERSITÀ DI BOLOGNA

The PhD project carried out by Stella Beglaryan is focused on the exploitation of conjugated polymers obtained (Polydiacetylenes – PDA) from the light-induced polymerization of tricosadynoic acid (TR) as photometric and fluorimetric sensors for specific groups of compounds.

TR is an amphiphilic substance that can form self-assembling supramolecular systems, like monomolecular layers or liposomes, alone or in mixtures with compounds having similar physic-chemical properties, under specific environmental conditions. Upon exposure to UV light, these assemblies undergo polymerization through multiple bond addition, to provide blue-colored materials whose light absorbance and fluorimetric properties can be varied upon exposition to specific substances, opening the way to a possible use for detecting the presence of those substances in specific environments.

To the aim of improving the specificity of the substrate-sensor interaction, the project of Dr. Beglaryan has been finalized to synthesize unprecedented TR derivatives bearing a variety of different functional groups on the carboxylic head, still able to undergo photo-induced polymerization but now capable of perform selective interaction with substrates containing specific functional groups. The heads introduced comprise amines, aminoacids, boronic acid, fluorinated moieties and others.

Different classes of substrates have been chosen to be investigated for the detection: a) substances present on the protective surface of art paintings, including proteinaceous glues, siccative oils, terpenes, polysaccaridic materials; b) volatile organic compounds present in the environment as pollutants c) organophosphate pesticides possibly present in the environment.

The work has been performed within the frame of a joint collaborative project including the group of cultural heritage chemistry of the Department of Chemistry in Ravenna, and the group of Prof. Raz Jelinek in Ben Gurion University (Israel).

Thanks to the obtainment of a Marco polo grant Stella Beglaryan has joined for a three months internship the group of Prof. Uwe Bunz in the University of Heidelberg(Germany) working on a project on the synthesis of new cyano-substituted N-heteroacenes/arenes, having possible application as organic semiconductors.

During the PhD work, the candidate has gained a strong experience in organic synthesis and characterization through the use of instrumental techniques like GC-MS, HPLS, NMR and other. She has also achieved good skills in the exploitation of multivariate analysis to complex data matrixes.

Dr. Beglaryan has attended various educational activities in the specific field of her expertise, as well as conferences and symposia, where she could present the results of her research.

Il Coordinatore
Prof. Aldo Roda

Il Segretario
Prof. Massimo Guardigli



ALMA MATER STUDIORUM
UNIVERSITÀ DI BOLOGNA

The results obtained in the PhD of Dr. Beglaryan have been published in two scientific papers in high impact international journals, while another article is under revision.

Through the PhD experience, the candidate has achieved a deep understanding of the scientific issues involved in her project, and a good command of the experimental techniques exploited, showing a good attitude to the collaborative research work.

In my opinion Stella Beglaryan has carried out a good work for her PhD project and thesis.

The Board expresses a good score on the activity carried out by the candidate during the whole cycle of doctorate and considers her worthy to attain the PhD in Chemistry.

Le deliberazioni assunte nella presente seduta sono state redatte, lette, approvate e sottoscritte seduta stante.

Il verbale della presente seduta del Collegio dei docenti, dopo essere stato firmato e scansionato, sarà inserito, in formato .pdf, a cura del Coordinatore, nell'apposito applicativo informatico al link: <https://www.aric.unibo.it/DottoratoDiRicerca/verbalizzazioni/default.aspx> ed accessibile mediante l'utilizzo delle credenziali istituzionali (l'art. 5, comma 10 del "Regolamento per l'istituzione e il funzionamento dei corsi di dottorato di ricerca" DR n. 524 del 26/06/2013 prevede che: *"Delle riunioni e deliberazioni assunte dal Collegio dei docenti deve essere redatto verbale da archiviare, debitamente sottoscritto, nell'apposito applicativo di Ateneo entro cinque giorni lavorativi dalla data della riunione del Collegio"*).

Esauroto l'Ordine del Giorno, il Collegio dei Docenti del Corso di Dottorato in Chimica termina la seduta alle ore 16.10.

Il Presidente

Prof. Aldo Roda

Segretario

Prof. Massimo Guardigli

Il Coordinatore
Prof. Aldo Roda

Il Segretario
Prof. Massimo Guardigli



Ruprecht-Karls-Universität Heidelberg
Organisch-Chemisches Institut
Prof. Dr. Uwe Bunz

Organ.-Chem. Institut Im Neuenheimer Feld
270 D – 69120 Heidelberg

Heidelberg, March 16th 2017

Kerstin-A. Windisch
Tel.: (06221) 54-8408
Fax: (06221) 54-4205
Kerstin.Windisch@oci.uni-heidelberg.de

Thesis Manuscript Assessment Stella Beglaryan

Design and synthesis of new molecular tools for the detection of compounds used for the preservation of artworks and substances of environmental concern

This thesis is focused on a design and syntheses of new, deeply colored polydiacetylenes (PDA), based on 10,12-tricosadynoic acid (TRCDA or TR) derivatives. These PDAs have a supreme applicability in fields ranging from art work quality assessment to nerve gas sensing. Stella synthesized a whole pool of TR derivatives and examined both the distinct molecular interactions (leading to color changes of the PDA) with the tested analytes, and looked at the modulation of the overall structural organization and corresponding colorimetric properties of the sensor films. In particular, the diacetylene monomers examined by Stella were equipped with carboxylic acids, fluorine containing headgroups with different fluorine chain lengths, cleverly designed to enhance non polar and hydrophobic interaction, phenyl boronic acid moieties to establish polar/ionic interactions and eventually form boronic esters with diol and polyol-containing materials; she also prepared PDAs with ammonium head groups which promote ionic interactions with negatively charged compounds, and amino-acid ester derivatives for promoting protein-like hydrogen bonding with polar targets. The photophysical properties and sensing applications of the new PDAs were very carefully and cleverly investigated. Distinct color and fluorescence transitions were induced by various analytes - binding materials of paintings, volatile organic compounds (VOCs) and also commercially available organophosphate pesticides (OPs) as models for nerve gas. Chromatic transformations were correlated to the analyte structures and their properties. Overall, this study presents an attractive new array of TR derivatives, which were successfully employed in the colorimetric and/or fluorescent detection of organic compounds present in binders for art-colors and

pigments, VOCs and organophosphate pesticides.

In Chapter 7 Stella's research experience in my Laboratory at Heidelberg University, Germany is reported. The aim was to synthesize new cyano-substituted azaacenes, which might be attractive targets due to their ability to form weak hydrogen bonds with aromatic C, H-bonds and therefore lead to a tighter packing of the molecules in the solid state with concomitant better charge transport properties. The target molecules - totally novel dicyano-substituted diazaacenes were prepared by Pd-catalyzed coupling, with subsequent oxidation. Stella was very successful in doing so and prepared a whole series of novel materials. She recorded the spectroscopic and structural properties of these novel 2,3-dicyano-substituted azaacenes containing three to six annelated rings; She discovered that the position of the cyano groups with respect to the pyrazine ring (either one or two benzene rings separated from the azaacene unit) influences both the reduction potential but also the optical properties of these species. Thereby, the effect of the cyano groups is dependent upon its placement. This work has just appeared as paper in Chem. Eur. J.

Over all Stella did a superb thesis that would be graded "summa cum laude" in the German system.



Uwe Bunz, Ordinarius,

Chaired Professor (Chair I, Organisch-Chemisches Institut).



ARISTOTLE UNIVERSITY OF THESSALONIKI

LABORATORY OF ORGANIC CHEMISTRY
DEPARTMENT OF CHEMISTRY
54124, THESSALONIKI, GREECE
FAX: ++302310997679
E-mail: klitinas@chem.auth.gr
Prof. Konstantinos E. Litinas

Thessaloniki, March 28, 2017

To PhD Committee, University of Bologna

TO WHOM IT MAY CONCERN

PhD Thesis Manuscript Assessment

The Thesis of **Ms. Stella Beglaryan** entitled “Design and synthesis of new molecular tools for the detection of compounds used for the preservation of artworks and substances of environmental concern” presents the design and synthesis of 10,12-tricosadynoic acid (TRCDA) derivatives and especially polydiacetylenes (PDA). These PDAs have applications as colorimetric/fluorescence sensors for the detection of organic components of painting materials, volatile organic compounds (VOCs) and organophosphates (OPs). 2,3-Dicyano-substituted azaacenes containing 3 to 6 annelated rings were prepared also in an effort to get organic field effect transistors.

After the introduction describing the molecular properties and applications of PDA systems as chromatic sensors (Ch. 1), the significant, aim and impact of current study (Ch. 2) and the synthesis of TRCDA derivatives used in this study (Ch. 3), in Ch. 4 is referred the study of poly(methyl methacrylate) (PMMA)-supported PDA films as colorimetric sensors for the screening of organic components in painting materials. This is useful for the painting restoration and the conservation science. In Ch. 5 the silica gel aerogel-embedded PDA derivatives are studied upon exposure to low concentration of VOCs exhibiting rapid color/fluorescence response. The different color transformations can distinguish among the VOCs. In Ch. 6 different TRCDA derivatives are used for the detection of OPs. This could be interesting for the detection of compounds implicated in the pollution of the environment. In Ch. 7 are synthesized 2,3-dicyano-substituted azaacene derivatives containing 3 to 6 annelated benzene rings. One of the prepared compounds presented interesting properties as thin film transistor. In Ch. 8 the experimental details of all chapters are described.

All the above work appeared in four papers and three presentations, while there is material for one more publication.

Overall the results are interesting and this Thesis contribute significantly to the scientific knowledge of the special fields. I like to give congratulations to Ms. Stella Beglaryan (an ERASMUS-MUNDUS PhD candidate scholar, 2011-2012, under my supervision) for performing this excellent Thesis.

Sincerely,



Prof. Konstantinos E. Litinas



Prof. Raz Jelinek
Department of Chemistry
Ben Gurion University,
Beersheva 84105, Israel
Phone: +972-8-6461747
Fax: +972-8-6472943
E-mail: razj@bgu.ac.il

March 18, 2017

PhD Committee

University of Bologna

RE: PhD Thesis Stella Beglaryan

To whom it may concern,

Hereby I assess the PhD Thesis of Ms. Beglaryan entitled “Design and synthesis of new molecular tools for the detection of compounds used for the preservation of artworks and substances of environmental concern”. The thesis presents an original study of development of analytical tools for characterization of molecular components of artwork. The primary focus of the thesis is *polydiacetylene (PDA)*, a conjugated polymer exhibiting unique fluorescence and color properties. Ms. Beglaryan demonstrated that chemical functionalization of PDA systems enables their use as analytical platforms for varied analytes, particularly related to paint substances and artwork analysis. The results are interesting and significant and overall the thesis contribute to scientific knowledge and better insight into artwork analysis and preservation. Below I provide details about the thesis contents.

Chapter 1 in the thesis provides a thorough introduction to PDA systems, highlighting their use as chromatic sensors. The chapter succinctly describes the molecular parameters pertaining to PDA systems and how external stimuli affect PDA structural properties and concomitant chromatic transformations. The chapter also provides an overview of previous studies employing PDA as a transduction element in sensing platforms.

Chapter 2 summarizes the individual projects carried out and outlines the significance and Aims of the study.

Chapter 3 provides comprehensive information upon synthesis of varied diacetylene derivatives that could be employed for recognition and sensing of water pollutants. The Chapter outlines the molecular considerations for the design of specific headgroups exhibiting different properties such as polarity, hydrophobicity, etc., aimed at binding molecular targets in water.

Chapter 4 depicts a broad study of PDA derivative application towards analysis of paint constituents. The work presented in the Chapter summarizes the molecular and cooperative properties of PDA-based films and their use for colorimetric screening of varied paint materials. The study outlined in the Chapter demonstrates that the use of different PDA derivatives provides a powerful means for distinguishing among paint material families.

Chapter 5 discusses applicability of a PDA-based guest-host system – specifically PDA/aerogel assembly – towards detection and identification of volatile substances rather than soluble species. Ms. Beglaryan shows in this Chapter how embedded PDA derivatives distinguishes among different gases, and provides an array-based methodology capable of identification of specific volatile organic compounds (VOCs) through “colorimetric fingerprinting”.

Chapter 6 further expands the array-based detection concept, describing a detailed study in which PDA derivatives in thin film and vesicle environments have been employed for analysis of organophosphates in water. This accomplishment is significant as it might open the way for application of PDA derivatives as a platform for monitoring pesticide presence in water.

Chapter 7 focuses on a related class of compounds – novel cyano-substituted diazenes. The Chapter provides a thorough description of different synthetic pathways designed to modulate their assembly properties, particularly as core components in organic field effect transistors (OFETs).

Chapter 8 outlines all the experimental details for the different systems discussed in the other chapters.

Overall, the thesis of Stella Beglaryan presents an excellent demonstration of the significance for synthetic manipulation of conjugated polymer systems and their interesting scientific, technological, and practical applications. The work carried out by Ms. Beglaryan has been extensive and thorough, and constitutes a significant contribution to scientific knowledge.

Sincerely,

A handwritten signature in cursive script, appearing to read "Raz Jelinek".

Raz Jelinek, PhD

Abstract

Polydiacetylenes (PDAs) comprise a class of chromatic polymers which have attracted significant interest over the past 40 years as a promising platform for chemo- and bio-sensing. Specifically, the unique colorimetric and fluorescent transformations of PDA, induced by varied external stimuli, are core properties of these polymers, and have been widely exploited for diverse applications.

This thesis is mainly focused on a design and syntheses of new PDAs, based on 10,12-tricosadynoic acid (TRCDA or TR) derivatives and their practical application in various fields. A pool of TR derivatives were synthesized in order to examine both the distinct molecular interactions with the compounds tested, as well as modulate the overall structural organization and corresponding colorimetric properties of the sensor films. In particular, the diacetylene monomers examined displayed carboxylic acid (e.g., the commercial product TRCDA), fluorine containing headgroups with different fluorine chain lengths designed to enhance non polar interaction, phenyl boronic acid moiety to establish polar/ionic interactions and eventually form boronic esters with diols-containing materials, ammonium residue aimed to promote ionic interactions with negative compounds, and aminoacid ester derivatives for attaining protein-like hydrogen bonding with polar targets. Photophysical properties and sensing applications of the new PDAs were investigated. Distinct color and fluorescence transitions were induced by various analytes - binding materials of paintings, volatile organic compounds (VOCs), commercially available organophosphate pesticides(OPs). Chromatic transformations were correlated to the analyte structures and properties. Overall, this study presents a new array of TR derivatives which were successfully employed in the colorimetric and/or fluorescent detection of organic compounds present in binding materials of paintings, VOCs and organophosphate pesticides.

In Chapter 7 the research experience in the laboratory of Prof. Dr. Uwe Bunz at Heidelberg University, Germany is reported. The aim was to synthesize new cyano-substituted azaacenes, which might be attractive due to their ability to form weak hydrogen bonds with aromatic C, H-bonds and therefore lead to a tighter packing of the molecules in the solid state with concomitant better charge transport properties. The target molecules - totally novel dicyano-substituted diazaacenes were prepared by Pd-catalyzed coupling, with subsequent oxidation. Spectroscopic and structural properties of novel 2,3-dicyano-substituted azaacenes containing three to six annelated rings as a framework were obtained. An interesting observation is that the position of the cyano groups (either one or two benzene rings separated from the azaacene unit) influence both the reduction potential and thus the LUMO position, such, that the azaacenes in which the pyrazine units are closer positioned to the cyano substituents show a lower lying LUMO and a higher electron affinity.

List of publications

Danilo Malferrari, Stella Beglaryan, Paola Galletti, Margarita Ritenberg, Kaviya P. Kootery, Roman Volinsky, Sofiya Kolusheva, Raz Jelinek, Emilio Tagliavini, “Sviluppo di sensori colorimetrici a base di polidiacetilene per tensioattivi”, *Chimica e Industria* , January/ February 2015, pp. 38-43

Alexander Trachtenberg, Orit Malka, Kaviya P. Kootery, Stella Beglaryan, Danilo Malferrari, Paola Galletti, Silvia Prati, Rocco Mazzeo, Emilio Tagliavini and Raz Jelinek, “Colorimetric analysis of painting materials using polymer-supported polydiacetylene films”, *New J.Chem.*, 2016, 40, 9054-9059

Susmita Dolai, Susanta Kumar Bhunia, Stella S. Beglaryan, Sofiya Kolusheva, Leila Zeiri, and Raz Jelinek, “Colorimetric Polydiacetylene-Aerogel Detector for Volatile Organic Compounds (VOCs)”, *ACS Appl. Mater. Interfaces*, 2017, 9, 2891–2898

Matthias Müller[§], Stella S. Beglaryan[§], Silke Koser, Sebastian Hahn, Olena Tverskoy, Frank Rominger and Uwe H. F. Bunz, “Dicyano-Substituted Diazaacenes”, *Chem. Eur. J.* – accepted article(10.1002/chem.201700421).

List of Presentations

Poster presentation: “Second workshop SCI of green chemistry.” It has been granted the “Best Poster” Award. “Derivati dell’acido 10, 12 - tricosadinoico (TR) in matrice polimerica (PMMA) come sensori di tensioattivi in acqua”, Ferrara, **Italy** -13/06/2014

Poster presentation: “Sensori colorimetrici per l’identificazione di gomme impiegate come protettivi nei dipinti”, 3rd National Workshop on Green Chemistry, Portici, **Italy**-12/06/2015

Oral presentation: “Design and synthesis of new molecular tools for the detection of compounds used for the preservation of artworks and substances of environmental concern”, “XV Giornata della Chimica dell’Emilia Romagna.” Has been granted the “Best Oral Communication” Award, Modena, **Italy** - 18/12/2015

Internship

04/02/2016 – 04/05/2016 – “Synthesis and Characterization of Cyanated Diazaacenes”, the Organic Chemistry Institute, University of Heidelberg, **Germany**. (Supervisor: Prof. Dr. Uwe Bunz)

*This work is dedicated to my husband Aleksey,
my son David and daughter Diana, who,
with patience and understanding, were
waiting for this moment.*

Table of Contents

<i>Abstract</i>	1
CHAPTER 1.....	6
<i>Introduction</i>	6
1.1. Polydiacetylenes	6
1.2. Basic molecular properties of PDA	7
1.3. Common PDA derivatives	8
1.4. Applications of PDA systems	10
CHAPTER 2.....	14
<i>Significance, aim and impact of the study</i>	14
2.1. Chapter 4. Colorimetric sensors for the detection of binding materials.....	14
2.2. Chapter 5. Colorimetric sensors for the detection of VOCs.....	14
2.3. Chapter 6. Colorimetric sensors for the detection of organophosphate pecticides.....	15
2.4. Chapter 7. Synthesis and characterization of cyano-substituted azaacenes.	15
CHAPTER 3.....	16
<i>Array of colorimetric and fluorimetric sensors based on TR derivatives.</i>	16
3.1. A pool of derivatives aimed to detect organic compounds used in protective layers of paintings. 16	
3.2. A pool of derivatives aimed to detect water soluble pollutants.	18
3.3. A pool of derivatives aimed to partially substitute the TR to improve the sensor response.....	21
CHAPTER 4.....	25
<i>Colorimetric sensors for the detection of painting materials</i>	25
4.1. Introduction.....	25
4.2. Results	26
4.3. Discussion	31
4.4. Conclusions.....	32
CHAPTER 5.....	33
<i>Colorimetric Polydiacetylene-Aerogel Artificial Nose for Volatile Organic Compounds</i>	33
5.1. Introduction.....	33
5.2. Results and Discussion.....	34
5.3. Conclusions.....	39
CHAPTER 6.....	40
<i>Array of sensors for the detection of organophosphate pecticides.</i>	40
6.1. Introduction.....	40
6.2. Results and Discussion.....	41
6.3. Conclusion	46

CHAPTER 7.....	47
<i>Synthesis and characterization of dicyano-substituted diazaacenes.....</i>	47
7.1. Introduction.....	47
7.2. Results and Discussion.....	48
7.3. Conclusions.....	55
CHAPTER 8.....	56
<i>Experimental Section.....</i>	56
8.1. Chapter 3: Synthetic procedures of compounds 2-45.....	56
8.2. Chapter 4: Colorimetric sensors for the detection of binding materials.....	93
8.3. Chapter 5: Colorimetric sensors for the detection of VOCs	95
8.4. Chapter 6: Colorimetric sensors for the detection of OPs.	98
8.5. Chapter 7: Synthesis and characterization of cyano-substituted azaacenes.	99
CHAPTER 9.....	104
<i>Supplementary Information.....</i>	104
9.1. Chapter 3	104
9.2. Chapter 4	125
9.3. Chapter 5	127
9.4. Chapter 6	128
9.5. Chapter 7	130
Conclusions of the thesis	150
<i>Acknowledgements</i>	151
References	151

CHAPTER 1

Introduction

1.1. Polydiacetylenes

Since the first reports on PDA synthesis appeared at the end of the 1960s from the laboratory of Wegner^{1,2} these molecules have captured the imagination of scientists and technologists alike due to their unique chromatic properties. Specifically, it has been shown that certain diacetylene monomers can be aligned in solutions and polymerized through ultraviolet (UV) irradiation, producing a conjugated PDA network^{3,4}. The polymerization only proceeds when the diacetylenes are arranged in a lattice with appropriate geometry and the propagating species is believed to be a dicarbene⁵. This topochemical constraint means that polymerization can only occur in solids or other highly ordered structures. Polymerization of self-assembled monomers leads to physical stabilization of the structure, increasing thermal stability and mechanical strength⁶. (Fig. 1). The unique feature of PDA systems has been the observation that the conjugated PDA networks often absorb light in the visible spectral region, thereby exhibiting color, in most cases blue^{7,8}. Moreover, conjugated PDA can undergo phase changes, induced by varied environmental stimuli, leading to dramatic colorimetric transformations that are visible to the naked eye (Fig. 1) paving the way to their use as sensing platform chemicals. Another attractive feature of PDA systems in the context of sensing applications has been the fluorescence properties; blue phase PDA is non-fluorescent while the red-phase configuration exhibits high fluorescence^{9,10,11}.

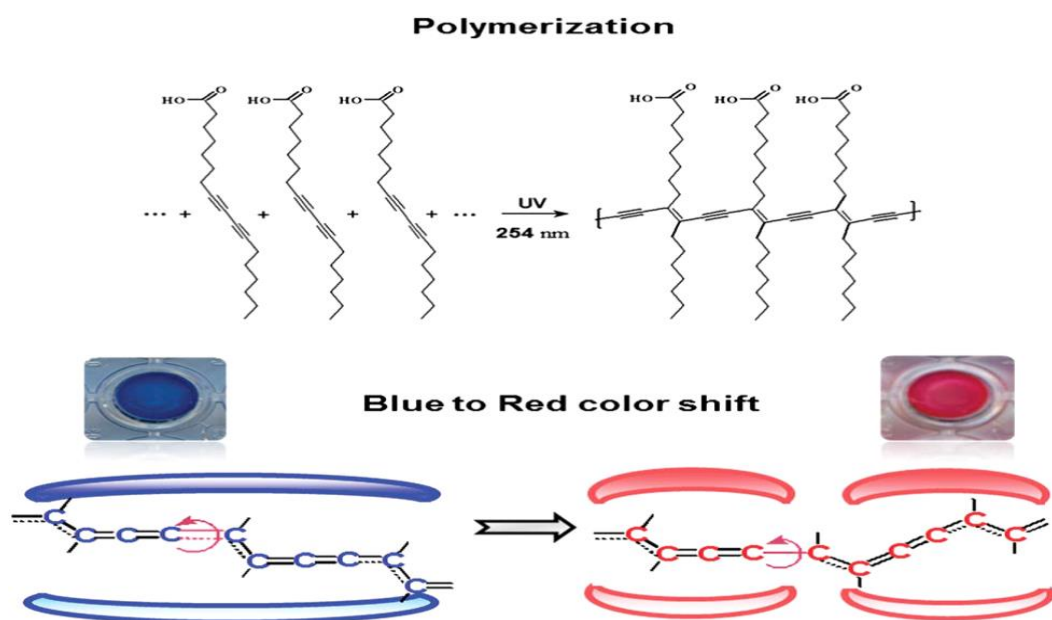


Figure 1. Colorimetric properties of polydiacetylenes^{3,4}.

Beside the intriguing chromatic properties of PDA, the diverse physical configurations of the PDA have attracted broad research interest. Self-assembled PDA materials have been prepared in many different forms. These forms can be divided into five different classes: Langmuir, LB, and LS films; self-assembled monolayers (SAMs); multilayer coatings; colloids; and immobilized colloids¹² (Fig. 2). Langmuir films and SAMs provide well-controlled platforms for studying

fundamental aspects of PDA materials. PDA coatings are relatively easy to prepare compared to Langmuir films and SAMs, though with less control of structure. PDA has been also assembled as components within other “host” matrixes, including inorganic matrixes^{13,14,15}, other polymers^{16,17}, and even living cells¹⁸. Remarkably, it has been shown that PDA generally retains its chromatic properties in these configurations, thus opening the way to construction of varied sensing assemblies.

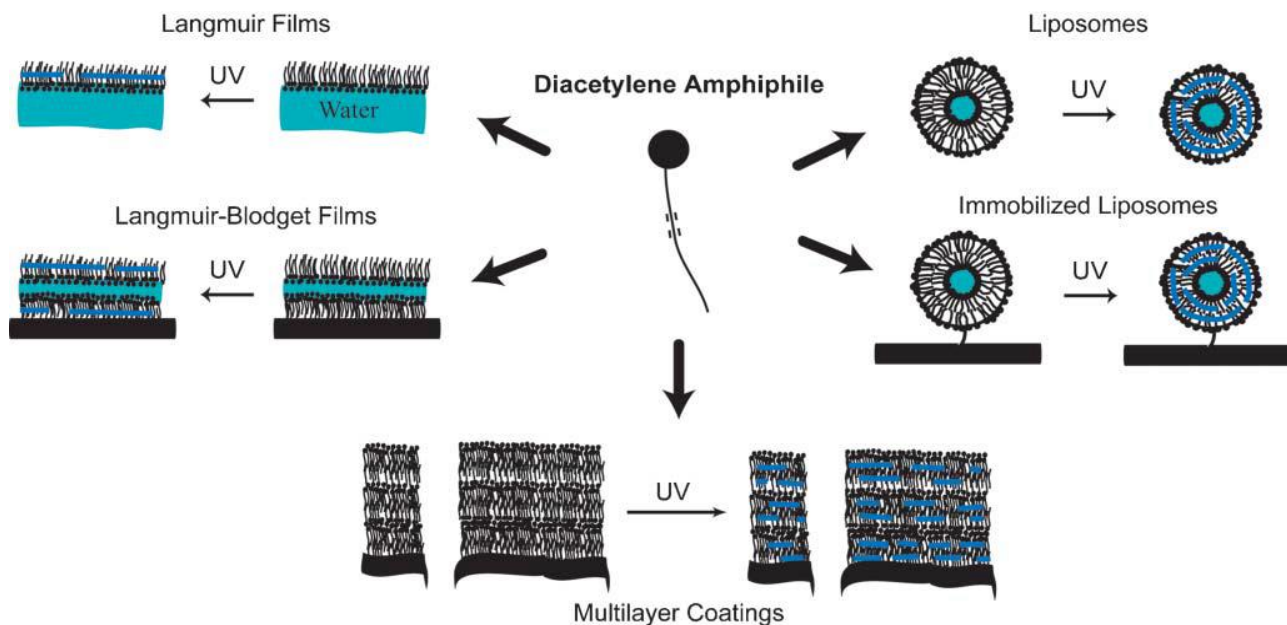


Figure 2. Diacetylene amphiphiles with a polar headgroup and diacetylene tail(s) form a variety of self assembled structures that can be photopolymerized¹⁹.

1.2. Basic molecular properties of PDA

The unique chromatic properties of PDA systems arise from the molecular properties of the polymer. PDA is formed through 1,4-addition of aligned diacetylenic monomers, initiated by ultraviolet (UV) irradiation (Fig. 1). The diacetylene monomers do not absorb light in the visible region, while polydiacetylene appears intense blue (absorption peak at around 650 nm) due to electron delocalization within the linear π -conjugated framework, and corresponding to a $\pi-\pi^*$ transition.

As indicated above, the colorimetric transformations of PDA, induced by a variety of external stimuli, have likely been the most interesting and technologically-attractive feature of PDA systems. The significant shift of the absorption peak from around 640 nm (the blue phase) to around 500 nm (the red phase) is ascribed to disruption of the conjugated network, resulting in shorter electronic delocalization lengths. The red phase of PDA is accompanied by intense fluorescence, contributing to utilization of the fluorescence properties in varied sensing applications.

Despite decades of studies, elucidating the exact mechanisms responsible for the chromatic transformations of PDA has not been fully accomplished. It has been recognized that the shifts in spectral absorbance are closely linked to structural modifications of the conjugated polymer framework²⁰. Early models accounting for the spectral/structural modulations proposed transformation of the polymer backbone from the ene–yne to a butatriene conformation²¹. Recent crystallographic and theoretical investigations have illuminated intimate structural aspects pertaining to the chromatic properties. In particular, it has been established that the pendant side-

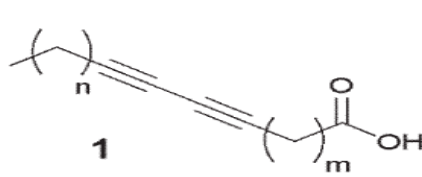
chains of PDA play a prominent role in affecting the chromatic transformations. Specifically, the interactions between the functional groups of the side-chains are believed to significantly affect the overall conformation of the polymer chain, primarily rotations around the C–C bonds (Fig. 1) affecting the planarity of the backbone and concomitant overlap between adjacent π orbitals²⁰. Indeed, theoretical calculations suggested that even rotation of a few degrees of the side-groups around the C–C bond would give rise to a significant change of the π –orbital overlap and resultant blue-red transition²².

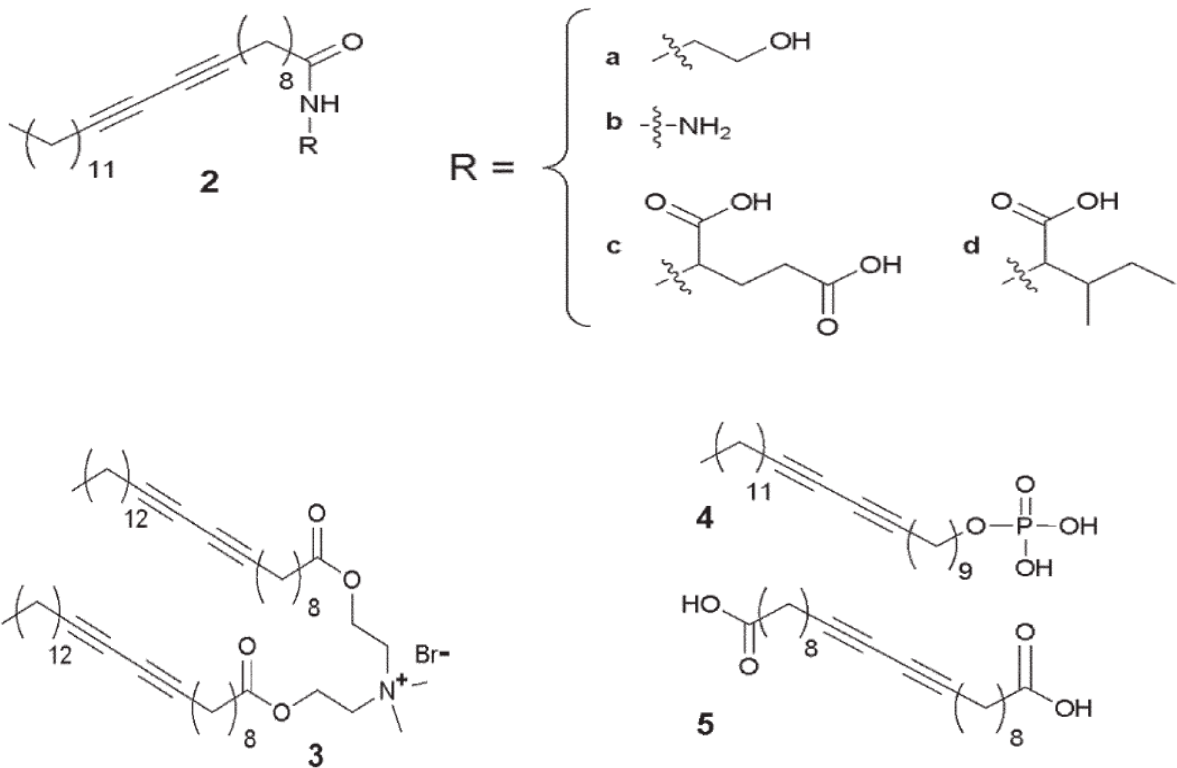
The realization that PDA side-chains exhibit significant effects upon the chromatic properties of the polymer has led to intense research aiming to modulate PDA spectral response through synthetic modifications of side-chain functional groups. Efforts have been directed, for example, to alter the crystal packing of the individual monomers – the essential precondition to photo-polymerization and the resultant linear polymer chains – via side-chain modification. A notable consequence of the close links between crystal packing and pendant side-chain orientation is the achievement of color reversibility. While most of the early work on supramolecular PDA assemblies demonstrated irreversible color transformations, there have been an increasing number of reports depicting color-change reversibility via chemical modification of the PDA side-chains, thus altering the molecular packing and topochemical transformations within the polymer modules^{23,24}.

1.3. Common PDA derivatives

Diacetylene monomers for self-assembled materials are composed of two parts: a polar headgroup and a hydrophobic tail containing the diacetylene moiety. Diacetylenes are usually prepared using the Cadiot–Chodkiewicz reaction consisting of the Cu(I) catalyzed coupling of an acetylene and a haloacetylene²⁵. A large variety of monomers have been synthesized with different polar headgroups and tail structures; some representative examples 1–5 are shown in Scheme 1. The hydrophobic portion of the amphiphile is generally composed of a single alkyl chain, but can also have multiple chains with a diacetylene group in one or more chains. Each tail can be broken down into three parts: the diacetylene group, a spacer between the headgroup and the diacetylene, and the terminal alkyl chain. Bolaamphiphiles, similar to 5, are an exception; they are membrane spanning with the two headgroups at the aqueous interfaces and the chain(s) linking the headgroups forming the hydrophobic region.

	<u>m,n</u>	<u>Abbreviation</u>
a	0,15	2,4 - HCDA
b	3,13	5,7 - DCDA
c	4,12	6,8 - DCDA
d	0,17	2,4 - TRCDA
e	8,9	10,12 - TRCDA
f	3,15	5,7 - TCDA
g	2,17	4,6 - PCDA
h	4,15	6,8 - PCDA
i	6,13	8,10 - PCDA
j	8,11	10,12 - PCDA
k	10,9	12,14 - PCDA
l	8,13	10,12 - HPCDA





Scheme 1. Diacetylene structures¹⁹.

Each element of the diacetylene amphiphile plays a crucial role in determining if an amphiphile will form a self-assembled material and, if it does, what properties that material will have. For instance, headgroup chirality strongly influences colloidal structure; amphiphilic monomers with achiral headgroups usually form spherical liposomes, whereas chiral amphiphiles often form non-spherical structures such as helices and tubules. The number and length of the tails largely controls the range of conditions under which an amphiphile will undergo self-assembly and the temperature of the melt transition (T_m) from “crystalline” chain packing to “liquid” chain packing.

One very interesting question with respect to self-assembled diacetylenes is how the position of the diacetylene relative to the headgroup affects the packing and polymerization of the monomers. Several groups have investigated the impact of this parameter on formation and polymerization of LB films^{26,27} and SAMs²⁸. Studies by Tieke and Lieser²⁶ and Tachibana²⁷ on diacetylene fatty acid LB films showed that the location of the diacetylenes affected the film stability and polymerization. As the diacetylene was moved closer to the headgroup the observed collapse pressures increased, indicating more stable films, but the extent of polymerization decreased and the generated polymer was red or yellow rather than blue. For example, 8,10-; 10,12-; and 12,14-pentacosadiynoic acid(PCDA) on an aqueous subphase with Cd²⁺ all polymerized blue and converted to red with extended UV irradiation, while 6,8-PCDA polymerized red and 4,6-PCDA polymerized weakly yellow²⁷. Fourier-transform infrared spectroscopy (FTIR) and X-ray diffraction (XRD) were used to estimate diyne tilt angle based on the space-filling model. The three that polymerized blue had angles around 45°, close to that observed in crystalline diacetylenes. The angle in red-polymerizing 6,8-PCDA was much smaller, around 18°, and in the yellow 4,6-PCDA was much larger, around 70°. These studies all indicate that a shorter spacer leads to better packing of the amphiphiles but poorer polymerization.

Most works in the field has predominantly focused upon the “standard” diacetylene monomers 5,7-PCDA and 10,12-TRCDA (Fig. 3). These monomers, currently commercially available, can be aligned in aqueous solutions and the hydrogen bond network maintained among the carboxylic headgroups enable the occurrence of ene–yne transformations and formation of the polymerized conjugated backbone system²⁹.

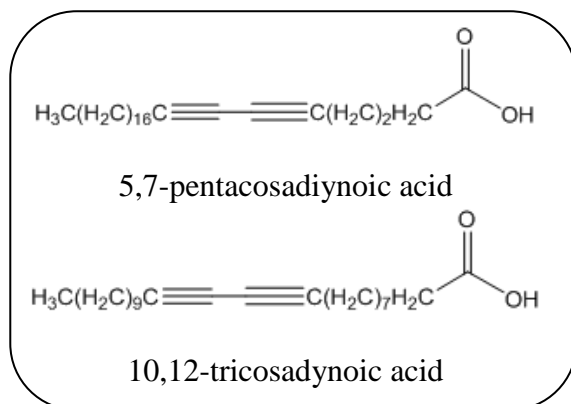


Figure 3 Diacetylene monomers²⁹.

1.4. Applications of PDA systems

Historically and up to the present, the main drawing point of PDA systems have been their remarkable chromatic sensing capabilities. In particular, the incorporation of diverse molecular recognition elements within PDA assemblies has made PDA a highly versatile sensing platform. Importantly, since the PDA headgroups are intrinsically negatively-charged³⁰, many reported biosensing applications have focused on detection of positively-charged amphiphilic molecules³¹. Inclusion of positive units within PDA assemblies, however, can bestow sensing capabilities of negative molecules as well. A recent example has been the use of liposomes comprising diacylenic units covalently displaying positive NH₃⁺ moieties for colorimetric detection of heparin, an important polyanionic biological molecule³². Interestingly, that study indicates that chromatic transformations did not occur in all cases in which positive units were displayed on the liposome surface; rather, color transitions were recorded only when the positive residues were attached to distinct molecular “arms”. Furthermore, the most pronounced chromatic response was induced when sizeable anionic polymers (i.e. heparin) were present in the tested solution, highlighting sensitivity of PDA systems to intimate variations even in electrostatic interactions between the analyte and vesicle surface.

The significance of steric factors in affecting the chromatic transformations of PDA vesicles induced by molecular recognition events was further analysed³³. That study utilized a micro-array liposome-based system to investigate the fluorescence changes induced by interactions between peptide components of the influenza virus (as well as the viral particles themselves) and their respective antibodies. Based upon the experimental data, the researchers have concluded that steric repulsion between vesicle-bound ligands play more significant roles in affecting the structural/chromatic transformations of PDA as compared to the binding strength between the analyte and vesicle-displayed recognition element (Fig. 4). This interpretation, if proven to be universal for PDA systems, is important, since it could shape the design of PDA-based sensors aiming to achieve optimal sensitivity.

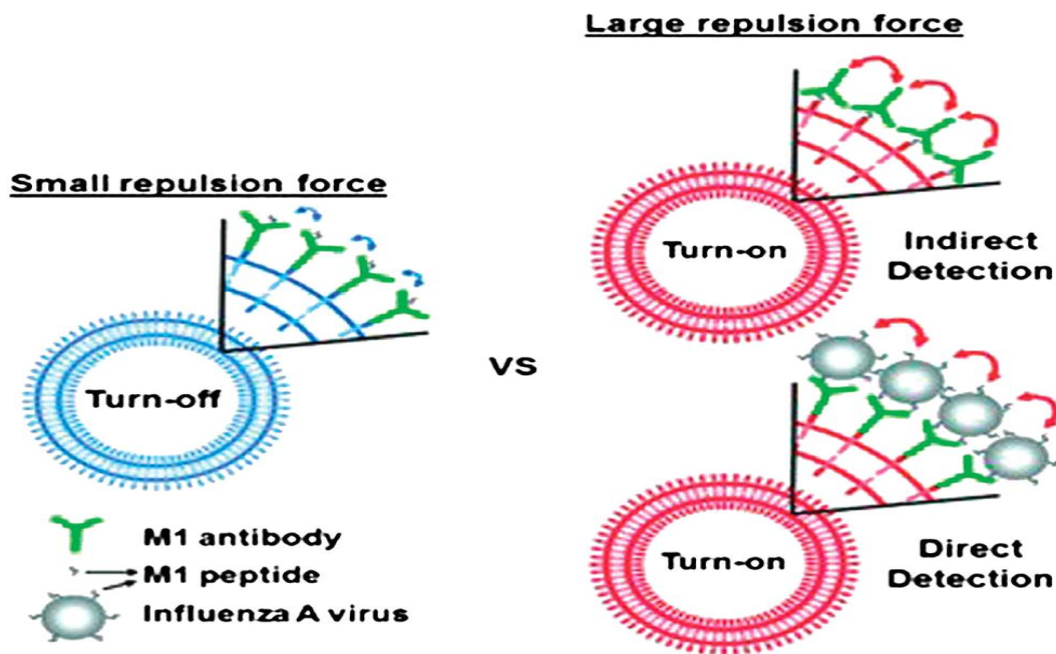


Figure 4 Significance of steric repulsion vs. analyte binding for PDA chromatic transitions. Effects of different stimuli upon the mechanical perturbation and concomitant color transformations of PDA vesicles³⁴.

An interesting vapor sensing application accomplished through a PDA-based approach has been recently reported³⁵. In that study, the researchers combined several notable features generating a potentially powerful sensing platform. First, they succeeded to couple diacetylene monomers to a filter paper, without adversely affecting the polymerization (and chromatic) properties of the PDA framework. Second, the coupled PDA–paper system exhibited sensitivity to vapors of VOCs, undergoing visible colorimetric transformations in the presence of the compounds in the gas phase. Moreover, to achieve specificity, the researchers prepared a matrix in which each component comprised a diacetylene monomer displaying a different headgroup. Together, the array of distinctly-functionalized PDA units produced colorimetric “fingerprints” for different VOCs, akin to “artificial nose” detection concepts³⁶.

In few cases, displayed functional units can bestow chromatic response to diagnostically-important anionic species. An example of such a system has been the construction of thin films comprising PDA derivatized with imidazolium units, and the use of such films for sensing anionic surfactants³⁷. Interestingly, the imidazolium-functionalized PDA exhibited unusual blue-yellow and blue-orange transformations (besides the more conventional blue-red changes), as well as reversibility of thermochromic transitions.

In some instances, the sensitivity of PDA detection schemes has been enhanced through more complex, hybrid detection schemes in which the PDA detector was coupled to orthogonal signal enhancement mechanisms. An example of such an approach has been a system for detection of the cancer marker prostate-specific antigen (PSA) through PDA chromatic response³⁸. The basic sensing approach relied on conjugating anti-PSA monoclonal antibodies (mAbs) onto the PDA vesicle surface. However, to amplify the chromatic signal magnetic beads coupled to polyclonal antibodies (pAbs) against PSA were further added to the reaction mixture. The consequent binding of the pAb–beads to the vesicles produced a significant mechanical perturbation giving rise to enhanced chromatic response of the PDA.

Coupling PDA with other functional materials could open avenues to intriguing novel applications. A recent study demonstrated that a solution of surfactants and diacetylene monomers

could be used as ink³⁹. Application of the diacetylene-containing ink onto paper through conventional inkjet printing produced chromatic patterns (Fig. 5). Remarkably, upon selection of the appropriate diacetylene monomers, the thermochromic transitions of the PDA-based ink were reversible—e.g. from blue to red upon heating, back to blue following cooling.

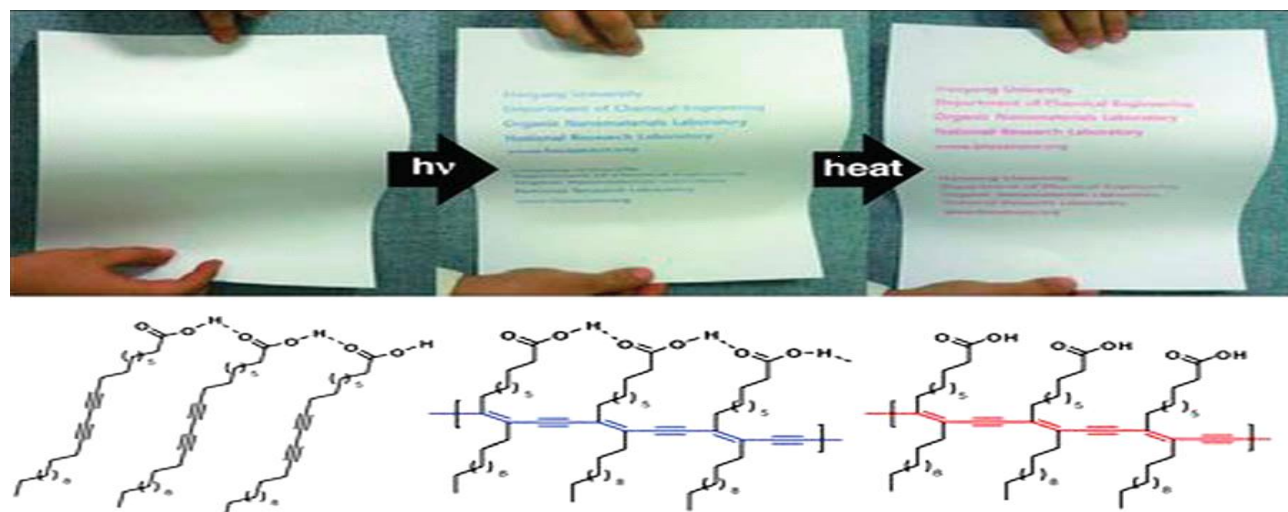


Figure 5. PDA-based inkjet printing. Photographs of a regular printer paper printed with a diacetylene–surfactant mixture. The diacetylene ink retains the chromatic properties – polymerized to the conjugated blue phase and undergoing the blue-red transition following heating³⁴.

Increasing the sensitivity of PDA chromatic properties to environmental stimuli through coupling to additional species has been a major driving force for research efforts aiming to create PDA-based sensing devices. Fig. 6 depicts a recent example of a PDA/sol–gel composite material for detection of bacterial biofilms⁴⁰. In that study, PDA/sol–gel films were assembled on glass substrates through a dip-coating technique⁴¹. Microscopic analysis of the resultant films indicated that distinct PDA domains were formed within the glassy sol–gel matrix. Remarkably, when the PDA/sol–gel films were placed in solutions containing biofilm-forming bacteria, they underwent gradual blue-red transformations.

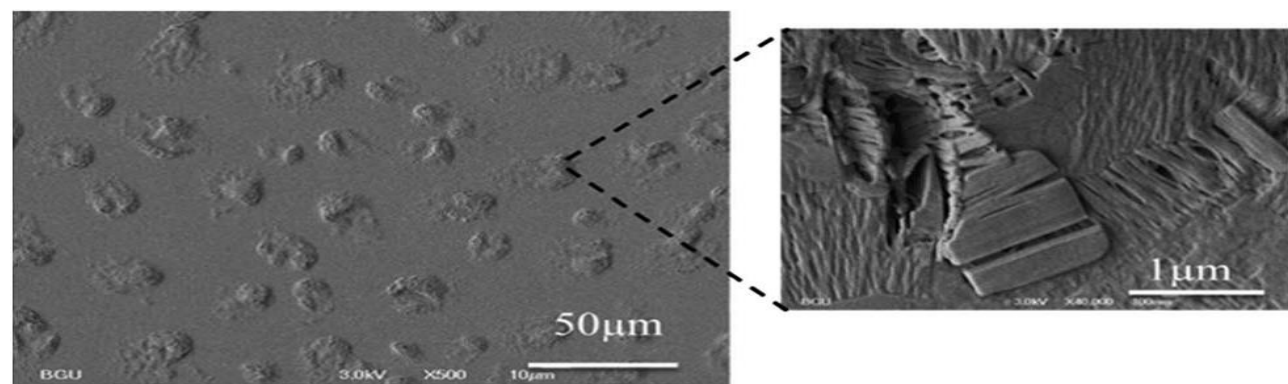


Figure 6. Dip-coated PDA/sol–gel film. SEM image showing the protruding PDA domains within the sol–gel matrix³⁴.

The colorimetric transitions (and corresponding fluorescent emission) were ascribed in that case to the dense biofilm matrix forming upon the PDA domains, consequently producing the localized mechanical stress inducing the structural modulation of PDA.

The conjugated network of PDA provides a useful means for fabricating rigid, stable supramolecular assemblies. A synthetic route has been recently presented in which diacetylenic amphiphile monomers were designed, subsequently forming micellar structures that could be used for gene delivery applications⁴². Fig. 7 depicts the experimental scheme. The diacetylene surfactant monomers in this case displayed positive moieties, designed to anchor DNA moieties – thus forming lipoplex-type assemblies⁴³. The polymerized PDA–surfactant micelles were stable in physiological solutions, and, importantly, exhibited lower cytotoxicity compared to conventional surfactant-based lipoplexes. Notably, the cationic PDA micelles were shown to be effective gene delivery vehicles, and photopolymerization actually enhanced their gene transfection efficiency. This result is likely related to the high stability of the conjugated polymer framework, facilitating better transport of the gene cargo to the cell nucleus compared to more conventional non crosslinked lipoplexes.

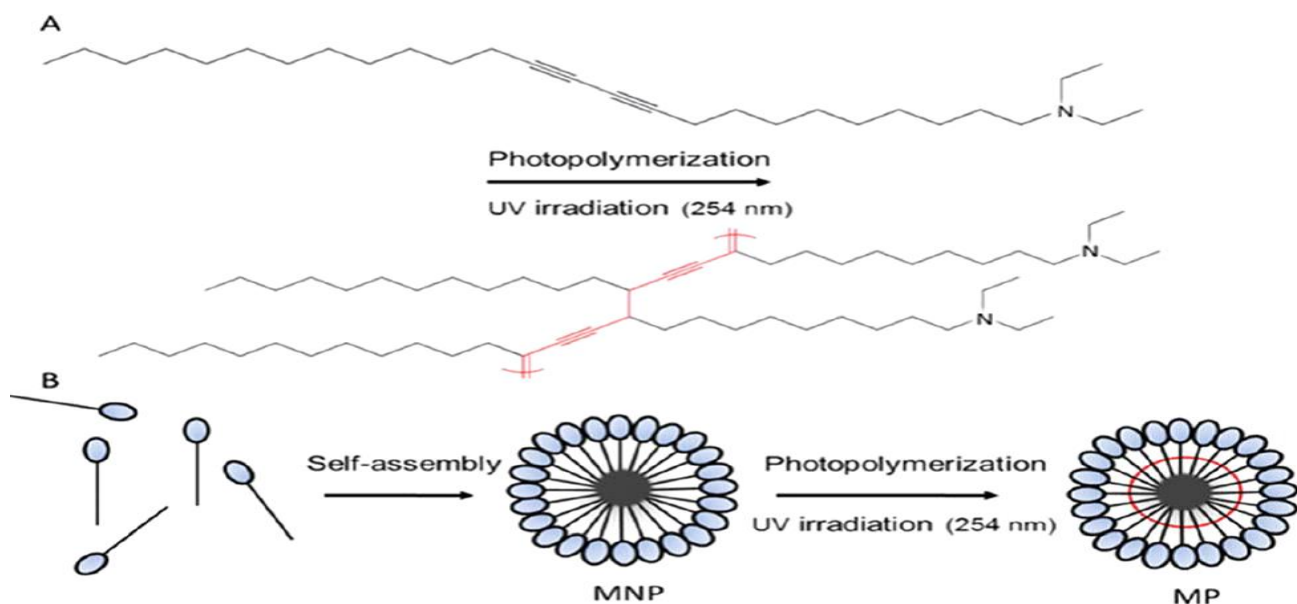


Figure 7. Cationic PDA micelles for gene delivery. Photopolymerization of the diacetylene–surfactant (A) and its micelle organization (B)³⁴.

CHAPTER 2

Significance, aim and impact of the study

The primary focus of the thesis is *polydiacetylene (PDA)*, a conjugated polymer exhibiting unique fluorescence and color properties. The original idea was to design and synthesize a pool of PDA derivatives, based on 10,12-tricosadynoic acid (TRCDA or TR), and demonstrate that chemical functionalization of these systems enables their use as analytical platforms for varied analytes, particularly related to artwork and environmental pollutants' analyses.

Even though a large variety of highly sensitive and specific PDA-based probes for the detection of various targets have been developed, considerable challenges remain in this field. For example, even though the PDA systems have been devised to respond specifically to interesting biologically and chemically important analytes, the cause of the blue-to-red color transition and fluorescent enhancement induced by various stimuli is still not well understood.

For practical applications as sensing platforms, the PDA systems must display good selectivities, sensitivities and stabilities. Although not fully investigated, the selectivity of a PDA sensing system is proposed to depend on the receptor moiety present in the headgroup of the PDA, which can be designed by using the principles guiding host–guest interactions between analytes and receptors. Also, the sensitivity of a sensing system is thought to be related to the degree of polymerization of self-assembled diacetylene monomers and the architecture of the PDA. Finally, because PDA sensing systems are susceptible to environmental factors, such as temperature, light, humidity and pH, their stabilities serve as a challenge to practical applications. A detailed understanding of all of these issues is needed in order for the PDA based sensors to gain widespread use. The overall aim of current study was to develop an array of new colorimetric or fluorimetric chemosensors with improved analyte selectivity and sensitivity.

List of Specific aims:

2.1. Chapter 4. Colorimetric sensors for the detection of binding materials.

Analysis of artworks and identification of their molecular components are of utmost importance for selecting proper conservation strategies and monitoring restoration. Accordingly, development of simple and readily applicable paint analysis assays is highly sought in conservation science and technology. The aim of this research was to design and synthesize new PDA derivatives and employ them as sensors for color analysis of organic constituents in painting materials. It was also interesting to investigate the interactions between the diacetylene headgroups and the tested compounds. Overall goal was to develop a cheaper and easy-operated tool for detecting the composition of protective layers of paintings, without damaging the artwork.

2.2. Chapter 5. Colorimetric sensors for the detection of VOCs.

VOCs might be harmful to human health and exposure to such vapors is considered hazardous and associated with varied pulmonary diseases. Detection of VOCs is thus essential for

early warning, monitoring of occupational hazards, and security applications. Despite the versatility of detection methods, however, current technologies are generally limited in term of practical, easy-to-apply VOC sensing, due to complexity and elaborate synthesis of the gas adsorption and/or transduction substances, high cost of the devices, and insufficient sensitivity / selectivity. The aim of present study was to fabricate a new hybrid PDA-aerogel, produced through a simple single-step method. The PDA-aerogel aimed to be employed for VOCs detection in order to exhibit better sensitivity and more rapid colorimetric response time. Importantly, the colorimetric and fluorescence response of the PDA-aerogel should be VOC-dependent, reflecting the distinct interactions of the VOC molecules with the aerogel-embedded PDA. Overall, the PDA-aerogel matrix aimed to be used as a platform for detection, visualization and speciation of VOCs.

2.3. Chapter 6. Colorimetric sensors for the detection of organophosphate pesticides.

Rapid detection of water pollutants is critical for assessing water quality and reducing the need for costly cleaning operations and drinking water treatment. Colorimetric sensors, in particular, should be attractive for monitoring water since color changes are visible to the naked eye, thereby not requiring specific instrumentation and expertise. To create a new pool of sensors aiming to detect water soluble pollutants, amino acid terminated TR derivatives were designed and synthesized. The chemical structures of amino acid headgroups are known to have a strong impact on the shape and properties of the resulting assemblies. The goal of this research was to develop sensitive and selective sensing technology for alerting on the presence of pollutants in water, such as organophosphate pesticides.

2.4. Chapter 7. Synthesis and characterization of cyano-substituted azaacenes.

Pentacene and triisopropylsilyl(TIPS)-pentacene are nowadays reference materials for organic field-effect transistors (OFETs) exhibiting excellent hole mobilities, but poor electron transport characteristics. Cyano-substituted azaacenes thought to be more attractive targets due to their ability to form weak hydrogen bonds with aromatic C, H-bonds and therefore lead to a tighter packing of the molecules in the solid state with concomitant better charge transport properties. In particular, we aimed to investigate if the cyano groups with respect to the pyrazine ring could influence both the reduction potential but also the optical properties of these species and if the effect of the cyano groups is dependent upon its placement. Electrochemical properties of new molecules have to reveal if they could be processed into thin film transistor as highly attractive n-channel semiconductor.

CHAPTER 3

Array of colorimetric and fluorimetric sensors based on TR derivatives.

3.1. A pool of derivatives aimed to detect organic compounds used in protective layers of paintings.

In Table 1 I present 10,12-tricosadiynoic acid derivatives in which the carboxylic residue was substituted with amines, amino acids, phenylboronic acid, and fluorinated alcohols. The adequate steric and ionic interactions between small, large, charged, branched, polar and protected groups can induce selective colorimetric change with various analytes.

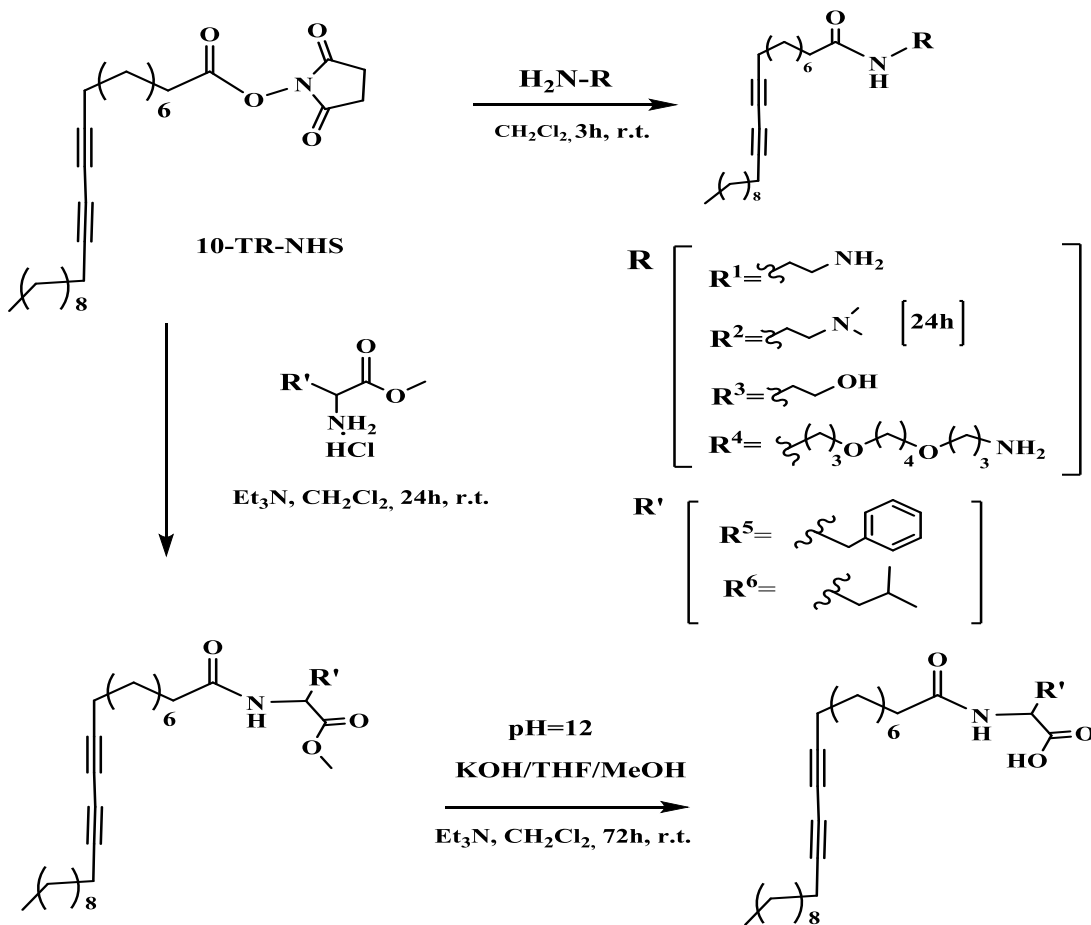
Table 1. 10,12-Tricosadiynoic acid (TRCDA or TR) derivatives.

Moieties	Acronyms	Entry	Moieties	Acronyms	Entry	Moieties	Acronyms	Entry
# 	TR-F3	2	# 	TR-MPhe	7	# 	TR-Leu	12
# 	TR-F17	3	# 	TR-MLeu	8	# 	TR-Phe	13
# 	TR-iF6	4	* 	TR-Cl	9	# 	TR-EDA	14
# 	TR-PhB	5	* 	TR-NHS	10	# 	TR-OH	15
# 	TR-N4	6	# 	TR-DMEDA	11	# 	TR-D3A	16

10,12-Tricosadiynoic acid derivatives were prepared by amide and ester formation. For amide synthesis commercially available 10,12-tricosadiynoic acid (TRCDA) was converted to a succinimidyl ester in the presence of N-hydroxysuccinimide (NHS) and N-(3-Dimethylaminopropyl)-N'-ethylcarbodiimide hydrochloride (EDC)(synthetic scheme is shown in

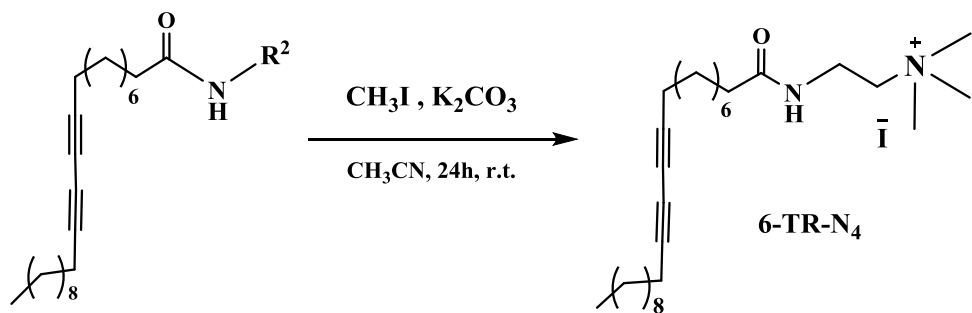
Experimental section)⁴⁴. Then, by nucleophilic substitution, it was reacted with amines⁴⁵ and amino acid methyl esters⁴⁶, with subsequent hydrolysis, to form different TR derivatives (Scheme 2).

Scheme 2. Synthetic routes for preparing amine and aminoacidic derivatives of TR.



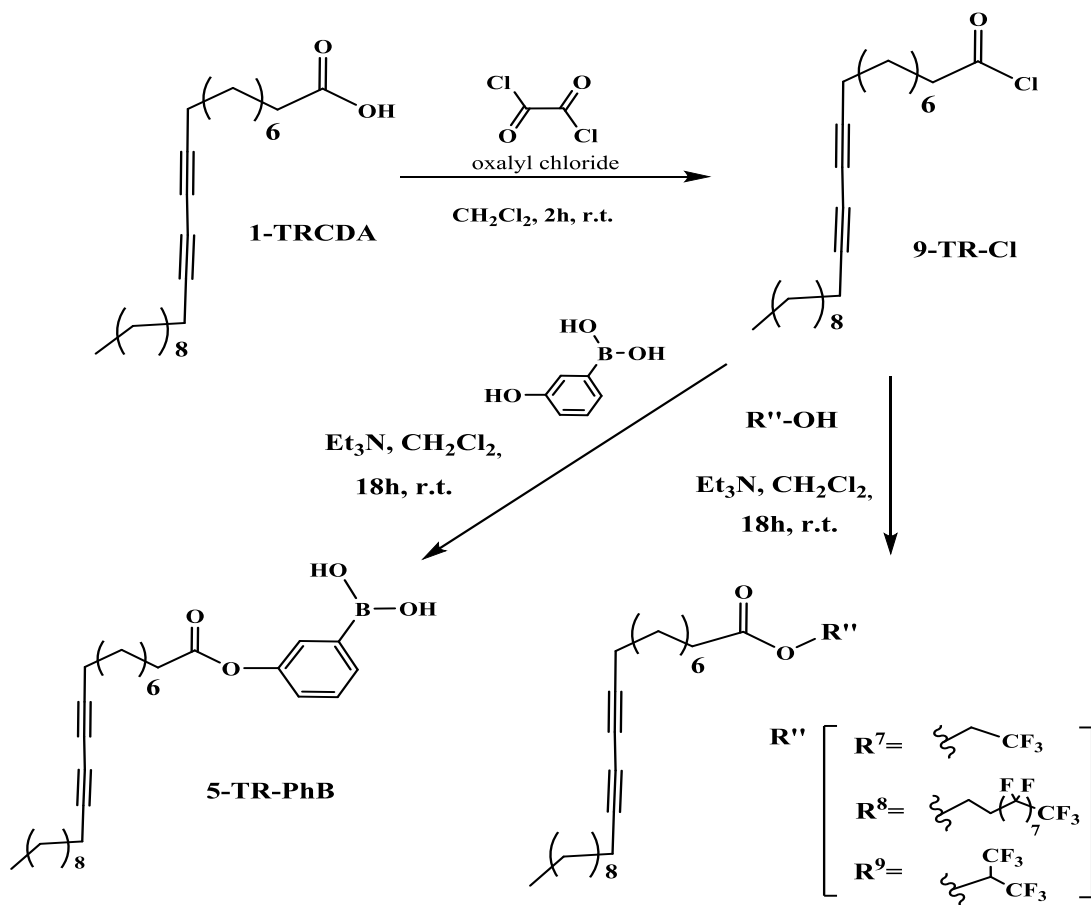
A monomer bearing a quaternary ammonium headgroup(TR-N4 **6**) was synthesized with excellent yields by refluxing with iodomethane a solution containing TR-DMEDA **11** (Scheme 3)⁴⁷.

Scheme 3. Synthesis of TR-TMEDA(TR-N4 **6**).



In order to prepare esters, TR was activated with oxalyl chloride and by further interaction with corresponding alcohols, phenylboronic acid and fluorinated TR derivatives have been isolated (Scheme 4)^{48,49}. As PDAs are sensitive to light and heat the reactions were performed under dark conditions at room temperature.

Scheme 4. Synthetic pathway of phenylboronic acid and fluorinated TR derivatives.



Compounds **2-16** obtained with good to excellent yields (52-93%, see Experimental Section), purified and characterized by standard spectroscopic techniques and are very stable(do not undergo polymerization) when stored at -20°C in the dark (procedures and characterization data can be found in the Experimental section 8.1. and NMR spectra are provided in the Supporting Information (SI) 9.1.).

Synthesized compounds were designed for sensing different classes of molecules employed as painting binders or in varnish formulation⁵⁰. They have been divided into different groups, taking into account their functionality: amine derivatives (**6, 11, 14-16**) - aimed to promote ionic interaction with negatively charged compounds; amino acidic (**7, 8, 12, 13**) - for attaining protein-like hydrogen bonding with polar targets; fluorinated (**2-4**) designed to enhance non polar interaction; and phenyl boronic acid derivative **5** to establish polar/ionic interactions and form boronic esters with diol-containing materials(results are published⁵¹ and detailed described in Chapter 4). Compound **7** was employed in the detection of VOCs⁵², details reported in the Chapter 5.

3.2. A pool of derivatives aimed to detect water soluble pollutants.

After successful application of derivatives **2-8** (details in Chapter 4) in the detection of binding materials of painting and VOCs, the idea to design new group of TR derivatives with different amino acidic moieties arose (Table 2). Amino acids were chosen as headgroups (entries **17, 22-33**) to create a compatible surface on the microstructures for protein-related applications. In

addition, amino acids are chiral and possess various charges, allowing surface charge and hydrophilicity to be manipulated in a controllable manner.

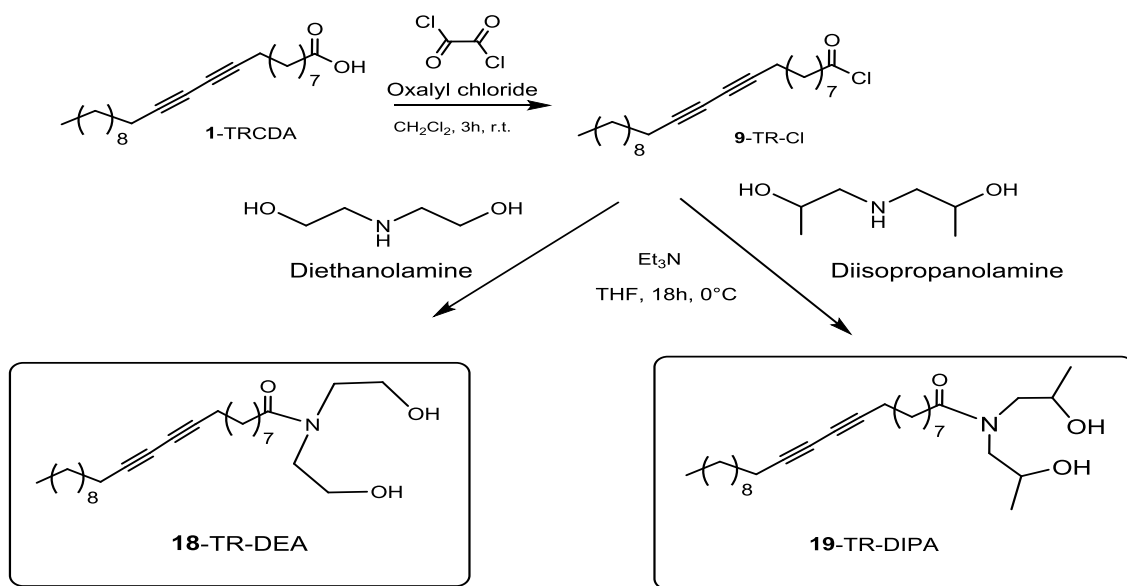
For increasing a sensitivity of the sensor towards water soluble pollutants, TR derivatives having small aromatic and hydrophilic headgroups (**18-21**) were also prepared. Some TR derivatives were synthesized as dipeptides (**31-33**). We believed that additional aromatic moiety will create more planar structure which will induce more intense signal.

Table 2. TR derivatives synthesized for the detection of water soluble pollutants.

Moieties	Acronyms	Entry	Moieties	Acronyms	Entry	Moieties	Acronyms	Entry
	TR-MGly	17		TR-MTyr	23		TR-MHis	28
	TR-DEA	18		TR-MTrp	24		TR-MLys-TR	29
	TR-DIPA	19		TR-Trp	25		TR-MArg-TR	30
	TR-Ph	20		TR-DMAsp	26		TR-Phe-Ba	31
	TR-Naph	21		TR-Asp	27		TR-Phe-MPhe	32
	TR-MCys	22						33

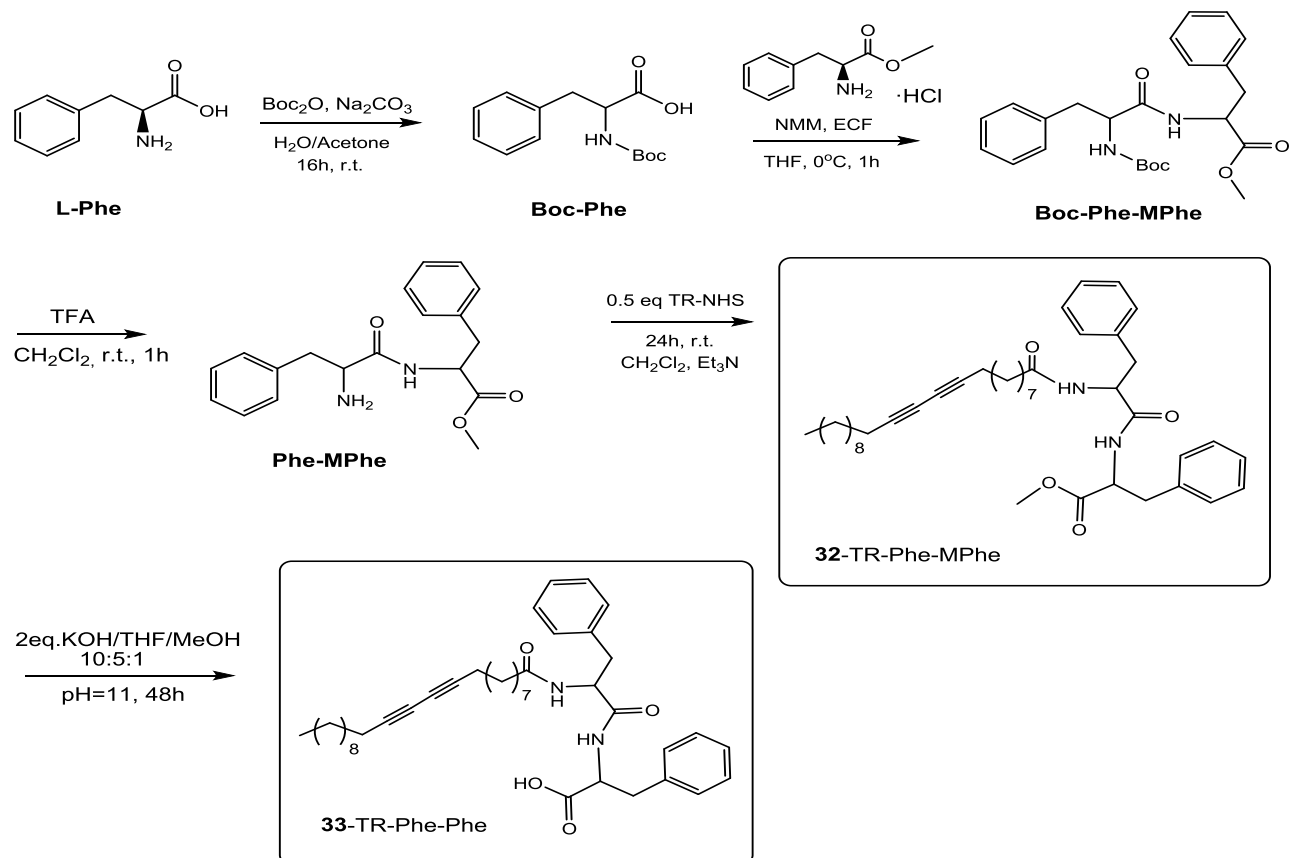
DEA derivatives exhibit a broad spectrum of biological activity, including antibacterial, antifungal, antitubercular, anticancer, local anesthetic, antiplatelet aggregation, and antioxidant⁵³. Amides derived from diethanolamine have great importance in surface active systems⁵⁴. Such promising synthetic and biological potential of DEA and its derivatives have prompted us to synthesize¹²⁷ TR-DEA **18** and its branched “relative” TR-DIPA **19** to sense some widely used organophosphate pesticides (detection tests with compounds **7**, **18**, **21**, **29**, are published as a Patent⁵⁵ and in more detailed reported in Chapter 6). Diethanolamide and diisopropanolamide synthesized by interaction with fatty acid chloride, by stirring overnight at 0°C (Scheme 5). TR-Ph **20** and TR-Naph **21** are synthesized following procedure of Scheme 4⁴⁹. Compounds **17**, **22-30** are synthesized by analogy with aminoacidic derivatives’ syntheses described in the Scheme 2⁴⁶.

Scheme 5. Synthetic route of TR-DEA **18** and TR-DIPA **19**



Compounds **31-33** were prepared using a multi-step procedure beginning with commercially available amino acids (Scheme 6). L-Phe was N-tBoc protected following standard procedures, coupled with MPhe and benzylamine using the mixed anhydride coupling (MAC) method, and then TFA deprotected to give Phe-Ba and Phe-MPhe⁵⁶. Target molecules **31-33** were obtained by following the procedure from Scheme 2⁴⁶.

Scheme 6. Synthesis of TR-dipeptide derivatives.



Compounds listed in Table 2 obtained with good to excellent yields (39-97%, see Experimental Section 8.1.), purified and characterized by standard spectroscopic techniques and are very stable (do not undergo polymerization) when stored at -20 °C in the dark (procedures and characterization data can be found in the Experimental section 8.1. and NMR spectra are provided in the SI 9.1.).

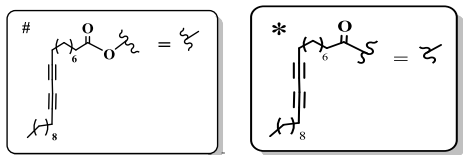
3.3. A pool of derivatives aimed to partially substitute the TR to improve the sensor response.

In Table 3 I present a pool of compounds (amphiphiles), designed and synthesized to improve response in the detection of water soluble pollutants and threats for human health, such as bacteria, metal ions, etc. I have synthesized amphiphilic compounds **34** – **38**, which aimed to partially substitute TR in vesicles or films to increase their stability, as well as TR derivatives containing polyethoxylated spacers with polar and apolar moieties (Entries **39**-**45**), aimed to selectively interact with biological molecules, metal ions, and other analytes (Table 3)⁵⁷.

We introduced in between a polyethoxylated chains so give more stability to liposomes, as well as to bring the detection unit more in contact with the analyte. In the substitution of neat TR – it would be also interesting to test compounds **2**, **20**, **21**. Combination of amphiphile **1** and TR derivatives(such as **39**, **40**-**43**, etc.) in a single hybrid micelle should permit the introduction of anchoring carboxylic groups for further functionalization.

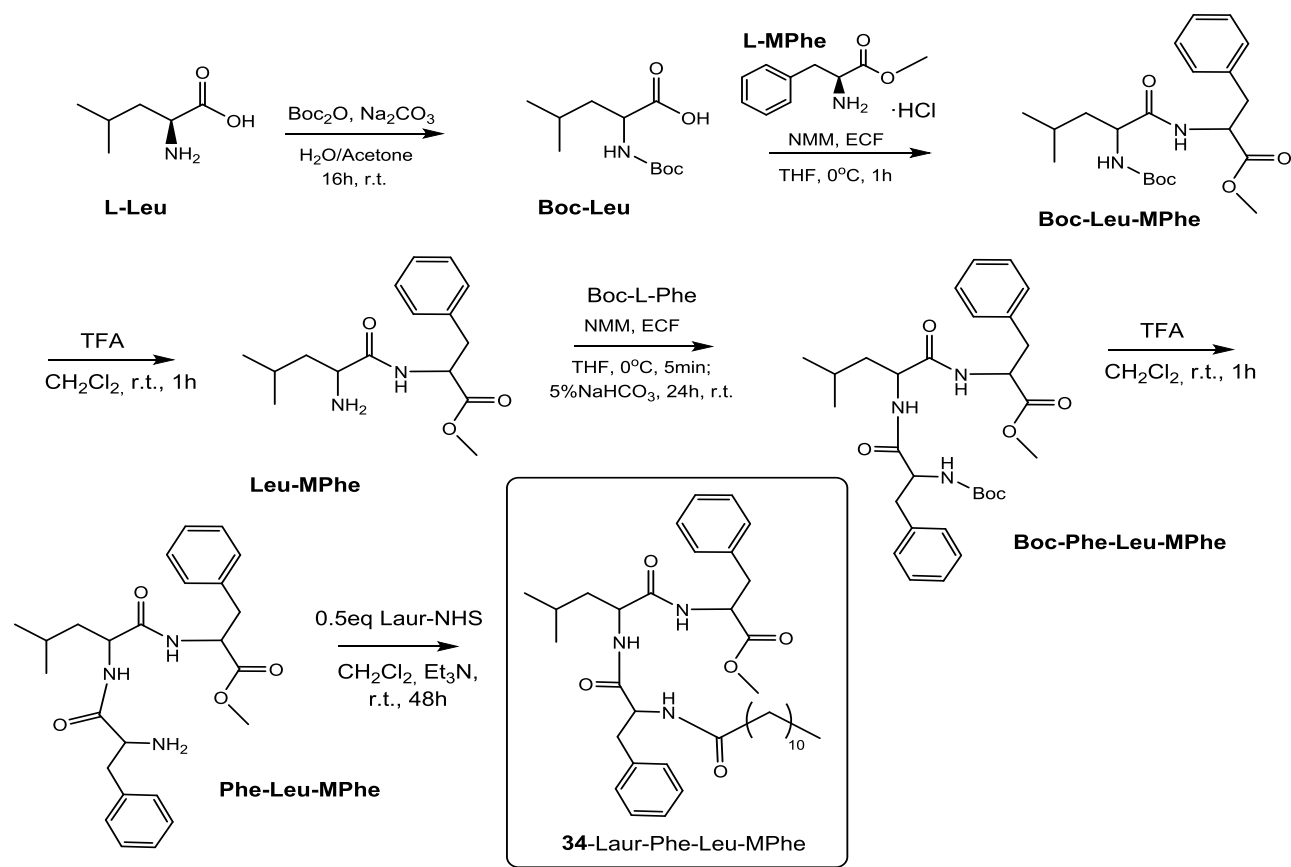
Table 3. Compounds synthesized for the detection of water soluble pollutants and substitution of TR.

Moieties	Acronyms	Entry	Moieties	Acronyms	Entry
	Laur-Phe-Leu-MPhe	34	#	TR-TEG-ABA	40
	Palm-Phe-MPhe	35	#	TR-TEG-F3	41
	Soya-Phe-Ba Soya-Phe-MPhe	36 37	#	TR-TEG-F17	42
	ADA-DANS	38	#	TR-3ET-DBA	43
#	TR-TEG-BENZ	39	#	TR-3ET-MP	44
*	TR-DMEDA-F17	45			



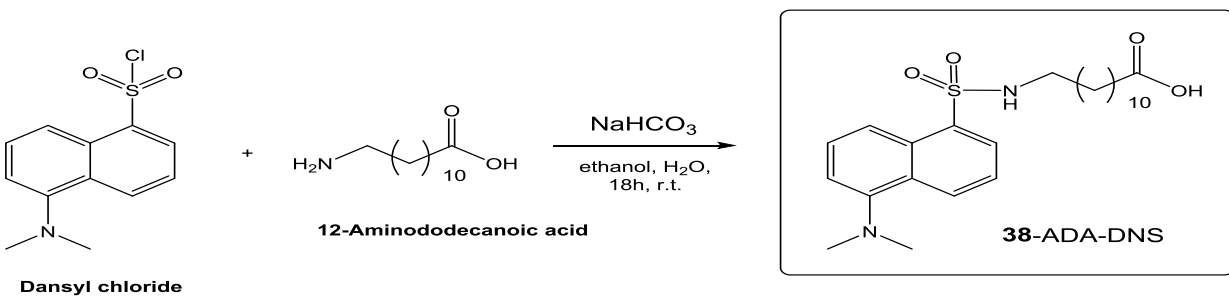
Compound **34** was synthesized modifying the procedure reported in Scheme 6. L-Leu was N-tBoc protected following standard procedures, coupled with MPhe using the MAC method, and then TFA deprotected to give Leu-MPhe, which was coupled with Boc-MPhe, and then TFA deprotected to give Boc-Phe-Leu-MPhe. Later by interaction with Laur-NHS, which was prepared by analogy with TR-NHS **10**, following procedure from Scheme 2, the target molecule **34** was obtained (Scheme 7).

Scheme 7. Multi-step procedure for preparing Laur-Phe-Leu-MPhe **34**.



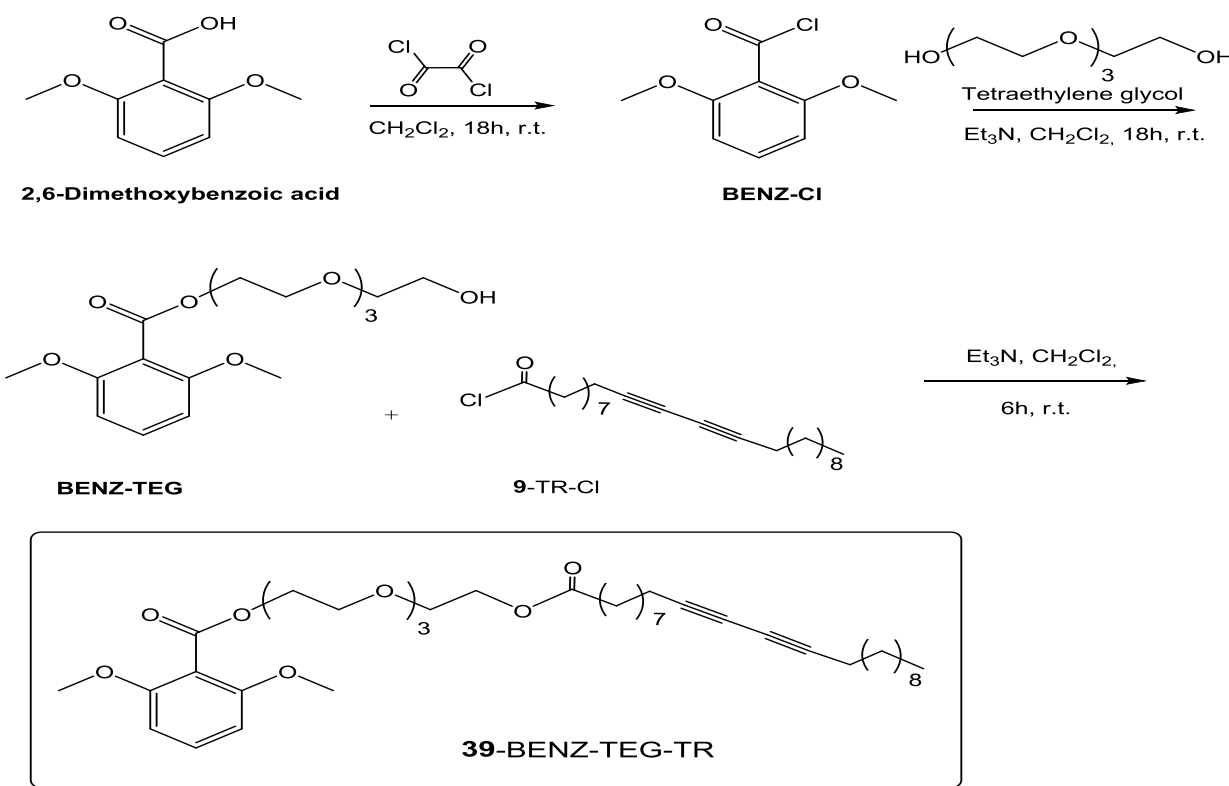
Dansyl-tagged fatty acid **38** was prepared by addition dropwise dansyl chloride to ethanol/water solution of 12-aminododecanoic acid (Scheme 8)¹²⁸.

Scheme 8. Synthesis of ADA-DANS **38**.

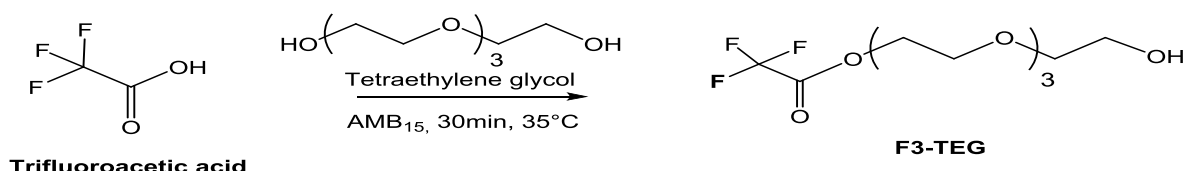


In Schemes 9-11 the synthetic procedures for compounds **39-44** are described. These linkers TEG and 3ET are flexible, water soluble, and have sufficient mobility to insert themselves into the bilayer of lyposomes at various depths⁵⁸. The interaction between water and polyethylene glycol (PEG) involves formation of hydrogen bonds between water molecules and oxygen atoms of PEG. When heated these bonds will be broken, which will cause a decrease in the PEG solubility.

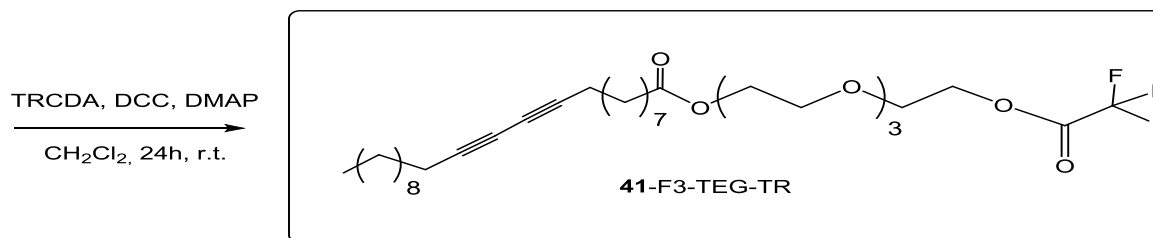
Scheme 9. Synthetic procedure for preparing compounds TR-TEG-BENZ **39** and TR-TEG-ABA **40**



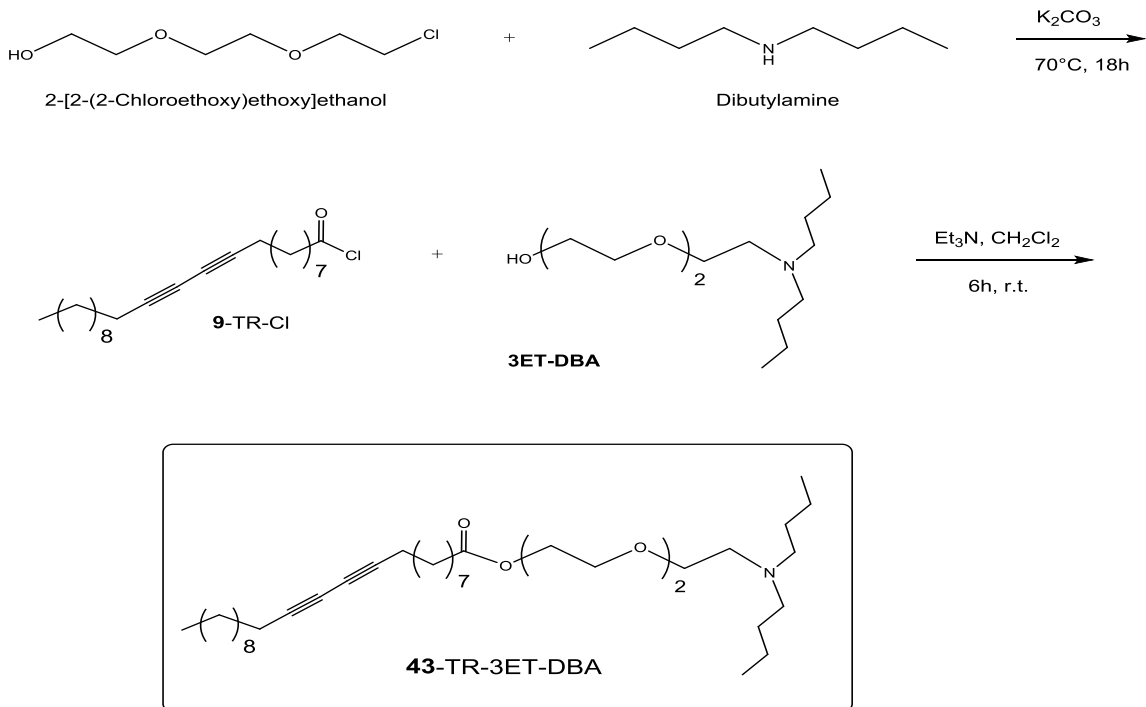
Scheme 10. Synthesis of compounds TR-TEG-F3 **41** and TR-TEG-F17 **42**



Trifluoroacetic acid



Scheme 11. Synthetic route for preparing TR-3ET-DBA **43** and TR-3ET-MP **44**.



Compound **45** was prepared by following the procedures of TR-N4 **6** from Schemes 2 and 3 with slight modifications.

Detailed syntheses and characterization data are reported in Chapter 8.1. of Experimental section and NMR spectra are available in SI 9.1.

CHAPTER 4

Colorimetric sensors for the detection of painting materials.

Analysis of artworks and identification of their molecular components are of utmost importance for selecting proper conservation strategies and monitoring restoration. Accordingly, development of simple and readily applicable paint analysis assays is highly sought in conservation science and technology. For this purpose, I designed and synthesized new derivatives of TRCDA listed in Table 1, which were then spin-coated upon poly(methyl methacrylate) (PMMA) substrates and employed for color analysis of organic constituents in painting materials. Distinct color transformations were recorded upon addition of paint compounds to different TR derivatives **2–8**(see Table 1 in Chapter 3). Quantitative analysis revealed that the colorimetric transitions were dictated by the interactions between the diacetylene headgroups and the tested compounds. This study underscores the significance of the diacetylene headgroup for molecular discrimination and points to the possible uses of the PMMA-supported PDA films for colorimetric screening of organic components in painting materials.

4.1. Introduction

Proper restoration of old paintings and artworks often necessitates identification of painting materials and diagnosis of their state of conservation. Cleaning operations of paintings are often necessary to remove the aged and yellowed varnish layer applied on the painting. However, the selective removal of the varnish layer may be difficult due to its thickness (10–50 mm) and the affinity to the painting surface. Thus, identification of organic compounds present both in the painting and in the varnish layers is of the utmost importance to identify the most suitable cleaning method. Moreover, the materials used as binders in painting layers or as ingredients in the formulation of varnishes belong to different organic classes, such as triglycerides (i.e., siccative oil used both as painting binders and in varnishes), terpenes (i.e., natural resins used in varnishes), proteinaceous materials (i.e., animal glue, egg, milk or casein used as binders and sometimes in varnishes), and polysaccharides (i.e., natural gums, used as binders and sometimes in varnishes). This poses additional challenges to the development of accurate and effective on-site identification methods.

Several analytical methods have been employed for paint analysis. Micro-destructive methods, such as gas chromatography-mass spectrometry (GC-MS) and high performance liquid chromatography (HPLC), enable specific identification of the organic compounds present in a paint sample⁵⁹. While these methods are very useful and informative, they cannot be applied during routine restoration work because they require technical expertise to carry out and analyse, and they could be expensive and time consuming. Portable Fourier transform infrared (FTIR) and Raman spectroscopies can be used to monitor the molecular compositions of the external painting layers⁵⁹. Development of simple on-site analytical systems has been lacking in conservation science. While such applications are technically challenging, introduction of such instruments would be of significant benefit in conservation and restoration work and maintaining cultural heritage.

In this chapter, I present application of spin-coated polydiacetylene (PDA) films containing different TR derivatives for *in situ* colorimetric sensing of a selection of organic materials present in paintings.

The premise of this work is that the interactions of the organic substances with the different headgroups would generate distinct colorimetric transformations within the PMMA-supported PDA films, aiding in distinguishing among the tested compounds. In particular, different PMMA-

supported PDA films were tested on not-aged painting materials in order to make a feasibility study and a screening of the most performing tools for the on-site analysis of paint materials.

4.2. Results

Fig. 8 outlines the structural features of the diacetylene monomer derivatives used in this study (prepared according to Scheme 1, 2, 3 in Chapter 3). In particular, I designed and synthetized different diacetylene headgroups in order to examine both the distinct molecular interactions with the compounds tested, as well as modulate the overall structural organization and corresponding colorimetric properties of the sensor films. In particular, the diacetylene monomers examined displayed carboxylic acid (e.g., the commercial product TRCDA, compound **1**), fluorine containing headgroups with different fluorine chain lengths designed to enhance non polar interaction (compounds **2**, **3** and **4**)⁴⁹, phenyl boronic acid (compound **5**)⁴⁸ designed to establish polar/ionic interactions and eventually form boronic esters with diols-containing materials with the aim of exhibiting affinity to carbohydrates⁶⁰, ammonium residue (compound **6**)⁴⁷ aimed to promote ionic interactions with negative compounds, and aminoacid ester derivatives (compounds **7** and **8**) for attaining protein-like hydrogen bonding with polar targets⁴⁶.

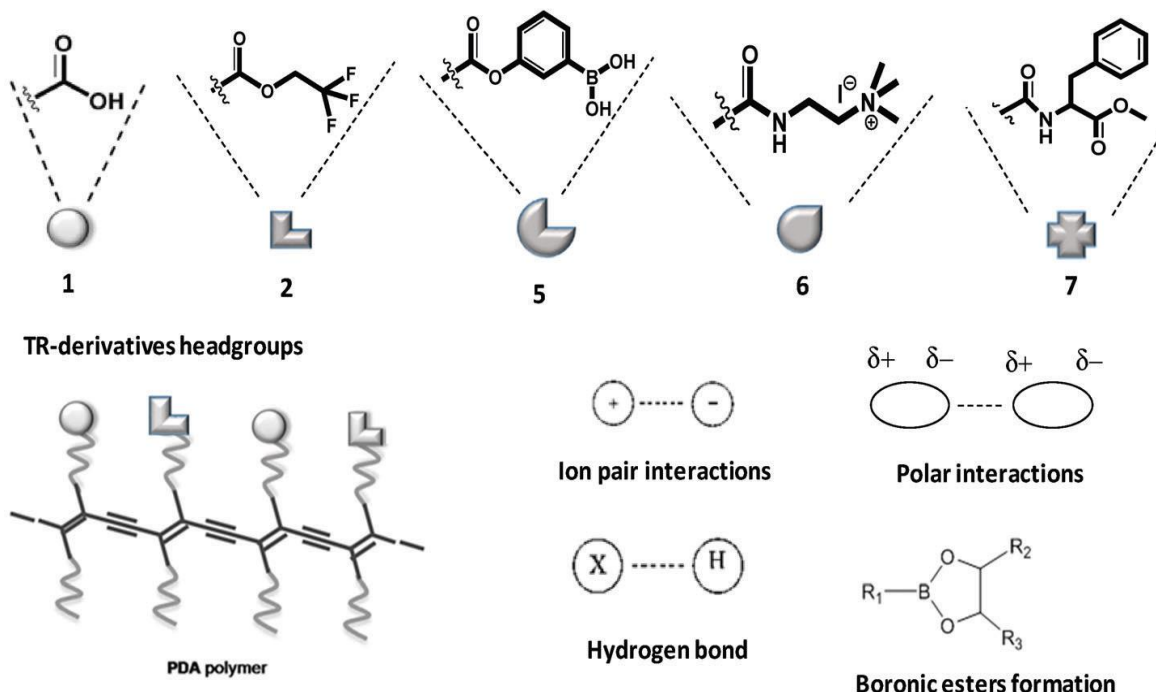


Figure 8. Structures of TR-derivatives and PDA polymers and possible intermolecular interactions between PDA and painting material components.

The color sensor films were assembled through spin-coating mixtures comprising the starting monomer (TRCDA, **1**) and the different functionalized-headgroup derivatives at a 1 : 1 mole ratio (TRCDA: derivative) upon PMMA disks. PMMA is a transparent polymer that is widely used in many applications, particularly as a glass substitute. The PMMA substrate intimately affects the deposited PDA films and endows interesting chromatic properties to the system, including chromatic reversibility induced by ultraviolet (UV) irradiation, and purple/red/orange/yellow color transformations affected by interactions with amphiphilic analytes⁶¹. Notably, we found that films comprising pure diacetylene derivatives exhibit lower stability and/or were too sensitive to

buffer/solvents, thereby rendering very high background signals. Following deposition and drying of the organic solvent, the films were subjected to UV (254 nm) irradiation to generate the blue polymerized polydiacetylene (PDA) phase.

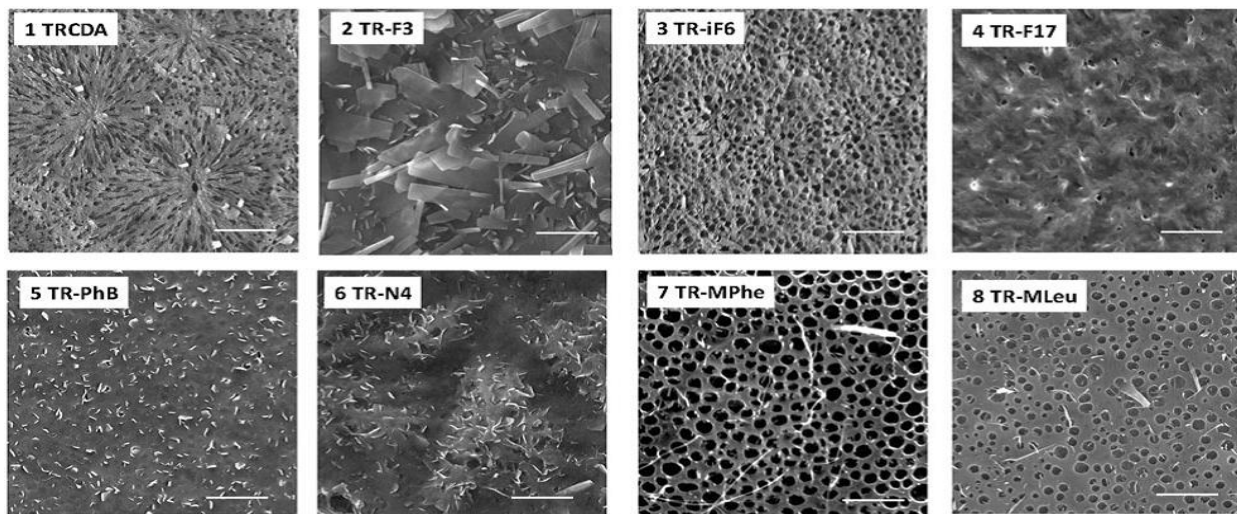


Figure 9. Scanning electron microscopy (SEM) of PMMA-supported diacetylene films. The films comprised the indicated derivatives and the TRCDA (**1**) monomer at 1 : 1 mole ratio. Scale bars correspond to 10 μm .

Fig. 9 presents the scanning electron microscopy (SEM) images of the PMMA-coated PDA films. The SEM experiments demonstrate significantly different surface morphologies among the PDA derivatives, and attest the pronounced effects of diacetylene headgroups upon film organization. In particular, the cooperative film properties, determined to a large extent by the distinct headgroups, might have generated different morphologies during the dewetting accompanying the spin coating process. Previous reports also underscored the significant effect of headgroup interactions in determining macro-scale organization of PDA assemblies⁶². While the SEM results in Fig. 9 reveal distinct macro-scale organizations of the spin-coated films, representative UV-vis spectra and Raman scattering data in Fig. 10 indicate that the PDA backbones within the different films exhibit the same chromatic properties, specifically the presence of the well-known blue and red PDA phases⁶³. Fig. 10A depicts the UV-vis spectra of a spin-coated PDA film in the blue phase (after polymerization), and after transformation to the red phase induced by placing the PMMA-supported film at 50 °C.

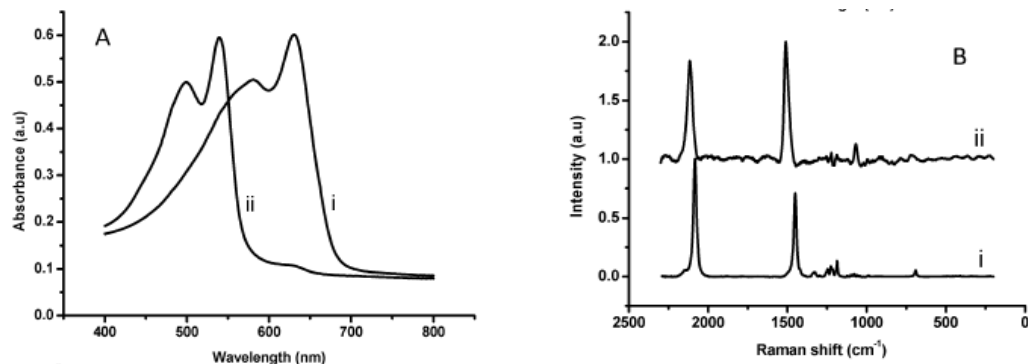


Figure 10. Spectroscopic characterization of PMMA-supported PDA films. (A) UV-vis spectra of blue (i) and red (ii) phase; (B) Raman scattering spectra of the blue (i) and red (ii) PDA film.

Importantly, similar spectral features corresponding to the blue-red transitions were recorded for the other PDA derivatives, indicating that the chromatic properties of the conjugated polymer

backbone were retained in all films. Indeed, the Raman scattering data in Fig. 10B corroborate this interpretation. The Raman spectral region corresponding to the conjugated alkyne–alkene groups initially featured the typical blue-phase signals at around 1450 cm^{-1} and 2090 cm^{-1} (Fig. 10B, i). Distinct peaks corresponding to red-phase PDA appeared at approximately 1520 cm^{-1} and 2125 cm^{-1} following heating (Fig. 10B, ii). Similar to the UV-vis results in Fig. 3A, Raman signals presented in Fig. 10B were recorded for all PDA derivative films prepared, confirming the formation of the conjugated PDA networks. Table 4 outlines the paint materials tested in this study. The selected substances belong to different classes of molecules employed as painting binders or in varnish formulation. In particular, the screened substances include polymerized triglycerides (linseed oil), proteinaceous compounds (fish glue, rabbit glue, and ovalbumine), terpenic compounds (mastic, dammar, colophony, and sandarac), and polysaccharide gums (arabic gum, gum karaya, ghatti gum, guar gum and gum tragacanth). Detailed compositions of the materials are provided in Table S1 in the SI 9.2. of Chapter 4⁵⁰.

Table 4. Paint substances used in the study⁵⁰.

<u>Paint Material</u>	<u>Family</u>	<u>Main Composition</u>
Linseed Oil	Tryglicerides	Polimerized tryglicerides, low chain carboxylic fatty acids
Ovalbumin	Proteinaceous	
Fish Glue, Rabbit Glue	Proteinaceous	Denaturated collagen
Sandarac	Terpenes	Diterpenic compounds, with a polimerized component
Mastic, Dammar	Terpenes	Triterpenic compounds
Colophony	Terpenes	Diterpenic compounds
Arabic, Karaya, Ghatti, Guar, Tragacanth Gums	Polysaccharides	Carbohydrates, monosaccharides % in SI

Fig. 11 presents the colorimetric responses of the PDA films comprising the different headgroup derivatives **2–8** upon incubation with the compounds outlined in Table 4.

In particular, the bar diagrams in Fig. 11A–D depict the percentage colorimetric response (%CR)⁶⁴ after subtraction of the buffer recorded upon incubation of the painting materials with the PDA films, calculated through comparison of the relative intensities of the UV-vis peaks at 500 nm (i.e., “red” peak in the UV-vis spectrum) and 640 nm (“blue” peak), see Experimental section 8.2.⁶⁵ Essentially, the %CR values reflect the degrees of blue-red transformations with respect to the reference solution (here a tri buffer pH 8.0). In particular, high %CRs correspond to more pronounced red appearance, whereas lower %CR values reflect less significant blue-red transformations (e.g., more blue PDA films)⁶⁶. Negative %CR values are occasionally recorded, likely reflecting the surface interactions of target analytes, which stabilize the PDA headgroups in comparison with the effects of buffer/solvents. Notably, the colorimetric data in Fig. 11 were grouped according to the solvent used, making sure the comparison of %CR is reliable in terms of compounds dissolution.

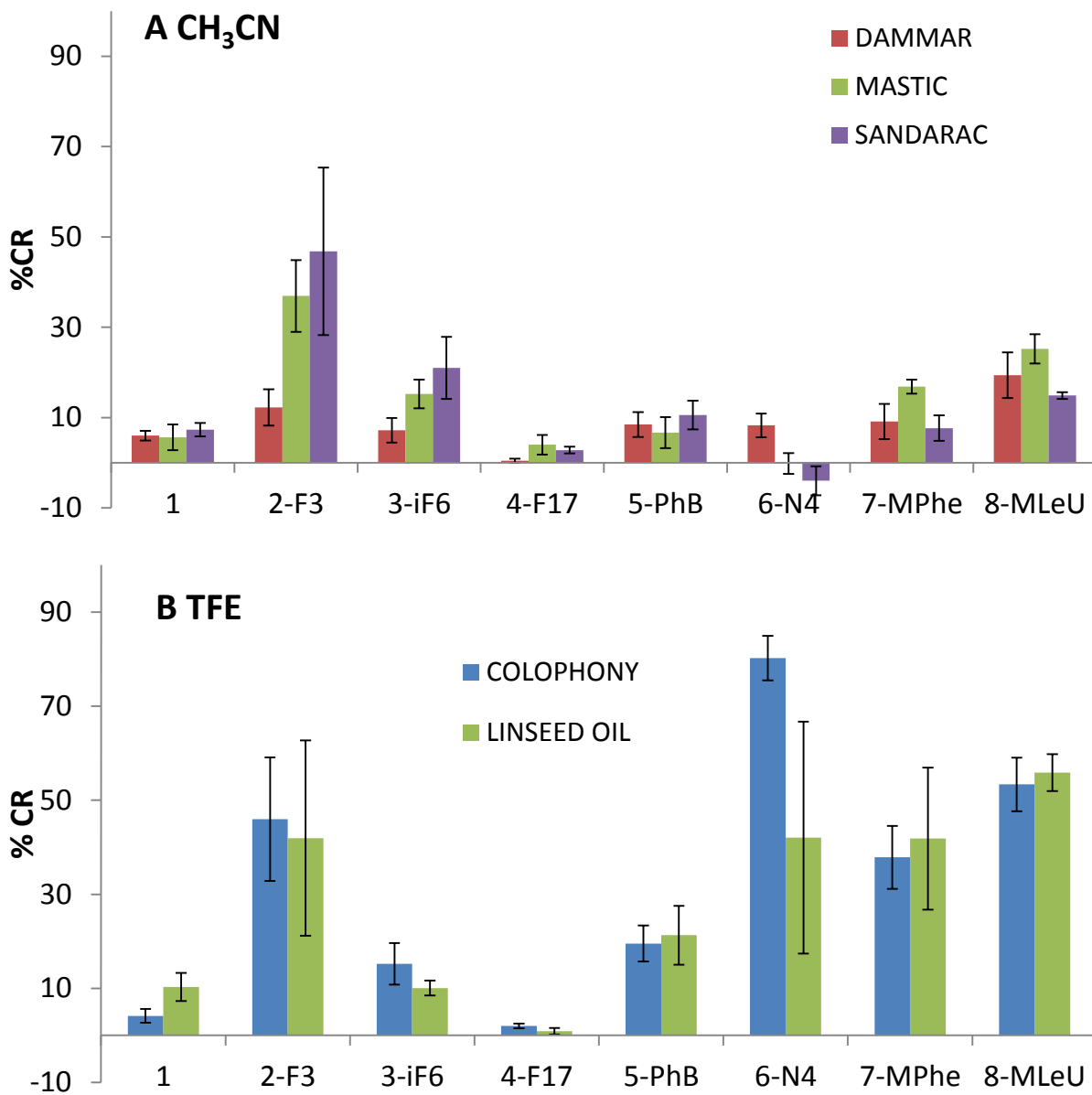


Fig. 11 shows significant variations both among the colorimetric responses of the PDA films to the different painting materials, as well as among the diacetylene derivatives used in the PMMA-supported films. Among the painting materials dissolved in acetonitrile (Fig. 11A, terpenic compounds), films comprising PDA units displaying fluorinated residues (i.e., monomers **2** and **3**) successfully distinguished between dammar, mastic, and sandarac resins. Derivative **2**, in particular, gave rise to the most significant blue-red transformations (%CR of 15, 40, and 50 induced by dammar, mastic, and sandarac, respectively, Fig. 11A). This specificity is likely ascribed to the terpenic apolar backbone interacting with the apolar terminus of fluorinated derivatives. The dammar and mastic are triterpenic resins with very similar composition, whereas sandarac is partially polymerized diterpenic materials⁶⁷. Among the diacetylene derivatives, monomer **2** exhibited the most versatile interactions, both polar through the ester moiety, as well as apolar affinity via the fluorinated group. Indeed, the significance of the fluorine containing PDA headgroups is supported by the observation of small %CR and no distinction among the terpenic compounds apparent in the films comprising the parent polymerized TRCDA (monomer **1**, Fig.

11A). Similarly, polar or charged residues (i.e., derivatives **5** and **6**) exhibited small %CR, which was similar to the parent diacetylene **1**, reflecting insignificant interactions with terpenes.

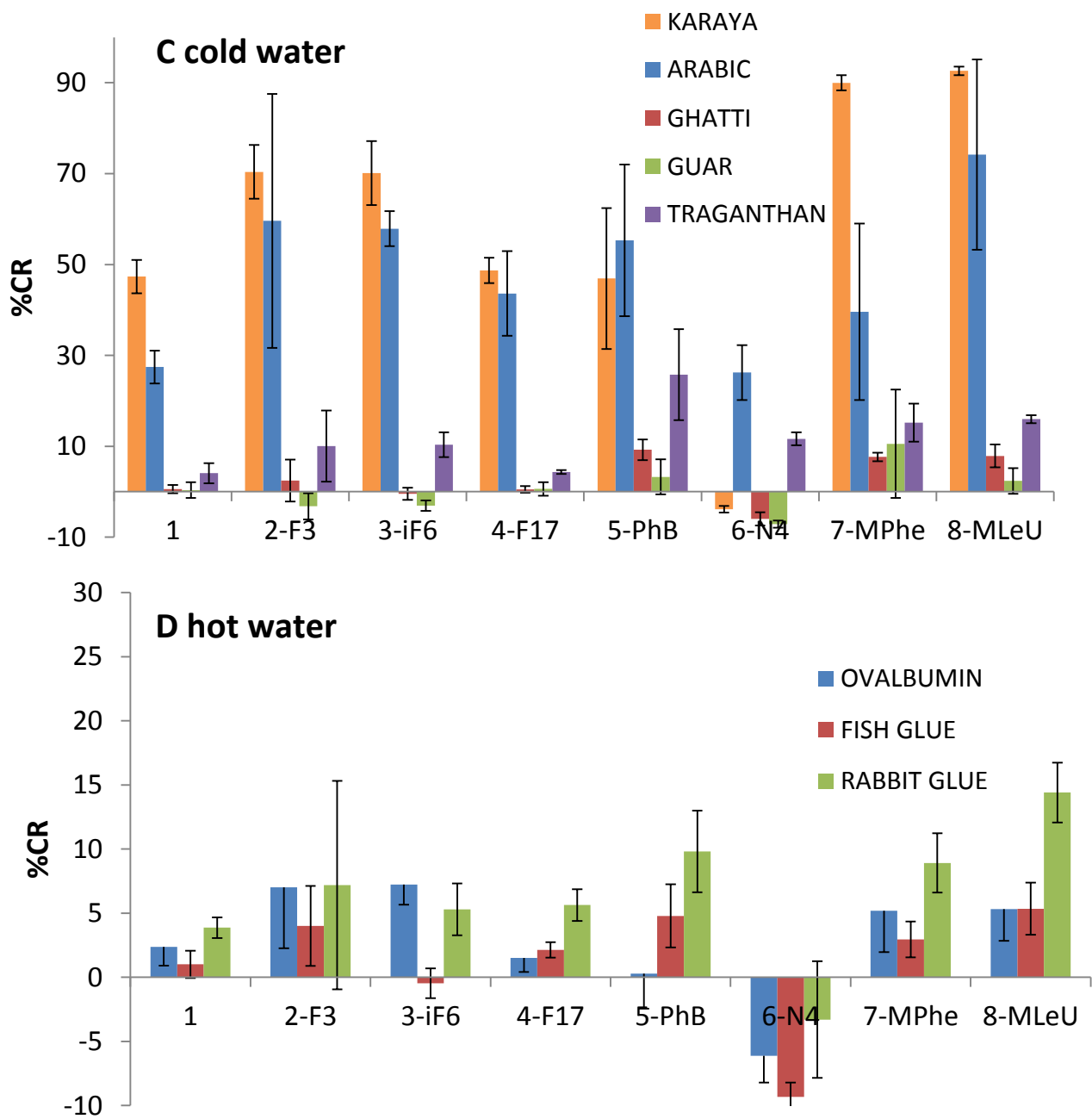


Figure 11. Colorimetric responses of PMMA-supported PDA films comprising different derivatives to paint substances. %CR values after subtraction of the buffer divided according to the solvent used for dissolving thematerial. (A) Materials dissolved in acetonitrile (terpenic compounds); (B) materials dissolved in trifluoroethanol TFE (triglycerides, colophony); (C) materials dissolved in cold water (gums); (D) materials dissolved in hot water (proteinaceous materials).

Fig. 11B depicts the colorimetric data recorded for colophony and linseed oil, substances that were only dissolved in trifluoroethanol (TFE). The bar diagram in Fig. 11B indicates that apolar fluorinated derivatives **3** and **4** produced low %CR due to lower solubility, whereas polar derivatives generated more pronounced %CR. Notably, only films comprising ionic positively-

charged headgroup, PDA derivative **6**, could distinguish between the two substances, possibly reflecting interactions of the amine residues with carboxylic acid functional groups in colophony.

Fig. 11C depicts the colorimetric transformations induced by paint substances solubilized in cold water, specifically gum derivatives with different saccharide compositions. Among these compounds, gum arabic and gum karaya induced the most pronounced blue-red transformations. Interestingly, Fig. 11C reveals that both the gums did not induce a colour change in the films comprising diacetylene **6**, which exhibits an ionic headgroup. Moreover, a clear distinction between the two gums was accomplished by films containing the parent diacetylene monomer **1** and derivatives **7** and **8**. Compound **8**, in fact, appears the most promising for screening other gums (Fig. 11C). This result points to hydrogen bonding and interactions between the polar headgroup of **7** and hydroxyl units in the carbohydrate gums, rather than boronate ester formation, as the most prominent factors affecting the colorimetric transformations.

The colorimetric results recorded upon interactions of the proteinaceous substances dissolved in hot water with the PDA/PMMA films (Fig. 1D) underscore low %CR values, likely reflecting weak interactions between the tested compounds and the PDA headgroups. Films comprising PDA derivatives **2**, **7**, and **8** generated %CR values that were somewhat higher than from the background, although the %CR signals could not be used for distinguishing among the tested substances. Nevertheless, identification of generic proteinaceous substances rather than the precise protein type may be sufficient for selecting a suitable paint restoration treatment.

In addition, it worth to mention that compound **12-16** were also tested for the detection of gums, but didn't show sufficient discrimination among signals(some color images are shown in SI Chapter 9.2., Fig. S43a).

4.3. Discussion

This study explores the use of PMMA-supported PDA films as colorimetric sensors for common constituents in artwork paint. In particular, I synthesized novel diacetylene derivatives displaying headgroups, exhibiting different molecular properties and functionalities, and spin-coated films comprising the polymerized diacetylene derivatives were prepared. Different PMMA-supported PDA films were tested on not-aged painting materials in order to evaluate the PDA platform for paint screening and analysis. The PMMA-supported PDA films featured distinct morphologies and particularly important, different colorimetric response upon interaction with paint materials.

The experimental data demonstrate that the extent of blue-red transformations of the PDA films was closely related to the affinity between the headgroup and tested analytes. In particular, the results point to the significance of polar, nonpolar, and electrostatic interactions between the PDA headgroup and paint constituents as fundamental parameters affecting the colour transitions. As such, this study points to the potential of the PDA/PMMA system as a viable tool for distinguishing among paint substances. Further studies will be performed to evaluate the response on aged and real paintings.

Polar interactions affecting enhanced colour transformations were demonstrated, for example, in the more pronounced transformations involving the fluorine-displaying headgroups, particularly derivatives **2** and **3**. These films gave rise to stronger blue-red transformations upon addition of different paint material families (e.g. Fig. 11A-C). The three fluorine-based PDA derivatives will be further tested to monitor the conservation state of terpenic varnishes considering that during ageing, they change their polarity and solubility. Thus, we expect a change in their response to the three derivatives at different level of apolarity compared with the non-aged materials.

While polar or apolar interactions (as well as combined polar/apolar effects involving different parts of the PDA framework) contributed to the colorimetric transformations and aided in distinguishing among paint substances, our results additionally illuminate other chemical effects modulating the colour response of the PDA films. Specifically, Fig. 11 revealed that hydrogen bonding and ionic interactions played significant roles in certain instances. These observations point to the possibility to employ different diacetylene derivatives in a comprehensive “colorimetric toolbox” for distinguishing paint analytes.

It should be emphasized that the experimental results presented in Fig. 11 suggest that ionic PDA films may be suitable to monitor the polarity changes of oil painting constituents. Indeed, siccative oils adopt three-dimensional networks upon drying, in which low molecular weight compounds formed during the polymerization are entrapped. In particular, dicarboxylic fatty acids are produced during the photo-polymerization of siccative oils and tend to increase in concentration due to ageing⁶⁷. In addition, degradation processes are responsible for the formation of free fatty acids and metal carboxylates, which further contribute to overall polarity changes in paintings.

PDA-derivatives capable to distinguish different types of gums may find applications not only in conservation science, but also in other disciplines, such as food production, in which gum formulation may be required⁶⁸. The colorimetric results obtained for the proteinaceous substances, for example, provided %CR values that were sufficiently different from the background colorimetric signals, even if it is not possible yet to clearly distinguish among the different materials. However, the PDA films might be applied to develop readily applicable tools for in situ identification of generic proteinaceous substances. Indeed, exact determination of the type of protein may not be necessary to define a suitable restoration treatment. Further studies will be performed to evaluate the ageing effect on the painting materials and to verify the applicability of the PDA-based sensors to other proteinaceous materials used in conservation. One example of application may be related to the evaluation of residues after the bio-cleaning procedures. Biotechnological researches have proposed the use of enzymes and bacteria as a cleaning method for the selective removal of specific class of compounds⁶⁹. When applied, conservators have to verify that any residue of the biological treatments was removed from the surface to avoid any interaction with the clean surface.

4.4. Conclusions

In conclusion, this study shows that different TR derivatives could distinguish among paint constituents. The film assembly might be employed as a simple, on-site platform for monitoring degradation processes and planning restoration intervention. Importantly, the colour transformations can be readily quantified using simple spectrophotometer instrumentation. Application of the colorimetric polydiacetylene film assay is simple and analysis can be readily carried out by the use of visible spectrophotometry. This study shows that the polydiacetylene technology might open new analytical avenues in molecular analysis, in general, painting restoration and conservation science, in particular.

CHAPTER 5

Colorimetric Polydiacetylene-Aerogel Artificial Nose for Volatile Organic Compounds.

A new hybrid system based on TR and TR derivatives embedded within aerogel pores has been constructed. The PDA-aerogel powder underwent dramatic color changes in the presence of VOCs, facilitated through infiltration of the gas molecules into the highly porous aerogel matrix and their interactions with the aerogel-embedded PDA units. The PDA-aerogel composite exhibited rapid color/ fluorescence response and enhanced signals upon exposure to low VOC concentrations. Encapsulation of TR derivatives displaying different headgroups within the aerogel produced distinct VOC-dependent color transformations, forming a PDA-aerogel “artificial nose”.

5.1. Introduction

VOCs might be harmful to human health, and exposure to such vapors is considered hazardous and associated with varied pulmonary diseases^{70,71,72,73}. Detection of VOCs is thus essential for early warning, monitoring of occupational hazards, and security applications. Varied techniques are currently employed for VOC detection and analysis, including gas chromatography-mass spectrometry⁷⁴, surface acoustic wave sensors⁷⁵, chemiresistor-based sensing⁷¹, and others^{76,77}. Identification of host materials capable of adsorption of VOCs is a fundamental requisite of effective sensing platforms. Aerogels, among the lowest density solid materials, have been employed in vapor sensor designs^{72,78,79}. Aerogels have been produced from diverse building blocks, comprising scaffolding of silicon⁸⁰, carbon⁸¹, metals⁸², metal oxides⁸³, organic polymers⁸⁴, and others. Hydrophobic silica aerogels, in particular, exhibit pronounced porous structures with very high internal surface area available for adsorption of guest molecules⁷⁸. Silica aerogels have been employed as insulation substances in the aerospace industry⁸⁵, sorption of miscible organic solvents in water⁷⁸, and sensing of air pollutants⁷². While silica aerogels are excellent gas adsorbents, the main challenge in using them for VOC sensing concerns the identity of signal transduction elements. A recent study has reported encapsulation of fluorescent carbon dots within aerogel pores and use of the hybrid matrix for aromatic VOC sensing⁷³.

In this chapter we report on a new VOC detection system comprising aerogel associated with PDA. While almost all published studies thus far have employed PDA systems in solution environments^{86,61,87,88}, few reports described applications of the polymer for gas sensing^{86,89}. Published PDA-based assemblies for VOC detection, however, are synthetically complex and/or exhibit limited sensing parameters, e.g., slow response time and low sensitivity⁸⁶.

Current research presents a new hybrid PDA–aerogel, produced through a simple single-step method. The PDA–aerogel was employed for VOC detection and exhibits excellent sensitivity and rapid colorimetric/fluorescence response. Importantly, the chromatic transformations of the PDA–aerogel were VOC-dependent, reflecting the distinct interactions of the VOC molecules with the aerogel-embedded PDA. Furthermore, “color fingerprinting” of VOCs was demonstrated by encapsulating in the aerogel matrix PDAs displaying different molecular headgroups. Overall, the PDA–aerogel matrix could be used as a platform for detection, visualization, and speciation of VOCs.

5.2. Results and Discussion

The simple preparation scheme of the polydiacetylene (PDA)-aerogel hybrid and representative VOC-induced color transformations are shown in Figure 12. The porous aerogel framework was first generated through high temperature silica annealing in the presence of pressurized nitrogen gas⁹⁰.

Following aerogel formation, the PDA precursor (TRCDA) was drop-casted on the aerogel powder. The TRCDA monomers were efficiently adsorbed and immobilized upon the hydrophobic domains within the aerogel pores⁷⁸. Irradiation of the TRCDA/aerogel construct with ultraviolet (UV) light induced polymerization of the aerogel-embedded TRCDA monomers, generating the blue-phase conjugated polydiacetylene (PDA). Importantly, the blue PDA appeared uniformly distributed within the aerogel powder, likely due to the high porosity of the aerogel. Figure 12 also illustrates the dramatic color transformations of the blue PDA/aerogel induced by exposure to different VOCs; notably, the photographs shown in Figure 12 (right) demonstrate that distinct VOC-dependent colors were generated.

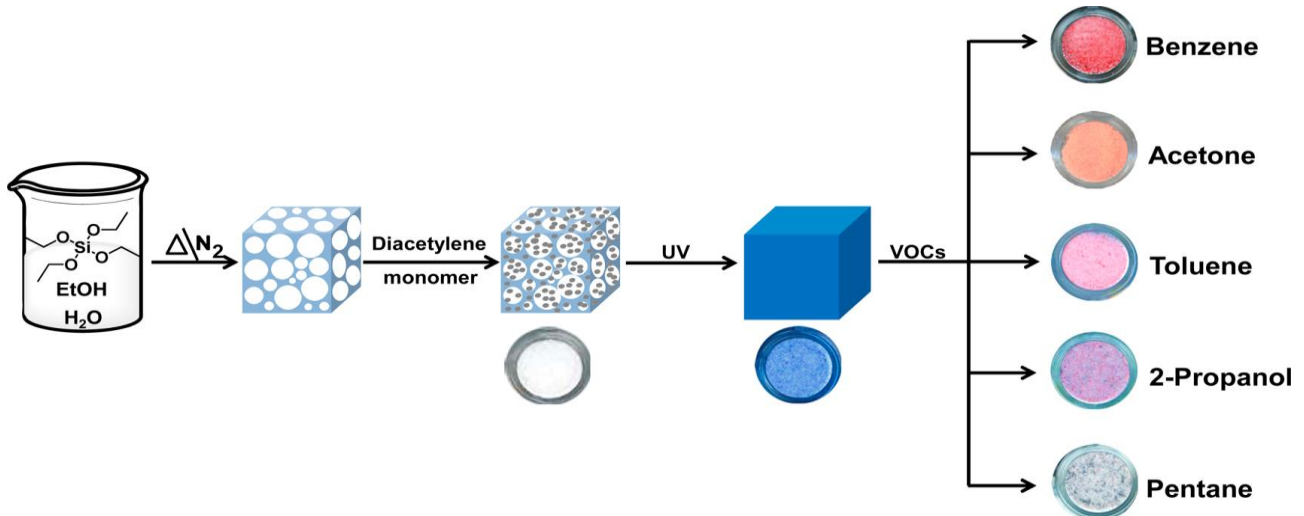


Figure 12. Synthesis of the polydiacetylene (PDA)-aerogel and its colorimetric properties. Schematic illustration of PDA-aerogel fabrication. The circled digital photographs depict the visible colors generated following exposure to different VOCs (concentrations 1000 ppm).

Characterization of the structural and physical properties of the hybrid PDA/aerogel was carried out (Figure 13). The representative scanning electron microscopy (SEM) image of the PDA/aerogel in Figure 13A is similar to the bare aerogel, displaying the typical hierarchical organization exhibiting high surface area⁷². The Brunauer-Emmett-Teller (BET) analysis in Figure 13B indicates a relatively high specific surface area ($265\text{m}^2/\text{g}$) suitable for adsorption of gas molecules. Specifically, the isotherms in Figure 13B,i exhibit type IV adsorption with a distinct hysteresis loop⁹¹. Figure 13B,ii further reveals high pore volume (0.34 cc/g) and sizable pore diameter (4.93 nm) of the PDA-aerogel. Overall, the BET analysis in Figure 13 underscores the high porosity of the PDA-aerogel and its applicability for efficient vapor adsorption.

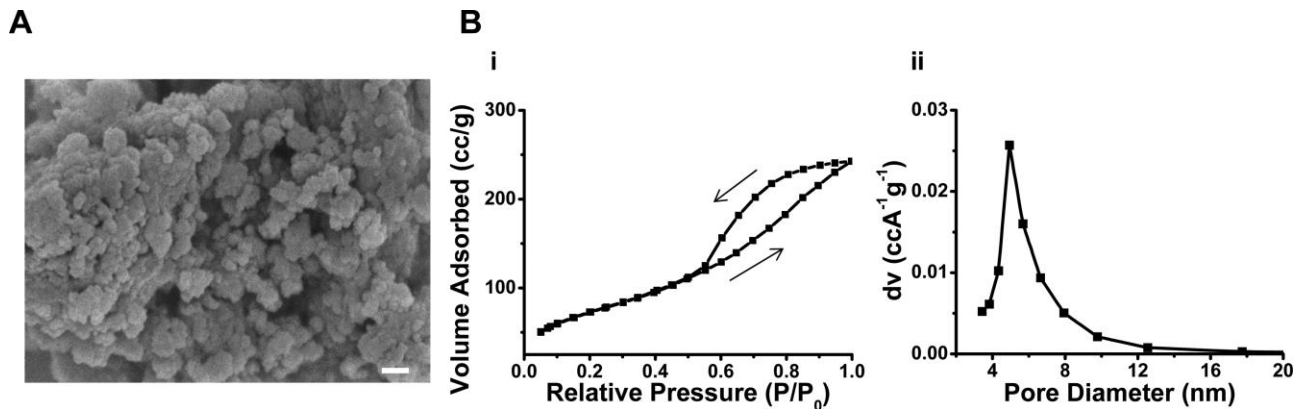


Figure 13. Characterization of the PDA–aerogel. (A) Scanning electron microscopy (SEM) image of the PDA/aerogel surface. The scale bar corresponds to 100 nm. (B) BET analysis: (i) N_2 adsorption–desorption isotherms of PDA/aerogel; (ii) pore size distribution curve indicating average pore diameter of 4.93 nm.

Figures 14–17 illustrate application of the PDA–aerogel construct for sensing VOCs. Figure 14 depicts spectroscopic and microscopic fluorescence analysis of the PDA–aerogel upon incubation with different VOCs, all applied at the same concentration (1000 ppm). Figure 14A reveals significantly different fluorescence emissions (excitation 482 nm) of the PDA–aerogel generated by the VOCs. Notably, the relative fluorescence emission intensities shown in Figure 14A echo the colorimetric transitions (Figure 12); previous studies similarly reported a direct correlation between the extent of blue–red transformations of PDA systems and the degree of fluorescence emission⁶¹. Accordingly, benzene and acetone vapors, which produced red and orange PDA–aerogels (Figure 12), gave rise to the most pronounced fluorescence emission (Figure 14A). Toluene and 2-propanol, which induced blue–purple transitions upon incubation with the PDA–aerogel (Figure 12) generated lower PDA fluorescence compared to benzene and acetone (Figure 14A), and pentane essentially gave rise to flat fluorescence emission (Figure 14A), reflecting the apparent quenching of PDA blue color by this vapor (Figure 12).

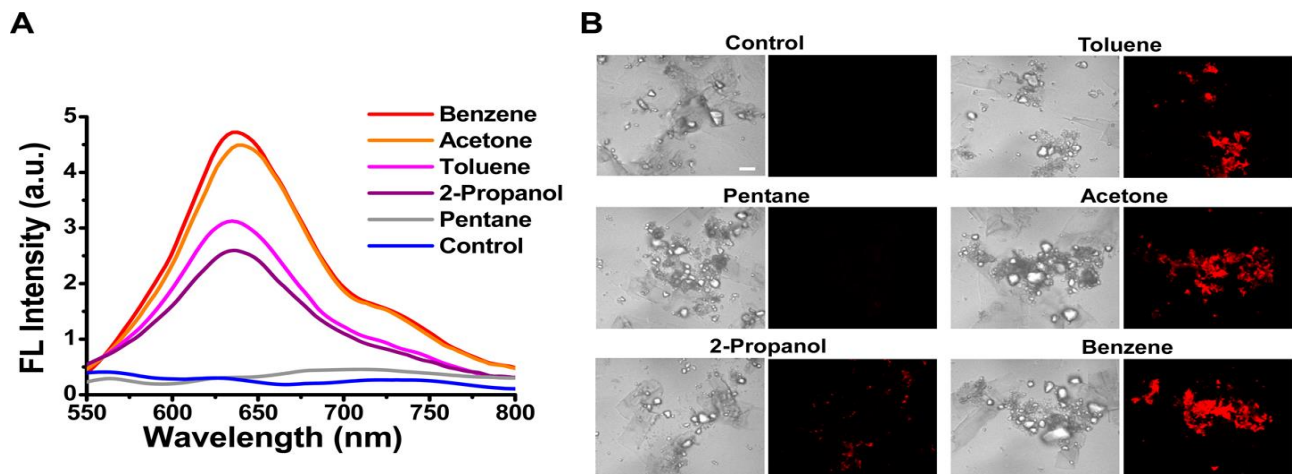


Figure 14. Fluorescence analysis of PDA–aerogel upon exposure to different VOCs. (A) Fluorescence emission spectra (excitation 482 nm) of PDA–aerogel following 60 min exposure to different VOCs (1000 ppm concentrations). (B) Confocal fluorescence microscopy images (excitation 488 nm) of PDA–aerogel after 60 min exposure to different VOCs. Scale bar corresponds to 10 μm .

The confocal microscopy images of the PDA–aerogel particulates presented in Figure 14B complement the fluorescence spectroscopy measurements and highlight the distinct VOC-induced fluorescence transformations. Specifically, Figure 14B reveals different intensities of PDA–aerogel

particles, depending upon the VOCs applied. Similar to the fluorescence results in Figure 14A, Figure 14B demonstrates that benzene and acetone induced the most fluorescently intense PDA-aerogel particulates, less fluorescent particles are apparent after exposure to toluene and 2-propanol, and no fluorescent particle were recorded upon exposure of the PDA-aerogel to pentane vapor.

Figure 15 highlights the sensitivity and fast chromatic response of the PDA-aerogel upon VOC exposure, and the contribution of the aerogel matrix to the unique chromatic properties of the hybrid material. Figure 15A presents fluorescence titration curves (excitation at 482 nm, emission at 635 nm) recorded upon exposure of the PDA–aerogel to different VOC concentrations. As apparent in Figure 15A, the detection thresholds for VOCs tested were between 100 and 200 ppm; this sensitivity is significantly better than previously reported PDA-based vapor sensors⁸⁶.

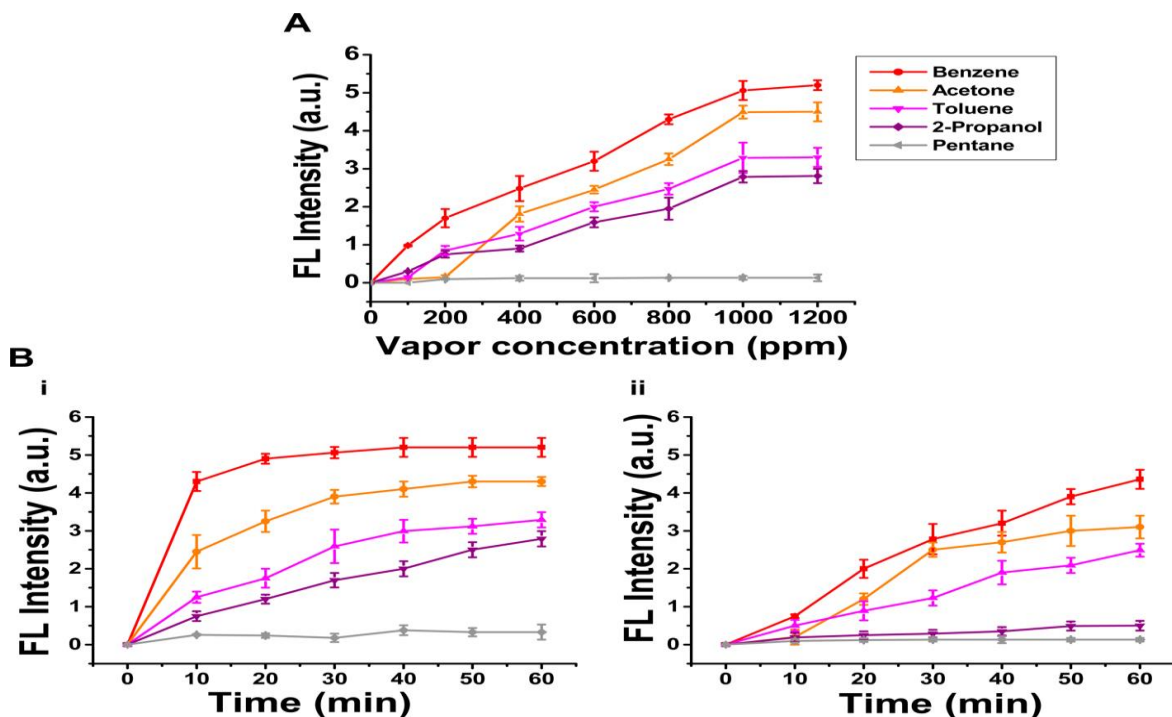


Figure 15. VOC-induced fluorescence emissions of PDA–aerogel. Fluorescence titration curves (A) and fluorescence kinetics (B) (excitation 482 nm, emission 635 nm) recorded in PDA–aerogel (i) and silica gel (ii) upon exposure to VOCs at concentrations of 1000 ppm.

Comparison of the fluorescence kinetic data of PDA-aerogel (Figure 15Bi) and PDA embedded within conventional silica gel matrix (Figure 15Bii) reveals faster and more pronounced fluorescence response upon VOC exposure of PDA-aerogel. This result points to the significance of the aerogel framework to the sensing performance; the pronounced porosity of the aerogel likely promoted adsorption of the guest vapor molecules, giving rise to the rapid chromatic response upon interactions with the pore-associated PDA. It should be also noted that chromatic image analysis⁹² (SI 9.3., Figure S47) yielded a similar kinetic profile as the fluorescence experiments depicted in Figure 15, underscoring the versatility of chromatic transformation detection methods (e.g., fluorescence emission or color change).

To account for the distinct VOC-induced chromatic transformations of the PDA–aerogel, we carried out Raman scattering analysis (Figure 16). Raman spectroscopy has been applied in numerous studies for characterization of the structural/photophysical transformations of PDA assemblies^{93,94,95}. In particular, Raman scattering experiments shed light on the molecular features of chromatically transformed PDA, through analysis of the shifts and intensities of the spectral peaks at around 1500 cm^{-1} (carbon–carbon double bond region) and 2100 cm^{-1} (carbon–carbon

triple bond)^{93,94}. Indeed, the relationships between the intensities of the Raman peaks corresponding to the blue PDA at 1450 and 2080 cm⁻¹, and red-phase PDA at 1515 and 2120 cm⁻¹, respectively, illuminate the VOC-induced chromatic transitions and relate these transitions to structural features of the PDA units. Specifically, the vapors of both benzene (Figure 16,vi) and acetone (Figure 16,v) gave rise to Raman signals ascribed to red-phase PDA⁹⁴, consistent with the pronounced color and fluorescence transformations induced by these VOCs (Figures 12 and 14, respectively). Figure 16,iv reveals that toluene similarly generated Raman spectral shifts associated with red-phase PDA. Interestingly, the Raman signature of 2-propanol vapor (Figure 16,iii), featuring Raman peaks at 1460 and 2105 cm⁻¹, indicates formation of a purple, intermediate PDA phase^{94,96}.

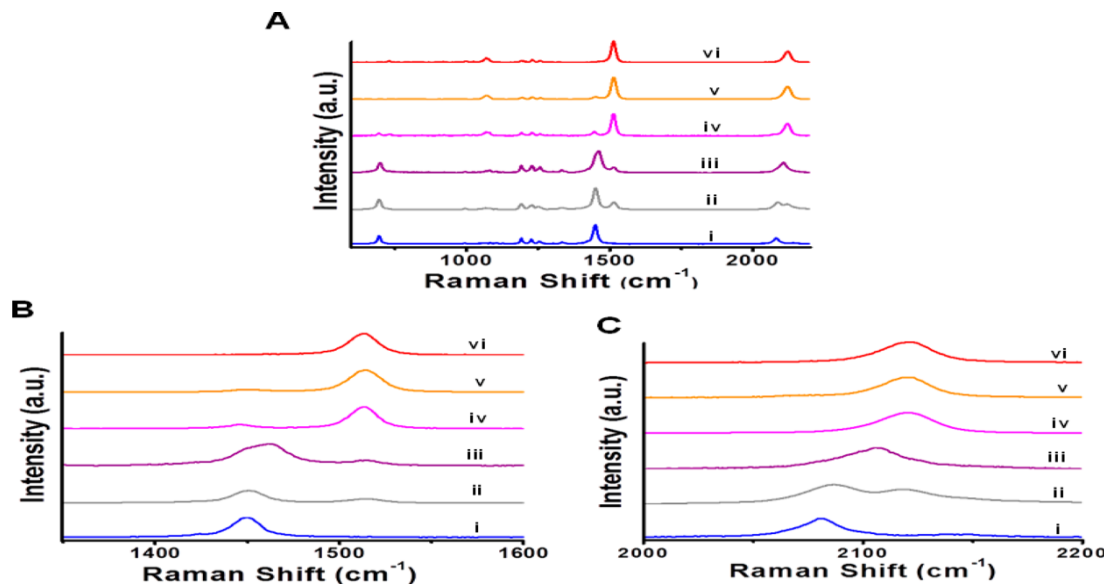


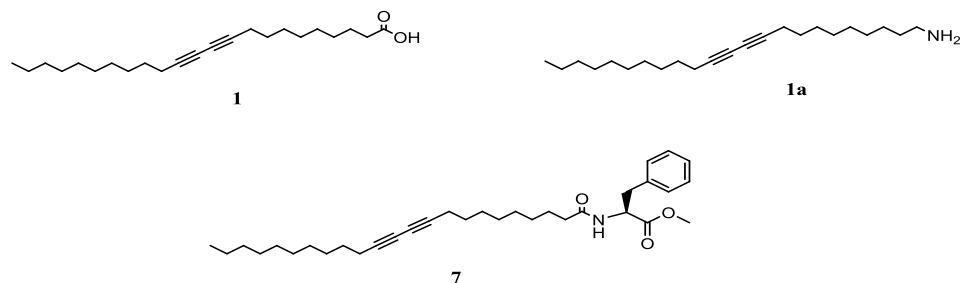
Figure 16. Raman spectra of PDA–aerogel. (A) Full spectral range; (B, C) magnified regions. (i) control; (ii) pentane; (iii) 2-propanol; (iv) toluene; (v) acetone; (vi) benzene. (B, C) Magnified images corresponding to the carbon–carbon double bond and carbon–carbon triple bond regions, respectively.

The variations of chromatic response (Figures 14 and 15) and Raman scattering data (Figure 16) likely correspond to different interactions of the VOCs with the PDA headgroup. Specifically, the amphiphilic nature of PDA, e.g., the polar headgroup and hydrophobic side chains, dictates that polarity and hydrophobicity of the target analyte constitute the primary factors affecting the degree of chromatic transformations^{86,94,97,98}. The interplay between these two parameters, however, might be complex. Acetone, for example, which is highly polar, induced a similar chromatic transition (Figures 14 and 15) and Raman shift (Figure 16) as benzene, which is apolar. Interestingly, 2-propanol, which is also polar⁹⁹, gave rise to only a mild chromatic transformation (Figures 14 and 15). This observation might be ascribed to the strong affinity between alcohols and the carboxylic moieties of PDA¹⁰⁰. Such interactions have been shown to stabilize the intermediate purple state of PDA⁹⁵.

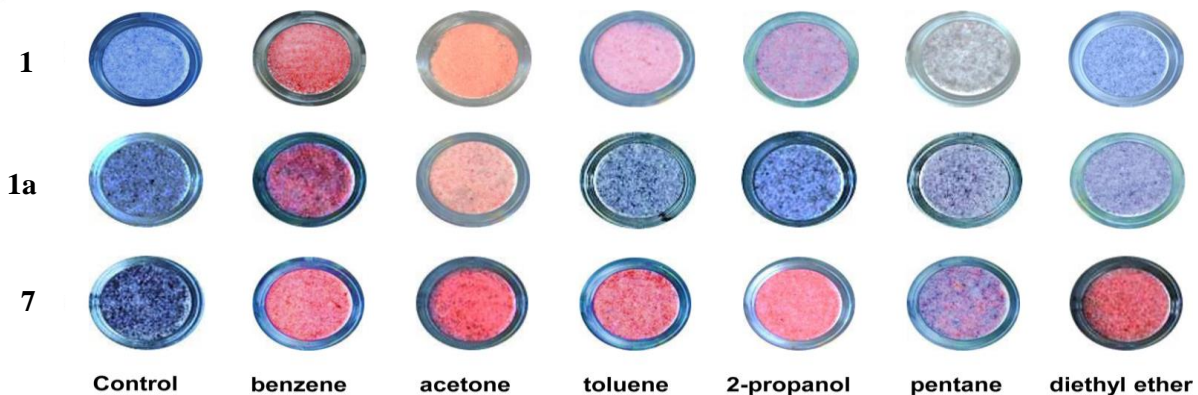
To explore application of the new PDA-aerogel platform for distinguishing among different vapors, we recorded the color transitions induced by VOCs in aerogels embedding PDA that was produced from monomers displaying different headgroups (Figure 17). Numerous studies have shown that modulation of the PDA headgroups exerted significant effects upon the chromatic properties of PDA systems and the color transformations^{61,88,101}. Figure 17A depicts the chemical structures of the three diacetylene monomers employed. The commercially available TR monomer (compound **1**) displays carboxylic moieties, the TR amine-functionalized **1a** exhibits a more polar headgroup, while **7** was functionalized with bulky, hydrophobic phenyl residues. The scanned photographs in Figure 17B and corresponding chromatic red-green-blue (RGB) signals⁹² in Figure

17C demonstrate significant variability in color transformations induced by the VOCs, which clearly depended upon the different embedded PDA.

A



B



C

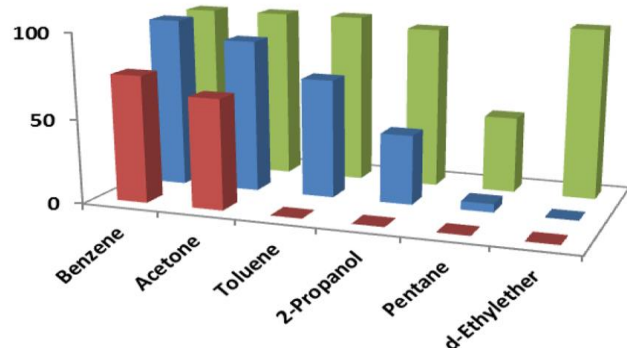


Figure 17. “Color fingerprinting” of VOCs using aerogel-embedded PDA derivatives. (A) Structures of the monomers employed; (B) scanned photographs of the PDA-aerogels after 60 min exposure to the VOCs (concentrations 1000 ppm); (C) chromatic (Red, Blue, Green: RGB) analysis⁹² of the recorded color responses depicted in (B). Height of the bars indicate more pronounced blue-red transformations. Red bars, 1; blue, 1a; green, 7.

Interestingly, Figure 17B indicates that the aerogel hybrid embedding the TR-MPhe derivative (e.g., monomer 7) produced much more pronounced blue-red transformations compared to the two other: TR and TR derivative. This result is ascribed to the hydrophobicity of the phenyl moieties exhibiting greater interactions with the aerogel-adsorbed VOC molecules. The different blue-red transformations induced in 3-aerogel by specific VOCs point to the significance of headgroup-analyte interactions in determining the extent of color change. For example, the more pronounced red color induced by benzene compared to n-pentane (Figure 17B) is likely ascribed to the high affinity between the benzene and phenyl rings; the corresponding interaction between the pentane hydrocarbon chain and the headgroup of 7 is expected to be less pronounced.

1-aerogel and **1a**-aerogel hybrids exhibited somewhat similar VOC-induced colors which were less significant than **7**-aerogel (Figure 17B, top rows), likely reflecting the polarities of their

headgroups. Color differences were apparent between **1**-aerogel and **1a**-aerogel, however, for most VOCs examined, confirming the roles of the PDA headgroup moieties as fundamental determinants of the colorimetric transformations. Distinctive color transformations were also recorded upon examination of two closely-related VOCs such as ethanol and **2**-propanol (SI 9.3., Figure S48). Overall, the PDA-aerogel color matrix in Figure 17B and the corresponding RGB pattern in Figure 17C provide compelling evidence for the feasibility of VOC “fingerprinting” through array-based pattern recognition methods, in which each array element comprised of a different TR derivative. PDA array-based sensing strategies have been reported^{61,51}. Powerful pattern-recognition methods for VOC detection have been also developed¹⁰².

5.3. Conclusions

We constructed a VOC sensor comprising PDA within the porous framework of a silica aerogel. The structural and physical properties of both the aerogel matrix and embedded PDA were retained following the fabrication procedure. The PDA-aerogel hybrid was used as a sensor for different VOCs, exploiting the porosity and high surface area for adsorption of the volatile compounds and their effects upon both the PDA color and fluorescence. Importantly, the observed chromatic modulation was dependent upon the electronic, structural features, and particularly the polarity of the VOCs. Accordingly, the PDA-aerogel vapor sensor could distinguish among different VOCs. The PDA-aerogel sensor exhibits notable practical advantages. Preparation of the hybrid material is straightforward, using inexpensive and readily available reagents. The actual sensing experiments are easy to perform and carried out through visible color transformations that could be also quantified using spectrophotometry.

CHAPTER 6

Array of sensors for the detection of organophosphate pesticides.

In this Chapter I present an array of colorimetric and fluorescent chemosensors designed and synthesized to detect OPs and other compounds causing environmental and/or health problems. An important analytical need is the detection of various compounds and pollutants in water, such as surfactants, heavy metals, oils, pesticides etc. with improved selectivity and sensitivity. Such target analytes are usually detected via dedicated instrumentation using often complex techniques that require technically-skilled operating personnel and are time-consuming. Furthermore, varied analytes cannot be detected using field operated instrumentation.

6.1. Introduction

Many organophosphorus (OP) based compounds are highly toxic and powerful inhibitors of acetylcholinesterases (AChE) that generate serious environmental and human health concerns. Organothiophosphates with a thiophosphoryl ($P=S$) functional group constitute a broad class of widely used pesticides. They are related to the more reactive phosphoryl ($P=O$) organophosphates, which include very lethal nerve agents and chemical warfare agents, such as, VX, Soman and Sarin. The most critical threat deriving from the intense utilization of organophosphate pesticides is towards workers assigned to their application and it is commonly faced through the use of personal protecting devices. Moreover, widespread and frequent commercial use of OP-based compounds in agricultural lands has resulted in their presence as residues in crops, livestock, and poultry products and also led to their migration into water bodies. Thus, the design of new sensors with improved analyte selectivity and sensitivity is of paramount importance in this area. Herein, I present some progress in the development of fluorescent chemo sensors towards toxic OP pesticides and related compounds.

Environmental pollution by organic chemicals continues to be one of the world's leading challenges to sustainable development. Modern developed and developing countries utilize millions¹⁰³ of synthetic organic compounds in their civilian, commercial, and defense sectors for an ever-expanding diversity of uses. Common applications include plastics, lubricants, refrigerants, fuels, solvents, preservatives, surfactants, dispersants and pesticides. As a result of widespread global usage coupled with improper handling practices, many of these organic compounds enter the environment and cause air, water, and soil pollution. For example, pesticides and herbicides are applied directly to plants and soils, while accidental releases originate from spills, leaking pipes, underground storage tanks, waste dumps, and waste repositories. Many pesticides are sprayed in large amounts with only 1% reaching the intended target. Some of these contaminants have long half-lives and thus persist to varying degrees in the environment. They migrate through large regions of soil until they reach water reservoirs, where they may present an ecological or human-health threat¹⁰⁴. USA Environmental Protection Agency (EPA) has imposed strict regulations on the concentrations of many environmental contaminants in air and water¹⁰⁵. However, current monitoring methods for most organic contaminants are costly and time-intensive, and limitations in sampling and analytical techniques exist¹⁰⁶. Thus, there is a great demand for development of quick, simple and reliable methods for the detection of organic-based agricultural pesticides.

An alternative to classical methods for detection of OP pesticides is the design of optical sensors, *i.e.*, colorimetric or fluorimetric chemo sensors or reagents. One of the most convenient and simple means of chemical detection is the generation of an optical signal, for example, changes

in absorption or emission bands of the chemo sensor in the presence of the target analyte. Optical outputs have been used extensively in recent years for the development of chemo sensors for ion or neutral molecule recognition and sensing based on supramolecular concepts¹⁰⁷. Unfortunately, although the utility of optical detection is becoming increasingly appreciated in terms of both qualitative and quantitative analysis, the number of optical sensors currently available for OP compound detection is quite limited.

Fluorescence-based sensors, both biosensors and chemo sensors, offer significant advantages over other conventional methods for detection of OP compounds. The principal advantages of fluorescence are its high single-molecule sensitivity and in some most cases almost instantaneous response. Fluorescence methods are capable of measuring concentrations of analytes 10^6 times smaller than absorbance techniques¹⁰⁷. Thus, fluorescence techniques have been widely used in molecular biology and analytical chemistry but not extensively in the detection of OP pesticides.

6.2. Results and Discussion

In order to develop a new array of chemo sensors for more selective and sensitive detection of water soluble pollutants some of previously synthesized TR derivatives (Chapter 3, Table 1) have been tested upon interaction with widely used OPs (listed in Table 5). Relatively distinct color changes were observed in the case of interaction between TR-MPhe **7** and some aromatic OPs. Figure 18 shows some quantitative data of colorimetric responses when TR-MPhe **7** is treated with different OPs in different concentrations. We suppose that TR-MPhe **7** showed higher selectivity, mainly due to aromatic stacking between the two aromatic moieties of OP and **7**. The values were calculated from the UV-vis spectra. The control films were by definition zero.

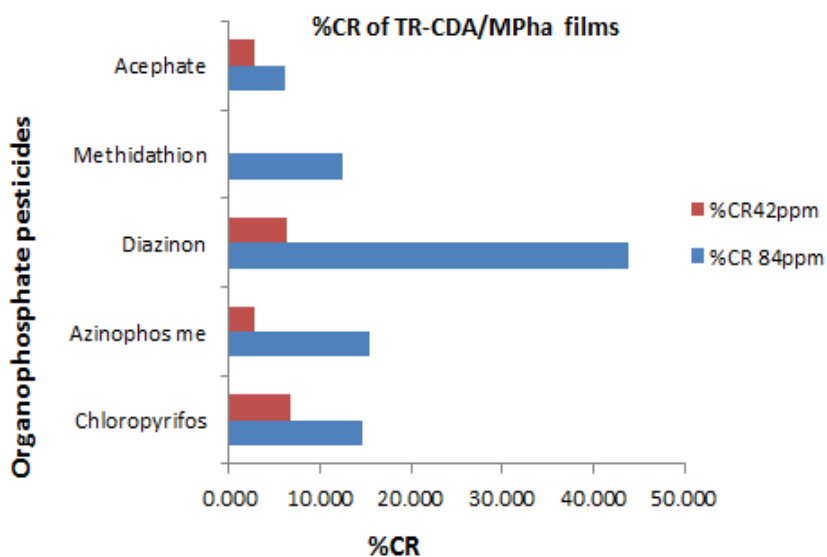


Figure 18. Colorimetric responses of compound **7** upon interaction with different OPs at different concentrations.

These preliminary results led us to the idea to design new group of TR derivatives with different amino acidic moieties **17, 22-30**, to be able selectively detect OPs of different structures. In order to increase a sensitivity of the sensor, TR derivatives having small and hydrophilic headgroups **18-21** were prepared, and some derivatives were synthesized as dipeptides **31-33** (Chapter 3, Table 2). We thought that additional aromatic moiety will create more planar structure which will induce more

intense signal⁵⁶. TR derivatives from Chapter 3, Tables 1 and 2 were tested upon interaction with OPs (listed in Table 5) and interesting results were obtained for the compounds **1**, **7**, **17**, **18**, **21**, **29**.

Table 5. Widely used and commercially available OPs tested in this study.

Structure	Name	Recom. conc.	Effects of overdose
	Chlorpyrifos	0.03 – 0.12%	Neurological, developmental autoimmune disorders
	Diazinon	<17 mg/kg^a	Cardiovascular, respiratory, gastrointestinal, nervous system and skin disorders
	Methidathion	0.2-0.11 mg/kg^b	Carcinogenicity, reproductive, developmental toxicity, neurotoxicity and acute toxicity
	Azinphos-methyl	<13.5%	Central nervous, endocrine, neuromuscular, immunological, cardiovascular and respiratory system disfunctions
	Acephate	≤50 mg/kg^c	Carcinogenicity, reproductive and developmental toxicity, neurotoxicity, and acute toxicity

^a<17 mg/kg of body-weight(mouse, oral, LD₅₀); 66 mg/kg (rat, oral, LD₅₀); 214 mg/kg (human, oral, TD_{L0})

^b35 mg/kg (Rat LD₅₀)

^chigh toxicity ≤50 mg/kg (acute oral LD₅₀); ≤0.05 mg/L(inhalation LD₅₀); ≤200 mg/kg(dermal LD₅₀)

Quantitative fluorescence emission data were recorded on TR-MPhe **7** by interaction with only two different structured OPs (Figure 19). Basically it was found definite sensitivity and selectivity of sensor towards aromatic OP. Color changes were tested also with faucet water, to which EDTA was added, to block or diminish the reactivity of background color, mainly induced by divalent ions. Kinetics of interaction has been controlled as well.

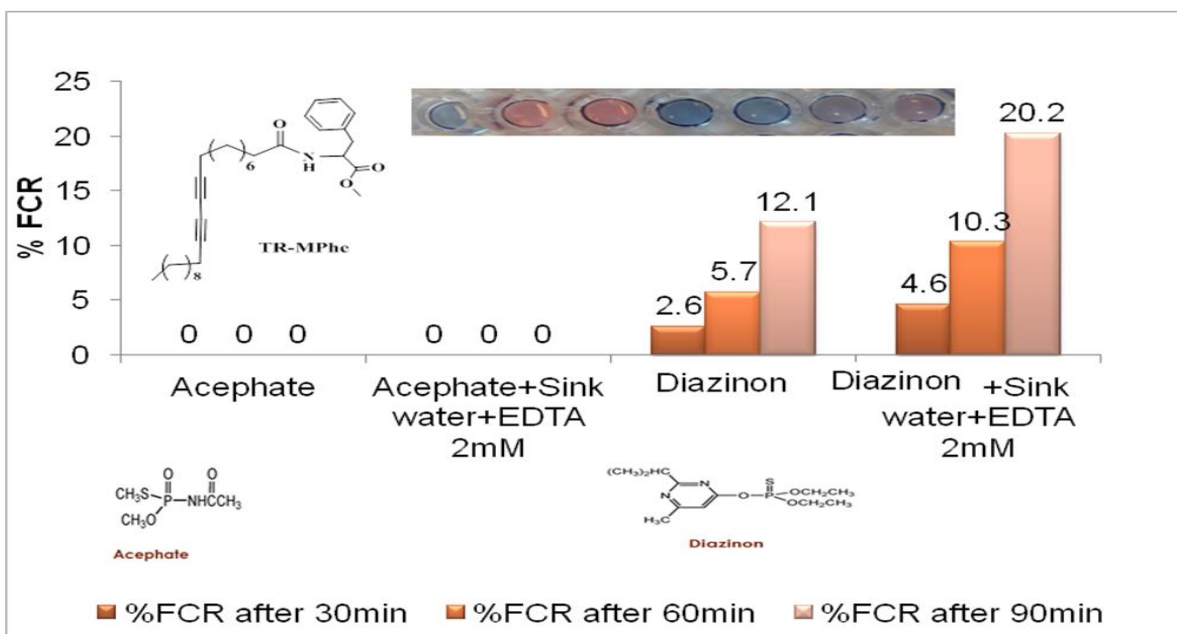


Figure 19. Interaction between TR-MPhe 7 and two different structured OPs

Fluorescence emission data were also recorded on the film containing double alkylated amino acid (TR-MLys-TR **29**) (Figure 20). This compound, as it was predicted, showed high selectivity towards linear OP. In this case signal received faster. So, we assume that, even if color changes are not well visible, the fluorescence intensities increase when OP is interacted with the similar structured TR derivative. The results shown in Figure 19 and 20 indicate that divalent metals do not cause great interference.

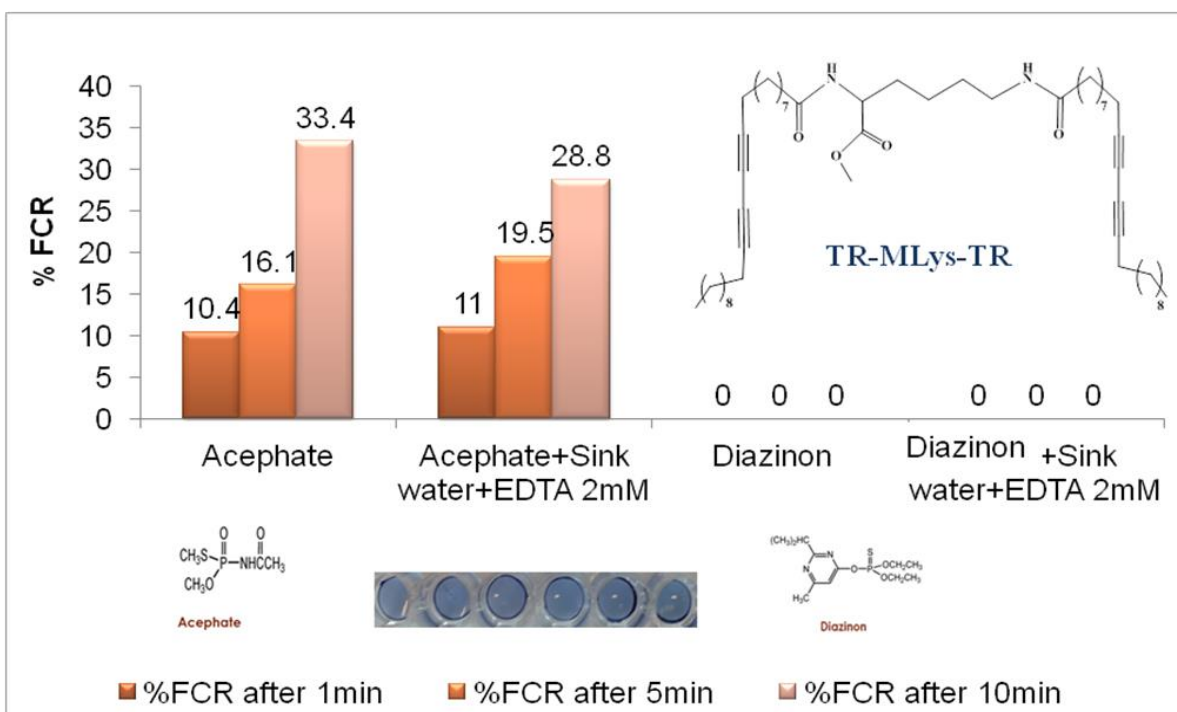
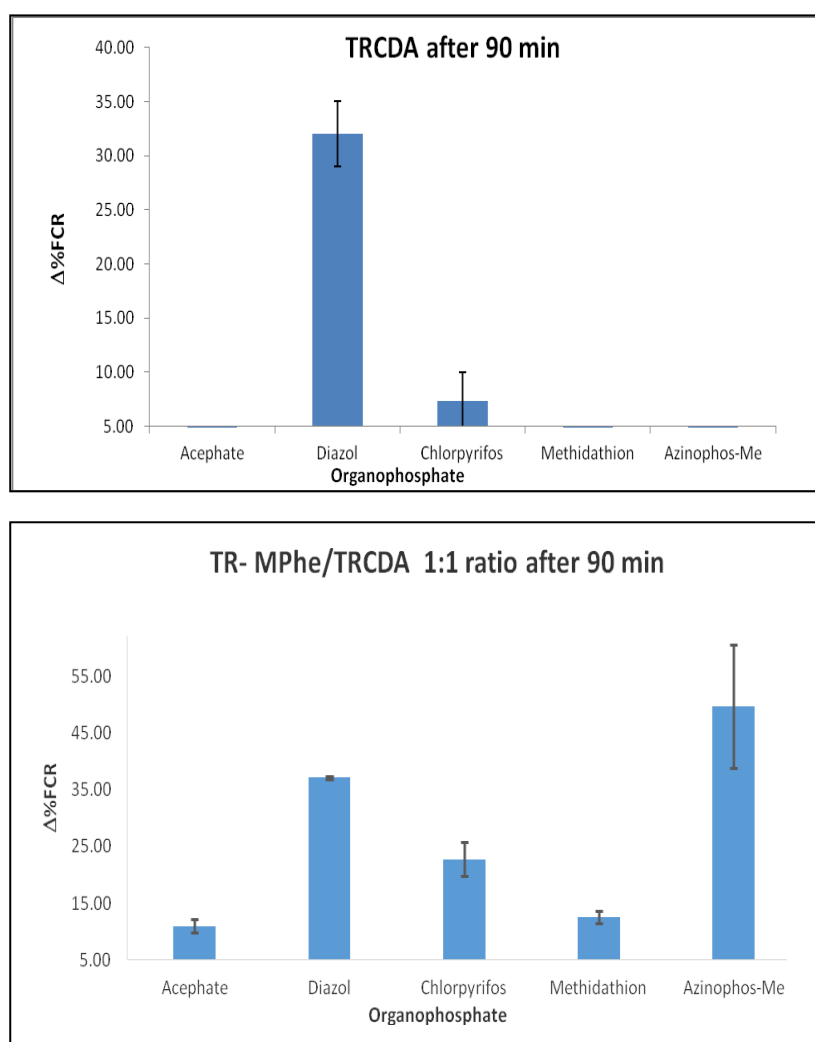
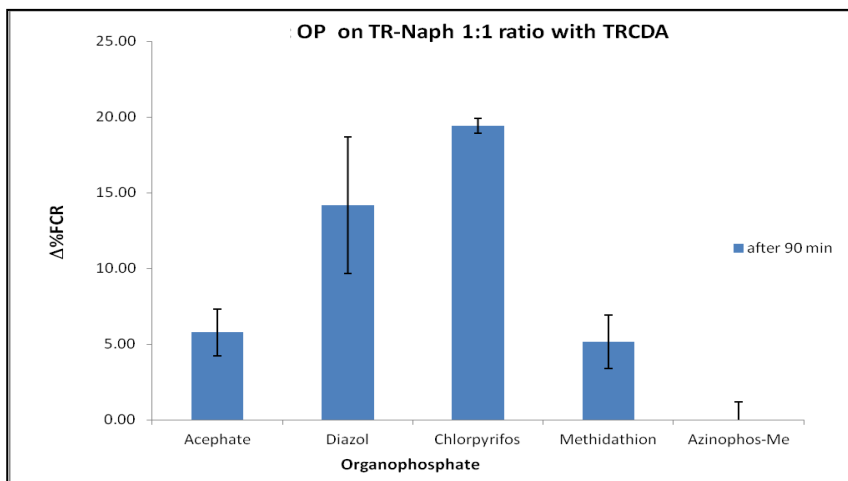
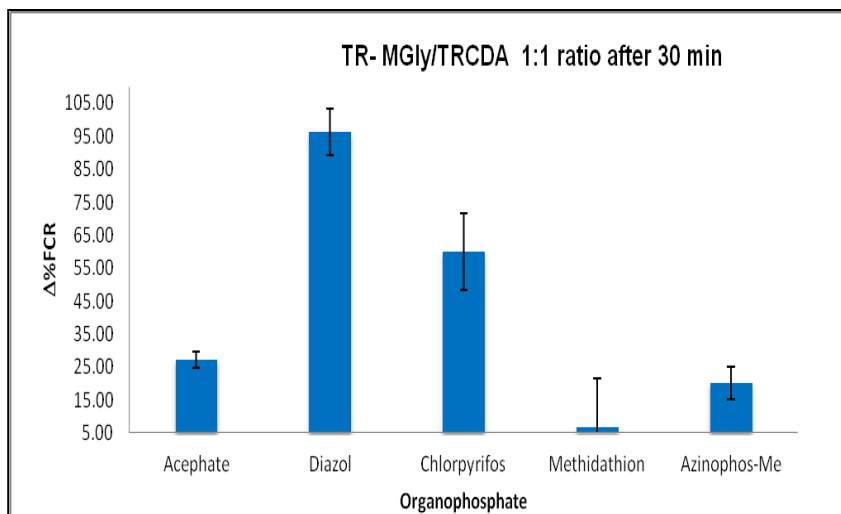
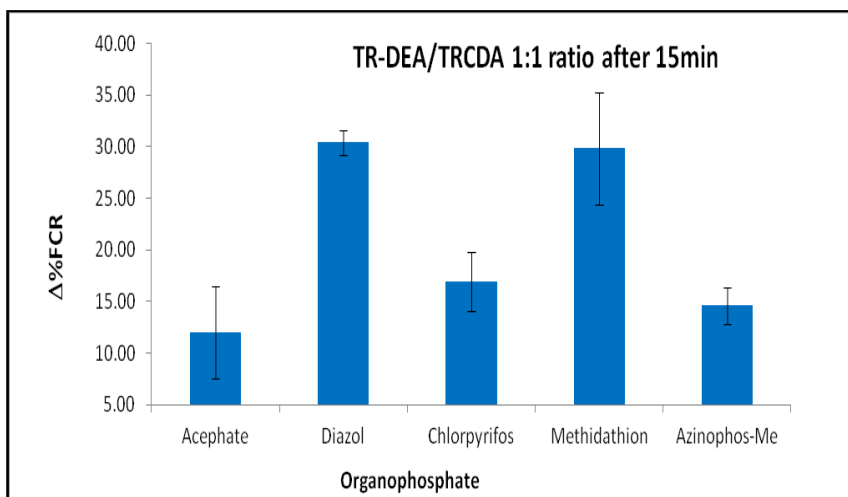


Figure 20. Interaction between TR-MLys-TR **29** and two different structured OPs

Fluorescence responses of PDA thin films were also recorded upon interaction with different OPs in concentration of 50 ppm (Figure 21a-e). Polymerized TR derivatives having small and hydrophilic headgroups showed higher detection sensitivity. For the sensor that consisted only of TRCDA **1** the best signal was obtained by interaction with Diazinon and low response with Chlorpyrifos (21a). Other signals below 5% considered unreliable. TR-MPhe **7**/TR (1:1) sensing system detected all OPs used in the study(21b). The best signals were observed by interaction with Diazinon, Chlorpyrifos and Azinphos-methyl. System TR-DEA **18**/TR (1:1) again detected all OPs, even in the shorter time (21c). The best signals were observed sensing Diazinon and Methidathion. Using system TR-MGly **17**/TR (1:1) very intense signals obtained by Diazinon and Chlorpyrifos (21d). Less sensitive system TR-Naph **21**/TR (1:1) also detected Chlorpyrifos and Diazinon(21e).





Figures 21(a-e). Interaction between compounds **1**, **7**, **17**, **18**, **21** and different OPs

In addition, experiments were performed adding the OPs (Table 5) to the other derivatives: TR-iF6 **4**, which didn't show significant changes and TR-3ET-DBA **43** at concentrations of 42 ppm and 2 ppm. For the compound **43** we observed slight changes. The %FCR values shown in SI 9.4. Fig.S49. do not necessarily reflect good sensitivity; the control also gave values of around 20%.

6.3. Conclusion

In conclusion: newly synthesized TR derivatives were tested for their possible detection of common used OPs. Emphasis was given to the preparation of sensing systems with improved sensitivity and selectivity, by changing the chemical structure of the headgroup and detecting a right target. TR derivatives **1**, **7**, **17**, **18**, **21**, **29** were able to distinguish between different OPs in 50ppm concentration. The highest sensitivity was obtained by TR/TR-MGly **17** sensing system. The best selectivity was observed with both TR/TR-DEA **18** & TR/TR-MPhe **7** sensors. The results show that the TR-based chemo sensor is rapid, sensitive, inexpensive, portable, and easy-to-use. New derivatives could be further tested on wider range of OPs, as well as in other studies, such as metal ion recognition¹⁰⁸, surfactants, bacteria, virus, cancer cells detection and drug-delivery¹⁰⁹. By taking advantage of the ease of functionalizing their potential use as colorimetric and fluorescent sensors or targeted delivery should be further investigated.

CHAPTER 7

Synthesis and characterization of dicyano-substituted diazaacenes

In this Chapter I report the synthesis, spectroscopic and structural properties of novel 2,3-dicyano-substituted azaacenes containing three to six annelated rings as a framework. The targets were prepared by Pd-catalyzed coupling of diamino-bis(*tri-iso-propylsilyl*ethynyl)benzene, -naphthalene and -anthracene with either 4,5-dibromophthalonitrile or 6,7-dibromonaphthalene-2,3-dicarbonitrile into the respective *N,N'*-dihydrodiazaacenes. Oxidation with MnO₂ or PbO₂ furnishes the dicyano-substituted diazaacenes in reasonable to good yields. An exception is the diazahexacene, where the *N,N'*-dihydrodiazaacene was difficult to oxidize. Most of the targets could be crystallized and pack in isolated pairs, stacks and brickwall motifs. The n-type behavior of these molecules was illustrated in a proof of concept organic field-effect transistor, showing mobilities up to $7 \cdot 10^{-3} \text{ cm}^2 \text{V}^{-1} \text{s}^{-1}$.

7.1. Introduction

In recent years, significant advances have been made in the field of organic n-type semiconductors, yet there is still a great demand for high-performing, air-stable organic n-channel-materials¹¹⁰. *N*-Heteroacenes are potentially such a class of attractive compounds; their low lying LUMO and promisingly high electron affinities combined with their acene topology make them supremely attractive.¹¹¹. Furthermore, the substitution of CH groups by pyridine-type nitrogen atoms increases their tendency to form π - π -interactions in the solid state, compared to their acene congeners, occasionally favoring brick wall over herringbone motives. Additionally, the introduction of pyridine or pyrazine motifs into acenes dramatically decreases their propensity towards oxidation¹¹². While the electron mobilities of nitrogen containing acenes can be as high as $3.3 \text{ cm}^2 \text{V}^{-1} \text{s}^{-1}$ for the symmetrical tetraazapentacene **6** (Figure 2, inset)¹¹³, they usually range from 10^{-3} – $10^{-1} \text{ cm}^2 \text{V}^{-1} \text{s}^{-1}$ in non-optimized devices¹¹⁴.

Some *N*-heteroacene-derivatives are known since the end of the 19th century, but the synthesis and property investigation of their larger representatives was difficult, not only due to their insolubility but also due to the lack of suitable oxidizing agents that would transform the *N,N'*-dihydrodiazaacenes into azaacenes. We have prepared and employed the diaminoarenes **1a-c** as powerful modular building blocks, facilitating an easy access to functionalized azaacenes employing both classical condensation reactions but also powerful Pd-catalyzed cyclizations^{111,113}.

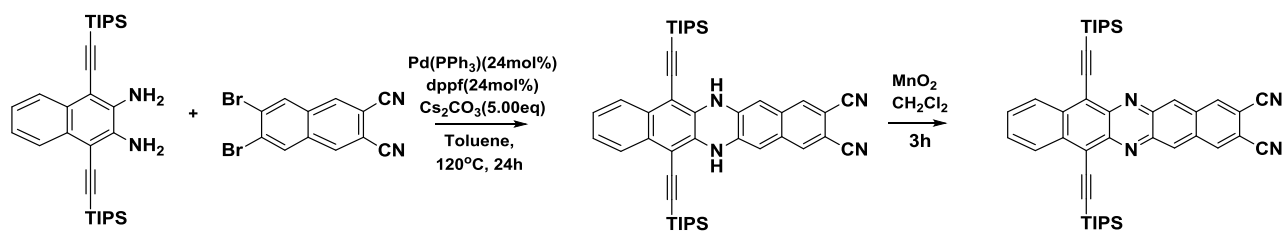
Up until now, there are no reports about cyano-carrying azaacenes, while fluorinated¹¹⁵ and other halogenated azaacenes have been prepared¹¹¹. Both fluorinated but also cyanated acenes are known and have been exploited in organic electronics applications¹¹⁶. A study by Houk and Winkler¹¹⁷ suggests that cyano-substituted azaacenes might be attractive targets due to their ability to form very weak hydrogen bonds with aromatic C, H bonds and therefore lead to a tighter packing of the cyanated azaacenes in the solid state with potentially concomitant better charge transport properties. We herein extend the modular Pd-catalyzed coupling approach towards the synthesis and characterization of novel dicyano-substituted diazaacenes with high electron affinities.

7.2. Results and Discussion

During my internship in Prof. U. Bunz's laboratory I prepared starting materials and studied the Pd-catalyzed coupling reactions between TIPS-substituted aromatic *ortho*-diamines (first synthesized in Prof. U. Bunz's laboratory¹¹⁸) and aromatic dihalides. As was planned new compounds, i.e. cyano-substituted novel azaacenes were synthesized and characterized (Scheme 12). 2,3-Dibromo-5,6-dicyanonaphthalene was prepared by reaction of 1,2-bis(dibromomethyl)-4,5-dibromobenzene with sodium iodide and fumaronitrile. The reaction proceeds by an iodide-induced 1,4-elimination of bromine to generate the corresponding *o*-quinonodimethane, which undergoes a Diels–Alder reaction with fumaronitrile, followed by rearomatization through elimination of hydrogen bromide¹¹⁹.

For the Pd-catalyzed coupling 1,4-bis((triisopropylsilyl)ethynyl)naphthalene-2,3-diamine was used to obtain desired azaacene. Crucial parameters for cyanation of *ortho*-substituted aryl halides are the reaction time and temperature and amount of catalysts. Typically, larger amount of catalysts, longer reaction times (>1 day) and higher temperatures (>120 °C) are required for effective cyanation.

Scheme 12. Synthesis of dicyano-functionalized TIPS azapentacenes.



Following synthetic Scheme 12, with slight modifications in reaction conditions, a pool of cyano-substituted azaacenes was synthesized and characterized. Synthetic approach towards **3** and **5** is straightforward. In both cases (Figure 22) the diamines **1a-c** are coupled towards the dinitriles **2** and **4**. Two different coupling strategies are successful: while the smaller benzene and naphthalene derivatives readily couple employing Pd(PPh₃)₄ with bis(diphenylphosphino)ferrocene (dppf) as co-ligand in toluene, the larger anthracene diamine requires more forcing conditions and the catalyst Pd-RuPhos was deployed in dioxane under microwave irradiation¹²⁰. The formed *N,N'*-dihydrodiazaacenes are immediately oxidized by manganese oxide or lead dioxide. The azaacenes are isolated after chromatography and crystallization. The poor overall yield of the hexacene **5c** is due to its limited stability under ambient conditions, the *N,N'*-dihydrodiazaacene always re-forms quickly.

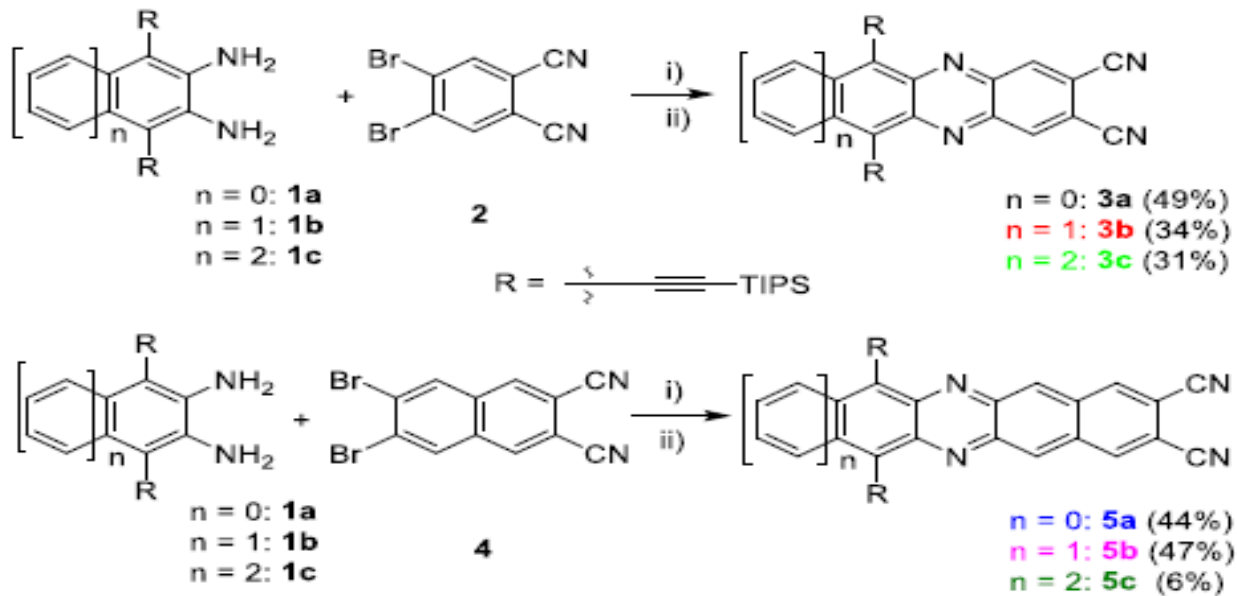
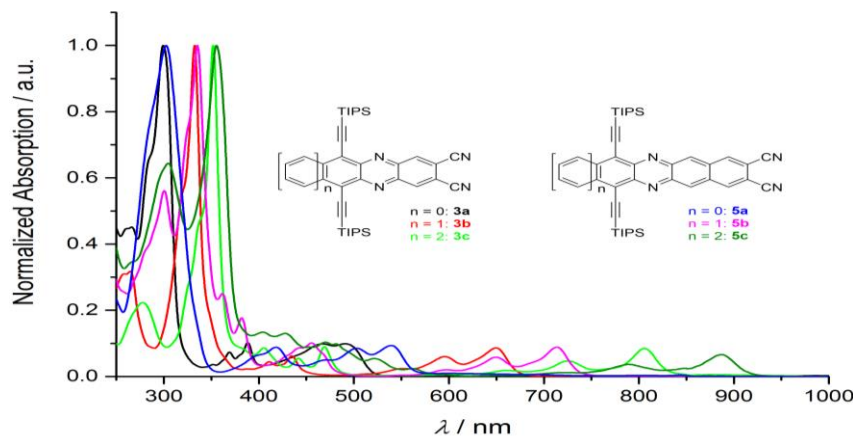


Figure 22. Synthesis of azaacenes **3a-c** and **5a-c**; i) $\text{Pd}(\text{PPh}_3)_4$ (10 mol%), dppf (10 mol%), Cs_2CO_3 , toluene, 120°C , 18 h or PdRuPhos (5 mol%), Cs_2CO_3 , dioxane, 120°C , 16 h, μW ; ii) exc. MnO_2 , CH_2Cl_2 , RT, 1 h or exc. PbO_2 , CH_2Cl_2 , RT, 1 h, sonic irradiation.

In Figure 23 the Uv-vis spectra of **3a-c**, **5a-c** and their non-cyanated congeners are shown^{113,120,121}. In Table 6 their photo-physical properties are listed. The hexacene **5c** has the most red shifted absorption. The addition of the two cyano groups leads to a red shift of the absorption by almost 90 nm. Similarly, for **5b** the red shift upon addition of the cyano groups is around 50 nm. For the diazapentacene **3c** this effect is even more distinct and a red shift of 110 nm is recorded when attaching the cyano groups.



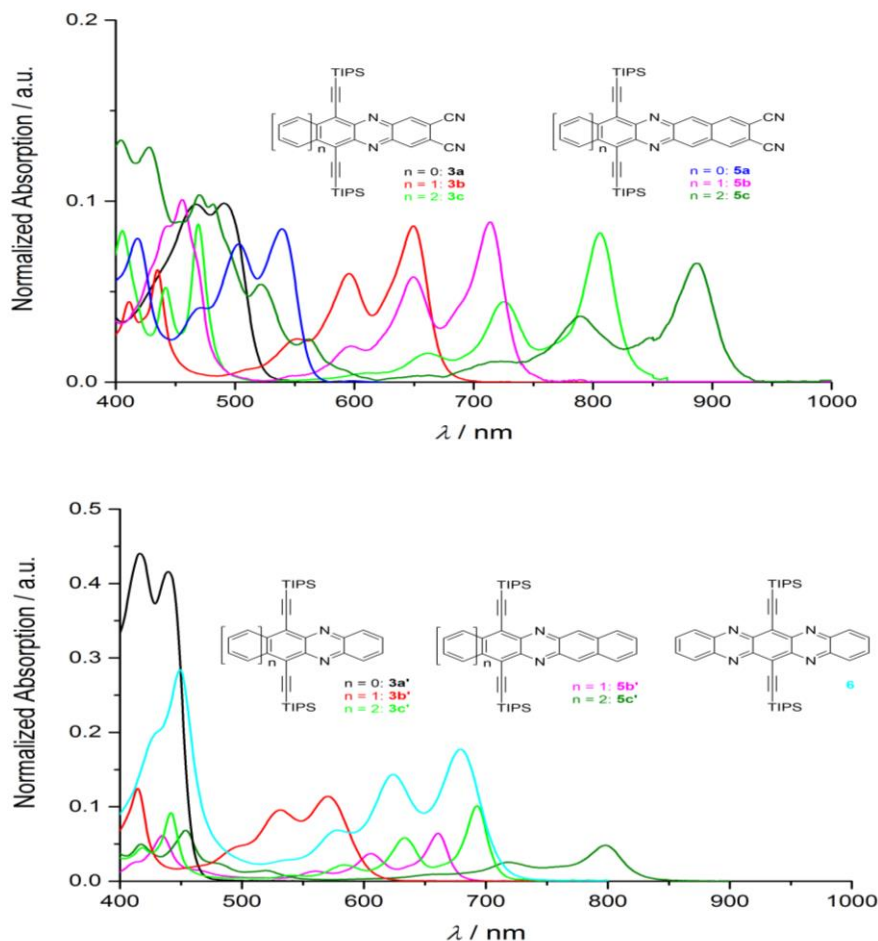


Figure 23. Top: UV-vis absorption spectra of **3a-c** and **5a-c** in *n*-hexane at room temperature; middle: spectra magnified to the region of the lowest energy maxima; bottom: UV-vis absorption spectra of the non-cyanated derivatives **3a'-c'**¹²¹ and **5b'** to **5c'**¹²⁰ as well as the tetraazapentacene **6**¹¹³ in *n*-hexane at room temperature.

For **3a** and **3b** similar but smaller effects are recorded. What is the reason for this quite dramatic shift? Quantum chemical calculations show that in the case of cyanation the LUMO level is stabilized between 0.7 and 0.8 eV, while the stabilization of the HOMO is less, viz. only 0.5 eV; A decreased HOMO-LUMO gap results.

Table 6. Photophysical properties of **3a-c** and **5a-c** in *n*-hexane at room temperature.

Compound	$\lambda_{\text{max, abs}} / \text{nm}$	$\lambda_{\text{onset}} / \text{nm}$	$E_{\text{g, opt}} / \text{eV}$
3a	491	522	2.38
3a' ¹²¹	440	460	2.69
3b	649	673	1.84
3b' ¹²¹	570	585	2.11
3c	805	833	1.49
3c' ¹²¹	693	709	1.75
5a	539	563	2.20

5b	714	734	1.69
5b' ¹²⁰	662	678	1.83
5c	886	917	1.35
5c' ¹²⁰	798	825	1.50
6 ¹¹³	679	711	1.74

In the case of the targets **5** the situation is similar. Figure 24 shows that the LUMO is distributed over the whole molecule including the cyano groups. The HOMOs of the targets **3** and **5**, on the other hand have larger coefficients on the side that is the furthest away from the cyano groups. In such a case, the electron accepting cyano groups strongly stabilize the LUMO, but are less efficient in stabilizing the HOMO.

Table 7. First reduction potentials measured by cyclic voltammetry (CV) in CH_2Cl_2 using Bu_4NPF_6 as electrolyte and Fc/Fc^+ as internal standard (-5.10 eV)¹²² at 0.1 mVs^{-1} ; frontier molecular orbital levels of **3a-c** and **5a-c** vs. vacuum level, estimated from UV-vis and CV experiments in *n*-hexane/ CH_2Cl_2 at room temperature; calculated using TURBOMOLE B3LYP/ def2TZVP//Gaussian 09 B3LYP/6-311++G**.

Compound	$E_{1/2\text{red1}}$	$E_{\text{LUMO, CV}}$	$E_{\text{HOMO, opt}}$	$E_{\text{LUMO, DFT}}$	$E_{\text{HOMO, DFT}}$
3a	-1.1	-4.0	-6.4	-3.9	-6.5
3a' ¹²¹	-1.7	-3.4	-6.1	-3.1	-6.0
3b	-0.8	-4.3	-6.1	-4.1	-6.0
3b' ¹²¹	-1.2	-3.9	-6.0	-3.4	-5.5
3c	-0.7	-4.4	-5.9	-4.2	-5.8
3c' ¹²¹	-1.1	-4.1	-5.8	-3.5	-5.3
5a	-1.1	-4.1	-6.3	-4.0	-6.3
5b	-0.8	-4.2	-6.0	-4.2	-5.9
5b' ¹²⁰	-1.0	-4.1	-5.9	-3.5	-5.5
6 ¹¹³	-0.8	-4.3	-6.1	-3.4	-5.3

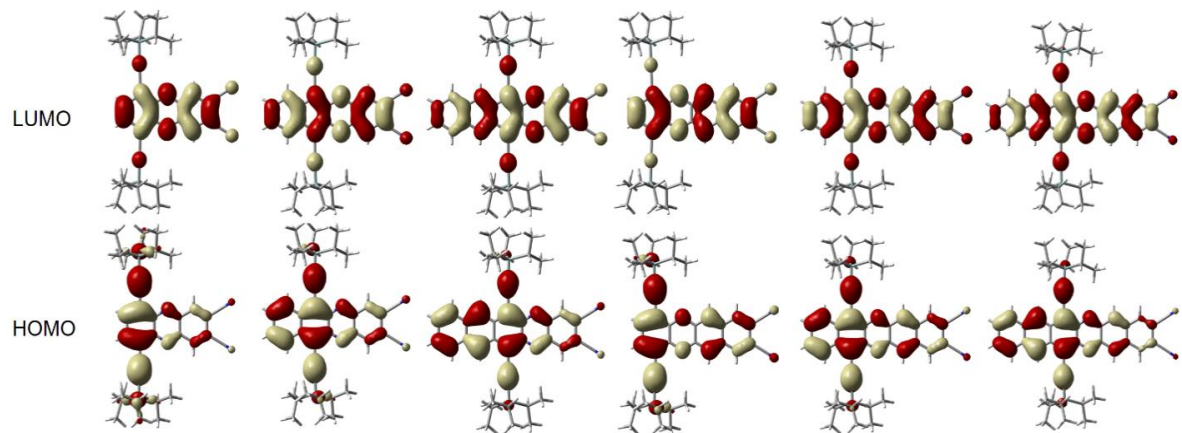


Figure 24. Frontier molecular orbitals of **3a-c** and **5a-c** vs. vacuum level (from left to right, respectively), calculated using TURBOMOLE B3LYP/ def2 TZVP//Gaussian 09 B3LYP/6-311++G**.

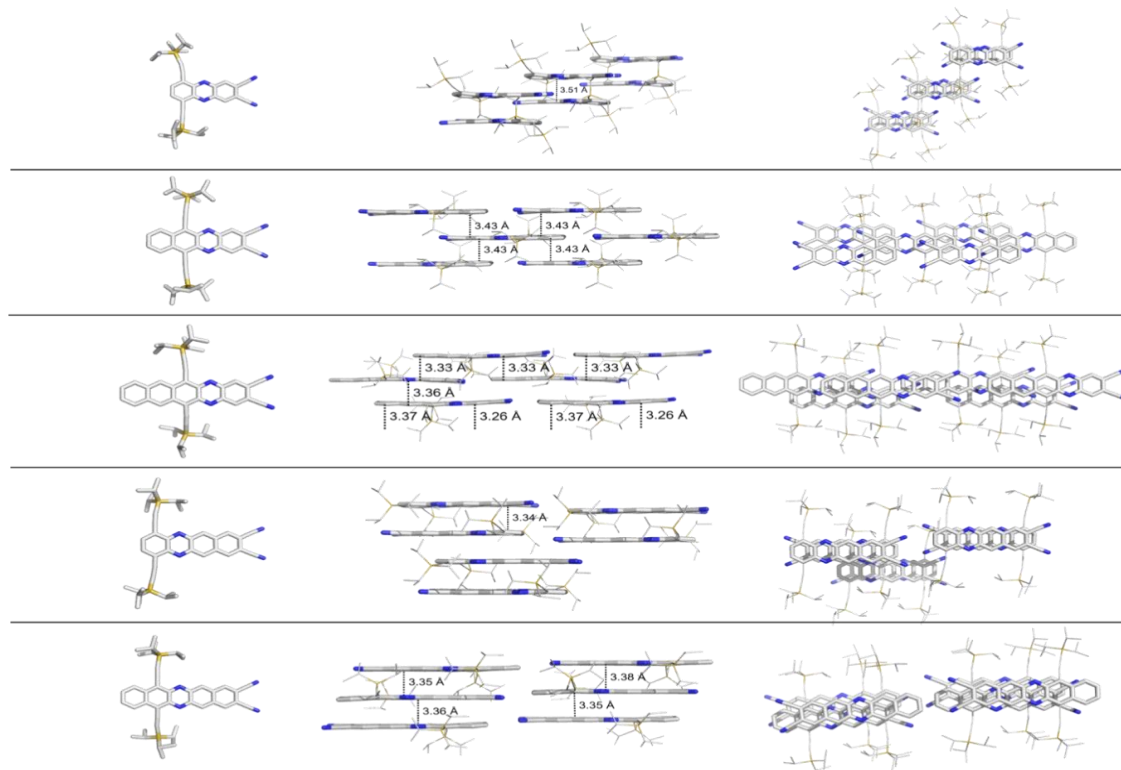


Figure 25. Solid-state structures of **3a-c** and **5a-b** (from top to bottom, respectively) as determined by X-ray analysis, showing dimer-type packings (**3a**, **5a**), brick-wall motifs (**3b**, **3c**) and slipped 1D-stacks (**5b**).

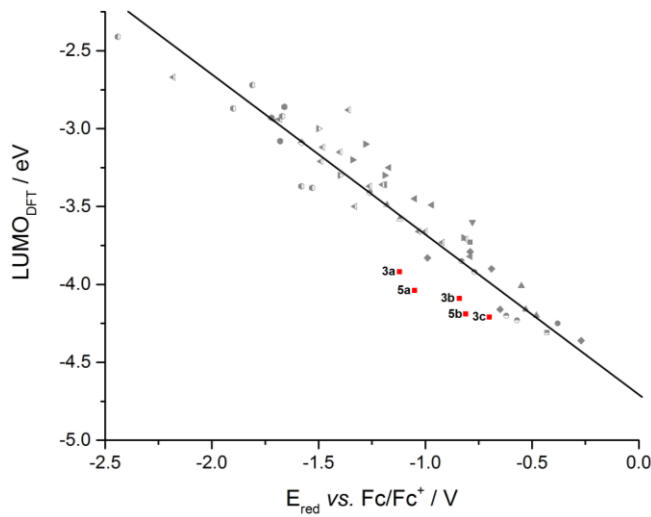


Figure 26. Correlation of the first reduction potentials of di-cyanated heteroacenes (red) as determined by cyclic voltammetry with the calculated DFT-LUMOs *vs.* that of nor-cyano heteroacenes (grey)¹²³. A more detailed version of this graph can be found in the SI(Chapter 9.5.).

The calculated stabilization of the LUMO does not fully translate into a facilitated chemical reduction potential, as the cyclic voltammetry data indicate (Table 7). The introduction of the two cyano groups leads to a reduction potential that is only 0.1-0.6V shifted towards more positive values, i.e. they are easier reduced, but not by as much as the calculated LUMO position suggests. Due to the low stability of the hexacene **5c**, we could not perform reliable cyclic voltammetry, so it is not included in this analysis.

The comparison of the experimental first reduction potential and the calculated LUMO-positions employing B3LYP/6-311++G** allows to compare these to other N-heteroacenes (Figure 26)¹²³. While the cyano compounds all show a linear LUMO/reduction potential correlation, the reduction potentials are all pushed towards more negative values compared to the non-cyano heteroacenes. The reason for this behavior is not entirely clear, but might be due to the differential solvation of neutral and radical anion, rendering the neutral cyano-compounds (relatively) less easily reduced than expected.

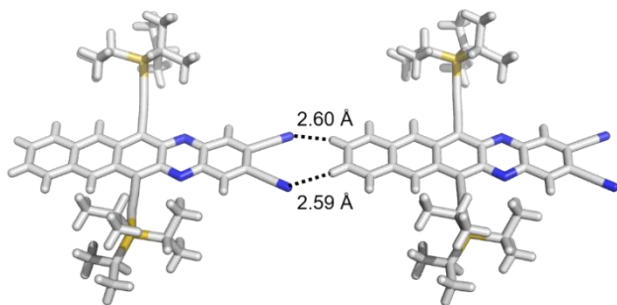


Figure 26. CN...CH-Interactions in the crystal structure of **3b**.

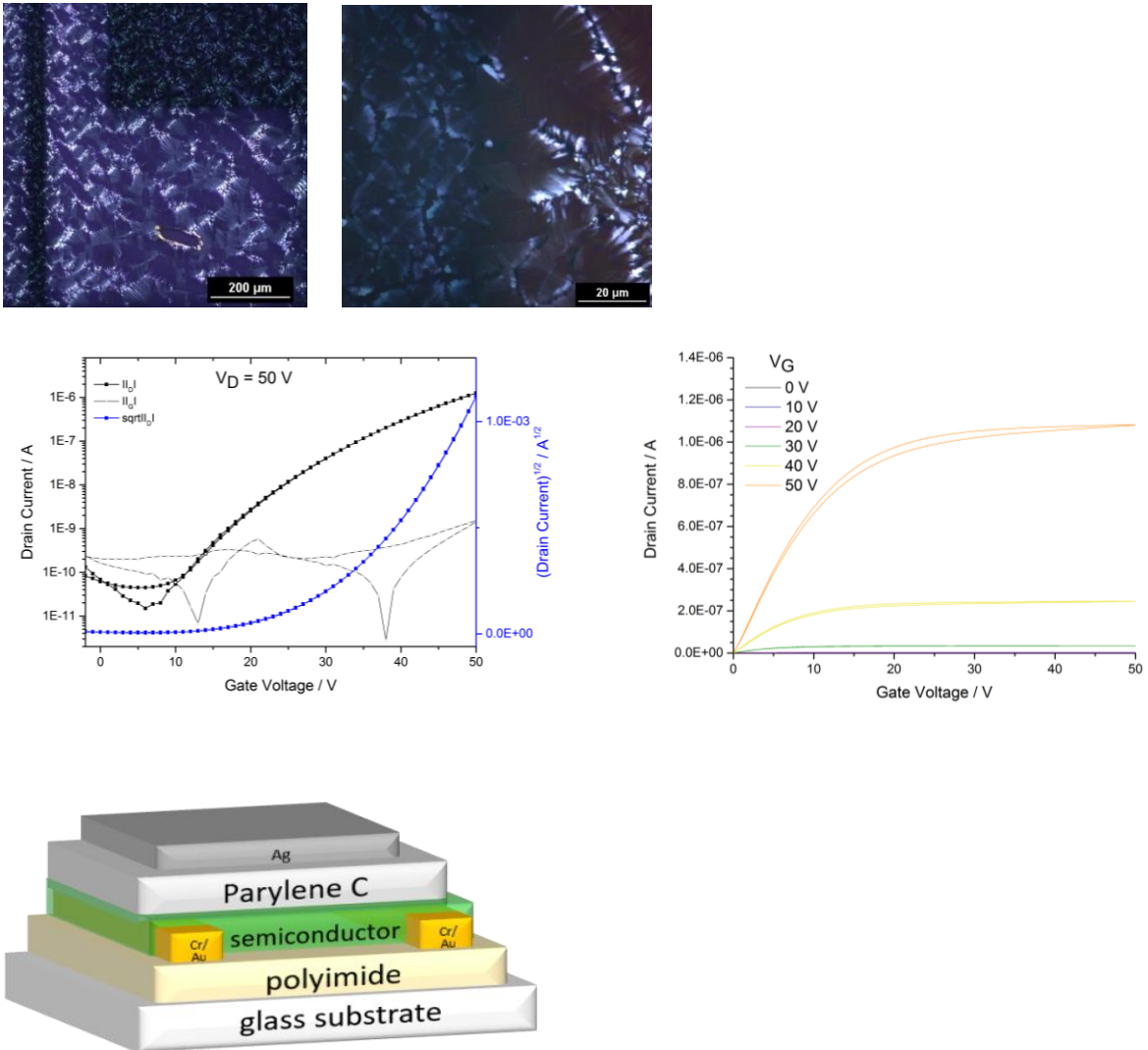


Figure 27. Top: Polycrystalline films of **3b** spun from tetraline on a polyimide substrate under cross-polarized light; middle: transfer and output characteristics of a bottom-contact/top-gate **3b**-FET with $W = 8$ mm and $L = 28.6 \mu\text{m}$. $\mu_e^{\text{max}} = 7 \cdot 10^{-3} \text{ cm}^2 \text{V}^{-1} \text{s}^{-1}$, $\mu_e^{\text{av}} = 6 \cdot 10^{-3} \text{ cm}^2 \text{V}^{-1} \text{s}^{-1}$, On/Off ratio = 10^4 - 10^5 , $V_{\text{Th}} = 32$ V; bottom: schematic device architecture.

We grew single crystalline specimen of the compounds **3a-c** and **5a,b**. Their structures and solid state packing are shown in Figure 25. For **3a** the molecules only form pairs that are held together by π - π -stacking with a distance of 3.51 \AA . In **3b** a brick wall motif forms, and the distances are 3.43 \AA with respect to each other. The target **3c** crystallizes with two independent molecules, which together form a brick wall motif. There is a significant number of non-equivalent distances from 3.26 \AA to 3.37 \AA . In **5a** we also observe pairs, their distance is 3.34 \AA . All of the pairs are oriented parallel to each other, but they are so much offset, that no real brick wall motif results. **5b** crystallizes with two independent molecules in the crystallographic cell. The molecules form stacks, displaying π - π -stacking with distances of 3.35 \AA / 3.36 \AA and 3.35 \AA / 3.38 \AA , respectively. These stacks do form a formal wall, but because of the lack of offset, these are more like one dimensional stacks that do not overlap with each other. An interesting aspect is the interaction of the cyano groups of the azaacenes with neighboring molecules (Figure 26). While the $\text{CN} \dots \text{H}$ -distances are long (2.6 \AA) and the CN -bonds are unchanged, there is probably something akin to an agostic interaction that is structure supporting in our dicyano-azaacenes.

These promising results motivated us to further investigate the semiconducting properties of the most promising candidates based on their solid state structures. We fabricated bottom-

contact/top-gate field effect transistors of **3b** on polyimide substrates, as its favorable brick wall packing motive should allow for an efficient charge transport. Gold with an adhesion layer of chromium underneath was thermally evaporated as source and drain contacts (Figure 27, bottom). Thin films of **3b** were spin-cast from tetraline solutions (10 mg/mL) and investigated via polarization microscopy images, showing crystallites with an average domain size of 20 µm (Figure 27 top). Vapor deposited parylene C was used as dielectric and the devices were finished with an evaporated silver gate electrode. The resulting thin-film transistors were characterized in a nitrogen filled glove box. Figure 27 (middle) displays the obtained transfer and output characteristics. The latter shows a good injection of electrons from the gold contacts into the material and nearly no hysteresis can be observed. The on/off ratio is 10^4 - 10^5 and the determined average electron mobility is $6 \cdot 10^{-3}$ cm²V⁻¹s⁻¹. Although the pentacene derivative **3c** should in theory exhibit an even better performance, we were despite great efforts not able to fabricate devices from it, as it shows significant dewetting from all common organic solvents on our substrates. Further investigations involving self-assembled monolayers are currently ongoing.

7.3. Conclusions

In conclusion, we have prepared a series of dicyano-substituted azaacenes, containing three to six rings. The targets were prepared by Pd-catalyzed coupling of suitable diamino-substituted arenes with either 4,5-dibromophthalonitrile or 6,7-dibromonaphthalene-2,3-dicarbonitrile. The resulting coupling products were oxidized by MnO₂ or by PbO₂ to give the desired azaacenes, which were investigated by optical spectroscopy, cyclic voltammetry and single crystal X-ray analysis. An interesting observation is that the position of the cyano groups (either one or two benzene rings separated from the azaacene unit) influence both the reduction potential and thus the LUMO position, such, that the azaacenes in which the pyrazine units are closer positioned to the cyano substituents show a lower lying LUMO and a higher electron affinity. The diazatetracene **3b** could be processed into a thin film transistor with electron mobilities of up to $7 \cdot 10^{-3}$ cm²V⁻¹s⁻¹.

CHAPTER 8

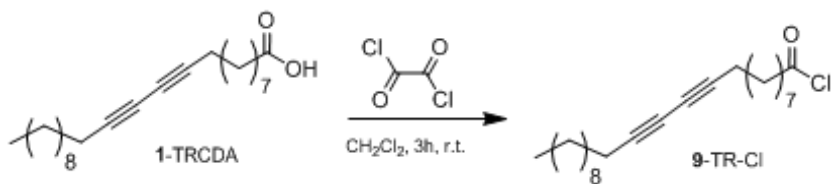
Experimental Section

8.1. Chapter 3: Synthetic procedures of compounds 2-45

Materials and methods

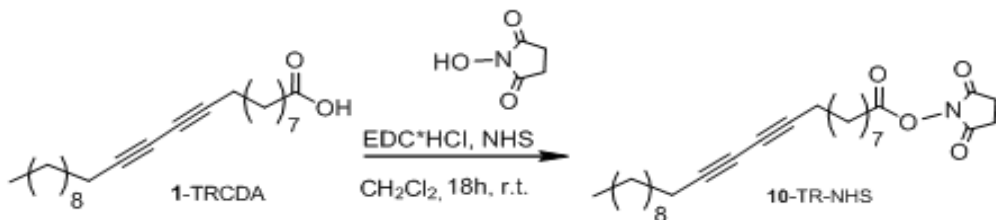
All reagents and solvents were purchased from Sigma-Aldrich Chemicals. The diacetylene monomer, 10,12-tricosadiynoic acid (TRCDA), was purchased from Aldrich (98% purity) and eventually purified to remove the polymerized part (if present) before use. Analytical thin-layer chromatography (TLC) was conducted on Sigma-Aldrich silica gel aluminum plates (60 Å, with fluorescent indicator) or silica gel 60 F-254 with a 0.2 mm layer thickness. For flash chromatography, 60 Å silica gel (Merck, 230–400 mesh) was employed. ¹H, ¹³C and ¹⁹F NMR spectra were obtained using a Varian Mercury 400 spectrometer with a 5 mm probe.

8.1.1. Synthesis of tricosa-10,12-diynoyl chloride (TR-Cl, 9)



Procedure was adopted from the previously reported one⁴⁸. Oxalylchloride (1.2 eq, 1.68 mmol) was added dropwise to a CH_2Cl_2 (15 mL) stirring solution containing **1** (1 eq, 1.40 mmol). The resulting mixture was stirred for 3h at r.t. Removal of the solvent under reduced pressure afforded the desired TR-Cl (**9**) in quantitative yield and the product was used for the next reaction without further purification. **Yield:** oily liquid (97 %). MW: Calcd for [M] $\text{C}_{23}\text{H}_{37}\text{ClO}$, 365. ¹H NMR (400 MHz, CDCl_3): δ = 0.84–0.88 (t, J =8.0, 7.1 Hz, 3H), 1.24–1.40 (m, 22H), 1.46–1.52 (m, 4H), 1.55–1.70 (m, 2H) 2.21–2.24 (t, 4H), 2.32–2.35 (t, 2H). ¹³C NMR (100 MHz, CDCl_3): δ = 169.6, 76.7, 65.3, 53.4, 35.3, 31.9, 29.5, 29.3, 29.1, 29.1, 29.0, 29.0, 28.9, 28.8, 28.8, 28.7, 28.6, 28.3, 24.2, 22.7, 19.2, 19.2, 14.1.

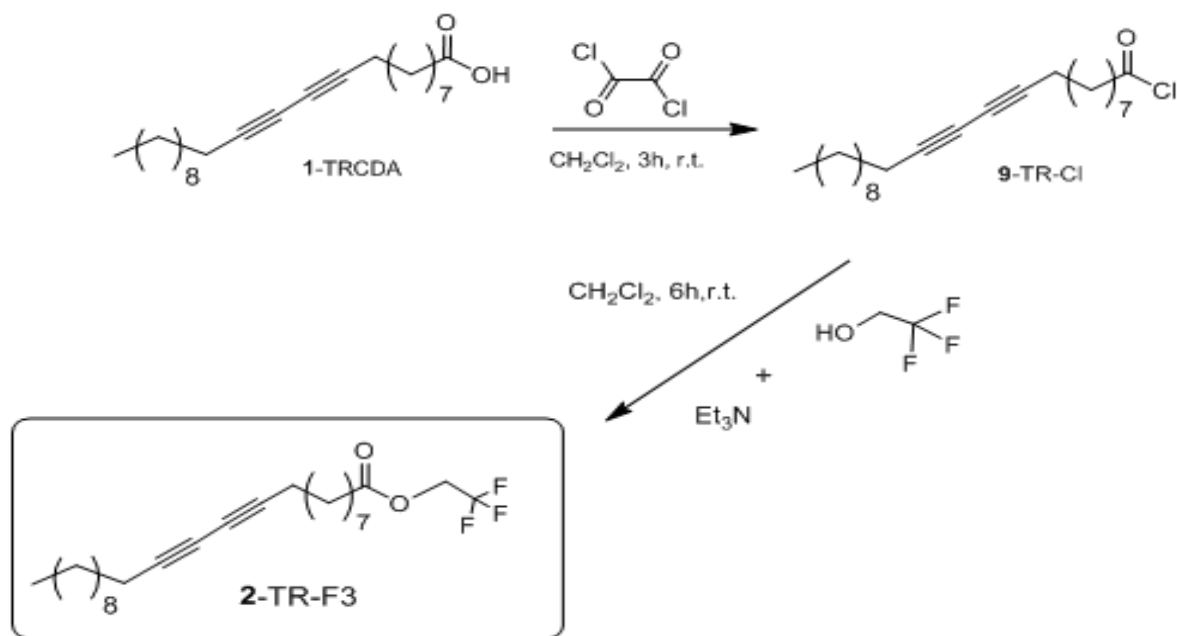
8.1.2. Synthesis of 2,5-dioxopyrrolidin-1-yl tricosa-10,12-diynoate (TR-NHS, 10)



Procedure was adopted from the previously reported one⁴⁴. 10,12 tricosadiynoic acid (TRCDA, **1**) (1 eq, 0.29 mmol) is solubilized in CH_2Cl_2 (3 mL) in a round bottom flask under a gentle flux of N_2 and avoiding light contact. N-Hydroxysuccinimide (NHS, 1.2 eq, 0.35 mmol) and N-(3-Dimethylaminopropyl)-N'-ethylcarbodiimide hydrochloride (EDC*HCl, 2 eq, 0.55 mmol) are solubilized in CH_2Cl_2 (5 mL) and mixed with a solution of **1** under stirring at r.t.. After 20 h, the

solvent is evaporated under reduced pressure. The mixture is extracted from water with diethyl ether (x2, 100 mL). The organic layers are recovered, dried with anhydrous Na₂SO₄, filtered and evaporated. TR-NHS **10** is used in the next step without further purification. **Yield:** white powder (98 %). MW: Calcd for [M] C₂₇H₄₁NO₄, 443.63. ¹H NMR (400 MHz, CDCl₃): δ = 0.84–0.87 (t, J=8.0, 7.1 Hz, 3H), 1.24–1.40 (m, 22H), 1.45–1.52 (m, 4H), 1.68–1.75 (m, 2H), 2.20–2.23 (t, 2H), 2.56–2.59 (t, 4H), 2.81 (s, 4H). ¹³C NMR (100 MHz, CDCl₃): δ = 169.2, 169.2, 168.6, 77.6, 77.4, 65.3, 65.2, 31.9, 30.9, 29.5, 29.5, 29.3, 29.1, 28.9, 28.8, 28.8, 28.7, 28.7, 28.3, 28.2, 25.6, 25.6, 24.5, 22.6, 19.2, 19.2, 14.1.

8.1.3. Synthesis of 2,2,2-trifluoroethyl tricosa-10,12-dynoate (TR-F3, **2**)

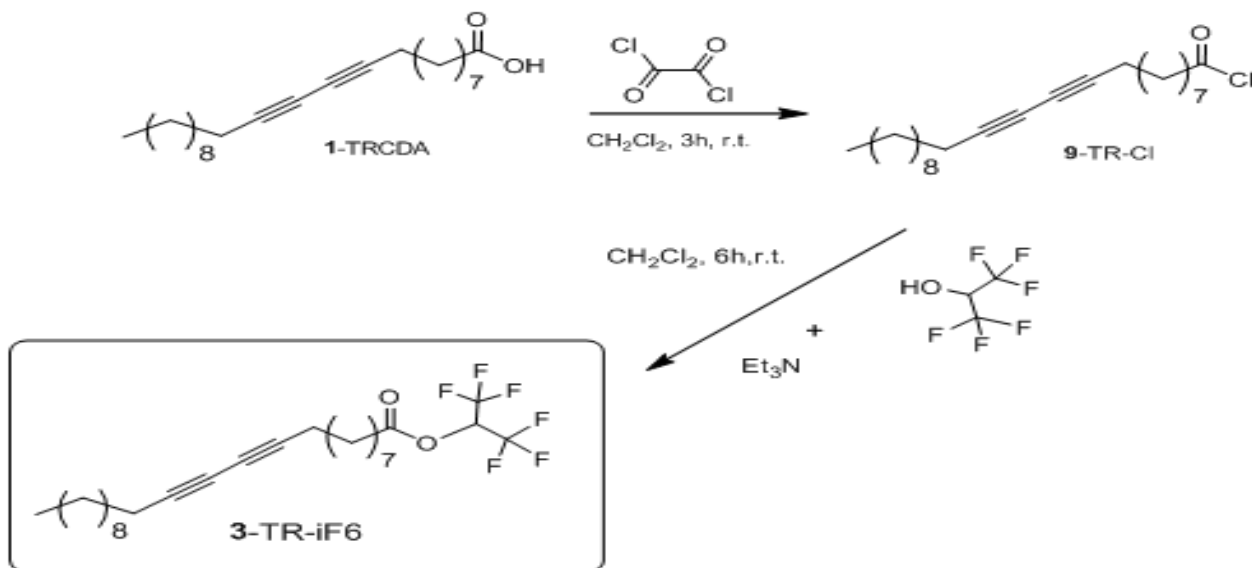


*Step 1. Synthesis of tricosa-10,12-dynoyl chloride (TR-Cl, **9**).*

*Step 2. Synthesis of 2,2,2-trifluoroethyl tricosa-10,12-dynoate (TR-F3, **2**).*

Procedure was adapted from a previously reported one⁴⁹. To a stirring solution of **9** (1 eq, 0.30 mmol) in CH₂Cl₂ (15 mL) was added 2,2,2-trifluoroethanol (2 eq, 0.60 mmol) and Et₃N (1.2 eq, 0.36 mmol); the resulting solution is stirred at r.t. for 6 h. The mixture is extracted from water with CH₂Cl₂ (x2, 50 mL). The organic layers are recovered, dried with anhydrous Na₂SO₄ and filtered. Evaporation of the solvent left a white solid, that was purified by column chromatography (AcOEt : cyclohexane = 1 : 9). **Yield:** white solid (88 %). MW: Calcd for [M] C₂₅H₃₉F₃O₂, 428.58. ¹H NMR (400 MHz, CDCl₃): δ = 0.84–0.88 (t, J=8.0, 7.1 Hz, 3H), 1.24–1.35 (m, 22H), 1.47–1.51 (m, 4H), 1.61–1.63 (m, 2H), 2.20–2.24 (t, 4H), 2.35–2.41 (t, 2H), 4.41–4.48 (q, 2H). ¹³C NMR (100 MHz, CDCl₃): δ = 173.4, 124.8, 77.6, 77.4, 77.3, 65.3, 65.2, 34.0, 31.9, 29.7, 29.6, 29.4, 29.3, 29.0, 28.8, 28.7, 28.3, 28.3, 28.1, 28.1, 24.7, 22.7, 19.2, 19.2, 14.1. ¹⁹F NMR (377 MHz, CDCl₃): δ = -73.90.

8.1.4. Synthesis of 1,1,1,3,3,3-hexafluoropropan-2-yl tricosa-10,12-dynoate (TR-iF6, **3**)

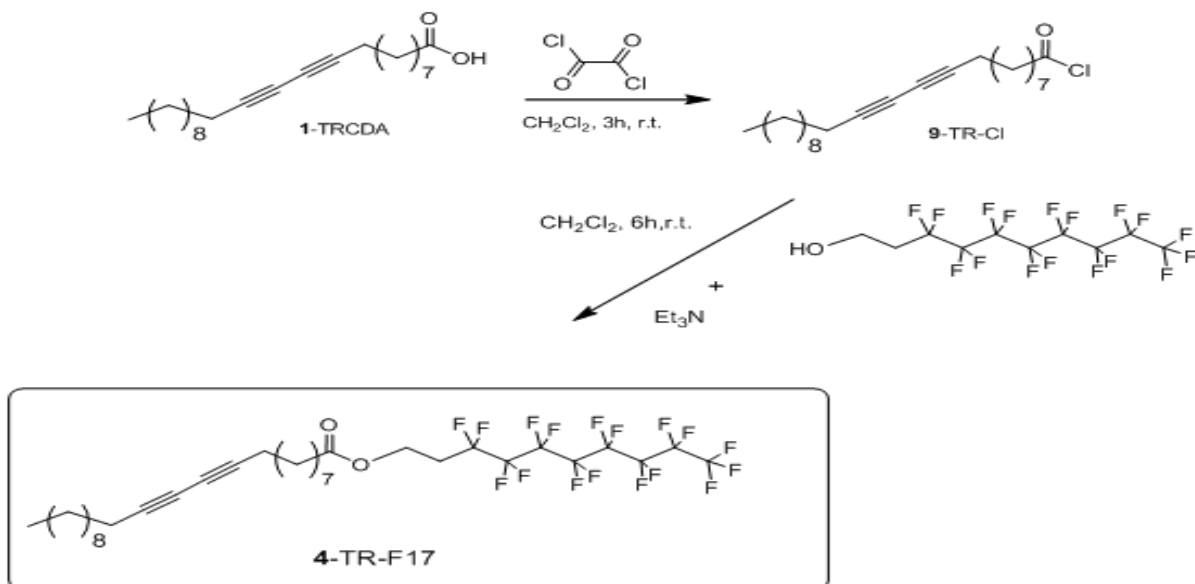


Step 1. Synthesis of **tricosa-10,12-diynoyl chloride** (TR-Cl, **9**).

*Step 2. Synthesis of 1,1,1,3,3,3-hexafluoropropan-2-yl tricosa-10,12-diynoate (TR-iF6, **3**).*

Procedure was adapted from a previously reported one⁴⁹. To a stirring solution of **9** (1 eq, 0.27 mmol) in CH₂Cl₂ was added 1,1,1,3,3,3-hexafluoropropanol (1.8 eq, 0.49 mmol) and Et₃N (1.2 eq, 0.36 mmol); the resulting solution is stirred at r.t. for 5 h. The mixture is extracted from water with CH₂Cl₂ (x2, 50 mL). The organic layers are recovered, dried with anhydrous Na₂SO₄ and filtered. Evaporation of the solvent left a liquid, that was purified by column chromatography (AcOEt : cyclohexane = 1 : 9). **Yield:** liquid (85 %). MW: Calcd for [M] C₂₆H₃₈F₆O₂, 496.54. ¹H NMR (400 MHz, CDCl₃): δ = 0.83-0.86 (t, J=8.0, 7.1 Hz, 3H), 1.22-1.37 (m, 22H), 1.44-1.47 (m, 4H), 1.61-1.67 (t, 2H), 2.19-2.22 (t, 4H), 2.45-2.49 (t, 2H), 5.70-5.76(quint, 1H). ¹³C NMR (100 MHz, CDCl₃): δ = 173.9, 110.0, 110.0, 95.4, 76.6, 76.6, 65.1, 65.1, 33.2, 31.8, 29.5, 29.4, 29.3, 29.3, 29.1, 28.8, 28.7, 28.6, 28.6, 28.3, 28.2, 24.5, 22.6, 19.2, 19.2, 14.1. ¹⁹F NMR (377 MHz, CDCl₃): δ = -73.43.

8.1.5. Synthesis of 3,3,4,4,5,5,6,6,7,7,8,8,9,9,10,10-heptadecafluorodecyl tricosa-10,12-diynoate (TR-F17, **4**)

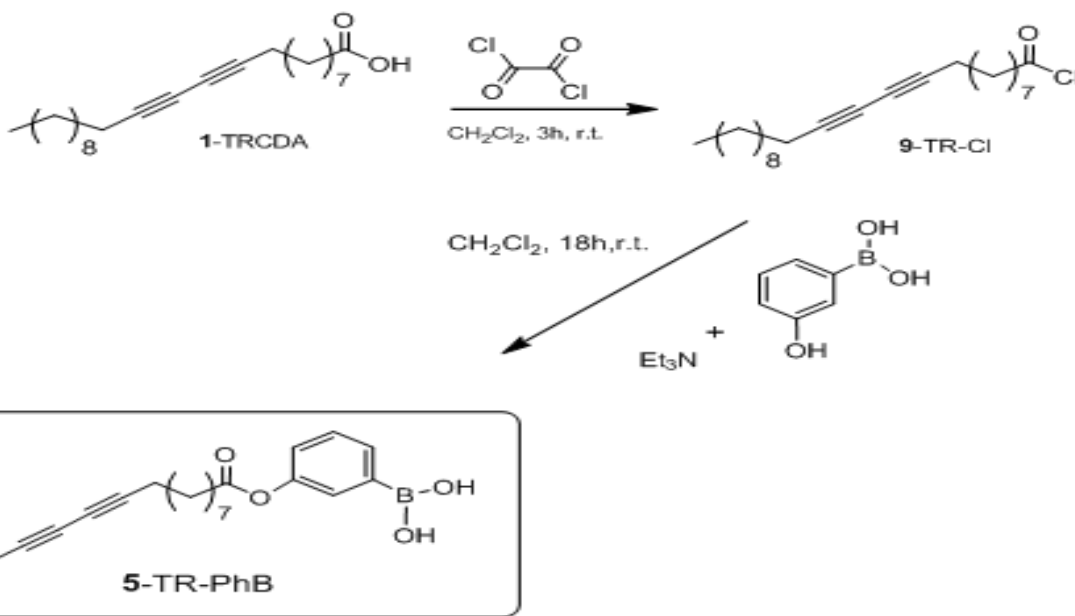


Step 1. Synthesis of tricosa-10,12-dynoyl chloride (TR-Cl, 9).

Step 2. Synthesis of 3,3,4,4,5,5,6,6,7,7,8,8,9,9,10,10-heptadecafluorodecyl tricosa-10,12-dynoate (TR-F17, 4).

Procedure was adapted from a previously reported one⁴⁹. To a stirring solution of **9** (1 eq, 0.27 mmol) in CH₂Cl₂ (10 mL) was added 1H, 1H, 2H, 2H, perfluoro-1-decanol (1.6 eq, 0.43 mmol) and Et₃N (1.2 eq, 0.32 mmol); the resulting solution is stirred at r.t. for 5 h. The mixture is extracted from water with CH₂Cl₂ (x2, 50 mL). The organic layers are recovered, dried with anhydrous Na₂SO₄ and filtered. Evaporation of the solvent left a liquid, that was purified by column chromatography (AcOEt : cyclohexane = 1 : 9). **Yield:** white solid (60 %). MW: Calcd for [M] C₃₃H₄₁F₁₇O₂, 792.66. ¹H NMR (400 MHz, CDCl₃): δ = 0.84-0.86 (t, J=8.0, 7.1 Hz, 3H), 1.24-1.41 (m, 22H), 1.47-1.49 (m, 4H), 1.53-1.55 (m, 2H), 2.20-2.24 (t, 4H), 2.28-2.32 (t, 2H), 2.39-2.51 (m, 2H), 4.34-4.37 (t, 2H). ¹³C NMR (100 MHz, CDCl₃): δ = 173.4, 124.8, 77.6, 77.4, 77.3, 65.3, 65.2, 56.1, 34.0, 31.9, 31.9, 30.8, 30.6, 30.4, 30.3, 29.7, 29.6, 29.5, 29.4, 29.3, 29.1, 29.0, 29.0, 28.9, 28.7, 28.3, 28.3, 24.7, 22.7, 19.2, 19.2, 14.1. ¹⁹F NMR (377 MHz, CDCl₃): δ = -80.744, -80.7773, -80.798, , -113.527, -113.570, -113.610, -113.653, -113.689, -121.678, -121.920,- 122.719, -123.572, -126.105.

8.1.6. Synthesis of (3-(tricosa-10,12-dynoyloxy)phenyl)boronic acid (TR-PhB, 5)



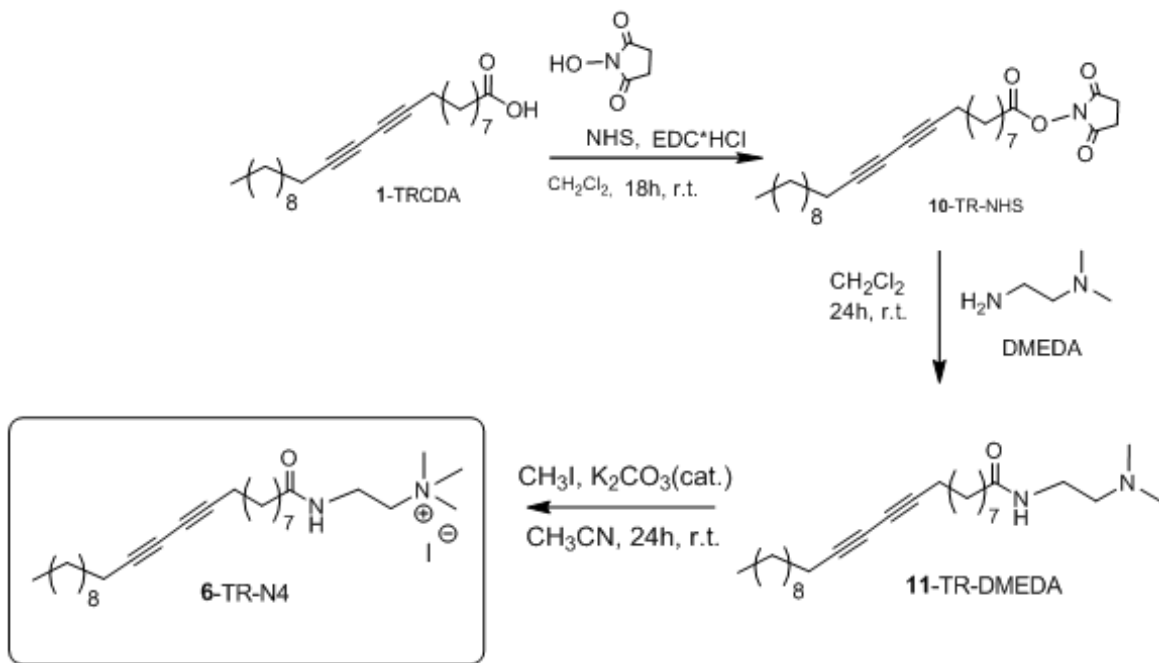
Step 1. Synthesis of tricosa-10,12-dynoyl chloride (TR-Cl, 9).

Step 2. Synthesis of (3-(tricosa-10,12-dynoyloxy)phenyl)boronic acid (TR-PhB, 5).

Procedure was adapted from a previously reported one⁴⁸. 3-Hydroxyphenylboronic acid (1.5 eq, 2.10 mmol) and Et₃N (3.4 eq, 4.70 mmol) were dissolved in CH₂Cl₂ and **9** (1 eq, 1.40 mmol) was dissolved in a small amount of anhydrous THF. The THF solution containing **9** was added dropwise into the CH₂Cl₂ solution. The resultant solution was stirred at room temperature overnight and concentrated in vacuum at r.t.. The crude residue was dissolved in a small amount of MeOH and added dropwise to water. Addition of small amount of HCl (1:9) water solution to MeOH solution resulted in the formation of white precipitates. The precipitates formed were filtered, washed with water and dried under N₂ to give the desired product. **Yield:** white solid (76 %). MW: Calcd for [M] C₂₉H₄₃BO₄, 466.4. ¹H NMR (400 MHz, CDCl₃): δ = 0.84-0.88 (t, J=8.0, 7.1 Hz, 3H), 1.24-

1.41 (m, 22H), 1.46–1.53 (m, 4H), 1.65–1.81 (m, 2H), 2.20–2.25 (m, 4H), 2.31–2.35 (t, 1H), 2.52–2.56 (t, 2H), 7.14–7.16 (d, $J=7.5$, 1.5 Hz, 1H), 7.29–7.31 (d, 1H), 7.37–7.43 (m, 2H), 7.51–7.58 (d, 1H). ^{13}C NMR (100 MHz, CDCl_3): δ = 178.8, 172.7, 150.6, 133.1, 129.2, 128.1, 126.2, 76.7, 65.3, 34.4, 33.8, 31.9, 30.3, 29.7, 29.5, 29.3, 29.1, 29.0, 28.9, 28.8, 28.7, 28.6, 28.3, 24.9, 24.6, 22.6, 19.2, 19.2, 14.1.

8.1.7. Synthesis of N,N,N-trimethyl-2-(tricos-10,12-dynamido)ethan-1-aminium iodide (TR-N4, 6)



Step 1. Synthesis of 2,5-dioxopyrrolidin-1-yl tricos-10,12-dynoate (TR-NHS, 10).

Step 2. Synthesis of N-(2-(dimethylamino)ethyl)tricos-10,12-dynamide (TR-DMEDA, 11).

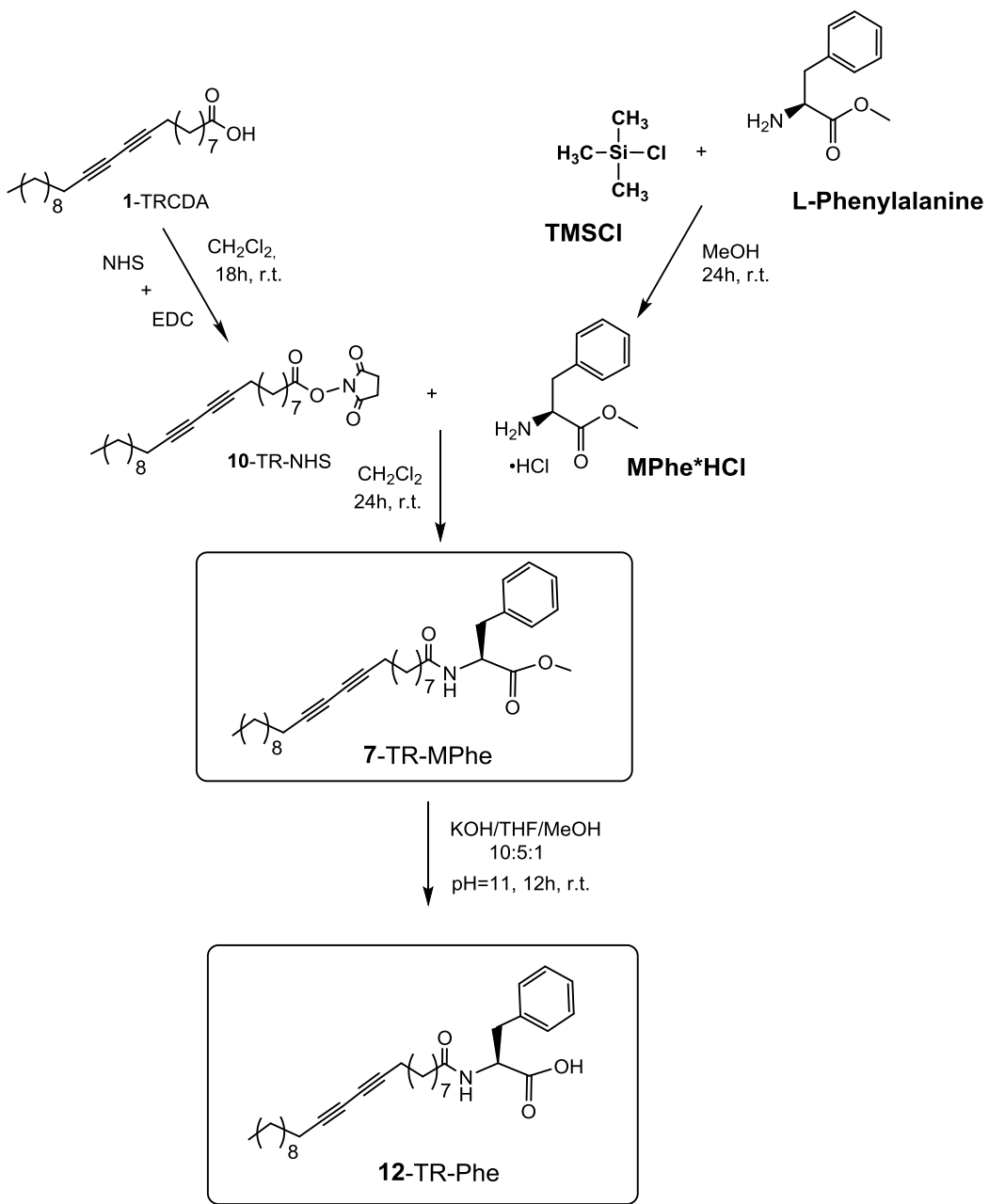
Procedure was adapted from a previously reported one⁴⁷. TR-NHS was added to a solution of N,N-dimethylethylenediamine (DMEDA, 2 eq, 0.45 mmol) in CH_2Cl_2 (10 mL). The resulting mixture was stirred for 24 h. After the solvent was evaporated, the residue was purified by a silica gel column ($\text{CH}_2\text{Cl}_2 : \text{CH}_3\text{OH} = 20 : 1$) to give TR-DMEDA **11**. **Yield:** white solid (96 %). MW: Calcd for [M] $\text{C}_{27}\text{H}_{48}\text{N}_2\text{O}$, 416.7. ^1H NMR (400 MHz, CDCl_3): δ = 0.84–0.87 (t, $J=8.0$, 7.1 Hz, 3H), 1.24–1.36 (m, 22H), 1.46–1.50 (mm, 6H), 2.14–2.24 (m, 8H), 2.41–2.50 (tt, 4H), 2.69 (s, 2H), 3.30–3.34 (q, 1H), 3.60–3.69 (t, 1H), 6.11 (s, 1H). ^{13}C NMR (100 MHz, CDCl_3) δ = 174.7, 76.9, 76.8, 65.6, 65.2, 65.2, 45.6, 45.6, 39.3, 36.3, 31.8, 29.5, 29.4, 29.3, 29.2, 29.1, 29.0, 28.9, 28.8, 28.3, 28.3, 28.1, 25.4, 22.6, 19.2, 19.2, 14.1.

Step 3. Synthesis of N,N,N-trimethyl-2-(tricos-10,12-dynamido)ethan-1-aminium iodide (TR-N4, 6).

Procedure was adapted from a previously reported one⁴⁷. To a solution containing TR-DMEDA **11** (1 eq, 0.24 mmol) in CH_3CN (10 mL), CH_3I (5.5 eq, 1.32 mmol) and K_2CO_3 (1.2 eq, 0.29 mmol) were added. The resulting suspension was stirred at r.t. for 24 h and filtered. After evaporation, the quantitative product TR-N4 **6** was obtained. **Yield:** white solid (80%). MW: Calcd for [M] $\text{C}_{28}\text{H}_{51}\text{IN}_2\text{O}$, 558.63. ^1H NMR (400 MHz, CDCl_3): δ = 0.84–0.88 (t, $J=8.0$, 7.1 Hz, 3H), 1.24–1.36 (m, 22H), 1.47–1.51 (t, 4H), 1.58–1.60 (t, 2H), 2.20–2.29 (m, 6H), 3.39 (s, 9H), 3.79–3.84 (m, 4H), 7.81 (s, 1H). ^{13}C NMR (100 MHz, CDCl_3) δ = 174.7, 76.9, 76.8, 65.6, 65.2, 65.2, 54.6, 54.6, 54.6,

36.3, 34.1, 31.8, 29.5, 29.4, 29.3, 29.2, 29.1, 29.0, 28.9, 28.8, 28.8, 28.3, 28.3, 25.4, 22.6, 19.2, 19.2, 14.1.

8.1.8. Synthesis of methyl tricosa-10,12-dienoylphenylalaninate (TR-MPhe, 7) and tricosa-10,12-dienoyl-L-phenylalanine (TR-Phe, 12)



*Step 1. Synthesis of L-phenylalanine methyl ester * HCl (MPhe * HCl).* Synthetic procedure has been adapted from a previously reported one¹²⁴.

Step 2. Synthesis of 2,5-dioxopyrrolidin-1-yl tricosa-10,12-dienoate (TR-NHS - 10)

Step 3. Synthesis of methyl tricosa-10,12-dienoylphenylalaninate (TR-MPhe - 7)

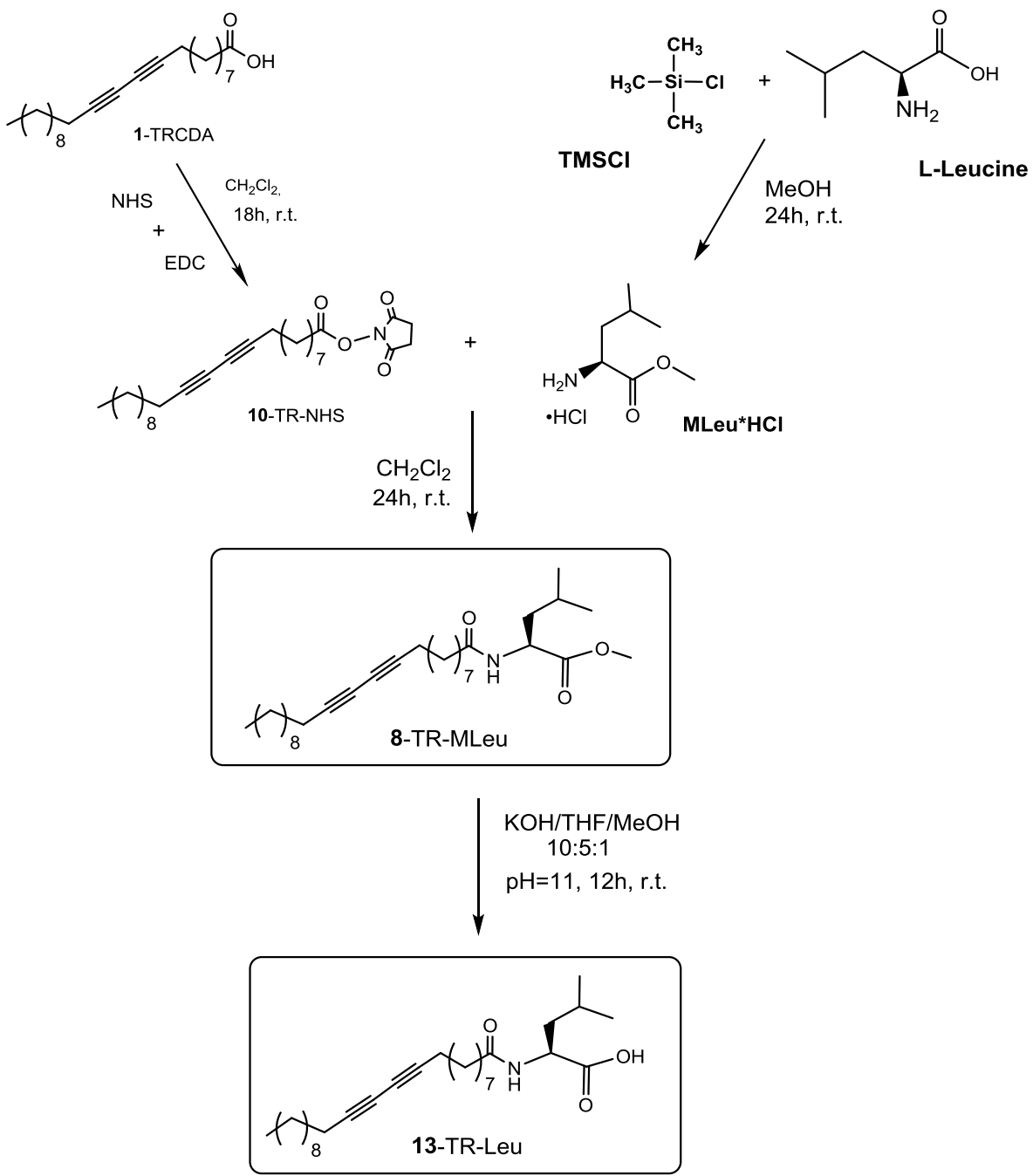
Procedure was adapted from a previously reported one⁴⁶. TR-NHS crude (1 eq, 0.24 mmol) is solubilized in CH_2Cl_2 (15 mL) in a round bottom flask under a gentle flux of N_2 and avoiding light

contact (wrapping the flask with an aluminum foil). MPhe*HCl (2 eq, 0.49 mmol) is added to the mixture followed by dropwise addition of triethylamine (Et_3N , 1.2 eq, 0.29 mmol). The reaction is stirred at r.t. for 24 h. After checking in TLC, extracted with CH_2Cl_2 /Brine solution and then the mixture is purified by column chromatography (ethylacetate : cyclohexane = 1 : 5 to 1 : 2 gradient elution) to yield the product. The solvent is removed under a gentle flux of N_2 . **Yield:** white powder TR-MPhe **7** (85 %). MW: Calcd for [M] $\text{C}_{33}\text{H}_{49}\text{NO}_3$, 507.37. ^1H NMR (400 MHz, CDCl_3): δ = 0.84–0.87 (t, J =8.0, 7.1 Hz, 3H), 1.24–1.41 (m, 22H), 1.45–1.57 (m, 6H), 2.12–2.23 (m, 6H), 3.04–3.16 (m, 2H), 3.71 (s, 3H), 4.86–4.91 (q, 1H), 5.82–5.84 (d, 1H), 7.06–7.08 (d, J =7.5, 1.5 Hz, 2H), 7.24–7.29 (d, 3H). ^{13}C NMR (100 MHz, CDCl_3): δ = 172.6, 172.1, 135.8, 129.2, 129.2, 128.5, 128.5, 127.1, 76.9, 76.9, 76.7, 65.3, 65.2, 52.8, 52.3, 37.9, 36.5, 31.2, 29.5, 29.4, 29.3, 29.1, 29.1, 29.0, 28.9, 28.7, 28.3, 28.3, 25.5, 22.6, 19.2, 19.2, 14.1.

Step 4. Synthesis of tricosa-10,12-diynoyl-L-phenylalanine (TR-Phe-12)

Compound **7** (100 mg, 0.197 mmol) was dissolved in 10:5:1 $\text{H}_2\text{O}/\text{THF}/\text{MeOH}$ (28 mL), and the pH of the solution was adjusted to 12–13 with 1 M KOH. The reaction mixture was stirred at 35 °C, and product formation was monitored by TLC (3:2 $\text{CH}_2\text{Cl}_2/\text{MeOH}$). The reaction was quenched after 12 h via the addition of Amberlist₁₅ (H⁺ form) ion-exchange resin to pH 4. The crude product was concentrated and extracted w/ethyl ether. TR-Phe **12** (75 mg) was isolated in 77% yield. MW: Calcd for [M] $\text{C}_{32}\text{H}_{47}\text{NO}_3$, 493.73. ^1H NMR (500 MHz, 3:2 $\text{CD}_3\text{OD}/\text{CDCl}_3$): δ = 0.88–0.92 (t, J =8.0, 7.1 Hz, 3H), 1.16–1.42 (m, 22H), 1.45–1.53 (m, 6H), 2.12–2.16 (t, 2H), 2.22–2.26 (t, 3H), 2.90–2.96 (m, 2H), 3.20–3.25 (dd, 2H), 3.73 (s, 1H), 4.66–4.69 (dd, 2H), 7.20–7.29 (m, 4H). ^{13}C NMR (125 MHz, 3:2 $\text{CD}_3\text{OD}/\text{CDCl}_3$): δ = 175.46, 174.84, 138.6, 128.6, 128.6, 127.7, 127.7, 125.9, 77.65, 77.65, 66.09, 66.09, 59.2, 37.20, 37.20, 32.77, 29.67, 29.67, 29.46, 28.9, 28.7, 28.7, 28.6, 28.4, 28.4, 28.1, 28.1, 25.83, 22.65, 19.56, 19.56, 14.1.

8.1.9. Synthesis of methyl tricosa-10,12-diynoylleucinate (TR-MLeu, 8) and tricosa-10,12-diynoyl-L-leucine (TR-Leu, 13)



*Step 1. Synthesis of leucine methyl ester * HCl (MLeu * HCl).* Synthetic procedure has been adapted from a previously reported one¹²⁴.

Step 2. Synthesis of 2,5-dioxopyrrolidin-1-yl tricosa-10,12-dynoate (TR-NHS - 10).

Step 3. Synthesis of methyl tricosa-10,12-dynoylleucinate (TR-MLeu - 8).

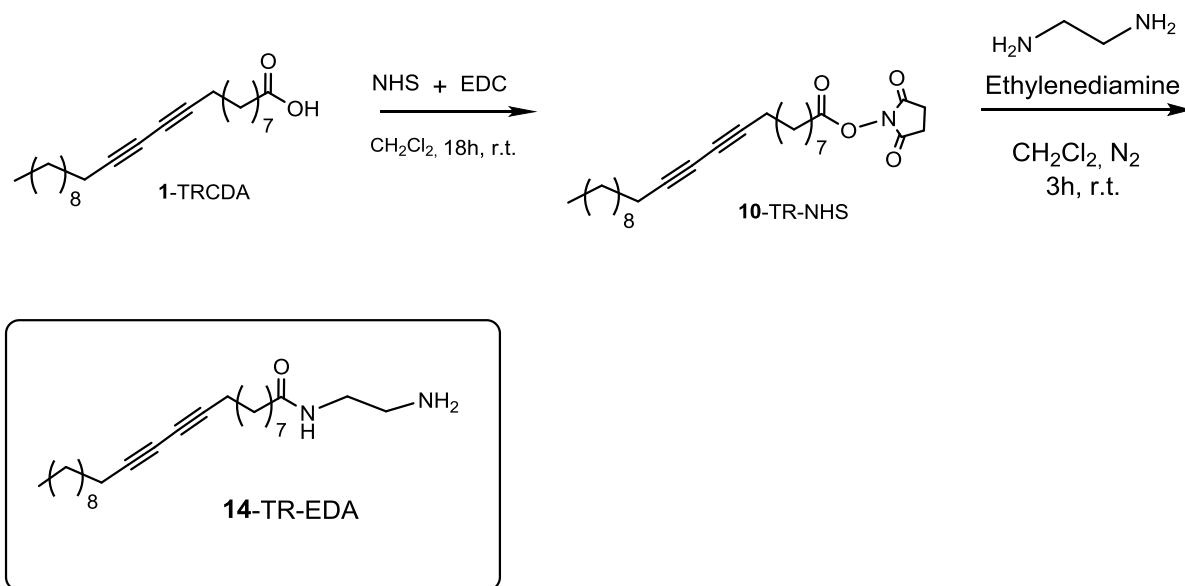
Procedure was adapted from a previously reported one⁴⁶. TR-NHS crude (1 eq, 0.24 mmol) is solubilized in CH_2Cl_2 (15 mL) in a round bottom flask under a gentle flux of N_2 and avoiding light contact. MLeu*HCl (2 eq, 0.49 mmol) is added to the mixture followed by dropwise addition of triethylamine (1.2 eq, 0.29 mmol). The reaction is stirred at r.t. for 24 h. Reaction monitored by Thin Layer Chromatography (TLC), the mixture is extracted with CH_2Cl_2 /Brine solution and then

purified with column chromatography (ethylacetate : cyclohexane = 1 : 5 to 1 : 2 gradient elution) to yield the product. The solvent is removed under a gentle flux of an inert gas. **Yield:** white solid TR-MLeu **8** (88 %). MW: Calcd for [M] C₃₀H₅₁NO₃, 473.39. ¹H NMR (400 MHz, CDCl₃): δ = 0.84–0.88 (t, J=8.0, 7.1 Hz, 3H), 0.91–0.94 (t, 6H), 1.24–1.41 (m, 22H), 1.45–1.52 (m, 6H), 1.55–1.66(m, 3H), 2.15–2.24 (m, 6H), 3.71 (s, 3H), 4.60–4.66 (m, 1H), 5.75–5.78 (d, 1H). ¹³C NMR (100 MHz, CDCl₃): δ = 173.7, 172.8, 76.7, 76.7, 65.2, 65.2, 52.2, 50.5, 41.8, 36.5, 31.9, 29.5, 29.5, 29.3, 28.9, 28.7, 28.7, 28.6, 28.3, 28.3, 28.1, 28.1, 25.5, 24.9, 22.8, 22.8, 22.7, 19.2, 19.2, 14.1.

Step 4. Synthesis of tricosa-10,12-diynoyl-L-leucine (TR-Leu - 13)

Compound **8** (214 mg, 0.425 mmol) was dissolved in 10:5:1 H₂O/THF/MeOH (60 mL), and the pH of the solution was adjusted to 12–13 with 1 M KOH. The reaction mixture was stirred at 35 °C, and product formation was monitored by TLC (3:2 CH₂Cl₂/MeOH). The reaction was quenched after 12 h via the addition of Amberlist₁₅ (H⁺ form) ion-exchange resin to pH 4. The crude product was concentrated and purified by reversed phase HPLC. TR-Leu **13** (112 mg) was isolated in 52% yield. MW: Calcd for [M] C₂₉H₄₉NO₃, 459.72. ¹H NMR (400 MHz, CD₃OD): δ = 0.84–0.88 (t, J=8.0, 7.1 Hz, 3H), 0.91–0.94 (t, 6H), 1.24–1.41 (m, 22H), 1.45–1.52 (m, 6H), 1.55–1.66 (m, 3H), 2.17–2.24 (m, 6H), 4.61–4.66 (m, 1H), 5.74–5.76 (d, 1H), 12.66 (s, 1H). ¹³C NMR (100 MHz, CD₃OD): δ = 173.7, 172.8, 76.7, 76.7, 65.2, 65.2, 56.9, 41.8, 36.5, 31.9, 29.5, 29.5, 29.3, 29.1, 28.8, 28.8, 28.6, 28.4, 28.4, 28.1, 28.1, 25.5, 24.9, 22.8, 22.8, 22.7, 19.2, 19.2, 14.1.

8.1.10. Synthesis of N-(2-aminoethyl)tricosa-10,12-diynamide (TR-EDA, 14)



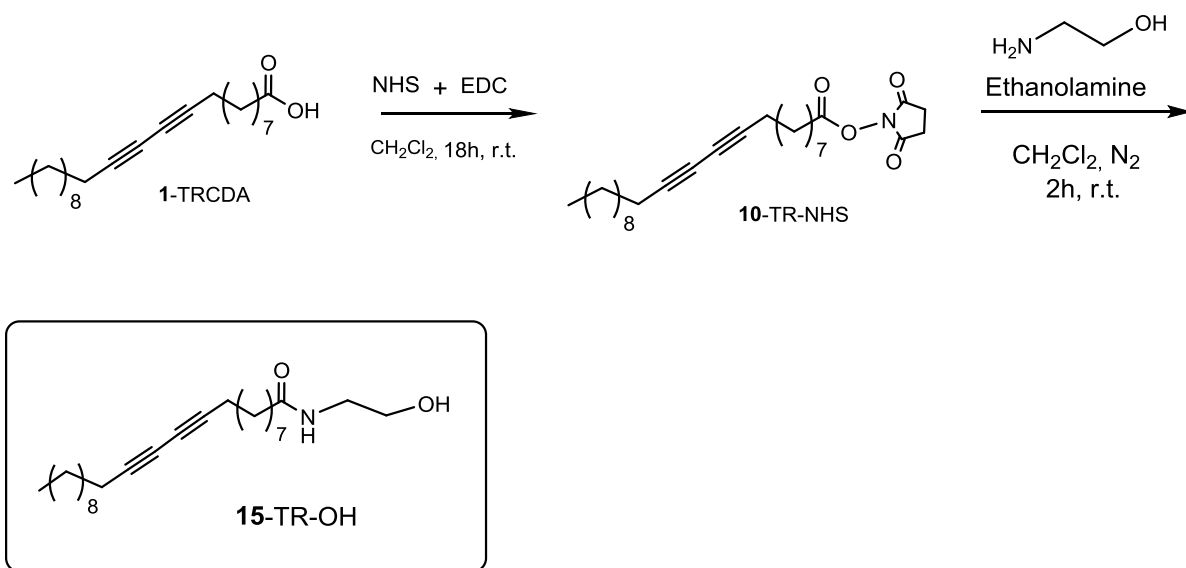
Step 1. Synthesis of 2,5-dioxopyrrolidin-1-yl tricosa-10,12-diynoate (TR-NHS - 10).

Step 2. Synthesis of N-(2-aminoethyl)tricosa-10,12-diynamide (TR-EDA- 14).

This reaction was carried out using modifications of the reported procedures¹²⁵. TR-NHS crude (1 eq, 0.25 mmol) was dissolved in methylene chloride (10 mL) and added dropwise into a solution of ethylenediamine (1.6 eq, 0.4mmol) in methylene chloride (2 mL). The mixture was then kept stirring for 4 h at room temperature. The mixture was extracted with methylene chloride (3 x 25 mL) and the organic phase was dried with sodium sulfate and rotary evaporated. The crude product was purified by column chromatography on silica gel eluted with a mixture of ethyl acetate and

methanol (70:30) to give N-(2-aminoethyl)deca-4,6-diynamide **14**, in 86% yield. Calcd for [M]C₂₅H₄₄N₂O, 388.64. ¹H NMR (400 MHz, CDCl₃): δ = 0.86–0.89 (t, J=8.0, 7.1 Hz, 3H), 1.23–1.30 (m, 22H), 1.46–1.53 (t, 8H), 2.15–2.28 (m, 6H), 2.89 (s, 2H), 3.32–3.37 (d, 2H), 6.16 (s, 1H). ¹³C NMR (100 MHz, CDCl₃): δ = 173.6, 77.5, 77.5, 65.3, 65.3, 41.6, 39.8, 36.8, 31.9, 29.6, 29.5, 29.3, 29.2, 29.2, 29.1, 28.9, 28.9, 28.7, 28.3, 25.7, 22.7, 19.2, 19.2, 14.1

8.1.11. Synthesis of N-(2-hydroxyethyl)tricos-a-10,12-diynamide (TR-OH, **15**)

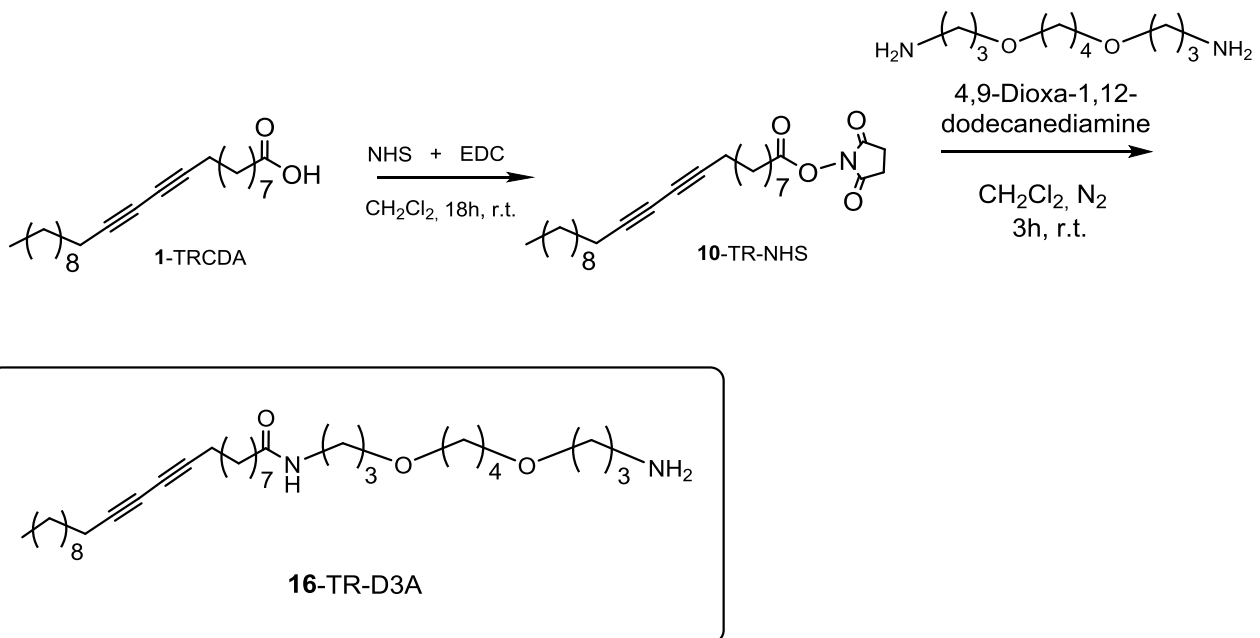


*Step 1. Synthesis of 2,5-dioxopyrrolidin-1-yl tricos-a-10,12-diynoate (TR-NHS - **10**).*

*Step 2. Synthesis of N-(2-hydroxyethyl)tricos-a-10,12-diynamide (TR-OH- **15**).*

This reaction was carried out using modifications of the reported procedure¹²⁶. TR-NHS crude (1 eq, 0.25 mmol) was dissolved in methylene chloride (10 mL) and added dropwise into a solution of ethanolamine (1.1 eq, 0.28 mmol) in methylene chloride (2 mL) followed by dropwise addition of triethylamine (1.2 eq, 0.3 mmol). The mixture was then kept stirring for 2 h at room temperature. The crude product was purified by column chromatography on silica gel eluted with a mixture of ethyl acetate and hexane (60:30) to give TR-OH **15**, in 73% yield. Calcd for [M]C₂₅H₄₃NO₂, 389.62. ¹H NMR (400 MHz, CDCl₃): δ = 0.86–0.89 (t, J=8.0, 7.1 Hz, 3H), 1.23–1.40 (m, 22H), 1.46–1.53 (t, 6H), 2.15–2.28 (m, 2H), 2.47–2.49 (m, 4H), 3.40–3.43 (d, 2H), 3.56–3.58 (t, 2H), 4.40 (s, 1H), 5.87 (s, 1H). ¹³C NMR (100 MHz, CDCl₃): δ = 173.6, 77.5, 77.5, 65.3, 65.3, 62.5, 41.6, 36.8, 31.9, 29.6, 29.6, 29.3, 28.9, 28.7, 28.7, 28.6, 28.4, 28.4, 28.1, 28.1, 25.6, 22.7, 19.2, 19.2, 14.1

8.1.12. Synthesis of N-(3-(4-(3-aminopropoxy)butoxy)propyl)tricos-a-10,12-diynamide (TR-D3A, **16**)

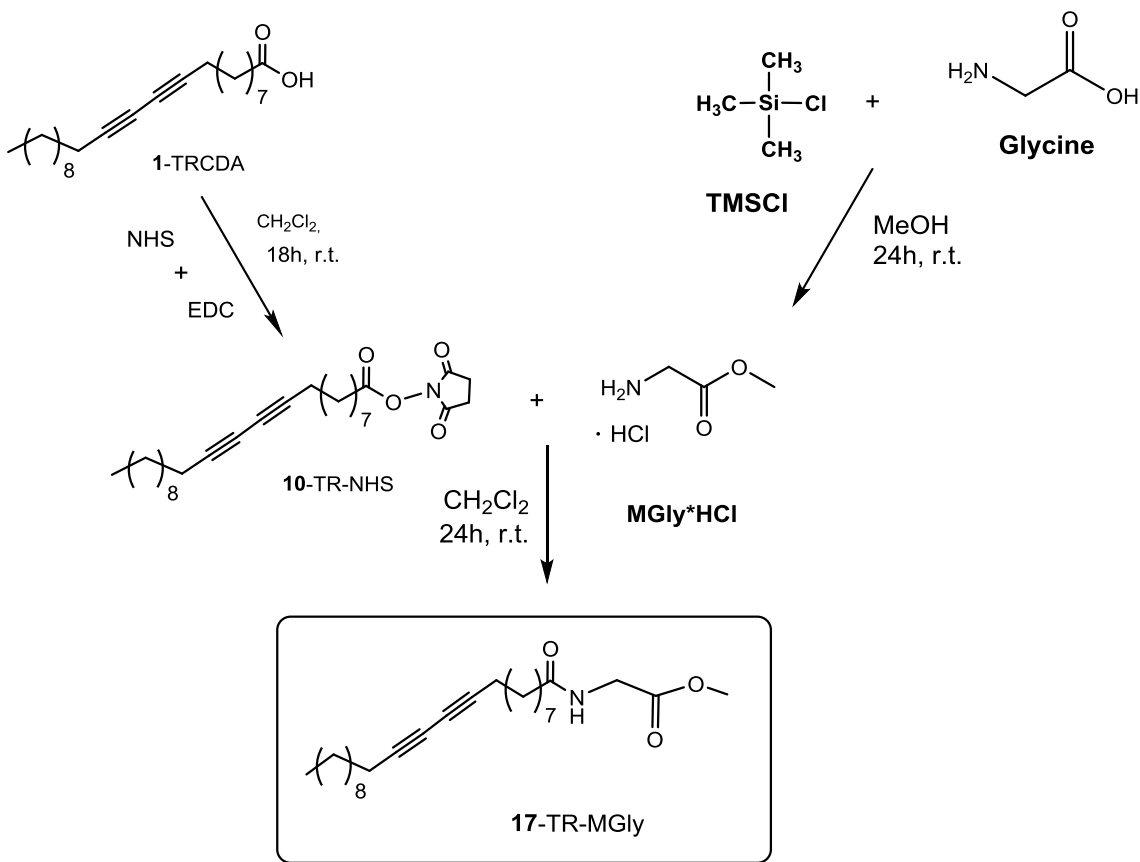


Step 1. Synthesis of 2,5-dioxopyrrolidin-1-yl tricosa-10,12-diynoate (TR-NHS - 10).

Step 2. Synthesis of N-(3-(4-(3-aminopropoxy)butoxy)propyl)tricosa-10,12-diynamide (TR-D3A-16).

This reaction was carried out using modifications of the procedures¹²⁵. TR-NHS crude (1 eq, 0.25 mmol) was dissolved in methylene chloride (10 mL) and added dropwise into a solution of D3A (1.2 eq, 0.3 mmol) in methylene chloride (2 mL). The mixture was then kept stirring for 3 h at room temperature. The crude product was purified by column chromatography on silica gel eluted with a mixture of ethyl acetate and methanol (60:40) to give TR-D3A **16**, in 93% yield. Calcd for [M]C₃₃H₆₀N₂O₃, 532.85. ¹H NMR (400 MHz, CDCl₃): δ = 0.84–0.87 (t, J=8.0, 7.1 Hz, 3H), 1.24–1.38 (m, 22H), 1.45–1.52 (mm, 12H), 2.10–2.14 (m, 4H), 2.20–2.23 (t, 2H), 2.59 (t, 4H), 2.71 (t, 2H), 3.06–3.09 (t, 2H), 3.29–3.56 (m, 8H), 6.16–6.19 (t, 1H). ¹³C NMR (100 MHz, CDCl₃): δ = 173.6, 77.5, 77.5, 72.3, 72.3, 65.3, 65.3, 64.7, 64.7, 39.8, 38.2, 36.8, 31.9, 29.6, 29.6, 29.6, 29.3, 29.1, 28.9, 28.7, 28.7, 28.6, 28.4, 28.4, 28.1, 28.1, 26.3, 26.3, 25.7, 22.7, 19.2, 19.2, 14.1

8.1.13. Synthesis of methyl tricosa-10,12-diynoylglycinate (TR-MGly, 17)



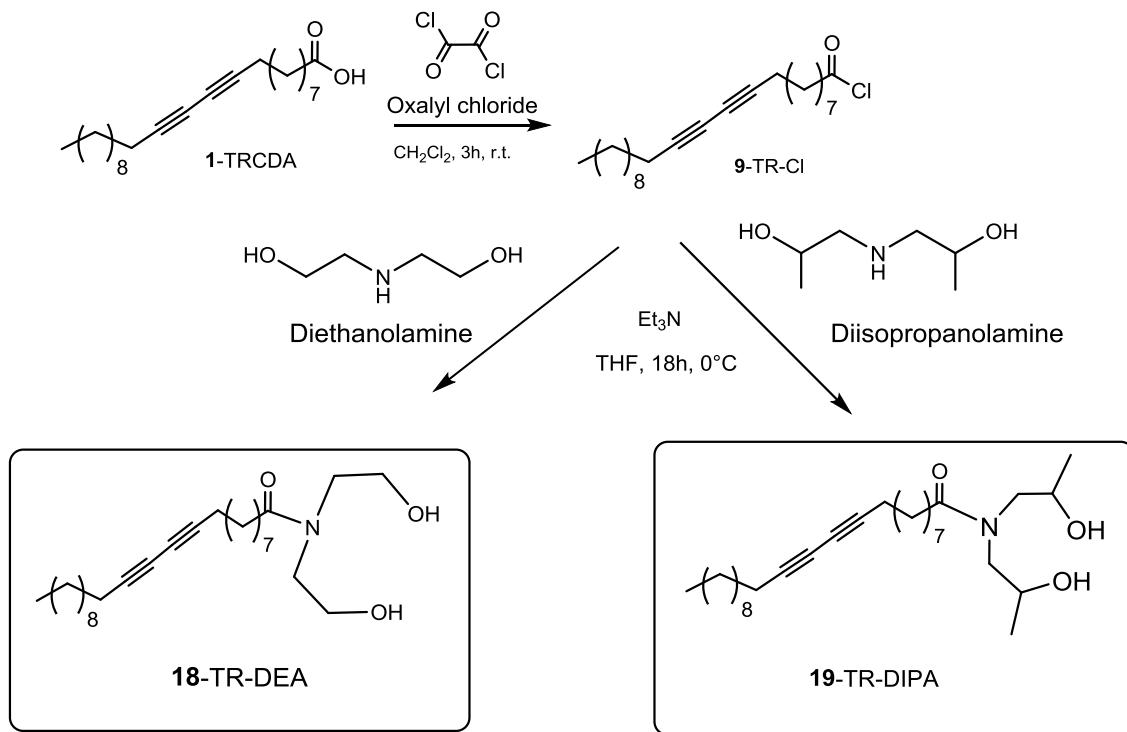
*Step 1. Synthesis of Glycine methyl ester * HCl (MGly * HCl).* Synthetic procedure has been adapted from a previously reported one¹²⁴.

*Step 2. Synthesis of 2,5-dioxopyrrolidin-1-yl tricos-a-10,12-dynoate (TR-NHS - **10**).*

*Step 3. Synthesis of Methyl tricos-a-10,12-dynoylglycinate (TR-MGly - **17**)*

Procedure was adapted from a previously reported one⁴⁶. TR-NHS crude (1 eq, 0.25 mmol) is solubilized in **CH₂Cl₂** (15 mL) in a round bottom flask under a gentle flux of **N₂** and avoiding light contact. MGly*HCl (3 eq, 0.75 mmol) is added to the mixture followed by dropwise addition of triethylamine (1.2 eq, 0.3 mmol). The reaction is stirred at r.t. for 24 h. Reaction monitored by Thin Layer Chromatography (TLC), the mixture purified with column chromatography (ethylacetate : cyclohexane = 1 : 5 to 1 : 2 gradient elution) to yield the product TR-MGly, **17**. The solvent is removed under a gentle flux of an inert gas. **Yield:** white solid (77 %). MW: Calcd for [M]C₂₆H₄₃NO₃, 417.63. ¹H NMR (400 MHz, CDCl₃): δ = 0.84–0.87 (t, J=8.0, 7.1 Hz, 3H), 1.23–1.36 (m, 22H), 1.46–1.49 (t, 6H), 1.60–1.65 (m, 2H), 2.20–2.23 (m, 4H), 3.74 (s, 3H), 4.02–4.04 (d, 2H), 5.93 (s, 1H). ¹³C NMR (100 MHz, CDCl₃): δ = 173.2, 170.6, 77.6, 77.6, 65.2, 65.2, 52.3, 41.2, 36.4, 31.9, 29.7, 29.4, 29.3, 29.1, 29.0, 28.9, 28.8, 28.7, 28.3, 28.2, 25.5, 22.6, 19.1, 19.1, 14.1.

8.1.14. Synthesis of N,N-bis(2-hydroxyethyl)tricos-a-10,12-dynamide (**TR-DEA**, **18**) and N,N-bis(2-hydroxypropyl)tricos-a-10,12-dynamide (**TR-DIPA**, **19**)



Step 1. Synthesis of tricos-10,12-dynoyl chloride (TR-Cl, 9).

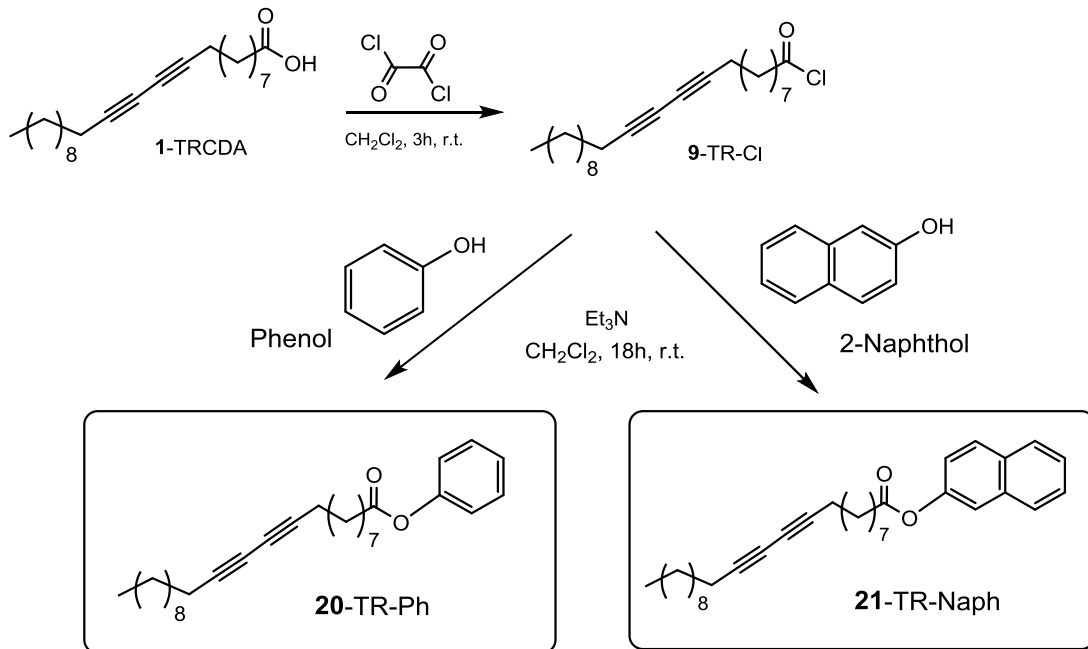
Step 2. Synthesis of N,N-bis(2-hydroxyethyl)tricos-10,12-dynamide (TR-DEA, 18).

Procedure was a modification of previously reported one¹²⁷. The THF solution containing diethanolamine (1.1 eq, 1.54 mmol) and Et₃N (1.2 eq, 1.68 mmol) were added to **9** (1 eq, 1.40 mmol). The resultant solution was stirred at 0°C overnight and concentrated in vacuum at r.t. After checking in TLC, extracted with CH₂Cl₂/Brine solution and then the mixture is purified by column chromatography (CH₂Cl₂ : MeOH = 9 : 1 to 4 : 1 gradient elution) to yield the TR-DEA **18** (86 %). MW: Calcd for [M] C₂₇H₄₇NO₃, 433.68. ¹H NMR (400 MHz, CDCl₃): δ = 0.84–0.88 (t, J=8.0, 7.1 Hz, 3H), 1.24–1.62 (m, 31H), 2.20–2.24 (t, 4H), 2.30–2.39 (m, 3H), 3.48–3.57 (tt, 3H), 3.77–3.87 (tt, 3H). ¹³C NMR (300 MHz, CDCl₃) δ = 173.3, 77.5, 77.5, 65.2, 65.2, 57.8, 57.8, 53.7, 53.7, 36.6, 31.8, 30.4, 29.6, 29.6, 29.4, 29.0, 28.7, 28.7, 28.6, 28.4, 28.4, 28.1, 28.1, 22.6, 19.2, 19.2, 14.1.

Step 2. Synthesis of N,N-bis(2-hydroxypropyl)tricos-10,12-dynamide (TR-DIPA, 19).

Procedure was a modification of previously reported one¹²⁷. The THF solution containing diisopropanolamine (1.1 eq, 1.54 mmol) and Et₃N (1.2 eq, 1.68 mmol) were added to **9** (1 eq, 1.40 mmol). The resultant solution was stirred at 0°C overnight and concentrated in vacuum at r.t. After checking in TLC, extracted with CH₂Cl₂/Brine solution and then the mixture is purified by column chromatography (CH₂Cl₂ : MeOH = 9 : 1 to 4 : 1 gradient elution) to yield the TR-DIPA **19** (82 %). MW: Calcd for [M] C₂₉H₅₁NO₃, 461.73. ¹H NMR (400 MHz, CDCl₃): δ = 0.81–0.88 (t, J=8.0, 7.1 Hz, 3H), 1.17–1.41 (d, 6H), 1.45–1.63 (m, 28H), 2.20–2.44 (m, 6H), 3.06–3.43 (mm, 4H), 3.98–4.22 (mm, 2H), 7.70 (s, 2H). ¹³C NMR (100 MHz, CDCl₃): δ = 173.6, 77.5, 77.5, 67.0, 67.0, 65.3, 65.3, 59.7, 59.7, 35.8, 31.9, 29.6, 29.6, 29.3, 29.2, 29.2, 29.1, 28.9, 28.7, 28.7, 28.3, 28.3, 25.6, 22.7, 21.4, 21.4, 19.2, 19.2, 14.1.

8.1.15. Synthesis of phenyl tricosa-10,12-dynoate (TR-Ph, 20) and naphthalen-2-yl tricosa-10,12-dynoate (TR-Naph, 21)



Step 1. Synthesis of tricosa-10,12-dynoyl chloride (TR-Cl, 9).

Step 2. Synthesis of phenyl tricosa-10,12-dynoate (TR-Ph, 20).

Procedure was a modification of previously reported one⁴⁹. Phenol (2 eq, 2.80 mmol) and Et_3N (3 eq, 4.20 mmol) were dissolved in CH_2Cl_2 and **9** (1 eq, 1.40 mmol) was dissolved in a small amount of anhydrous THF. The THF solution containing **9** was added dropwise into the CH_2Cl_2 solution. The resultant solution was stirred at room temperature overnight and concentrated in vacuum. After checking in TLC, extracted with CH_2Cl_2 /Brine solution, dried over Na_2SO_4 , filtered, solvent evaporated. Crude product is purified by column chromatography (EtOAc : Cyclohexane = 1 : 9 to 1 : 2 gradient elution) to yield the TR-Ph **20** (85 %). MW: Calcd for [M] $\text{C}_{29}\text{H}_{42}\text{O}_2$, 422.65. ^1H NMR (400 MHz, CDCl_3): δ = 0.85–0.88 (t, J =8.0, 7.1 Hz, 3H), 1.24–1.42 (m, 22H), 1.46–1.53 (m, 4H), 1.70–1.77 (q, 2H) 2.20–2.25 (m, 4H), 2.52–2.55 (t, 2H), 7.05–7.07 (t, J =7.5, 1.5 Hz, 2H), 7.18–7.22 (t, 2H), 7.34–7.38 (t, 1H). ^{13}C NMR (100 MHz, CDCl_3): δ = 172.7, 150.6, 129.2, 129.2, 126.2, 120.4, 120.4, 76.7, 76.7, 65.3, 65.3, 33.8, 31.9, 29.3, 29.3, 29.1, 29.1, 28.9, 28.5, 28.5, 28.3, 28.3, 28.1, 28.1, 24.9, 22.6, 19.2, 19.2, 14.1.

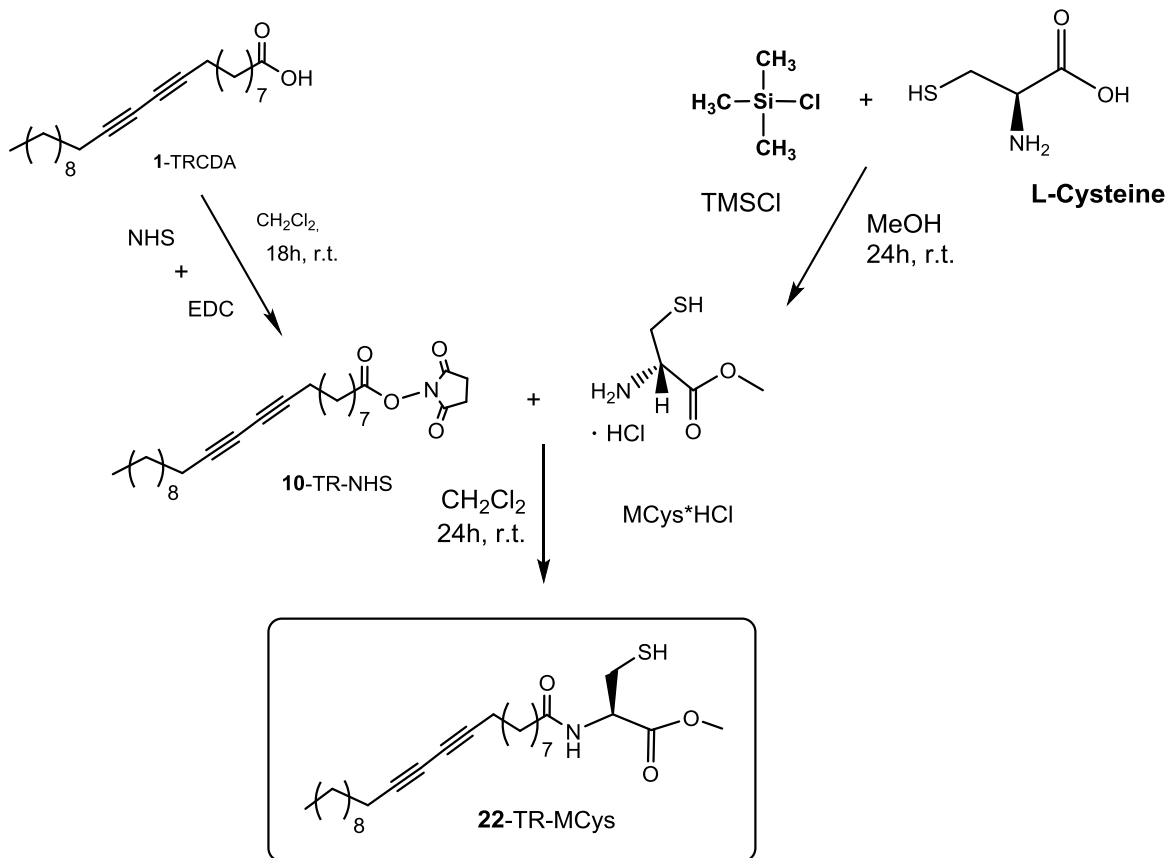
Step 1. Synthesis of tricosa-10,12-dynoyl chloride (TR-Cl, 9).

Step 2. Synthesis of naphthalen-2-yl tricosa-10,12-dynoate (TR-Naph, 21)

Procedure was a modification of previously reported one⁴⁹. Naphthol (2 eq, 2.80 mmol) and Et_3N (3 eq, 4.20 mmol) were dissolved in CH_2Cl_2 and **9** (1 eq, 1.40 mmol) was dissolved in a small amount of anhydrous THF. The THF solution containing **9** was added dropwise into the CH_2Cl_2 solution. The resultant solution was stirred at room temperature overnight and concentrated in vacuum. After checking in TLC, extracted with CH_2Cl_2 /Brine solution, dried over Na_2SO_4 , filtered, solvent

evaporated. Crude product is purified by column chromatography (EtOAc : Cyclohexane = 1 : 9 to 1 : 2 gradient elution) to yield the TR-Naph **21** (95%). MW: Calcd for [M] C₃₃H₄₄O₂, 472.71. ¹H NMR (400 MHz, CDCl₃): δ = 0.85–0.88 (t, J=8.0, 7.1 Hz, 3H), 1.28–1.55 (m, 26H), 1.74–1.81 (m, 2H), 2.20–2.26 (m, 4H), 2.57–2.61 (t, 2H), 7.19–7.22 (d, J=7.5, 1.5 Hz, 1H), 7.42–7.52 (m, 2H), 7.53–7.54 (s, 1H), 7.77–7.84 (m, 3H). ¹³C NMR (100 MHz, CDCl₃): δ = 172.7, 150.6, 135.6, 132.0, 129.2, 127.7, 127.7, 126.2, 125.1, 123.3, 120.4, 76.7, 76.7, 65.3, 65.3, 33.8, 31.9, 29.3, 29.3, 29.1, 29.1, 28.9, 28.5, 28.5, 28.3, 28.3, 28.1, 28.1, 24.9, 22.6, 19.2, 19.2, 14.1.

8.1.16. Synthesis of methyl tricosa-10,12-diynoyl-L-cysteinate (TR-MCys, **22**)



*Step 1. Synthesis of Glycine methyl ester * HCl (MCys * HCl).* Synthetic procedure has been adapted from a previously reported one¹²⁴.

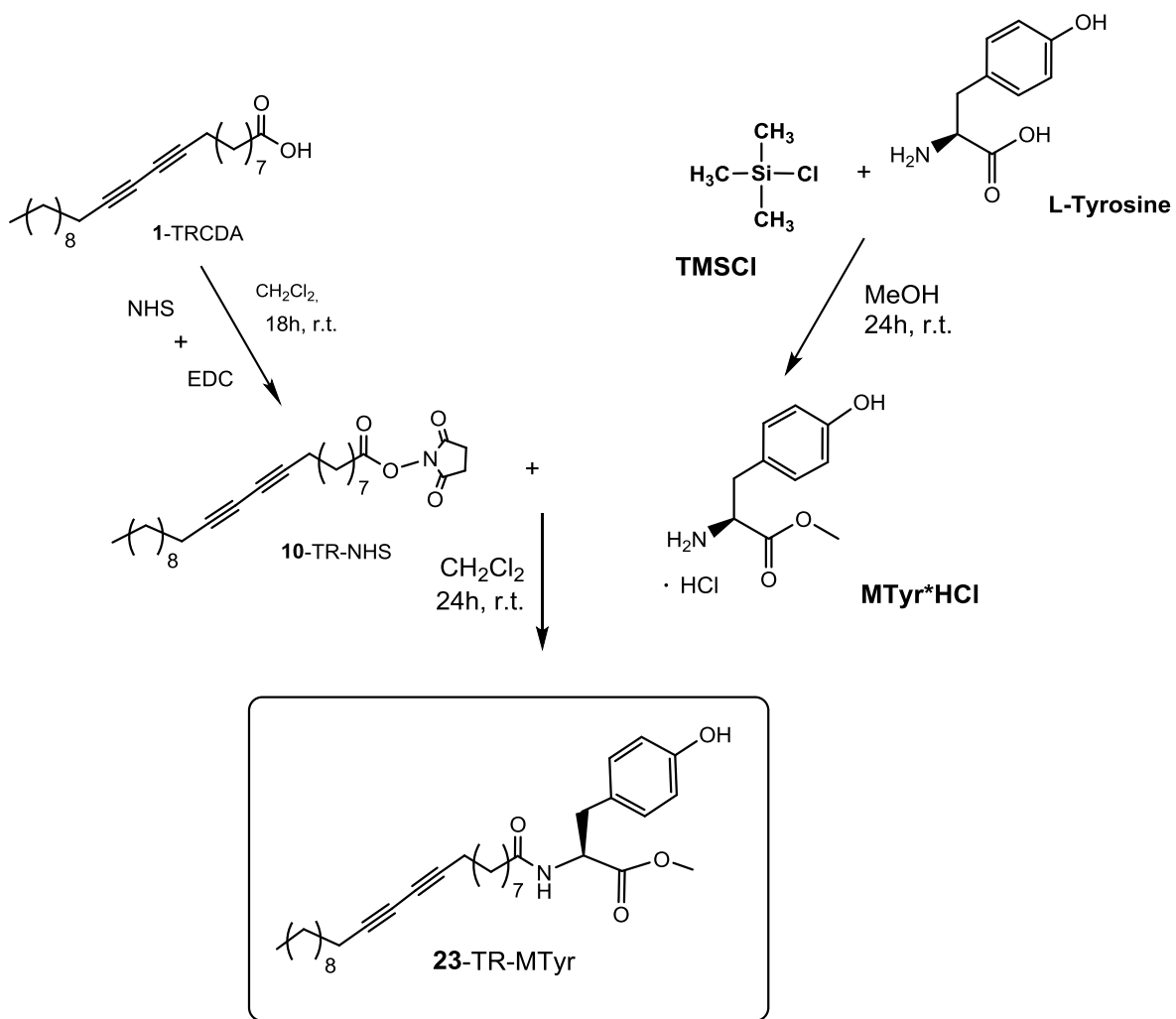
*Step 2. Synthesis of 2,5-dioxopyrrolidin-1-yl tricosa-10,12-diynoate (TR-NHS - **10**).*

*Step 3. Synthesis of Methyl tricosa-10,12-diynoyl-L-cysteinate (TR-MCys- **22**)*

Procedure was a modification of previously reported one⁴⁶. TR-NHS crude (1 eq, 0.25 mmol) is solubilized in CH₂Cl₂ (15 mL) in a round bottom flask under a gentle flux of N₂ and avoiding light contact. MCys*HCl (3 eq, 0.75 mmol) is added to the mixture followed by dropwise addition of triethylamine (1.2 eq, 0.3 mmol). The reaction is stirred at r.t. for 24 h. Reaction monitored by Thin Layer Chromatography (TLC), the mixture purified with column chromatography (CH₂Cl₂ : MeOH = 20 : 1 to 1 : 20 gradient elution) to yield the product TR-MCys, **22**. The solvent is removed under a gentle flux of an inert gas. **Yield:** white solid (28 %). MW: Calcd for [M] C₂₇H₄₅NO₃S, 463.72. ¹H NMR (400 MHz, CD₃OD): δ = 0.84–0.87 (t, J=8.0, 7.1 Hz, 3H), 1.23–1.39 (m, 22H), 1.43–1.93 (m, 7H), 2.05–2.08 (q, 2H), 2.12–2.15 (m, 4H), 3.17–3.24 (m, 2H), 3.77 (s, 3H), 4.83–5.05 (m, 1H),

6.98 (s, 1H). ^{13}C NMR (100 MHz, CDCl_3): $\delta = 173.8, 171.2, 77.4, 77.4, 65.3, 65.3, 55.3, 50.2, 36.4, 31.9, 29.7, 29.7, 29.4, 28.9, 28.7, 28.7, 28.6, 28.4, 28.4, 28.1, 28.1, 26.7, 25.5, 22.6, 19.1, 19.1, 14.1$.

8.1.17. Synthesis of methyl tricosa-10,12-diynoyl-L-tyrosinate (TR-Tyr, 23)



*Step 1. Synthesis of L-tyrosine methyl ester * HCl (MTyr * HCl).* Synthetic procedure has been adapted from a previously reported one¹²⁴.

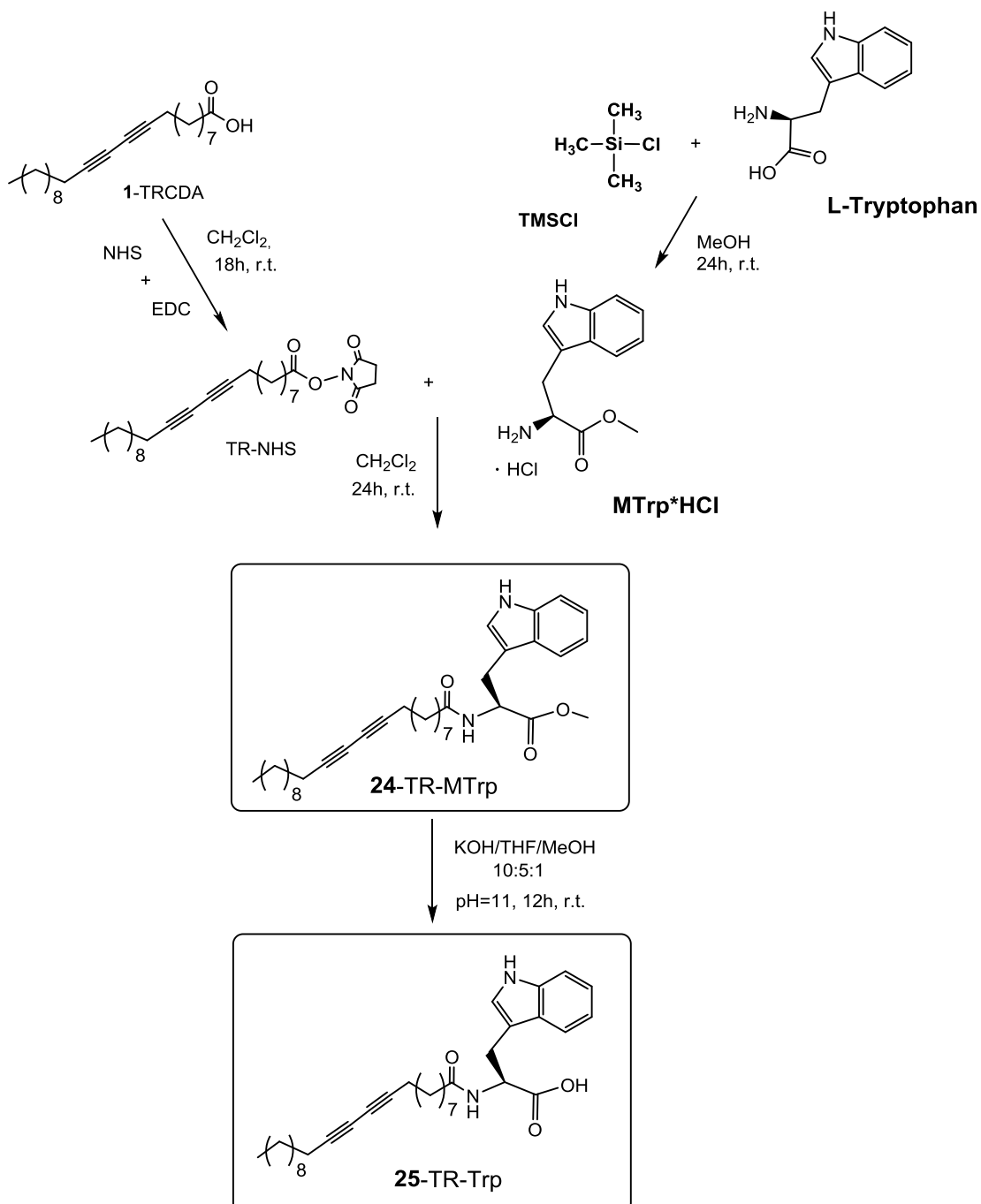
Step 2. Synthesis of 2,5-dioxopyrrolidin-1-yl tricos-10,12-diynoate (TR-NHS - 10)

Step 3. Synthesis of methyl tricosa-10,12-diynoyl-L-tyrosinate (TR-MTyr - 23)

Procedure was a modification of previously reported one⁴⁶. TR-NHS crude (1 eq, 0.24 mmol) is solubilized in CH_2Cl_2 (15 mL) in a round bottom flask under a gentle flux of N_2 and avoiding light contact (wrapping the flask with an aluminum foil). MTyr*HCl (3 eq, 0.72 mmol) is added to the mixture followed by dropwise addition of triethylamine (Et_3N , 1.2 eq, 0.29 mmol). The reaction is stirred at r.t. for 24 h. After checking in TLC, extracted with CH_2Cl_2 /Brine solution and then the mixture is purified by column chromatography ($\text{CH}_2\text{Cl}_2 : \text{MeOH} = 9 : 1$ to $1 : 1$ gradient elution) to yield the product. The solvent is removed under a gentle flux of N_2 . **Yield:** TR-Tyr 23, white

powder (85 %). MW: Calcd for [M] C₃₃H₄₉NO₄, 523.76. ¹H NMR (400 MHz, CDCl₃): δ = 0.84–0.87 (t, J=8.0, 7.1 Hz, 3H), 1.24–1.41 (m, 22H), 1.45–1.57 (m, 6H), 2.10–2.13 (t, 2H), 2.24–2.27 (t, 4H), 3.05–3.12 (m, 2H), 3.46 (s, 3H), 3.93–4.01 (t, 1H), 6.68–6.96 (dd, J=7.5, 1.5 Hz, 4H), 7.24 (s, 1H), 12.02 (s, 1H). ¹³C NMR (100 MHz, CDCl₃): δ = 172.6, 172.1, 155.7, 130.2, 130.2, 129.2, 115.8, 115.8, 75.0, 75.0, 65.2, 65.2, 56.8, 51.9, 36.8, 36.5, 31.9, 29.6, 29.6, 28.9, 28.7, 28.7, 28.6, 28.4, 28.4, 28.1, 28.1, 25.5, 22.6, 19.2, 19.2, 14.1.

8.1.18. Synthesis of methyl tricosa-10,12-diynoyl-L-tryptophanate (TR-MTrp, 24) and tricosa-10,12-diynoyl-L-tryptophan (TR-Trp, 25)



*Step 1. Synthesis of L-Tryptophan methyl ester * HCl (MTrp * HCl).* Synthetic procedure has been adapted from a previously reported one¹²⁴.

Step 2. Synthesis of 2,5-dioxopyrrolidin-1-yl tricosa-10,12-diynoate (TR-NHS - 10)

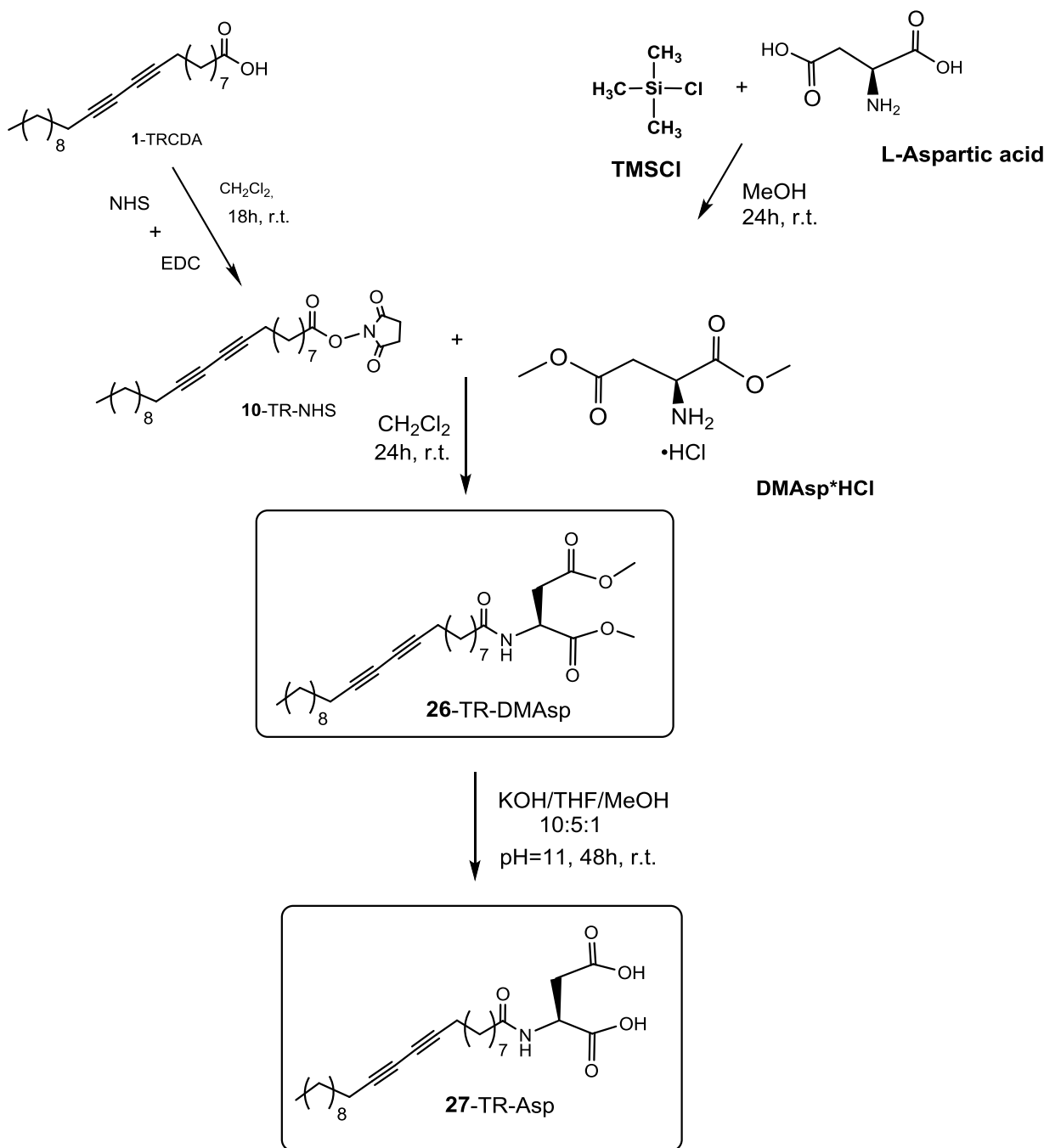
Step 3. Synthesis of methyl tricosa-10,12-diynoyl-L-tryptophanate (TR-MTrp - 24)

Procedure was a modification of previously reported one⁴⁶. TR-NHS crude (1 eq, 0.24 mmol) is solubilized in CH₂Cl₂ (15 mL) in a round bottom flask under a gentle flux of N₂ and avoiding light contact (wrapping the flask with an aluminum foil). MTrp*HCl (2 eq, 0.49 mmol) is added to the mixture followed by dropwise addition of triethylamine (Et₃N, 1.2 eq, 0.29 mmol). The reaction is stirred at r.t. for 24 h. After checking in TLC, extracted with CH₂Cl₂/Brine solution and then the mixture is purified by column chromatography (ethylacetate : cyclohexane = 1 : 5 to 5 : 1 gradient elution) to yield the TR-MTrp **24**. The solvent is removed under a gentle flux of N₂. **Yield:** white powder (80 %). MW: Calcd for [M] C₃₅H₅₀N₂O₃, 546.8. ¹H NMR (400 MHz, CDCl₃): δ = 0.84–0.87 (t, J=8.0, 7.1 Hz, 3H), 1.24–1.41 (m, 22H), 1.43–1.57 (m, 6H), 2.08–2.22 (tt, 6H), 3.26–3.32 (mm, 2H), 3.71 (s, 3H), 4.89–4.96 (q, 1H), 5.90–5.94 (d, 1H), 6.96 (s, 1H), 7.08–7.20 (tt, J=7.5, 1.5 Hz, 2H), 7.35–7.39 (d, 1H), 7.50–7.52 (d, 1H), 8.08 (s, 1H), 10.38 (s, 1H). ¹³C NMR (100 MHz, CDCl₃): δ = 172.6, 172.1, 135.8, 129.2, 123.0, 121.7, 119.8, 118.8, 111.1, 110.7, 76.7, 76.7, 65.2, 65.2, 57.8, 52.3, 36.5, 31.8, 29.6, 29.6, 29.3, 28.9, 28.7, 28.7, 28.6, 28.5, 28.4, 28.4, 28.1, 28.1, 25.5, 22.6, 19.2, 19.2, 14.1.

Step 4. Synthesis of tricosa-10,12-diynoyl-L-tryptophan (TR-Trp - 25)

Compound **24** (110 mg, 0.189 mmol) was dissolved in 10:5:1 H₂O/THF/MeOH (32 mL), and the pH of the solution was adjusted to 11 with 1 M KOH. The reaction mixture was stirred at 35 °C, and product formation was monitored by TLC (2:1 EtOAc/Cyclohexane). The reaction was quenched after 12 h via the addition of Amberlist₁₅ (H⁺ form) ion-exchange resin to pH 4. The crude product was concentrated and extracted w/ethyl ether. TR-Trp **25** (60 mg) was isolated in 60% yield (white brownish film). MW: Calcd for [M] C₃₄H₄₈N₂O₃, 532.77. ¹H NMR (400 MHz, Ether-d₁₀): δ = 0.84–0.88 (t, J=8.0, 7.1 Hz, 3H), 1.15 (s, 1H), 1.24–1.40 (m, 22H), 1.44–1.53 (m, 6H), 2.05–2.08 (t, 2H), 2.18–2.22 (q, 4H), 3.06–3.39 (qq, 2H), 4.56–4.59 (t, 1H), 4.79–4.84 (s, 1H), 6.96–6.99 (t, J=7.5, 1.5 Hz, 1H), 7.03–7.08 (t, 1H), 7.24–7.27 (d, 1H), 7.52–7.57 (d, 1H), 7.68 (s, 1H), 12.68 (s, 1H). ¹³C NMR (125 MHz, 3:2 CD₃OD/CDCl₃): δ=175.0, 174.6, 136.8, 127.4, 123.0, 121.7, 119.8, 118.8, 111.1, 109.7, 77.6, 77.6, 66.1, 66.1, 60.3, 37.2, 32.7, 29.6, 29.3, 28.9, 28.7, 28.7, 28.6, 28.4, 28.2, 28.1, 28.1, 25.8, 22.6, 19.5, 19.5, 14.1.

8.1.19. Synthesis of dimethyl tricosa-10,12-diynoylaspartate (TR-DMAsp, **26**) and tricosa-10,12-diynoylaspartic acid (TR-Asp, **27**)



Step 1. Synthesis of L-Aspartic acid dimethyl ester * HCl (DMAsp* HCl). Synthetic procedure has been adapted from a previously reported one¹²⁴.

Step 2. Synthesis of 2,5-dioxopyrrolidin-1-yl tricos-10,12-dynoate (TR-NHS - 10)

Step 3. Synthesis of dimethyl tricos-10,12-dynoylaspartate (TR-DMAsp - 26)

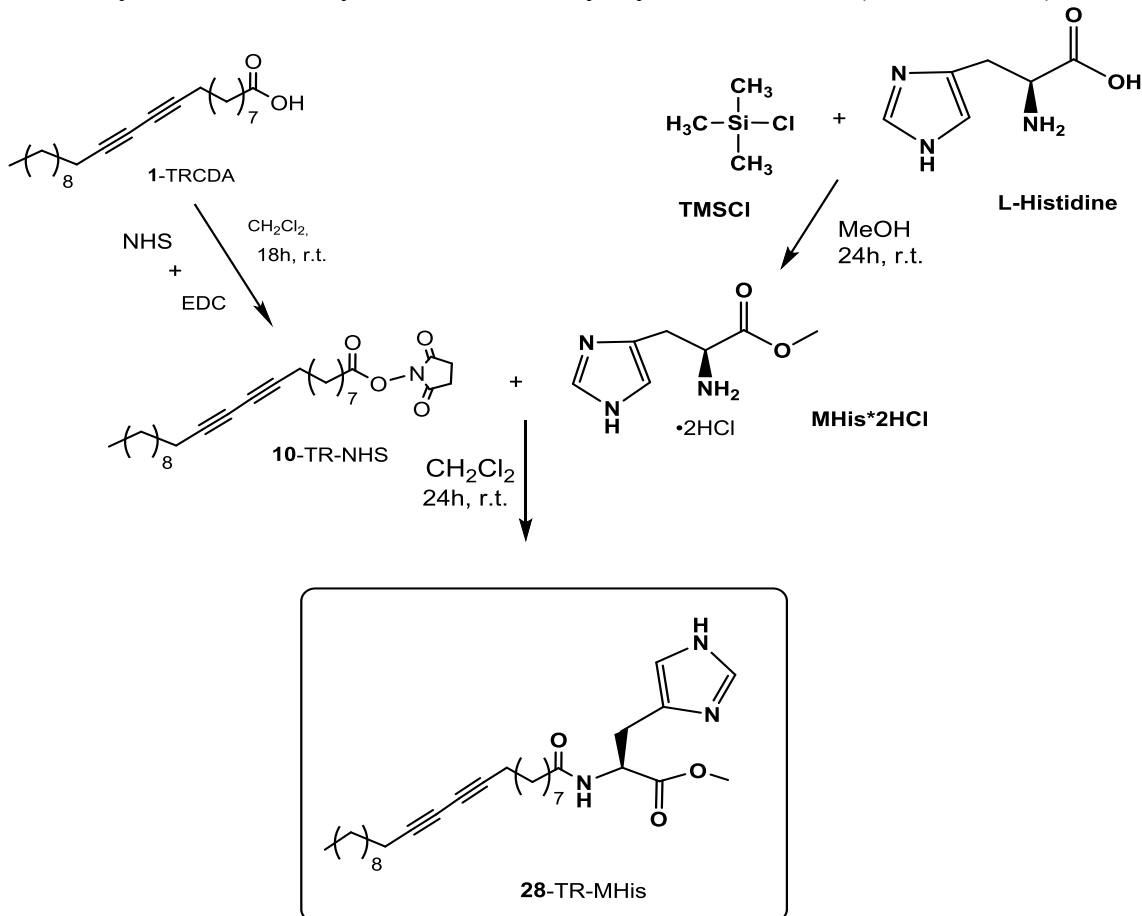
Procedure was a modification of previously reported one⁴⁶. TR-NHS crude (1 eq, 0.24 mmol) is solubilized in CH_2Cl_2 (15 mL) in a round bottom flask under a gentle flux of N_2 and avoiding light contact (wrapping the flask with an aluminum foil). DMAsp*HCl (2.5 eq, 0.60 mmol) is added to the mixture followed by dropwise addition of triethylamine (Et_3N , 2 eq, 0.49 mmol). The reaction is stirred at r.t. for 24 h. After checking in TLC, extracted with CH_2Cl_2 /Brine solution and then the

mixture is purified by column chromatography (CH_2Cl_2 : MeOH = 9 : 1 to 1 : 1 gradient elution) to yield the TR-DMAasp **26**. The solvent is removed under a gentle flux of N_2 . Yield: white powder (97 %). MW: Calcd for [M] $\text{C}_{29}\text{H}_{47}\text{NO}_5$, 489.7. ^1H NMR (400 MHz, 3:2 $\text{CD}_3\text{OD}/\text{CDCl}_3$): δ = 0.84–0.87 (t, J =8.0, 7.1 Hz, 3H), 1.24–1.41 (m, 22H), 1.45–1.57 (m, 6H), 2.05–2.08 (t, 2H), 2.28–2.32 (m, 4H), 2.47–2.51 (mm, 2H), 2.99 (s, 3H), 3.48 (s, 3H), 3.71 (m, 1H), 5.29 (s, 1H). ^{13}C NMR (100 MHz, 3:2 $\text{CD}_3\text{OD}/\text{CDCl}_3$): δ = 173.9, 171.5, 169.3, 76.7, 76.7, 65.2, 65.2, 55.8, 52.3, 52.3, 37.0, 36.5, 31.8, 29.5, 29.5, 29.3, 28.9, 28.7, 28.7, 28.6, 28.3, 28.3, 28.1, 28.1, 25.5, 22.6, 19.2, 19.2, 14.1.

Step 4. Synthesis of tricosa-10,12-diynoylaspartic acid (TR-Asp-27)

Compound **26** (167 mg, 0.341 mmol) was dissolved in 10:5:1 $\text{H}_2\text{O}/\text{THF}/\text{MeOH}$ (100 mL), and the pH of the solution was adjusted to 11 with 1 M KOH. The reaction mixture was stirred at 35 °C, and product formation was monitored by TLC (CH_2Cl_2 : MeOH = 4 : 1). The reaction was quenched after 48 h via the addition of Amberlist₁₅ (H⁺ form) ion-exchange resin to pH 4. The crude product was concentrated and extracted w/ethyl ether, solvent removed under a gentle flux of N_2 . TR-Asp **27** (62 mg) was isolated in 35% yield (white powder). MW: Calcd for [M] $\text{C}_{27}\text{H}_{43}\text{NO}_5$, 461.64. ^1H NMR (400 MHz, CD_3OD): δ = 0.84–0.88 (t, J =8.0, 7.1 Hz, 3H), 1.24–1.65 (m, 22H), 1.83–1.90 (mm, 6H), 2.05–2.08 (t, 2H), 2.46–2.51 (t, 4H), 3.69–3.72 (mm, 2H), 4.33–4.37 (m, 1H), 5.28 (s, 1H), 12.56 (s, 2H). ^{13}C NMR (100 MHz, CD_3OD): δ = 173.7, 173.3, 172.3, 76.7, 76.7, 65.2, 65.2, 54.3, 36.5, 35.9, 31.9, 29.5, 29.5, 29.3, 28.9, 28.7, 28.7, 28.6, 28.4, 28.4, 28.1, 28.1, 25.5, 22.8, 19.2, 19.2, 14.1.

8.1.20. Synthesis of methyl tricosa-10,12-diynoyl-L-histidinate (TR-MHis, **28**)



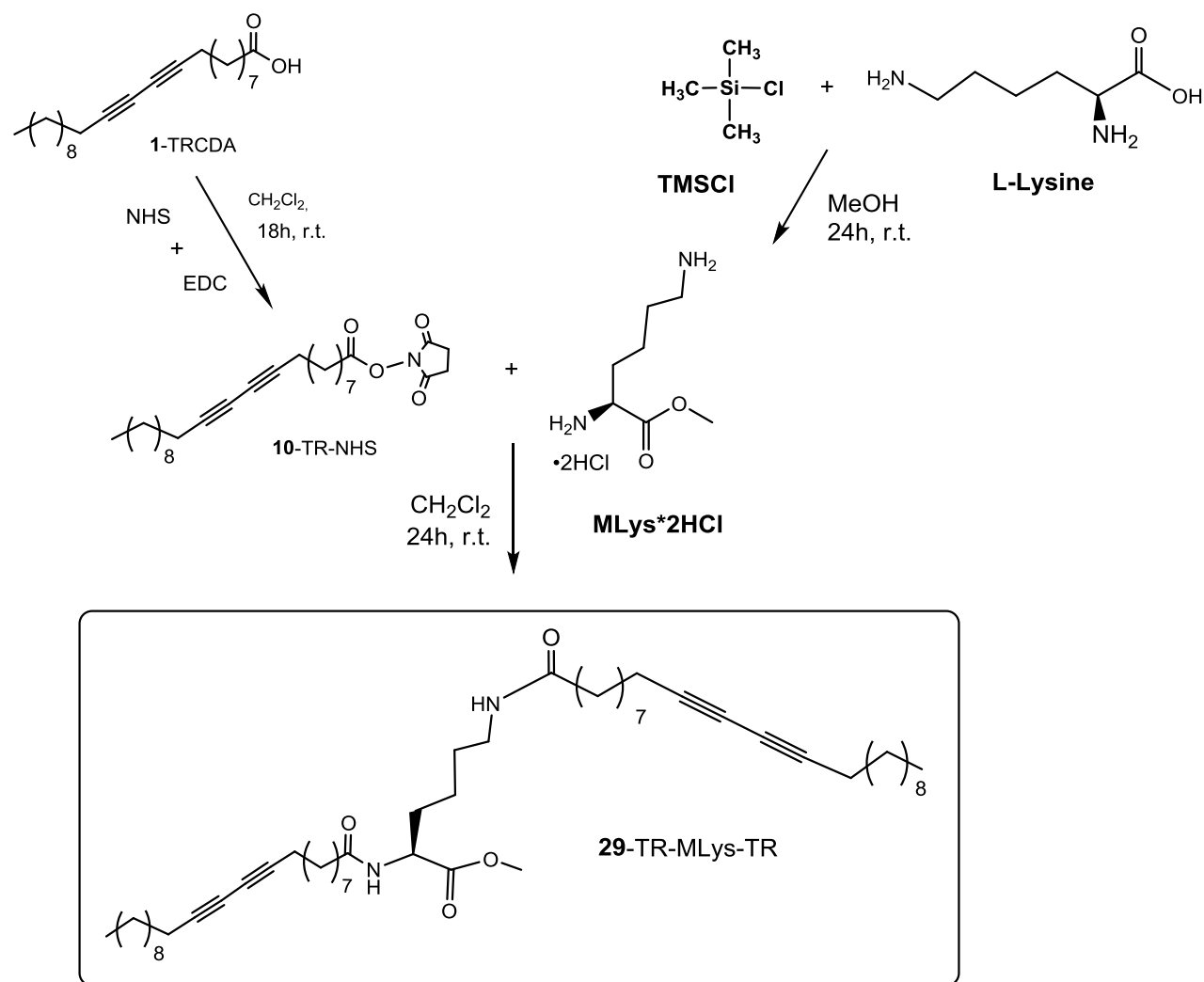
*Step 1. Synthesis of L-Histidine methyl ester dihydrochloride (MHis * 2HCl).* Synthetic procedure has been adapted from a previously reported one¹²⁴.

Step 2. Synthesis of 2,5-dioxopyrrolidin-1-yl tricos-10,12-dynoate (TR-NHS - 10).

Step 3. Synthesis of methyl tricos-10,12-dynoyl-L-histidinate (TR-MHis - 28)

Procedure was a modification of previously reported one⁴⁶. TR-NHS crude (1 eq, 0.25 mmol) is solubilized in CH₂Cl₂ (5 mL) in a round bottom flask under a gentle flux of N₂ and avoiding light contact. MHis*2HCl (2 eq, 0.5 mmol) is added to the mixture followed by dropwise addition of triethylamine (1.2 eq, 0.3 mmol). The reaction is stirred at r.t. for 24 h. Reaction monitored by Thin Layer Chromatography (TLC), the mixture purified with column chromatography (CH₂Cl₂ : MeOH = 20 : 1 to 1 : 20 gradient elution), the solvents are removed under a gentle flux of an inert gas to isolate the product, TR-MHis, **28**, with 45 % yield. MW: Calcd for [M] C₃₀H₄₇N₃O₃, 497.72. ¹H NMR (400 MHz, CDCl₃): δ = 0.84–0.87 (t, J=8.0, 7.1 Hz, 3H), 1.24–1.37 (m, 22H), 1.43–1.51 (mm, 6H), 2.05–2.08 (t, 2H), 2.40–2.45 (t, 4H), 2.68 (s, 3H), 3.17–3.22 (mm, 2H), 4.98 (t, 1H), 5.18 (d, 1H), 7.23 (s, 1H), 7.54 (d, J=7.5, 1.5 Hz, 1H), 12.78 (s, 1H). ¹³C NMR (100 MHz, CDCl₃): δ = 173.6, 171.7, 137.4, 124.6, 114.0, 76.7, 76.7, 65.2, 65.2, 56.2, 52.2, 36.5, 31.9, 29.6, 29.6, 29.3, 28.9, 28.7, 28.7, 28.6, 28.4, 28.4, 28.1, 28.1, 25.7, 22.7, 19.2, 19.2, 14.1.

8.1.21. Synthesis of methyl N², N⁶-di(tricos-10,12-dynoyl)lysinate (TR-MLys-TR, 24)



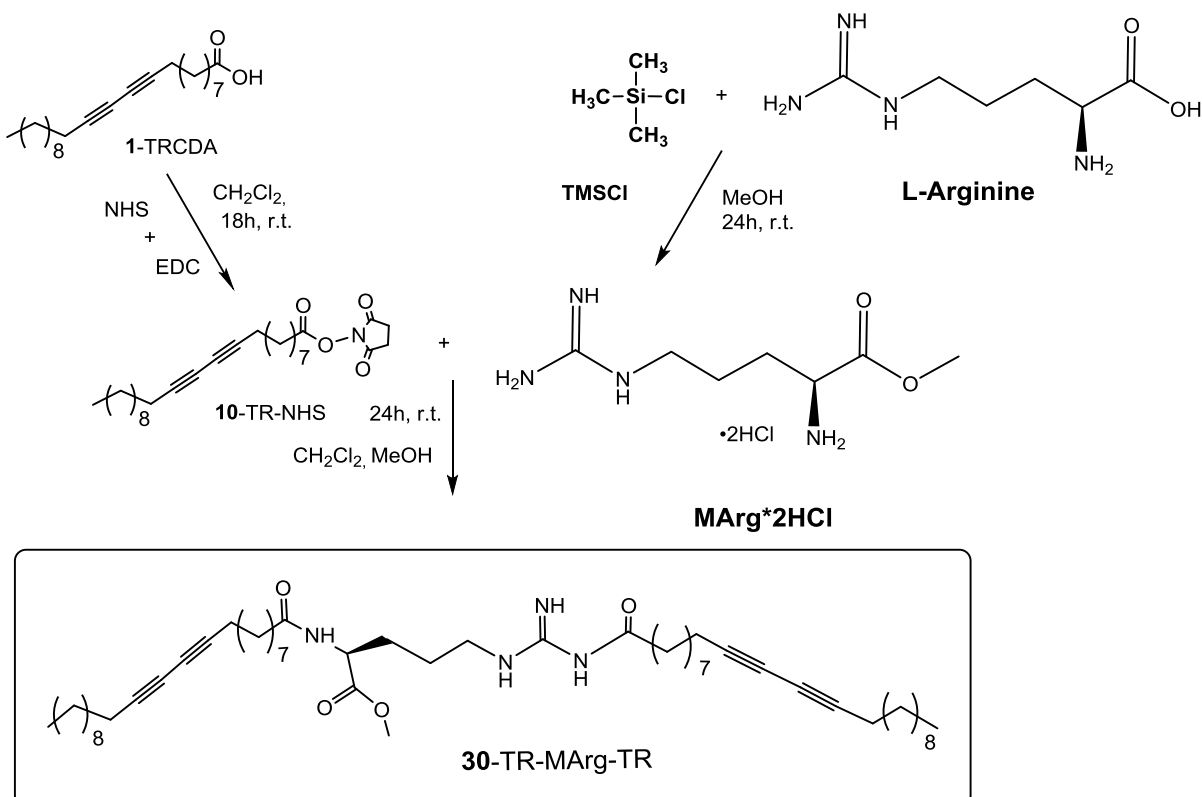
*Step 1. Synthesis of L-Lysine methyl ester * 2HCl (MLys * 2HCl).* Synthetic procedure has been adapted from a previously reported one¹²⁴.

Step 2. Synthesis of 2,5-dioxopyrrolidin-1-yl tricoso-10,12-diynoate (TR-NHS - 10).

Step 3. Synthesis of methyl N²,N⁶-di(tricoso-10,12-diynoyl)lysinate (TR-MLys-TR- 29)

Procedure was a modification of previously reported one⁴⁶. TR-NHS crude (1 eq, 0.25 mmol) is solubilized in CH₂Cl₂ (5 mL) in a round bottom flask under a gentle flux of N₂ and avoiding light contact. MLys*2HCl (0.5 eq, 0.125 mmol) is added to the mixture followed by dropwise addition of triethylamine (1.2 eq, 0.3 mmol). The reaction is stirred at r.t. for 24 h. Reaction monitored by Thin Layer Chromatography (TLC), the mixture purified with column chromatography (ethylacetate : cyclohexane = 1 : 5 to 2 : 1 gradient elution), the solvents are removed under a gentle flux of an inert gas to isolate the product, TR-MLys-TR, **29**, with 89 % yield. MW: Calcd for [M] C₅₃H₈₈N₂O₄, 817.30. ¹H NMR (400 MHz, CDCl₃): δ = 0.85–0.88 (t, J=8.0, 7.0 Hz, 6H), 1.24–1.41 (t, 46H), 1.45–1.76 (m, 14H), 1.80–1.88 (m, 2H), 2.15–2.18 (t, 4H), 2.20–2.24 (t, 8H), 3.18–3.24 (q, 2H), 3.66 (s, 3H), 4.51–4.60 (q, 1H), 5.63–5.66 (s, 1H), 6.17–6.20 (d, 1H). ¹³C NMR (100 MHz, CDCl₃): δ = 173.7, 172.8, 172.6, 76.7, 76.7, 76.7, 65.2, 65.2, 65.2, 65.2, 56.2, 52.2, 41.8, 36.5, 36.5, 31.9, 31.9, 30.9, 29.7, 29.6, 29.6, 29.6, 29.6, 29.3, 29.3, 28.9, 28.9, 28.7, 28.7, 28.7, 28.6, 28.6, 28.4, 28.4, 28.4, 28.1, 28.1, 28.1, 25.5, 25.5, 22.9, 22.9, 22.9, 19.2, 19.2, 19.2, 14.1, 14.1.

8.1.22. Synthesis of methyl N²,N⁶-di(tricoso-10,12-diynoyl)argininate (TR-MArg-TR, **30**)



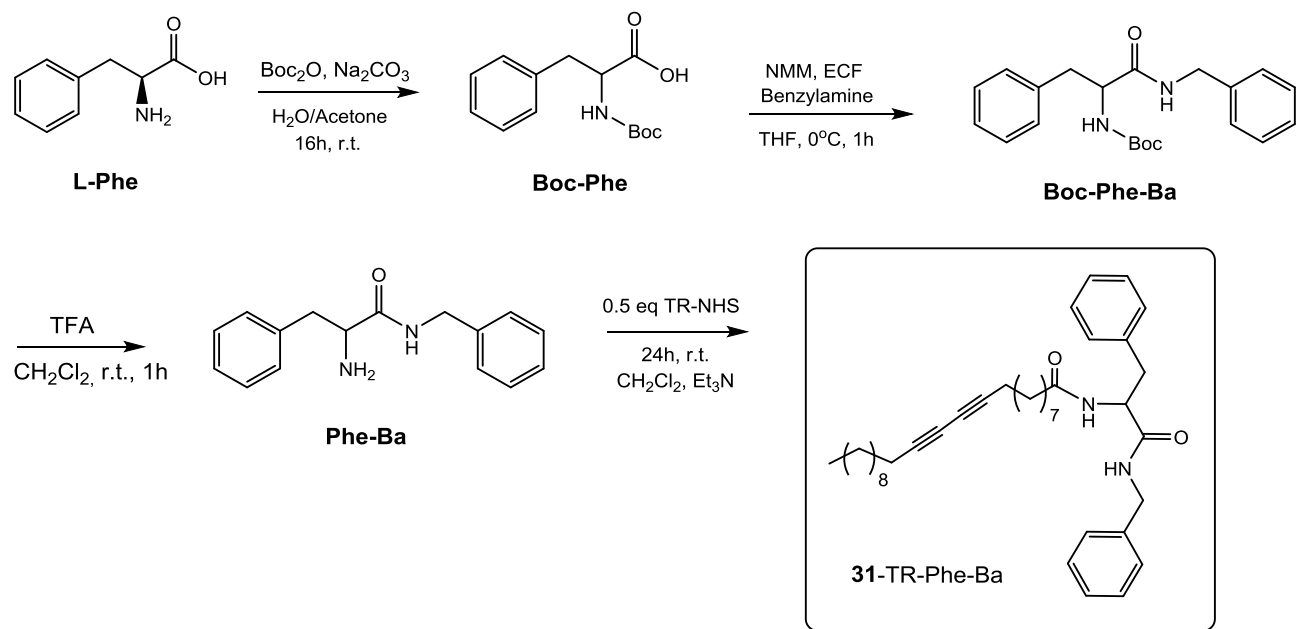
*Step 1. Synthesis of L-Arginine methyl ester * 2HCl (MArg * 2HCl).* Synthetic procedure has been adapted from a previously reported one¹²⁴.

Step 2. Synthesis of 2,5-dioxopyrrolidin-1-yl tricosa-10,12-diynoate (TR-NHS - 10).

Step 3. Synthesis of methyl N²,N⁹-di(tricosa-10,12-diynoyl)argininate (TR-MArg-TR - 30)

Procedure was a modification of previously reported one⁴⁶. TR-NHS crude (1 eq, 0.25 mmol) is solubilized in CH₂Cl₂ (5 mL) in a round bottom flask under a gentle flux of N₂ and avoiding light contact. MArg*2HCl (0.5 eq, 0.125 mmol) dissolved in a little amount MeOH is added to the mixture followed by dropwise addition of triethylamine (1.2 eq, 0.3 mmol). The reaction is stirred at r.t. for 24 h. Reaction monitored by Thin Layer Chromatography (TLC), the mixture purified with column chromatography (CH₂Cl₂ : MeOH = 9 : 1 to 1 : 1 gradient elution), the solvents are removed under a gentle flux of an inert gas to isolate the product, TR MArg-TR, **30**, with 61 % yield. MW: Calcd for [M] C₅₃H₈₈N₄O₄, 845.31. ¹H NMR (400 MHz, CDCl₃): δ = 0.84–0.88 (t, J=8.0, 7.0 Hz, 6H), 1.12–1.42 (m, 42H), 1.44–1.53 (m, 4H), 1.57–1.80 (m, 5H), 1.88–1.95 (m, 2H), 2.20–2.26 (q, 2H), 2.41–2.44 (t, 1H), 2.63 (s, 2H), 3.16–3.24 (q, 9H), 3.30–3.40 (m, 9H), 3.73 (s, 3H), 4.41–4.44 (q, 1H), 7.55 (s, 1H), 8.43 (s, 1H). ¹³C NMR (100 MHz, CDCl₃): δ = 175.2, 173.7, 172.8, 155.4, 76.7, 76.7, 76.7, 76.7, 65.2, 65.2, 65.2, 56.2, 52.2, 44.8, 36.5, 36.3, 31.9, 31.9, 30.0, 29.6, 29.6, 29.6, 29.6, 29.3, 29.3, 28.9, 28.9, 28.7, 28.7, 28.7, 28.7, 28.6, 28.6, 28.4, 28.4, 28.4, 28.1, 28.1, 28.1, 28.1, 25.5, 25.3, 24.6, 22.7, 22.7, 19.2, 19.2, 19.2, 19.2, 14.1, 14.1.

8.1.23. Synthesis of N-(1-(benzylamino)-1-oxo-3-phenylpropan-2-yl) and tricosa-10,12-diynamide (TR-Phe-Ba, **31**)



Step 1. Synthesis of (tert-butoxycarbonyl)phenylalanine (Boc-Phe). Synthetic procedure has been adapted from a previously reported one⁵⁶.

Step 2. Synthesis of tert-butyl (1-(benzylamino)-1-oxo-3-phenylpropan-2-yl)carbamate (Boc-Phe-Ba). Synthetic procedure has been adapted from a previously reported one⁵⁶.

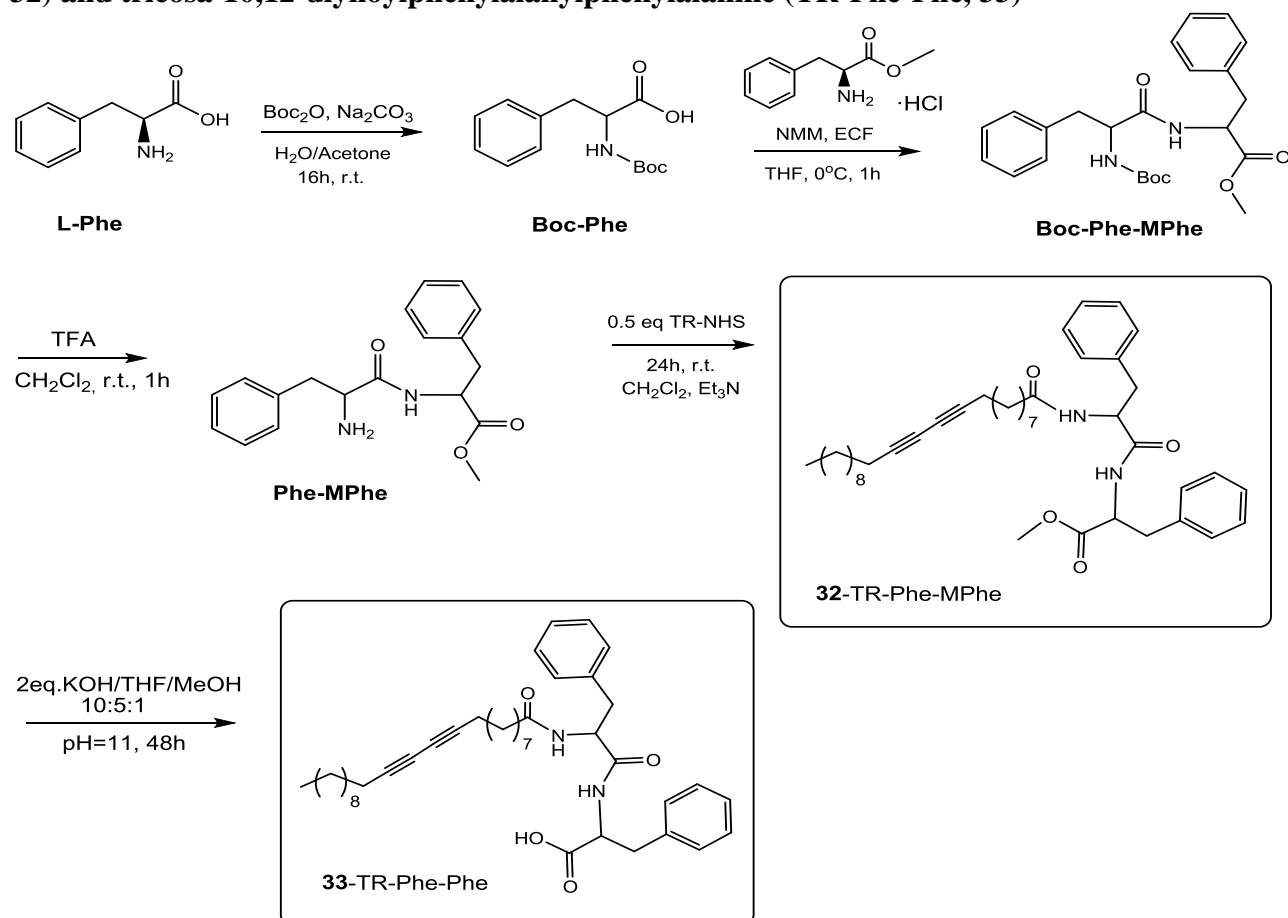
Step 3. Deprotection. 2-amino-N-benzyl-3-phenylpropanamide (Phe-Ba). Synthetic procedure has been adapted from a previously reported one⁵⁶.

Step 4. Synthesis of 2,5-dioxopyrrolidin-1-yl tricosa-10,12-diynoate (TR-NHS - 10)

Step 5. Synthesis of N-(1-(benzylamino)-1-oxo-3-phenylpropan-2-yl)tricosa-10,12-diynamide (TR-Phe-Ba, 31)

Procedure was a modification of previously reported one⁴⁶. TR-NHS crude (1 eq, 0.24 mmol) is solubilized in CH₂Cl₂ (15 mL) in a round bottom flask under a gentle flux of N₂ and avoiding light contact (wrapping the flask with an aluminum foil). Phe-Ba (2 eq, 0.49 mmol) is added to the mixture followed by dropwise addition of triethylamine (1.2 eq, 0.29 mmol). The reaction is stirred at r.t. for 24 h. After checking in TLC, extracted with CH₂Cl₂/Brine solution and then the mixture is purified by column chromatography (CH₂Cl₂ : MeOH = 90 : 1 to 1 : 90) to yield the product TR-Phe-Ba **31**. The solvent is removed under a gentle flux of N₂. **Yield:** white powder (84 %). MW: Calcd for [M] C₃₉H₅₄N₂O₂, 582.87. ¹H NMR (400 MHz, CDCl₃): δ = 0.84–0.88 (t, J=8.0, 7.1 Hz, 3H), 1.23–1.42 (m, 22H), 1.45–1.57 (m, 6H), 2.11–2.15 (t, 2H), 2.20–2.34(t, 4H), 2.98–3.12 (qq, 2H), 4.25–4.36 (m, 2H), 4.60–4.65 (q, 1H), 6.02 (s, 1H), 6.08–6.10 (d, 1H), 7.04–7.06 (t, J=7.5, 1.5 Hz, 2H), 7.16–7.27 (m, 8H). ¹³C NMR (100 MHz, CDCl₃): δ = 178.1, 170.1, 170.8, 162.5, 137.5, 136.6, 129.3, 128.7, 128.6, 127.6, 127.5, 127.0, 77.6, 76.7, 65.3, 65.2, 54.6, 45.5, 43.5, 38.5, 36.5, 34.8, 31.9, 29.5, 29.3, 29.1, 29.0, 28.9, 28.8, 28.7, 28.3, 28.2, 26.2, 25.5, 22.7, 19.2, 19.1, 14.1.

8.1.24. Synthesis of methyl tricosa-10,12-diynoylphenylalanylphenylalaninate (TR-Phe-MPhe, 32) and tricosa-10,12-diynoylphenylalanylphenylalanine (TR-Phe-Phe, 33)



Step 1. Synthesis of (tert-butoxycarbonyl)phenylalanine (Boc-Phe). Synthetic procedure has been adapted from a previously reported one⁵⁶.

Step 2. Synthesis of methyl (tert-butoxycarbonyl)phenylalanylphenylalaninate (Boc-Phe-MPhe). Synthetic procedure has been adapted from a previously reported one⁵⁶.

Step 3. Deprotection. methyl phenylalanylphenylalaninate (Phe-MPhe). Synthetic procedure has been adapted from a previously reported one⁵⁶.

Step 4. Synthesis of 2,5-dioxopyrrolidin-1-yl tricosa-10,12-diynoate (TR-NHS - 10)

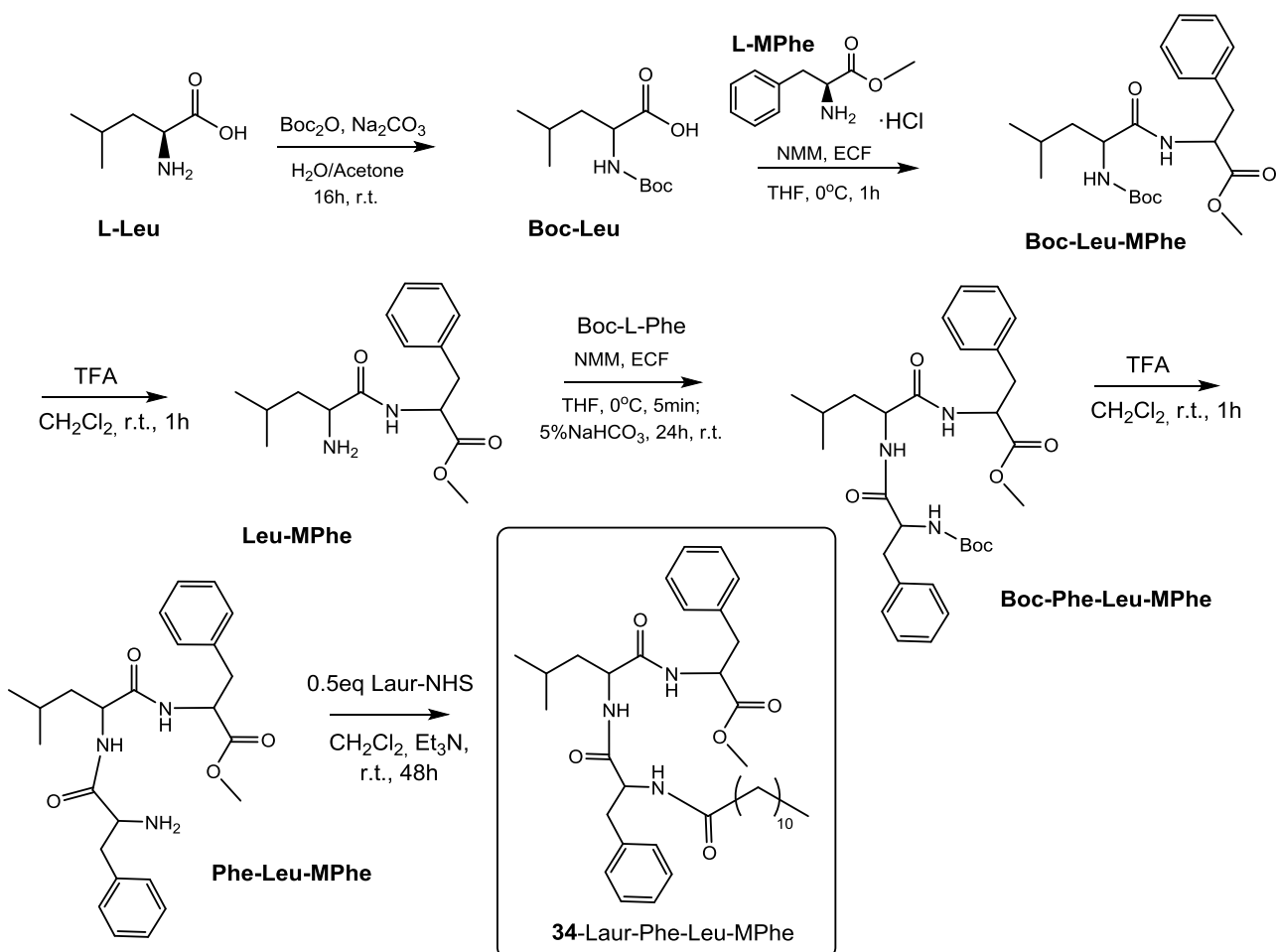
Step 5. Synthesis of methyl tricosa-10,12-diynoylphenylalanylphenylalaninate (TR-Phe-MPhe, 32)

Procedure was a modification of previously reported one⁴⁶. TR-NHS crude (1 eq, 0.8 mmol) is solubilized in CH₂Cl₂ (15 mL) in a round bottom flask under a gentle flux of N₂ and avoiding light contact (wrapping the flask with an aluminum foil). Phe-MPhe (2 eq, 1.6 mmol) is added to the mixture followed by dropwise addition of triethylamine Et₃N (1.2 eq, 0.96 mmol). The reaction is stirred at r.t. for 24 h. After checking in TLC, extracted with CH₂Cl₂/Brine solution and then the mixture is purified by column chromatography (CH₂Cl₂ : MeOH = 90 : 1 to 1 : 90) to yield the product TR-Phe-MPhe **32**. The solvent is removed under a gentle flux of N₂. Yield: white powder (80 %). MW: Calcd for [M] C₄₂H₅₈N₂O₄, 654.94. ¹H NMR (400 MHz, CDCl₃): δ = 0.84–0.88 (t, J=8.0, 7.1 Hz, 3H), 1.18–1.41 (m, 22H), 1.46–1.51 (t, 6H), 1.59–1.60 (s, 2H), 2.07–2.11 (t, 2H), 2.20–2.23 (t, 4H), 2.93–3.09 (m, 4H), 3.66–3.68 (t, 3H), 4.58–4.74 (qq, 2H), 5.90–5.92 (d, 1H), 6.18–6.20 (d, 1H), 6.96–6.98 (d, J=7.5, 1.5 Hz, 2H), 7.09–7.25 (m, 6H), 7.16–7.27. ¹³C NMR (100 MHz, CDCl₃): δ = 173.8, 171.7, 171.5, 136.7, 136.6, 128.6, 128.6, 128.6, 128.6, 127.7, 127.7, 127.7, 127.7, 125.9, 125.9, 76.7, 76.7, 65.2, 65.2, 58.7, 56.7, 51.9, 37.4, 36.8, 36.2, 31.9, 29.5, 29.5, 29.3, 28.9, 28.7, 28.7, 28.6, 28.4, 28.4, 28.1, 28.1, 25.5, 22.8, 19.2, 19.2, 14.1.

Step 6. Synthesis of tricosa-10,12-diynoylphenylalanylphenylalanine (TR-Phe-Phe, 33)

Compound **32** (523 mg, 0.8 mmol) was dissolved in 10:5:1 H₂O/THF/MeOH (172 mL), and the pH of the solution was adjusted to 11 with 1 M KOH. The reaction mixture was stirred at 35 °C, and product formation was monitored by TLC (CH₂Cl₂ : MeOH = 20 : 1). The reaction was quenched after 48 h via the addition of Amberlist₁₅ (H⁺ form) ion-exchange resin to pH 4. The crude product was concentrated and extracted w/ethyl ether, solvent removed under a gentle flux of N₂. TR-Phe-Phe **33** (346 mg) was isolated in 54% yield (white transparent film). MW: Calcd for [M] C₄₁H₅₆N₂O₄, 640.91 ¹H NMR (400 MHz, Ether-d₁₀): ¹H NMR (500 MHz, 3:2 CD₃OD/CDCl₃): δ = 0.84–0.88 (t, J=8.0, 7.1 Hz, 3H), 1.18–1.41 (m, 22H), 1.44–1.57 (m, 6H), 2.05–2.08 (t, 2H), 2.47–2.51 (t, 4H), 2.96–3.14 (m, 4H), 4.08–4.11 (m, 1H), 4.38 (s, 1H), 4.62–4.80 (m, 1H), 6.45 (s, 1H), 7.03–7.07 (d, J=7.5, 1.5 Hz, 2H), 7.16–7.22 (m, 8H), 12.89 (s, 1H). ¹³C NMR (125 MHz, 3:2 CD₃OD/CDCl₃): δ = 174.7, 173.9, 171.7, 136.6, 136.6, 128.6, 128.6, 128.6, 127.7, 127.7, 127.7, 127.7, 125.9, 125.9, 75.0, 75.0, 64.4, 64.4, 59.2, 58.7, 37.4, 36.5, 36.1, 31.9, 29.6, 29.6, 29.3, 28.9, 28.7, 28.7, 28.6, 28.4, 28.4, 28.1, 25.6, 22.7, 19.2, 19.2, 14.1.

8.1.25. Synthesis of methyl dodecanoylphenylalanylleucylphenylalaninate (Laur-Phe-Leu-MPhe, 34)



Step 1. Synthesis of (*tert*-butoxycarbonyl)leucine (Boc-Leu). Synthetic procedure has been adapted from a previously reported one⁵⁶.

Step 2. Synthesis of methyl (*tert*-butoxycarbonyl)leucylphenylalaninate (Boc-Leu-MPhe). Synthetic procedure has been adapted from a previously reported one⁵⁶.

Step 3. Deprotection. Methyl leucylphenylalaninate (Leu-MPhe). Synthetic procedure has been adapted from a previously reported one⁵⁶.

Step 4. Synthesis of methyl (*tert*-butoxycarbonyl)phenylalanylleucylphenylalaninate (Boc-Phe-Leu-MPhe). Synthetic procedure has been adapted from a previously reported one⁵⁶.

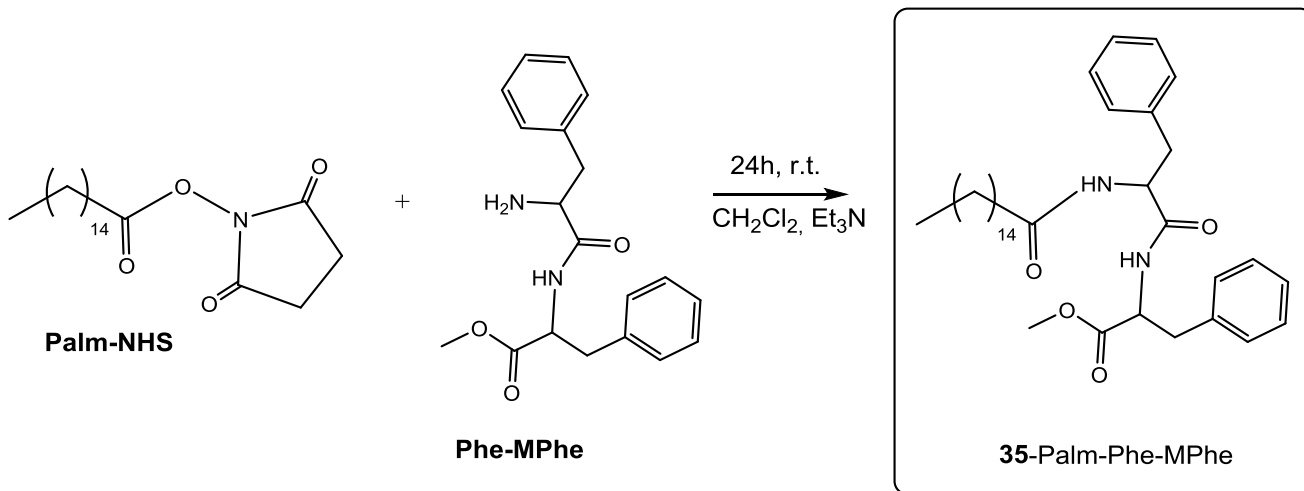
Step 5. Deprotection. Methyl phenylalanylleucylphenylalaninate (Phe-Leu-MPhe)
Synthetic procedure has been adapted from a previously reported one⁵⁶.

Step 6. Synthesis of 2,5-dioxopyrrolidin-1-yl dodecanoate (Laur-NHS-10a, by analogy with TR-NHS-10)

Step 7. Synthesis of methyl dodecanoylphenylalanylleucylphenylalaninate (Laur-Phe-Leu-MPhe, 34)

Procedure was a modification of previously reported one⁴⁶. Laur-NHS crude (1 eq, 0.67 mmol) is solubilized in CH₂Cl₂ (15 mL) in a round bottom flask under a gentle flux of N₂ and avoiding light contact (wrapping the flask with an aluminum foil). Phe-Leu-MPhe (2 eq, 1.33 mmol) is added to the mixture followed by dropwise addition of triethylamine Et₃N (1.2 eq, 0.8 mmol). The reaction is stirred at r.t. for 24 h. After checking in TLC, extracted with CH₂Cl₂/Brine solution and then the mixture is purified by column chromatography (CH₂Cl₂ : MeOH = 90 : 1 to 1 : 90) to yield the product Laur-Phe-Leu-MPhe **34**. The solvent is removed under a gentle flux of N₂. **Yield:** white powder 333mg (80 %). MW: Calcd for [M] C₃₇H₅₅N₃O₅, 621.86. ¹H NMR (400 MHz, CDCl₃): δ = 0.65–1.05 (m, 9H), 1.18–1.90 (mm, 21H), 2.05–2.14 (t, J=8.0, 6.8 Hz, 2H), 2.98–3.16 (dm, 4H), 3.67 (s, 3H), 4.30–4.37 (q, 1H), 4.62–4.66 (q, 1H), 4.77–4.82 (q, 1H), 6.01–6.07 (d, 1H), 6.39–6.45 (d, 1H), 6.50–6.55 (d, 1H), 7.09–7.22 (dd, J=7.5, 1.5 Hz, 10H). ¹³C NMR (100 MHz, CDCl₃): δ = 173.5, 171.9, 171.7, 171.6, 136.2, 135.9, 128.6, 128.6, 128.5, 128.5, 128.3, 128.3, 128.2, 128.2, 127.3, 127.2, 54.0, 53.8, 52.6, 52.2, 41.2, 37.6, 37.4, 36.8, 31.9, 29.6, 29.6, 29.5, 29.5, 29.4, 29.3, 25.6, 25.0, 22.7, 22.6, 22.2, 14.1.

8.1.26. Synthesis of methyl palmitoylphenylalanylphenylalaninate (Palm-Phe-MPhe, **35**)



*Step 1. Synthesis of 2,5-dioxopyrrolidin-1-yl palmitate (Palm-NHS-**10b**, by analogy with TR-NHS-**10**)*

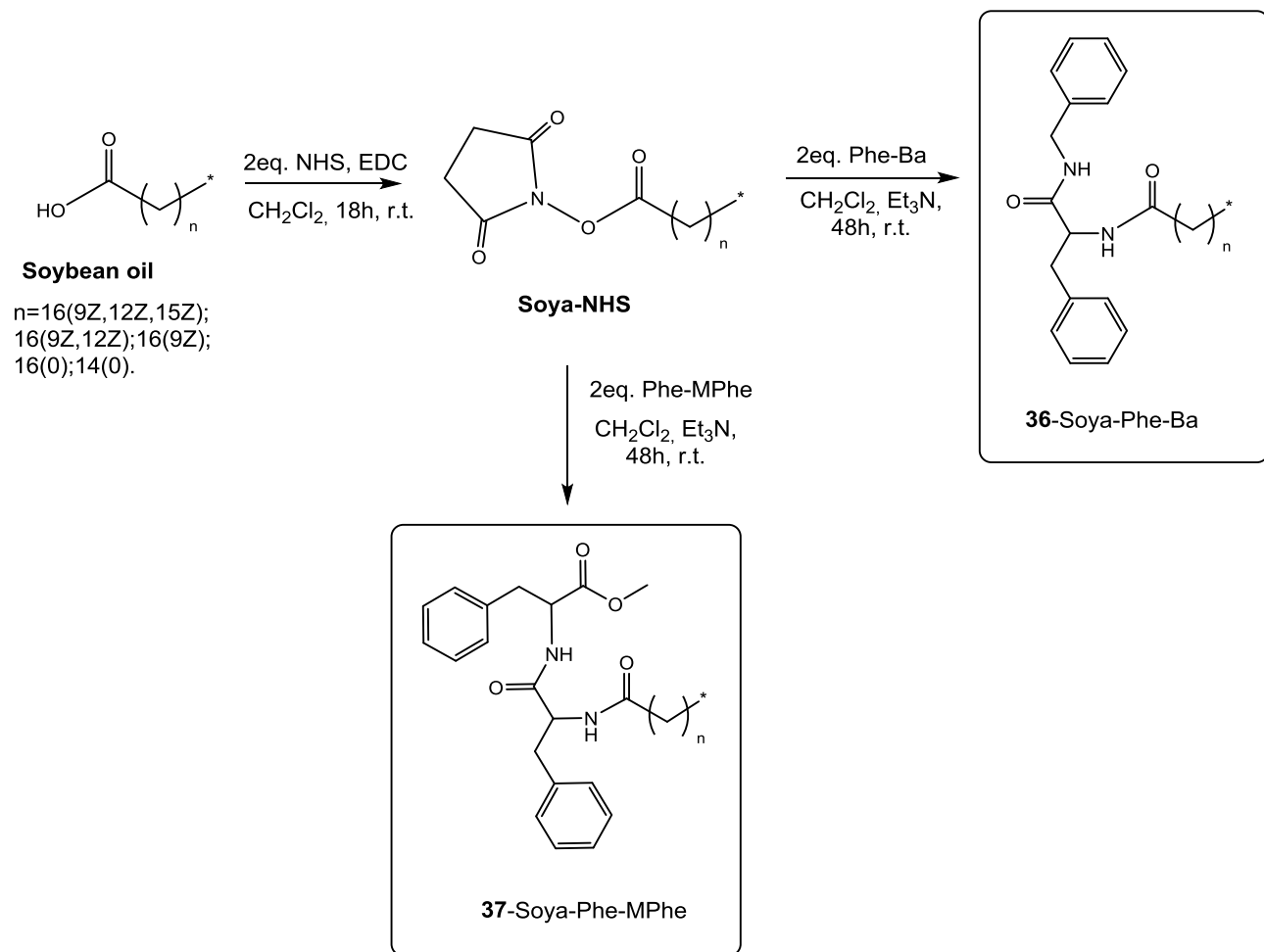
*Step 2. Synthesis of methyl phenylalanylphenylalaninate (Phe-MPhe, starting of TR-Phe-MPhe, **30**)*

*Step 3. Synthesis of methyl palmitoylphenylalanylphenylalaninate (Palm-Phe-MPhe, **35**, by analogy with TR-Phe-MPhe, **32**)*

Procedure was a modification of previously reported one⁴⁶. Palm-NHS crude (1 eq, 0.8 mmol) is solubilized in CH₂Cl₂ (15 mL) and added to the Phe-MPhe (2 eq, 1.6 mmol), followed by dropwise addition of triethylamine Et₃N (1.2 eq, 0.96 mmol). The reaction is stirred at r.t. for 24 h. After checking in TLC, extracted with CH₂Cl₂/Brine solution and then the mixture is purified by column chromatography (1:9 to 2:1 EtOAc/hexanes) to yield the product Palm-Phe-MPhe **35**. Yield: white transparent film (82 %). MW: Calcd for [M] C₃₅H₅₂N₂O₄, 564.81. ¹H NMR (400 MHz, CDCl₃): δ = 0.84–0.88 (t, J=8.0, 7.0 Hz, 3H), 1.24–1.29 (m, 22H), 1.53–1.57 (t, 4H), 2.05–2.13 (t, 2H), 2.93–3.10 (m, 4H), 3.64 (s, 3H), 4.58–4.63 (q, 1H), 4.70–4.76 (q, 1H), 5.91–5.96 (d, 1H), 6.17–6.20 (d, 1H), 6.95–6.98 (d, J=7.5, 1.5 Hz, 2H), 7.18–7.23 (m, 8H). ¹³C NMR (100 MHz, CDCl₃): δ = 173.5,

171.9, 171.7, 136.6, 136.6, 128.6, 128.6, 128.5, 128.5, 128.3, 128.3, 128.2, 128.2, 125.9, 125.9, 58.7, 56.5, 52.2, 37.4, 36.8, 36.1, 31.9, 29.6, 29.6, 29.6, 29.5, 29.5, 29.4, 29.3, 28.9, 28.6, 25.6, 22.6, 14.1.

8.1.27. Synthesis of Soya-phenylalanine-benzylamine(Soya-Phe-Ba, **36**)and Soya-phenylalanine-methylphenylalanine(Soya-Phe-MPhe, **37**)



*Step 1. Synthesis of Soya-NHS-**10c**, by analogy with TR-NHS-**10**.*

*Step 2. Synthesis of 2-amino-N-benzyl-3-phenylpropanamide (Phe-Ba, starting of TR-Phe-Ba, **31**)*

*Step 3. Synthesis of methyl phenylalanylphenylalaninate (Phe-MPhe, starting of TR-Phe-MPhe, **32**)*

*Step 4. Synthesis of Soya-phenylalanine-benzylamine (Soya-Phe-Ba, **36**, by analogy with TR-Phe-Ba, **31**)*

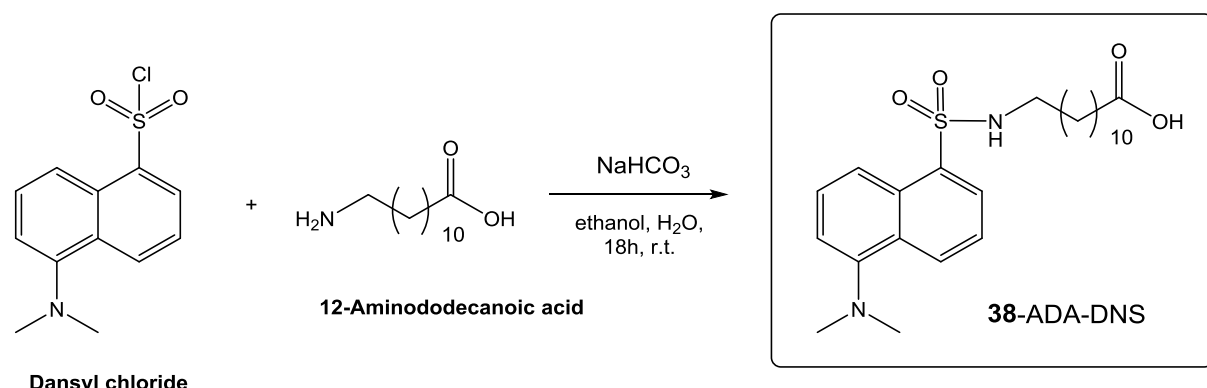
Procedure was a modification of previously reported one⁴⁶. Soya-NHS crude (1 eq, 0.8 mmol) is solubilized in CH₂Cl₂ (15 mL) and added to the Phe-Ba (2 eq, 1.6 mmol), followed by dropwise addition of triethylamine Et₃N (1.2 eq, 0.96 mmol). The reaction is stirred at r.t. for 48 h. After checking in TLC, extracted with CH₂Cl₂/Brine solution and then the mixture is purified by column

chromatography (1:9 to 2:1 EtOAc/hexanes) to yield the product Soya-Phe-Ba **34**. Yield: light brown solid (85 %). MW: ~ 500.86.

Step 5. Synthesis of Soya-phenylalanine-methylphenylalanine (Soya-Phe-MPhe, **37, by analogy with TR-Phe-MPhe, **32**)**

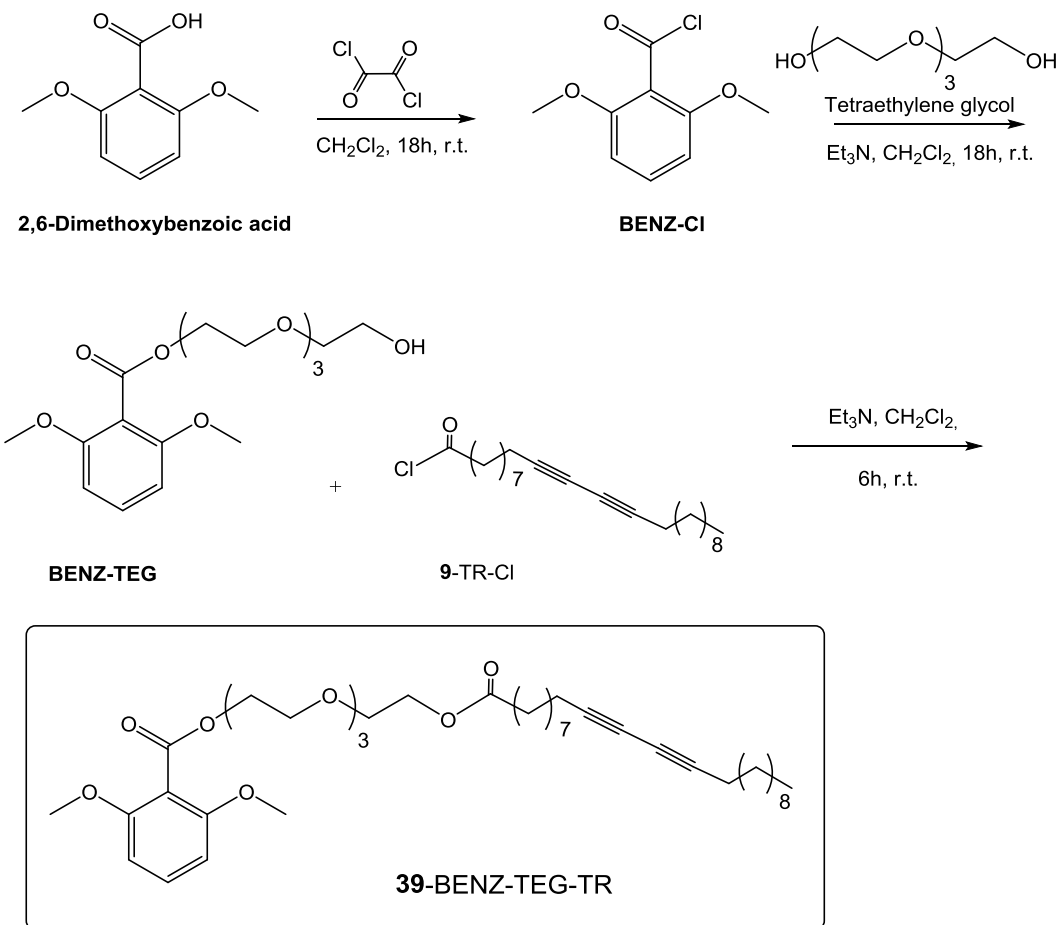
Procedure was a modification of previously reported one⁴⁶. Soya-NHS crude (1 eq, 0.8 mmol) is solubilized in CH₂Cl₂ (15 mL) and added to the Phe-MPhe (2 eq, 1.6 mmol), followed by dropwise addition of triethylamine Et₃N (1.2 eq, 0.96 mmol). The reaction is stirred at r.t. for 48 h. After checking in TLC, extracted with CH₂Cl₂/Brine solution and then the mixture is purified by column chromatography (1:9 to 2:1 EtOAc/hexanes) to yield the product Soya-Phe-MPhe **35**. Yield: light yellow solid (90 %). MW: ~ 547.7.

8.1.28. Synthesis of 12-((5-(dimethylamino)naphthalene)-1-sulfonamido)dodecanoic acid (ADA-DNS, **38)**



Synthesis was carried out using modification of the reported procedure¹²⁸. NaHCO₃ (1 mmol) was dissolved in 2.5 ml of water. To this solution was added 12-aminododecanoic acid (0.25 mmol), followed by 7.5 ml of ethanol. The fatty acid was dissolved with mild heating (some NaHCO₃ precipitated at this point). After cooling to room temperature, DNS-Cl (0.75 mmol) was added, and the reaction was stirred in the dark at room temperature. After 4 h, the reaction was stopped with 1.0 ml of 1 N HCl. Ethanol and water were added to obtain 30 ml of ethanol/water (1 : 1). The products were dissolved with heating, then crystallized overnight at -20°C. The precipitate was harvested on glass fiber filter paper, washed with cold water, and dissolved in chloroform/methanol (99 : 1). Reaction mixture was purified by column chromatography (CH₂Cl₂ : MeOH = 99.5 : 0.5 to 99 : 2 gradient elution) to yield the ADA-DNS **38**, (yield 39%). MW: Calcd for [M] C₂₄H₃₆N₂O₄S, 448.62. ¹H NMR (400 MHz, CDCl₃): δ = 1.08–1.37 (m, 14H), 1.56–1.64 (quint, 4H), 2.31–2.35 (t, 2H), 2.84–2.89 (s, 6H), 4.79–4.82 (t, 2H), 7.18–7.24 (d, 2H), 7.50–7.57 (m, 2H), 8.22–8.30 (dd, 2H), 8.53–8.55 (d, 1H), 11.87 (s, 1H). ¹³C NMR (300 MHz, CDCl₃) δ = 178.3, 151.3, 147.3, 133.2, 128.3, 127.9, 126.6, 124.0, 123.7, 119.9, 117.6, 46.2, 46.2, 42.8, 34.0, 29.6, 29.6, 29.3, 29.3, 29.1, 29.0, 26.7, 24.7.

8.1.29. Synthesis of 13-oxo-3,6,9,12-tetraoxapentatriaconta-22,24-diyn-1-yl 2,6-dimethoxybenzoate (TR-TEG-BENZ, **39)**



Step 1. Synthesis of **2,6-dimethoxybenzoyl chloride**(BENZ-Cl, by analogy with TR-Cl, **9**)

Step 2. Synthesis of **2-(2-(2-hydroxyethoxy)ethoxy)ethyl 2,6-dimethoxybenzoate** (BENZ-TEG)

Procedure was adapted from a previously reported one⁴⁹. Tetraethylene glycol (1.5 eq, 1.5 mmol) and Et₃N (3.4 eq, 3.4 mmol) were dissolved in CH₂Cl₂ and **BENZ-Cl** (1 eq, 1 mmol) was dissolved in a small amount of anhydrous THF. The THF solution containing **BENZ-Cl** was added dropwise into the CH₂Cl₂ solution. The resultant solution was stirred at room temperature overnight and concentrated in vacuum at r.t. The crude residue was dissolved in a small amount of MeOH and added dropwise to water. Addition of small amount of HCl (1:9) water solution to MeOH solution resulted in the formation of white precipitates. The precipitates formed were filtered, washed with water and dried yielding **BENZ-TEG** (36 %). MW: Calcd for [M] C₁₇H₂₆O₈, 358.39. ¹H NMR (400 MHz, CDCl₃): δ = 3.56-2.58 (t, J=8.0, 7.1 Hz, 10H), 3.63-3.70 (tt, 2H), 3.77-3.80 (q, 8H), 4.45-4.48 (t, 2H), 5.27(s, 1H), 6.51-6.54 (d, J=7.5, 1.5 Hz, 2H), 7.26-7.28 (m, 1H). ¹³C NMR (100 MHz, CDCl₃): δ = 108.8, 162.7, 162.5, 133.5, 106.2, 106.1, 101.5, 71.0, 70.8, 70.7, 70.3, 70.1, 69.3, 64.7, 61.3, 55.8, 55.6.

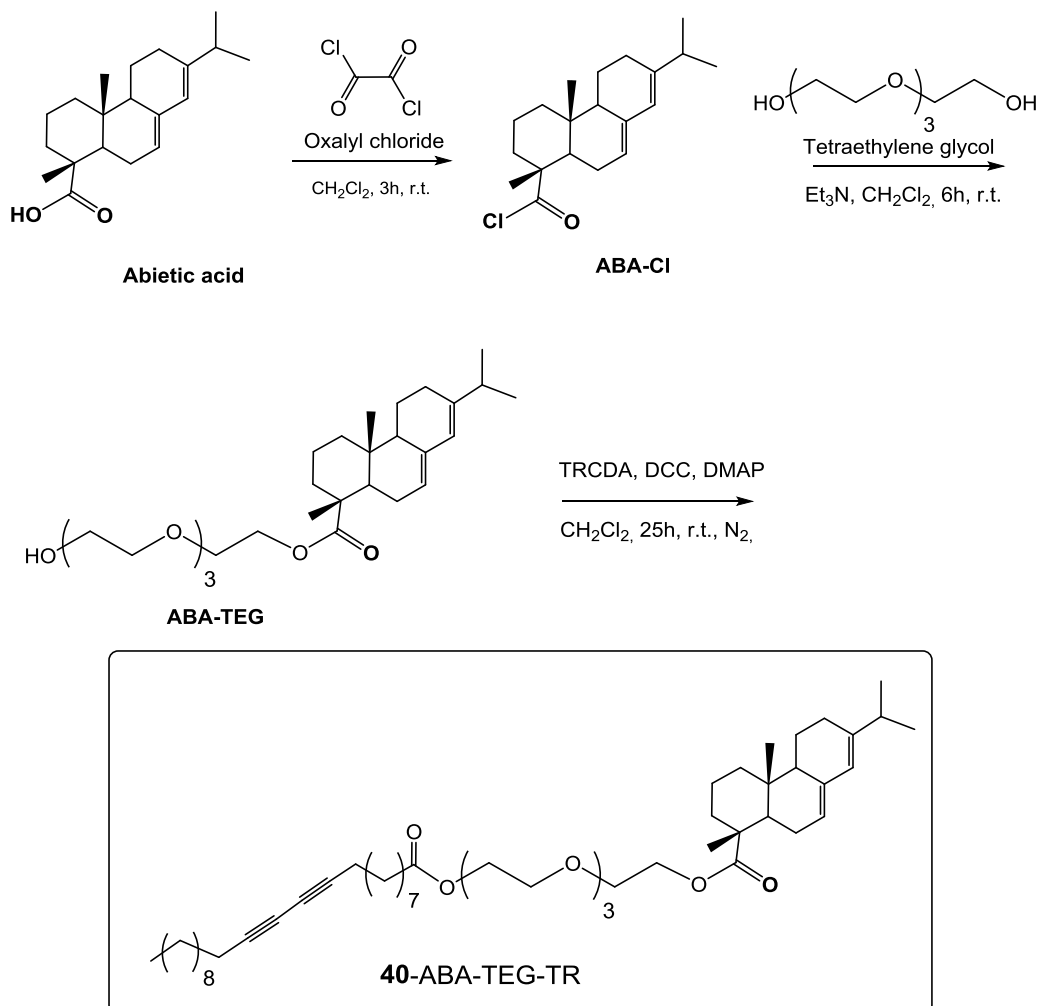
Step 3. Synthesis of **tricoso-10,12-diynoyl chloride** (TR-Cl, **9**).

Step 4. Synthesis of **13-oxo-3,6,9,12-tetraoxapentatriaconta-22,24-diyn-1-yl 2,6-dimethoxybenzoate** (TR-TEG-BENZ, **39**).

Procedure was adapted from a previously reported one⁴⁹. **BENZ-TEG** (1.5 eq, 0.36 mmol) and Et₃N (3.4 eq, 0.82 mmol) were dissolved in CH₂Cl₂ and TR-Cl **9** (1 eq, 0.24 mmol) was dissolved

in a small amount of anhydrous THF. The THF solution containing **TR-Cl** was added dropwise into the CH_2Cl_2 solution. The resultant solution was stirred at room temperature 6h and concentrated in vacuum at r.t.. The crude residue was dissolved in a small amount of MeOH and added dropwise to water. Addition of small amount of HCl (1:9) water solution to MeOH solution resulted in the formation of white precipitates. The precipitates formed were filtered, washed with water and dried yielding **TR-TEG-BENZ 39** (48 %). MW: Calcd for [M] $\text{C}_{40}\text{H}_{62}\text{O}_9$, 686.93. ^1H NMR (400 MHz, CDCl_3): δ = 0.84-0.88 (t, 3H), 1.24-1.37 (m, 23H), 1.46-1.51 (m, 2H), 1.57-1.61 (m, 3H), 2.20-2.32 (tt, 6H), 3.60-3.68 (m, 10H), 3.77-3.80 (s, 6H), 4.18-4.20 (t, 2H), 4.45-4.47 (t, 2H), 6.52-6.54 (d, 2H), 7.26-7.28 (t, 3H). ^{13}C NMR (100 MHz, CDCl_3): δ = 173.1, 170.5, 162.1, 162.1, 135.0, 106.8, 106.8, 101.5, 75.0, 75.0, 70.4, 70.4, 70.1, 70.1, 69.3, 69.3, 66.7, 64.4, 64.4, 64.3, 55.8, 55.8, 33.9, 31.9, 29.6, 29.6, 29.3, 29.3, 29.0, 28.7, 28.7, 28.4, 28.4, 28.1, 28.1, 25.0, 22.7, 19.2, 19.2, 14.1.

8.1.30. Synthesis of 13-oxo-3,6,9,12-tetraoxapentatriaconta-22,24-diyn-1-yl (*1R,4aR*)-7-isopropyl-1,4a-dimethyl-1,2,3,4,4a,4b,5,6,10,10a-decahydrophenanthrene-1-carboxylate (**TR-TEG-ABA, 40**)



Step 1. Synthesis of (*1R,4aR*)-7-isopropyl-1,4a-dimethyl-1,2,3,4,4a,4b,5,6,10,10a-decahydrophenanthrene-1-carboxyl chloride (ABA-Cl, by analogy with BENZ-Cl)

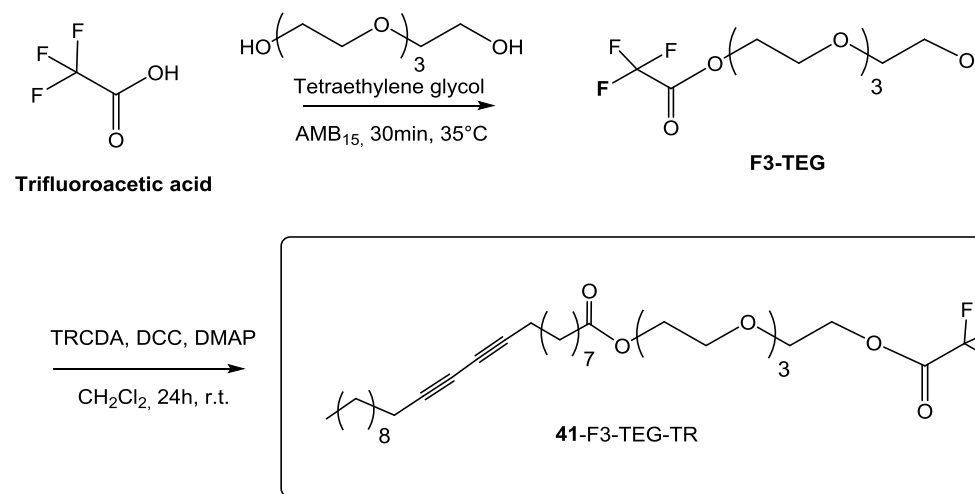
Step 2. Synthesis of **2-(2-(2-hydroxyethoxy)ethoxy)ethoxyethyl (1*R*,4*a*R)-7-isopropyl-1,4*a*-dimethyl-1,2,3,4,4*a*,4*b*,5,6,10,10*a*-decahydronaphthalene-1-carboxylate** (ABA-TEG, by analogy with BENZ-TEG)

Step 3. Synthesis of **tricosa-10,12-diyenyl chloride** (TR-Cl, **9**).

Step 4. Synthesis of **13-oxo-3,6,9,12-tetraoxapentatriaconta-22,24-diyen-1-yl (1*R*,4*a*R)-7-isopropyl-1,4*a*-dimethyl-1,2,3,4,4*a*,4*b*,5,6,10,10*a*-decahydronaphthalene-1-carboxylate** (TR-TEG-ABA, **40**).

Procedure was modified from previously reported ones¹²⁹ **ABA-TEG** (1eq, 0.63 mmol) was dissolved in dry dichloromethane under N₂ atmosphere, to this solution **TRCDA 1** (2eq, 1.26 mmol), DMAP (1eq, 0.63 mmol) and DCC (1.5 eq, 0.95 mmol) was added. This reaction mixture was stirred at room temperature for 24 h, and then the reaction mixture was filtered and the clear solution was evaporated to dryness. The crude product was purified by silica column chromatography using ethyl acetate and petroleum ether as eluents (1:9-1:4). The desired compound **TR-TEG-ABA 40** was collected in the third fraction in 52% yield. MW: Calcd for [M] C₅₁H₈₂O₇, 807.21. ¹H NMR (400 MHz, CDCl₃): δ = 0.84-0.88 (t, J=8.0, 6.8 Hz, 9H), 0.97-1.00 (m, 3H) 1.09-1.63 (m, 44H), 2.15-2.44 (mm, 8H), 2.78-2.87 (m, 1H), 3.61-3.68 (m, 8H), 4.17-4.22 (m, 4H), 5.25-5.31 (m, 1H), 5.75 (s, 1H), 6.83 (s, 1H), 6.95-7.00 (d, 1H), 7.16-7.18 (d, J=6.2, -1.0 Hz, 2H). ¹³C NMR (100 MHz, CDCl₃): δ = 177.9, 173.1, 146.0, 135.5, 122.4, 121.2, 75.0, 75.0, 70.4, 70.4, 70.1, 70.1, 69.3, 69.3, 67.5, 66.9, 64.4, 64.4, 64.3, 51.3, 46.8, 45.1, 39.2, 37.8, 34.8, 34.5, 33.9, 31.9, 29.6, 29.6, 29.3, 29.0, 28.7, 28.7, 28.4, 28.4, 28.1, 28.1, 26.6, 25.0, 23.5, 22.7, 22.7, 21.9, 21.9, 19.2, 19.2, 18.7, 17.0, 14.6, 14.1.

8.1.31. Synthesis of 14,14,14-trifluoro-13-oxo-3,6,9,12-tetraoxatetradecyl tricosa-10,12-diynoate (**TR-TEG-F3, 41**)



Step 1. Synthesis of **2-(2-(2-hydroxyethoxy)ethoxy)ethoxyethyl 2,2,2-trifluoroacetate** (F3-TEG)

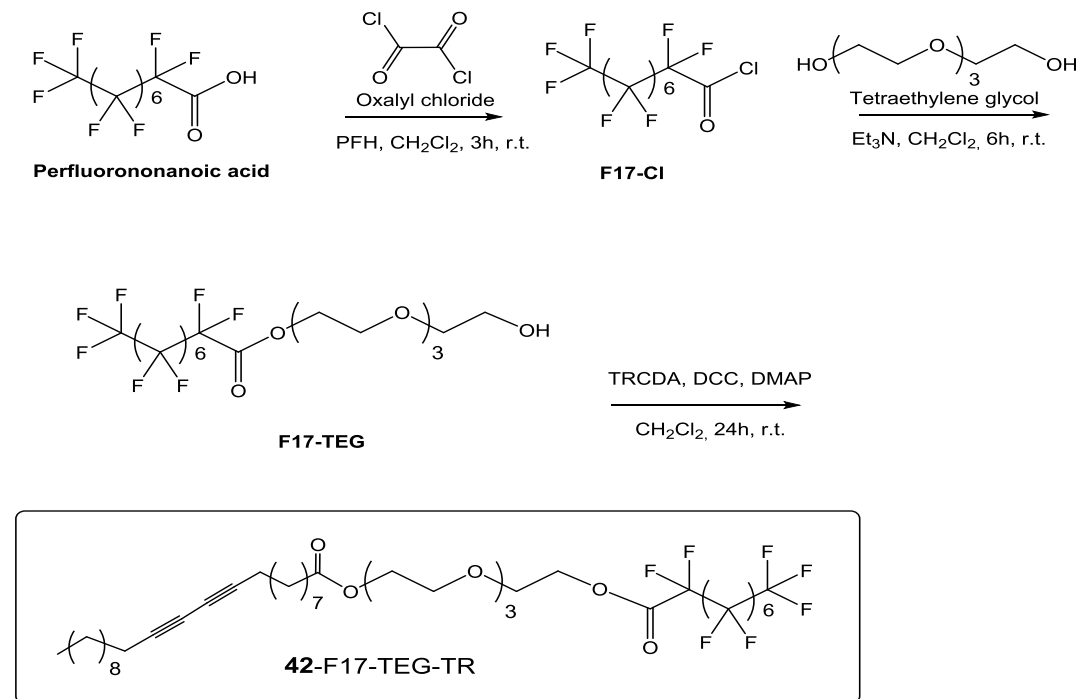
Procedure was a modification of previously reported one⁵⁷. Trifluoracetic acid (1 eq, 2 mmol) was added to tetraethylene glycol (4 eq, 8 mmol) followed by addition of catalytic amount of Amberlyst₁₅(0.1 eq 0.2 mmol). The reaction was stirred at 35°C for 30 min, filtered and extracted

with DCM, dried over MgSO₄, solvent evaporated. The crude product was purified by silica column chromatography using ethyl acetate and petroleum ether as eluents (1:4 - 9:1). The desired compound **F3-TEG** was isolated in 85 % yield. MW: Calcd for [M] C₁₀H₁₇F₃O₆, 290.24. ¹H NMR (400 MHz, CDCl₃): δ = 3.60-3.78 (mm, 14H), 4.45-4.48 (m, 2H), 6.98 (s, 1H). ¹³C NMR (100 MHz, CDCl₃): δ = 162.0, 115.1, 70.6, 70.6, 70.5, 70.3, 69.2, 65.3, 61.7. ¹⁹F NMR (377 MHz, CDCl₃): δ = -75.0, -75.0, -76.0.

Step 2 . Synthesis of 14,14,14-trifluoro-13-oxo-3,6,9,12-tetraoxatetradecyl tricosa-10,12-diynoate (TR-TEG-F3, 41).

Procedure was modified from previously reported ones¹²⁹. **F3-TEG** (1.5eq, 0.33 mmol) was dissolved in dry dichloromethane under N₂ atmosphere, to this solution **TRCDA 1** (2eq, 0.44 mmol), DMAP (1eq, 0.22 mmol) and DCC (1.5 eq, 0.33 mmol) was added. This reaction mixture was stirred at room temperature for 24 h, and then the reaction mixture was filtered and the clear solution was evaporated to dryness. The crude product was purified by silica column chromatography using ethyl acetate and petroleum ether as eluents (1:9-1:2). The desired compound **TR-TEG-F3 39** was collected in the third fraction in 32% yield. MW: Calcd for [M] C₃₃H₅₃F₃O₇, 618.78. ¹H NMR (400 MHz, CDCl₃): δ = 0.84–0.88 (t, J=8.0, 7.1 Hz, 3H), 1.24–1.41 (m, 22H), 1.45–1.61 (mm, 6H), 2.20–2.24 (t, 4H), 2.29–2.32 (t, 2H), 3.58–3.72 (mm, 14H), 4.20–4.23 (quint, 2H). ¹³C NMR (100 MHz, CDCl₃): δ = 173.9, 158.3, 117.4, 77.6, 77.4, 77.3, 77.0, 76.7, 72.5, 70.6, 70.5, 70.5, 70.3, 69.2, 63.3, 61.7, 34.1, 31.9, 29.5, 29.5, 29.3, 29.1, 29.0, 28.8, 28.8, 28.7, 28.3, 28.3, 24.8, 22.7, 19.2, 19.2, 14.1. ¹⁹F NMR (377 MHz, CDCl₃): δ = -75.0, -75.0, -76.0.

8.1.32. Synthesis of 14,14,15,15,16,16,17,17,18,18,19,19,20,20,21,21,21-heptadecafluoro-13-oxo-3,6,9,12-tetraoxahenicosyl tricosa-10,12-diynoate (TR-TEG-F17, 42)



Step 1. Synthesis of 2,2,3,3,4,4,5,5,6,6,7,7,8,8,9,9,9-heptadecafluorononanoyl chloride (F17-Cl, by analogy with TR-Cl 9).

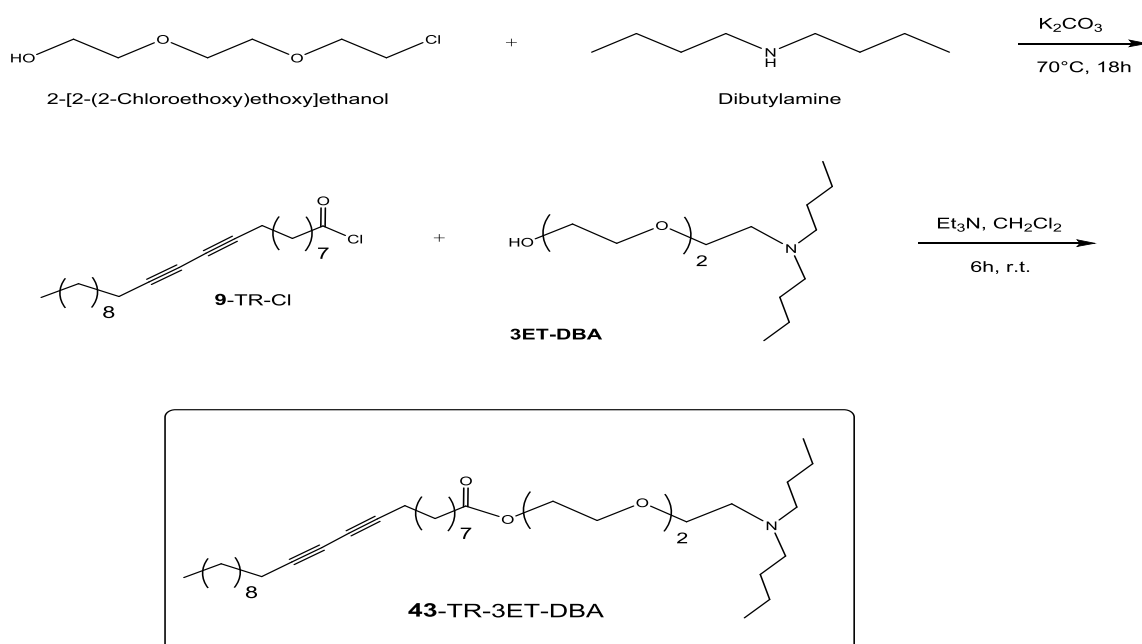
Step 2 . Synthesis of 2-(2-(2-hydroxyethoxy)ethoxy)ethyl 2,2,3,3,4,4,5,5,6,6,7,7,8,8,9,9,9-heptadecafluorononanoate (F17-TEG)

Procedure was a modification of previously reported one⁵⁷. **F17-Cl** (1 eq, 2 mmol) was added to tetraethylene glycol (4 eq, 8 mmol) followed by addition of catalytic amount of Amberlyst₁₅ (0.1 eq 0.2 mmol). The reaction was stirred at 35°C for 30 min, filtered and extracted with DCM, dried over MgSO₄, solvent evaporated. The crude product was purified by silica column chromatography using ethyl acetate and petroleum ether as eluents (1:4 - 9:1). The desired compound **F17-TEG** was isolated in 73 % yield. MW: Calcd for [M] C₁₇H₁₇F₁₇O₆, 640.29. ¹H NMR (400 MHz, CDCl₃): δ = 3.07-3.15(t, 3H), 3.58-3.70 (mm, 14H). ¹³C NMR (100 MHz, CDCl₃): δ = 162.0, 120.7, 115.1, 112.4, 112.4, 112.1, 111.9, 109.5, 107.3, 70.6, 70.6, 70.6, 70.5, 70.3, 69.2, 66.9, 61.7. ¹⁹F NMR (377 MHz, CDCl₃): δ = -82.4, -82.4, -82.4, -120.0, -120.0, -122.5, -122.6, -122.6, -122.7, -123.7, -123.8, -123.9, -123.9, -124.0, -127.6, -127.7, -127.2.

Step 3. Synthesis of 14,14,14-trifluoro-13-oxo-3,6,9,12-tetraoxatetradecyl tricosa-10,12-diynoate (TR-TEG-F17, 42).

Procedure was modified from previously reported ones¹²⁹. **F17-TEG** (1.5eq, 0.33 mmol) was dissolved in dry dichloromethane under N₂ atmosphere, to this solution **TRCDA 1** (2eq, 0.44 mmol), DMAP (1eq, 0.22 mmol) and DCC (1.5 eq, 0.33 mmol) was added. This reaction mixture was stirred at room temperature for 24 h, and then the reaction mixture was filtered and the clear solution was evaporated to dryness. The crude product was purified by silica column chromatography using ethyl acetate and petroleum ether as eluents (1:9-1:2). The desired compound **TR-TEG-F17 42** was collected in the third fraction in 44% yield. MW: Calcd for [M] C₄₀H₅₃F₁₇O₇, 968.83. ¹H NMR (400 MHz, CDCl₃): δ = 0.84–0.88 (t, J=8.0, 7.1 Hz, 3H), 1.24–1.41 (m, 22H), 1.45–1.61 (mm, 6H), 2.20–2.24 (t, 4H), 2.29–2.32 (t, 2H), 3.58–3.72 (mm, 14H), 4.20–4.23 (quint, 2H). ¹³C NMR (100 MHz, CDCl₃): δ = 173.9, 158.3, 120.3, 117.4, 112.4, 112.4, 112.1, 111.9, 108.5, 107.3, 76.7, 76.7, 70.5, 70.5, 70.3, 70.3, 69.2, 69.2, 66.9, 66.9, 64.4, 64.4, 34.1, 31.9, 29.5, 29.5, 29.3, 29.3, 29.0, 28.7, 28.7, 28.3, 28.3, 28.1, 28.1, 24.8, 22.7, 19.2, 19.2, 14.1. ¹⁹F NMR (377 MHz, CDCl₃): δ = -82.4, -82.4, -82.4, -120.0, -120.0, -122.5, -122.6, -122.6, -122.7, -123.7, -123.8, -123.9, -123.9, -124.0, -127.6, -127.7, -127.2.

8.1.33. Synthesis of 2-(2-(2-(dibutylamino)ethoxy)ethoxy)ethyl tricosa-10,12-diynoate (TR-3ET-DBA, 43)



Step 1. Synthesis of **2-(2-(dibutylamino)ethoxy)ethoxyethan-1-ol** (3ET-DBA)

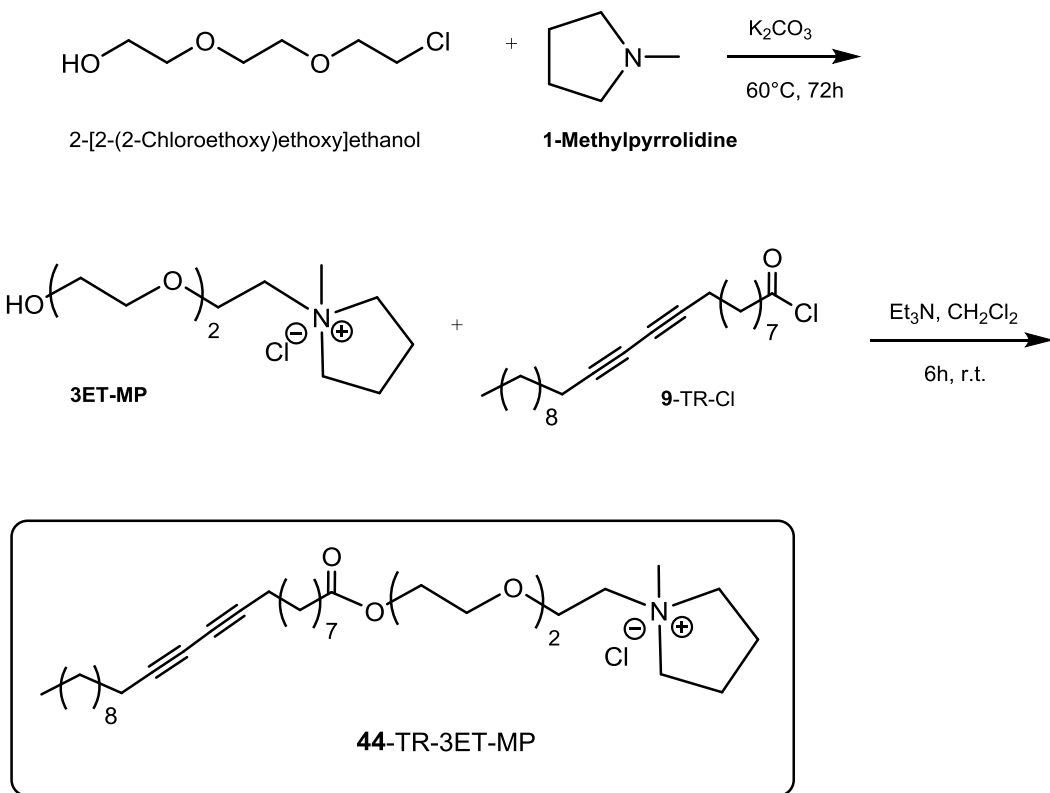
Procedure was modified from previously reported one⁴⁸. To the 2-[2-(2-Chloroethoxy)ethoxy]ethanol (1 eq, 3 mmol) and dibutylamine (1.2 eq, 3.6 mmol) K₂CO₃ (1.5 eq, 4.5 mmol) was added and reaction was stirred overnight at 70°C. Reaction mixture was filtered and dissolved in a small amount of CH₂Cl₂/MeOH and extracted with water. The organic layer is recovered, dried with anhydrous Na₂SO₄ and filtered. Crude product concentrated and purified by column chromatography (AcOEt : cyclohexane = 1 : 9 – 9 : 1). Desired compound **3ET-DBA** was isolated (76 %). MW: Calcd for [M] C₁₄H₃₁NO₃, 261.39. ¹H NMR (400 MHz, CDCl₃): δ = 0.88-0.91 (t, 6H), 1.23-1.32 (m, 4H), 1.41-1.49 (quint, 4H), 2.52 (s, 4H), 2.69- 2.72 (t, 2H), 2.85-2.88 (t, 1H), 3.58-3.75 (mm, 10H). ¹³C NMR (100 MHz, CDCl₃): δ = 70.4, 70.3, 70.1, 69.8, 61.3, 55.8, 55.8, 51.4, 30.5, 30.5, 20.4, 20.4, 13.8, 13.8.

Step 2. Synthesis of **tricosa-10,12-diynoyl chloride** (TR-Cl, **9**).

Step 3. Synthesis of **2-(2-(dibutylamino)ethoxy)ethoxyethyl tricosa-10,12-diynoate** (TR-3ET-DBA, **43**).

Procedure was adapted from a previously reported one⁴⁸. To a stirring solution of **9** (1 eq, 0.55 mmol) in CH₂Cl₂ (15 mL) was added **3ET-DBA** (1.2 eq, 0.66 mmol) and Et₃N (1 eq, 0.55 mmol); the resulting solution is stirred at r.t. for 6 h. The mixture is extracted from water with CH₂Cl₂ (x2, 50 mL). The organic layers are recovered, dried with anhydrous Na₂SO₄ and filtered. Solvent evaporated and the crude product was purified by column chromatography (AcOEt : cyclohexane = 1 : 2 – 95 : 5). **Yield:** 38 % of TR-3ET-DBA **43**. MW: Calcd for [M] C₃₇H₆₇NO₄, 589.95. ¹H NMR (400 MHz, CDCl₃): δ = 0.84-0.90 (t, J=8.0, 7.0 Hz, 9H), 1.23-1.61 (m, 39H), 2.20-2.67 (m, 10H), 3.52-3.69 (mm, 8H), 4.19-4.22 (t, 2H). ¹³C NMR (100 MHz, CDCl₃): δ = 173.1, 75.0, 75.0, 70.1, 70.1, 69.8, 69.3, 66.9, 64.4, 64.4, 56.9, 56.9, 51.4, 33.9, 31.9, 30.5, 30.5, 29.6, 29.6, 29.3, 29.3, 29.0, 28.7, 28.7, 28.4, 28.4, 28.1, 28.1, 25.0, 22.7, 19.2, 19.2, 14.1, 13.8, 13.8.

8.1.34. Synthesis of 1-methyl-1-(2-(2-(tricosa-10,12-diynoyloxy)ethoxy)ethoxyethyl)pyrrolidin-1-i um chloride (TR-3ET-DBA, **44)**



Step 1. Synthesis of **2-(2-(2-ethoxy)ethoxy)ethyl-1-methylpyrrolidinium chloride** (**3ET-MP**)

Procedure was modified from previously reported one¹³⁰. To the 2-[2-(2-Chloroethoxy)ethoxy]ethanol (1 eq, 3 mmol) and 1-methylpyrrolidine (1.2 eq, 3.6 mmol) K_2CO_3 (1.5 eq, 4.5 mmol) was added and reaction was stirred overnight at 60°C . Reaction mixture was filtered and dissolved in a small amount of $\text{CH}_2\text{Cl}_2/\text{MeOH}$ and extracted with water. The organic layer is recovered, dried with anhydrous Na_2SO_4 and filtered. Crude product concentrated and purified by column chromatography ($\text{AcOEt : cyclohexane} = 1 : 4 - 95 : 5$). Desired compound **3ET-MP** was isolated (44 %). MW: Calcd for [M] $\text{C}_{11}\text{H}_{24}\text{ClNO}_3$, 253.77. ^1H NMR (400 MHz, CDCl_3): $\delta = 2.19\text{-}2.28$ (t, 4H), 3.26-3.34 (t, 3H), 3.56-3.73 (mm, 10H), 3.83 (s, 3H), 3.88-4.06 (dd, 3H), 5.28 (s, 1H). ^{13}C NMR (100 MHz, CDCl_3): $\delta = 70.4, 70.3, 70.1, 69.8, 64.9, 64.9, 62.5, 61.3, 51.4, 22.1, 22.1$.

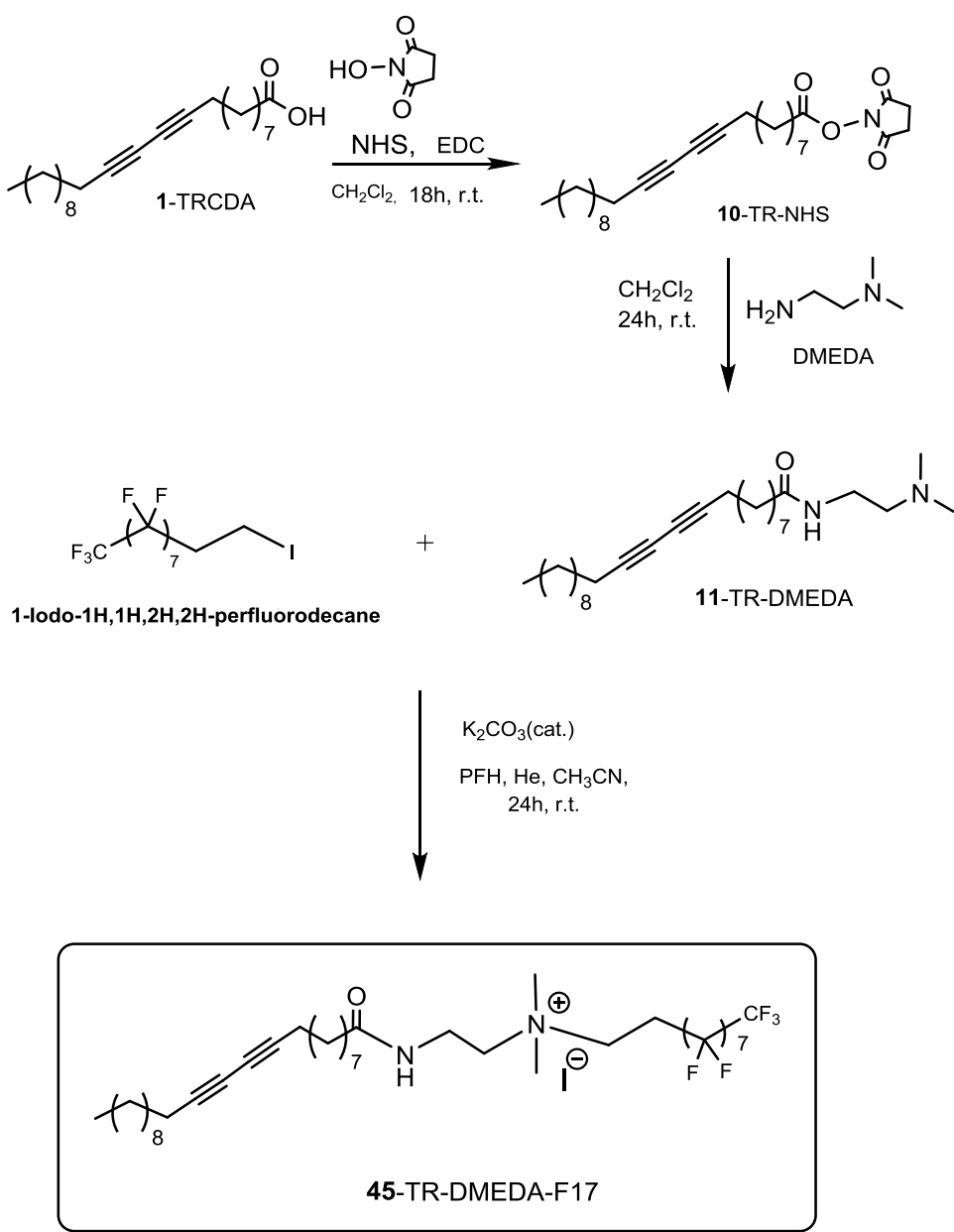
Step 2. Synthesis of **tricos-10,12-dienoyl chloride** (**TR-Cl, 9**).

Step 3. Synthesis of **1-methyl-1-(2-(2-(tricos-10,12-dienoyloxy)ethoxy)ethoxy)ethylpyrrolidin-1-iun chloride** (**TR-3ET-MP, 44**).

Procedure was adapted from a previously reported one⁴⁸. To a stirring solution of **9** (1 eq, 0.55 mmol) in CH_2Cl_2 (15 mL) was added **3ET-MP** (1.2 eq, 0.66 mmol) and Et_3N (1.2 eq, 0.66 mmol); the resulting solution is stirred at r.t. for 6 h. The mixture is extracted from water with CH_2Cl_2 (x2, 50 mL). The crude residue was dissolved in a small amount of MeOH and added dropwise to water. Addition of small amount of HCl (1:9) water solution to MeOH solution resulted in the formation of white precipitates. The precipitates formed were filtered, washed with water and dried under N_2 to give the desired product. **Yield:** 83 % of TR-3ET-MP **44**. MW: Calcd for [M] $\text{C}_{34}\text{H}_{60}\text{ClNO}_4$,

582.31. ^1H NMR (400 MHz, CDCl_3): δ = 0.84-0.88 (t, $J=8.0$, 7.1 Hz, 3H), 1.21-1.83 (m, 32H), 2.18-2.36 (mm, 6H), 3.04-3.11 (m, 4H), 3.28-3.31 (t, 4H), 3.44 (s, 1H), 3.62-4.10 (mm, 6H), 4.17-4.21 (t, 2H), 4.43-4.46 (t, 2H). ^{13}C NMR (100 MHz, CDCl_3): δ = 173.1, 75.0, 75.0, 70.1, 70.1, 69.3, 67.8, 66.9, 64.9, 64.9, 64.4, 64.4, 62.5, 49.8, 33.9, 31.9, 29.6, 29.6, 29.3, 29.3, 29.0, 28.7, 28.7, 28.4, 28.4, 28.1, 28.1, 25.0, 22.7, 22.1, 22.1, 19.2, 19.2, 14.1.

8.1.35. Synthesis of 3,3,4,4,5,5,6,6,7,7,8,8,9,9,10,10,10-heptadecafluoro-N,N-dimethyl-N-(2-(tricosa-10,12-diynamido)ethyl)decan-1-aminium iodide (TR-DMEDA-F17, 45)



Step 1. Synthesis of 2,5-dioxopyrrolidin-1-yl tricosa-10,12-diynoate (TR-NHS, 10).

Step 2. Synthesis of N-(2-(dimethylamino)ethyl)tricos-10,12-diynamide (TR-DMEDA, 11).

Step 3. Synthesis of 3,3,4,4,5,5,6,6,7,7,8,8,9,9,10,10,10-heptadecafluoro-N,N-dimethyl-N-(2-(tricos-10,12-diynamido)ethyl)decan-1-aminium iodide (TR-DMEDA-F17, 45).

Procedure was modified from previously reported one⁴⁷. To a solution containing TR-DMEDA (1 eq, 0.24 mmol) in CH₃CN (10 mL), 1-Iodo-1H,1H,2H,2H-perfluorodecane (2 eq, 0.48 mmol) in PFH and K₂CO₃ (2 eq, 0.48 mmol) were added. The resulting suspension was stirred at r.t. for 24 h and filtered. After evaporation of solvents, the quantitative product TR-DMEDA-F17 **45** was obtained. **Yield:** white solid (75%). MW: Calcd for [M] C₃₇H₅₂F₁₇IN₂O, 990.71. ¹H NMR (400 MHz, CDCl₃): δ = 0.83–0.87 (t, J=8.0, 7.1 Hz, 3H), 1.11–1.28 (m, 22H), 1.35–1.44 (m, 10H), 1.55(s, 6H), 2.03–2.15 (m, 4H), 2.60–2.80 (m, 4H), 3.22–3.25 (t, 2H), 5.27 (s, 1H). ¹³C NMR (100 MHz, CDCl₃) δ = 172.8, 118.7, 118.5, 112.7, 112.7, 112.4, 111.9, 111.7, 109.5, 76.67, 76.67, 65.26, 65.26, 63.2, 52.3, 52.3, 50.8, 36.5, 33.6, 31.9, 29.6, 29.6, 29.3, 28.9, 28.7, 28.7, 28.6, 28.4, 28.4, 28.1, 28.1, 25.6, 22.7, 19.4, 19.3, 19.3, 14.1.

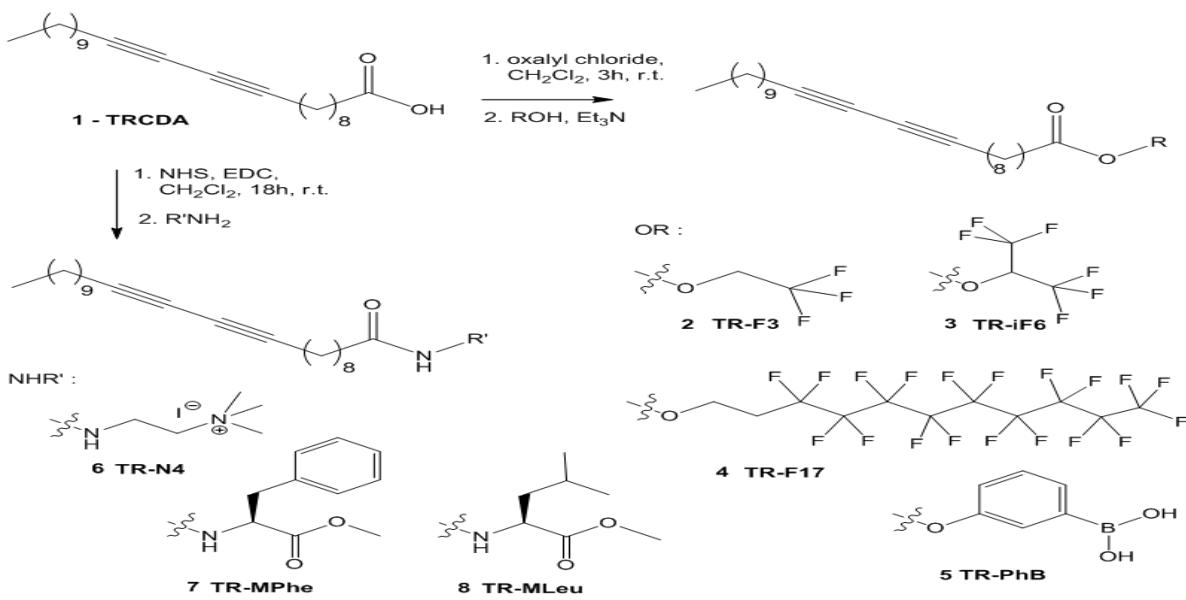
8.2. Chapter 4: Colorimetric sensors for the detection of binding materials

8.2.1. Materials

All solvents were purchased from Sigma-Aldrich Chemicals. The diacetylene monomer, 10,12-tricosadiynoic acid (TRCDA), was purchased from Aldrich (98% purity) and eventually purified to remove the polymerized part (if present) before use. For natural gums study, arabic, ghatti, tragacanth, guar and karaya gums were purchased from Sigma Aldrich. Analytical thin-layer chromatography (TLC) was conducted on Sigma-Aldrich silica gel aluminum plates (60 Å, with fluorescent indicator) or silica gel 60 F-254 with a 0.2 mm layer thickness. For flash chromatography, 60 Å silica gel (Merck, 230–400 mesh) was employed. ¹H, ¹³C and ¹⁹F NMR spectra were obtained using a Varian Mercury 400 spectrometer with a 5 mm probe.

8.2.2. Synthesis of diacetylene monomer derivatives

Synthesis routes developed for synthesizing the TRCDA derivatives **2–8** are summarized in Scheme 1. All synthesis routes started from 10,12-tricosadiynoic acid (TRCDA) **1**. Ester derivatives were prepared by treating **1** with oxalyl chloride and the suitable fluorinated alcohol to obtain **2–4** or phenylboronic acid to obtain **5**. Amide derivatives **6–8** were prepared by activating **1** via its hydroxysuccinamide derivative, in the presence of EDC, and then coupling with the corresponding amine or amino-acid methyl ester. All diacetylene derivatives **2–8** were characterized by standard analytical and spectroscopic techniques and proved very stable when stored under nitrogen (or at -20 °C) in the dark. Details on synthesis and spectroscopic data are reported in the Chapter 8.1. and Chapter 9.1.



Scheme 1 General synthetic pathways to TR-ester derivatives **2–5**, and TR-amide derivatives **6–8**.

8.2.3. Film preparation

40 mg of TRCDA and TR derivatives (mole ratio 3 : 1) were dissolved in a solvent mixture comprising 500 mL CH_2Cl_2 and 500 mL THF. 40 mL of this solution was placed upon a PMMA disk (0.5 cm diameter). After 30 seconds, spin coating was carried out at 1500 rpm for 30 seconds. The films were subsequently UV irradiated (254 nm) for 0.3 minutes in a UV oven, yielding blue-phase PDA.

8.2.4. Colorimetric measurements and analysis

The organic painting material samples were solubilized in different solvents (outlined in the Results section) at a concentration of 10 mg mL^{-1} and placed upon the spin-coated PDA films and incubated for 90 minutes. Ultraviolet (UV)-vis spectroscopy measurements were subsequently carried out at 25 °C on a Varioskan (Thermo, Finland) in a wavelength range of 400–800 nm.

Percentage colorimetric response (%CR) was calculated after baseline correction of the UV-vis absorbance spectrum, according to the equation:

$$\% \text{CR} = [(\text{PB}_0 - \text{PB}_i)/\text{PB}_0] \times 100$$

where $\text{PB} = \text{A}_{\text{blue}}/(\text{A}_{\text{blue}} + \text{A}_{\text{red}})$, A_{blue} = absorbance at 640 nm, A_{red} = absorbance at 500 nm, PB_0 corresponds to the control film, and PB_i corresponds to the sample. Reference %CR was registered on tris buffer with pH 8.0.

8.2.5. Analytical techniques

8.2.5.1. Scanning electron microscopy (SEM)

SEM images were recorded on a JEOL JSM-7400F (Tokyo, Japan) scanning electron microscope. Images were taken after sputtering a thin film of Au (~15 nm thickness) over the substrates for better contrast and minimum charging.

8.2.5.2. Raman scattering

The Raman system comprised a Jobin-Yvon LabRam HR 800 micro-Raman system, equipped with a synapse CCD detector. The excitation sources were an Argon laser (514.5 nm) and a He–Ne laser (633 nm), both exhibiting 3 mW power. The full laser power was reduced by 1000 using ND filters to prevent affecting the measurements. The laser was focused with a $\times 100$ objective to a spot of around 1 mm². The grating used was a 600 g mm⁻¹ and the confocal hole of 100 mm with exposure times of 10–60 seconds.

8.3. Chapter 5: Colorimetric sensors for the detection of VOCs

8.3.1. Materials

Tetraethylorthosilicate (TEOS) was purchased from Sigma-Aldrich, USA. The diacetylene monomer 10,12-tricosadiynoic acid (TRCDA) was purchased from Alfa-Aesar, England. Tetrahydrofuran (THF) and diethyl ether were purchased from Bio-Lab Ltd. Dichloromethane (DCM), ammonium hydroxide (NH₄OH), chloroform (CHCl₃), methanol, dimethylformamide (DMF), and acetone were purchased from Frutarom Ltd. (Haifa, Israel). Benzene was purchased from Merck. Lauroyl chloride was bought from TCI, Japan. Chloroform, toluene, pentane, and n-hexane were purchased from Daejung Chemicals, Korea. Ethanol was purchased from J. T. Baker. Tetrahydrofuran was purchased from Acros Organics, USA. Ethyl acetate and concentrated hydrochloric acid (HCl) were purchased from Bio-Lab Ltd. (Jerusalem, Israel). 2-Propanol was bought from SDFCL, India. All the reagents and solvents were used as received without further purification.

8.3.2. Aerogel Synthesis

Wet silica gel was prepared according to previous report^{72,73} Briefly, 5 mL of TEOS, 15 mL of anhydrous ethanol (EtOH), 5 mL of distilled water, and 5 µL of concentrated hydrochloric acid were mixed in a 100 mL flask and stirred in a 60°C water bath for 90 min. Subsequently, 25 mL of ethanol, 13 mL of distilled water, and 15 µL of NH₄OH were added to the solution and stirred for 30 min under the same temperature. The prepared wet silica gel was coated with parafilm before it was further dried and transferred into 200 mL of anhydrous ethanol and placed in GCF1400 atm furnace under ultrapure N₂ gas atmosphere. Afterward, the outlet was closed while the ultrapure N₂

was continuously passed into the autoclave and reached 1 MPa. The temperature was first raised quickly from room temperature to 200 °C, increased slowly to 246 °C, followed by 260 °C for 3h at 2 MPa N₂ gas pressure. Finally, the white colored silica aerogel were obtained after opening the autoclave.

8.3.3. Diacetylene Monomers Synthesis

8.3.3.1. 10, 12-Tricosadiyn Amine (TR-NH2)

Synthesis of 10, 12-tricosadiyn amine was carried out through a two-step pathway⁶¹⁵⁵. Briefly, 570 mg of TRCDA was dissolved in 20 mL of DCM. Then 2 mL of oxalyl chloride was added into TRCDA solution under an argon atmosphere. Several drops of DMF were then added as catalyst followed by stirring overnight at room temperature. Then solvent was evaporated, and the residue was dissolved in dry THF (20 mL). The solution was then slowly added to 30 mL of NH₄OH (25%) in an ice bath and stirred overnight. The solvent was evaporated, and the residue was purified and added to 30 mL of diethyl ether. LiAlH₄ (550 mg) was added to it while keeping the solution in an ice bath under overnight stirring and then poured into a saturated solution of NH₄Cl. The aqueous layer was then extracted with ethyl acetate. The combined organic layer was washed with saturated NaCl solution and then dried with MgSO₄, filtered, and evaporated. The residue was purified with column chromatography over silica gel.

8.3.3.2. Methyl Tricosa-10,12-diynoylphenylalaninate (TR-MPhe)

Methyl tricosa-10,12-diynoylphenylalaninate (TR-MPhe) was synthesized according to published protocols⁵¹. Phenylalanine (3 mmol) and trimethylsilyl chloride (6 mmol) are stirred in MeOH (10 mL) at rt for 24 h. The solvent was evaporated under reduced pressure, and the crude (MPhe*HCl) was used with TR-NHS without further purifications. TRCDA (0.29 mmol) was solubilized in DCM (3 mL). N-Hydroxysuccinimide (0.35 mmol) and 1-ethyl-3-(dimethylamino)propyl carbodiimide (0.55 mmol) were solubilized in DCM (5 mL) and mixed to the solution of TRCDA under stirring at room temperature. After 20 h, the solvent was evaporated under reduced pressure followed by extraction from water with diethyl ether. The organic layers were recovered, dried with anhydrous Na₂SO₄, filtered, and evaporated to get TR-NHS and dissolved in DCM. MPhe*HCl (0.49 mmol) was added to the mixture followed by dropwise addition of triethylamine (0.29 mmol) with stirring for 24 h. Then the product was purified by column chromatography.

8.3.4. Synthesis of PDA–Aerogel

PDA–aerogel was fabricated by different techniques using different TRCDA derivatives. First, 570 mg of TRCDA was dissolved in 20 mL of DCM. Then the solution was filtered through a membrane filter (Millex, Nylon, 0.45 µm). Then 20 µL of the filtered TRCDA solution was drop-casted on 10 mg of aerogel powder. Then the TRCDA–aerogel was irradiated with ultraviolet light

(254 nm) for 0.5 min to produce the polymerized, blue phase of polydiacetylene. TRCDA and TR-NH₂ or TR-MPhe mixtures were mixed at 5:1 ratio in the case of diacetylene derivative mixtures.

8.3.5. VOC Sensing

Predetermined quantities of organic liquids were placed in a 500 mL closed glass container to obtain desired vapor pressures using a MiniRAE Lite (PID). In parallel, 50 mg of PDA-aerogel was placed in the sealed container and incubated prior to colorimetric and fluorescence analysis (Chapter 9.3., Figure S3).

8.3.6. Instrumentation and Characterization

Scanning electron microscopy (SEM) experiments were conducted using a JEOL (Tokyo, Japan) model JSM-7400F scanning electron microscope. Images were taken after sputtering a thin film of gold over the substrates for better contrast and minimum charging. Fluorescence emission spectra of the PDAs–aerogel were recorded on a Varioskan plate reader using 482 nm excitation wavelength. Confocal microscopy images of PDAs-aerogel were acquired on an UltraVIEW system (PerkinElmer Life Sciences, Waltham, MA) equipped with an Axiovert-200 M microscope (Zeiss, Oberkochen, Germany) and a Plan-Neofluar 63 \times /1.4 oil objective. The excitation wavelength at 488 nm was produced by an argon/krypton laser. Emitted light was passed through a barrier filter (580–700 nm). Surface area, pore volume, and pore diameters of the PDA-aerogel were measured by a BET instrument (Quantachrome High Speed gas sorption analyzer NOVA-1200e). Degassing of the PDA-aerogel was carried out for 21h in order to evaporate all traces of solvents and moisture followed by N₂ adsorption-desorption in liquid nitrogen. Raman spectra were recorded with a Horiba–Jobin–Yvon LabRam HR 800 micro-Raman system, equipped with a Synapse CCD detector. The excitation source was an He-Ne laser (633 nm), with a power of 5 mW. To protect the samples the laser power was reduced by 1000 using ND filters. The laser was focused with x100 \times long-focallength objective to a spot of about 1 μ m. Measurements were taken with the 600 g mm⁻¹ grating and a confocal hole of 100 μ m with a typical exposure time of 1 min.

8.3.7. Chromatic (Red–Green–Blue, RGB) Analysis

Multiwell plates containing multicolored dust PDA–aerogel were scanned in transmitted mode on an Epson 4990 photo scanner to produce 2400 dpi, 24-bit color depth red-green-blue (RGB) images. Digital colorimetric analysis (DCA) was performed by extracting RGB channels values for each pixel within the sample spots in the scanned images, and the color change values were estimated using Matlab R2010 scientific software (The Mathworks, Inc., MA, USA). Briefly, DCA handles the standard “red-green-blue” (sRGB) model, essentially translating every color signal into three distinct values corresponding to the intensities of red (R), green (G), and blue (B) color channels.

Accordingly, the relative intensity of a particular RGB component in a scanned image can be described as the chromaticity level. For example, the red chromaticity level (r) in each pixel was figured as

$$r = R/(R + B + G)$$

where R (red), G (green), and B (blue) are the three primary color components. For a defined surface area within a PDA-based sensor well, we classified a quantitative parameter denoted chromatic response that represents the total blue-red transformations of the pixels encompassed in the area,

$$\% \text{RGB} = (r_{\text{sample}} - r_0)/(r_{\text{max}} - r_0) \times 100\%$$

where r_{sample} is the average red chromaticity level of all pixels in the scanned surface, r_0 is the average red level calculated in a blank surface (blue sensor well), and r_{max} is the average red chromaticity level of the maximal blue-red transition, an area of the sensor well in which the most pronounced blue-red transition was induced (positive control). In essence, the calculated %RGB is the normalized change in the red chromaticity level within the sensor well surface on which the tested sample was deposited.

8.4. Chapter 6: Colorimetric sensors for the detection of OPs.

8.4.1. Materials and methods

Sonication of 4 mL vials with the mixed solutions of OP + buffer was conducted for 1-2 minutes. The vial was vortexed for a few seconds at the lowest possible speed, and the mixed solution (300 pL) was immediately transferred into the appropriate well over the TR/TR derivatives coated Perspex. Special care should be taken to ensure that the Perspex is not partly floating in the solution and bubbles are to be removed if necessary. The order of addition should be preserved in the following experiments according to the different OP. A "control" sample containing TFE and Tris buffer at a molar ratio of 1:20 should be added last in the order of addition. The 48 well plate was incubated for 90 minutes in the incubator at 27.0°C - 28.0°C. Then fluorometric scanning was performed. Results of different TR derivatives for several organophosphate pesticides are provided in Chapter 6, Figures 21a-e. Films were prepared at various ratios 1:1, 1:3, 2:3, 1:6, and 1:9 as compared to the monomer having a small hydrophilic headgroup (**1**-TRCDA).

8.4.2. Synthesis of TRCDA monomers

Amphiphiles discussed in the Chapter 6 were prepared according to the procedures detailed described in Chapter 3 and synthetic procedures described in Chapter 8.1. Detailed analytical data of the compounds are provided in the Chapter 9.1.

8.4.3. Vesicle preparation

A liposome solution containing unmodified 10, 12-tricosadiynoic acid (**1**, TRCDA) and receptor modified TRCDA was prepared using an earlier reported procedure⁵⁵. According to that, a mixture containing the diacetylene amphiphiles and diacetylene carboxylic acid **1** in a molar ratio of 10 : 90, respectively, was dissolved in dichloromethane in a 25 mL round bottom flask. The solvent was evaporated by a stream of N₂ gas and an appropriate amount of buffered aqueous solution (HEPES 10 mmol, pH = 7.2) was added to the flask to give the desired concentration of the lipid (1 × 10-3 M). This solution was sonicated at 75–80°C for 40 min. The resulting milky solution was filtered through a syringe filter (pore size: 1 mm, filter: 15 mm) while hot, the filtrate was cooled and stored at 0°C overnight. The self-assembled vesicles were polymerized at room temperature by irradiating the solutions with light of 254 nm wavelength for 5 to 10 min, whereby the colourless vesicle solution turned blue. The average size of the liposomes was 150–250 nm as determined by dynamic light scattering (DLS). The stability of the vesicles depends on the concentration of the vesicles. Highly concentrated vesicle solutions are unstable and the vesicles will precipitate over time. More diluted samples are very stable when stored at 4°C (> 3 month test period).

8.5. Chapter 7: Synthesis and characterization of cyano-substituted azaacenes.

8.5.1. Materials and Methods

4,5-Dibromophthalonitrile¹³¹ and 6,7-dibromonaphthalene-2,3-dicarbonitrile¹³² were synthesized according to literature procedures. A Monowave 300 reactor from Anton Paar with an external IR temperature sensor was used for microwave reactions. The palladium precatalyst PdRuPhos was purchased from Sigma-Aldrich. Column chromatography was performed using silica gel from Macherey, Nagel & Co. (particle size: 0.032–0.062 mm). NMR spectra were recorded on Bruker Avance Spectrometers using the specified frequency. Chemical shifts (δ) are given in parts per million (ppm) relative to internal solvent signals¹³³. The following abbreviations describe the signal multiplicities: s = singlet, d = doublet, dd = doublet of doublets, m = multiplet. High-resolution mass spectra (HRMS) were obtained by matrix-assisted laser desorption/ionization (MALDI), electrospray ionisation (SI) or direct analysis in real time (DART) experiments. CV measurements were performed on a VersaSTAT 3 potentiostat by Princeton Applied Research. UV-vis spectra were recorded on a Jasco V670. Optical microscopy was performed on a Nikon LV100i-Pol microscope under cross-polarized light. Computational studies were carried out using DFT calculations on Turbomole 6.3.1 or Gaussian 09. Geometry optimizations were performed using the B3LYP functional and def2-TZVP basis set. At this geometry, the absolute energy and FMO energies were assigned by a single-point approach at the B3LYP/6-311++G** level¹³⁴. CCDC 1529783 (3a), 1529784 (3b), 1529785 (3c), 1529786 (5a), 1529787 (5b) contain the supplementary crystallographic data for this paper. These data can be obtained free of charge from The Cambridge Crystallographic Data Centre via www.ccdc.cam.ac.uk/data_request/cif.

8.5.2. General Procedure 1 (GP1)

A solution of ortho-diamine (1.00 eq.), ortho-dibromide (1.00 eq.), Pd(PPh₃)₄ (10 mol%), dppf (10 mol%) and cesium carbonate (6.00 eq.) in dry toluene (5 mL) was stirred under argon at

120 °C for 18 h in a sealed vial. Water was added, the phases were separated and the aqueous layer was extracted with dichloromethane (3 x 10 mL). The combined organic layers were washed with brine, dried over MgSO₄ and filtered. The solvent was removed under reduced pressure and the crude product was purified by flash column chromatography.

8.5.3. General Procedure 2 (GP2)

A solution of ortho-diamine (1.10 eq.), ortho-dibromide (1.00 eq.) and PdRuPhos (5 mol%) in dry 1,4-dioxane (3 mL) was degassed for 10 min. Subsequently, cesium carbonate (4.00 eq.) was added under argon and the mixture was stirred for 16 h at 120 °C under microwave irradiation. Water was added, the phases were separated and the aqueous layer was extracted with dichloromethane (3 x 10 mL). The combined organic layers were washed with brine, dried over MgSO₄ and filtered. The solvent was removed under reduced pressure and the crude product was purified by flash column chromatography.

8.5.4. General Procedure 3 (GP3)

A mixture of *N,N'*-dihydroazaacene (1.00 eq.) and MnO₂ (20.0 eq.) in dichloromethane (5 mL) was stirred at room temperature for 1 h. The reaction mixture was filtered through celite, the solvent was evaporated under reduced pressure and the crude product was purified by flash column chromatography.

6,9-Bis((tri-*iso*-propylsilyl)ethynyl)phenazine-2,3-dicarbonitrile (3a)

GP1 was applied to the *ortho*-diamine **1a** (300 mg, 639 µmol, 1.00 eq.) using 4,5-dibromophthalonitrile (201 mg, 704 µmol, 1.10 eq.), Pd(PPh₃)₄ (73.8 mg, 63.9 µmol, 0.10 eq.) dppf (35.4 mg, 63.9 µmol, 0.10 eq.) and cesium carbonate (832 mg, 2.56 mmol, 4.00 eq.). The crude product was purified by flash column chromatography (silica gel, petroleum ether/ethyl acetate 98:2) and directly subjected to **GP3** due to its instability under ambient conditions. After purification by flash column chromatography (silica gel, petroleum ether/dichloromethane 90:10), **3a** could be obtained as an orange solid (184 mg, 311 µmol, 49% over two steps). M.p. 187–188 °C; ¹H NMR (300 MHz, CDCl₃, 25 °C): δ = 8.74 (s, 2H), 8.09 (s, 2H), 1.25 (s, 42H); ¹³C NMR (101 MHz, CDCl₃, 25 °C) δ = 145.52, 142.48, 139.05, 136.54, 125.03, 115.10, 114.22, 103.56, 102.19, 18.92, 11.59; IR (neat): ν (cm⁻¹) = 2941, 2864, 1567, 1506, 1457, 1366, 1349, 1035, 880, 794; UV-vis (CH₂Cl₂): λ_{max} = 483 nm; HR-MS (DART): *m/z* calcd. for C₃₆H₄₆N₄Si₂: [M]⁺ 591.3334, found: 591.3329, correct isotope distribution; elemental analysis: calcd. for C₃₆H₄₆N₄Si₂: C 73.17, H 7.85, N 9.48, found: C 73.07, H 7.95, N 8.99.

6,11-Bis((tri-*iso*-propylsilyl)ethynyl)benzo[*b*]phenazine-2,3-dicarbonitrile(3b)

GP1 was applied to the *ortho*-diamine **1b** (50 mg, 96.4 µmol, 1.00 eq.) using 4,5-dibromophthalonitrile (30 mg, 106 µmol, 1.10 eq.), Pd(PPh₃)₄ (10 mg, 9.64 µmol, 0.10 eq.) dppf (5.3 mg, 9.64 µmol, 0.10 eq.) and cesium carbonate (125 mg, 384 µmol, 4.00 eq.). The crude product was purified by flash column chromatography (silica gel, petroleum ether/ethyl acetate 99:1) and directly subjected to **GP3** due to its instability under ambient conditions. After purification by flash column chromatography (silica gel, petroleum ether/ethyl acetate 98:2), **3b** could be obtained as dark blue needles (21.3 mg, 33.2 µmol, 34% over two steps). M.p. 297–298

[°]C; ¹H NMR (600 MHz, CDCl₃, 25°C): δ = 8.75 – 8.69 (m, 2H), 8.24 – 8.21 (m, 2H), 7.42 (s, 2H), 2.25 – 2.09 (m, 42H); ¹³C NMR (151 MHz, CDCl₃, 25°C): δ = 134.86, 132.84, 129.82, 126.47, 125.16, 115.83, 115.23, 105.63, 101.54, 98.93, 18.98, 11.37. IR (neat): ν(cm⁻¹) = 2939, 2890, 2232, 2132, 1460, 1440, 1390, 1042, 880, 784; UV-vis (CH₂Cl₂): λ_{max} = 652 nm; HR-MS (ESI): *m/z* calcd. for C₄₀H₄₉N₄Si₂: [M+H]⁺ 641.3490, found: 641.3497, correct isotope distribution; elemental analysis: calcd. for C₄₀H₄₈N₄Si₂: C 74.95, H 7.55, N 8.74, found: C 74.75, H 7.78, N 8.79.

6,13-Bis((tri-*iso*-propylsilyl)ethynyl)naphtho[2,3-*b*]phenazine-2,3-dicarbonitrile (**3c**)

GP2 was applied to the *ortho*-diamine **1c** (102 mg, 179 μmol, 1.10 eq.) using 4,5-dibromophthalonitrile (46.4 mg, 162 μmol, 1.00 eq.), cesium carbonate (211 mg, 648 μmol, 4.00 eq.) and PdRuPhos (6.6 mg, 8.08 μmol, 0.05 eq.) in dry 1,4-dioxane(3 mL). Flash column chromatography (silica gel, petroleum ether/dichloromethane 70:30) yielded **3c-H₂** as a green solid (36 mg, 51.9 μmol, 32%). M.p. 344–346 °C (decomp.); ¹H NMR (500 MHz, CDCl₃, 25°C): δ = 8.27 (s, 2H), 7.80 (dd, J = 6.3, 3.3 Hz, 2H), 7.39 (dd, J = 6.4, 3.2 Hz, 2H), 6.77 (s, 2H), 6.45 (s, 2H), 1.36 – 1.21 (m, 42H); ¹³C NMR (101 MHz, CDCl₃, 25°C): δ = 133.76, 132.86, 132.27, 128.10, 128.07, 126.04, 123.80, 115.81, 115.77, 109.16, 106.20, 100.20, 99.33, 19.05, 11.52; IR (neat): ν(cm⁻¹) = 3374, 2940, 2888, 2225, 2141, 1582, 1460, 1438, 876, 743; UV-vis (CH₂Cl₂): λ_{max} = 481 nm; HR-MS (DART): *m/z* calcd. for C₄₄H₅₂N₄Si₂: [M]⁺ 692.3725, found: 692.3730, correct isotope distribution; elemental analysis: calcd. for C₄₄H₅₂N₄Si₂: C 76.25, H 7.56, N 8.08, found: C 75.61, H 7.69, N 8.08.

3c-H₂ (25.0 mg, 36.1 μmol, 1.00 eq.) was subjected to **GP3**. After purification by flash column chromatography (silica gel, petroleum ether/dichloromethane 70:30 to 60:40), **3** could be obtained as a dark green solid (24.1 mg, 34.9 μmol, 97%).

M.p. >350 °C; ¹H NMR (500 MHz, CDCl₃, 25°C): δ = 9.43 (s, 2H), 8.71 (s, 2H), 8.08 – 8.02 (m, 2H), 7.59 – 7.53 (m, 2H), 1.39 – 1.31 (m, 42H); ¹³C NMR (126 MHz, CDCl₃, 25°C): δ = 142.70, 141.68, 140.01, 134.13, 133.85, 128.96, 128.07, 127.56, 122.21, 115.30, 113.51, 112.74, 102.97, 19.11, 11.76; IR (neat): ν(cm⁻¹) = 2939, 2862, 2231, 2145, 1538, 1461, 1376, 881, 751, 661; UV-vis (CH₂Cl₂): λ_{max} = 811 nm; HR-MS (DART): *m/z* calcd. for C₄₄H₅₀N₄Si₂: [M]⁺ 690.3574, found: 690.3569, correct isotope distribution; elemental analysis: calcd. for C₄₄H₅₀N₄Si₂: C 76.47, H 7.29, N 8.11, found: C 75.26, H 7.19, N 7.49.

1,4-Bis((tri-*iso*-propylsilyl)ethynyl)benzo[*b*]phenazine-8,9-dicarbonitrile (**5a**)

GP1 was applied to the *ortho*-diamine **1a** (300 mg, 639 μmol, 1.00 eq.) using 6,7-dibromonaphthalene-2,3-dicarbonitrile (248 mg, 738 μmol, 1.10 eq.), Pd(PPh₃)₄ (73 mg, 63.9 μmol, 0.10 eq.) dppf (35.4 mg, 63.9 μmol, 0.10 eq.) and cesium carbonate (834 mg, 2.56 mmol, 4.00 eq.). The crude product was purified by flash column chromatography (silica gel, petroleum ether/ethyl acetate 95:5) and directly subjected to **GP3** due to its instability under ambient conditions. After purification by flash column chromatography (silica gel, petroleum ether/dichloromethane 75:25) **5a** could be obtained as a dark red solid (182 mg, 284 μmol, 44% over two steps).

M.p. 307–308 °C (decomp.); ¹H NMR (400 MHz, CDCl₃, 25°C): δ 8.91 (s, 2H), 8.61 (s, 2H), 8.03 (s, 2H), 1.32 – 1.30 (m, 42H); ¹³C NMR (101 MHz, CDCl₃, 25°C): δ = 145.45, 141.21, 138.18,

135.79, 131.56, 131.51, 124.98, 115.60, 109.76, 102.79, 19.01, 11.69; IR (neat): ν (cm⁻¹) = 2939, 2862, 2234, 2149, 1461, 1448, 1382, 1357, 1036, 784; UV-vis (CH₂Cl₂): λ_{max} = 538 nm; HR-MS (DART): *m/z* calcd. for C₄₀H₄₈N₄Si₂: [M]⁻ 640.3423, found: 640.3434, correct isotope distribution; elemental analysis: calcd. for C₄₀H₄₈N₄Si₂: C 74.95, H, 7.55, N 8.74, found: C 74.87, H 7.63, N 8.82.

7,12-Bis((tri-*iso*-propylsilyl)ethynyl)dibenzo[*b,i*]phenazine-2,3-dicarbonitrile (5b)

GP1 was applied to the *ortho*-diamine **1b** (100 mg, 192 μ mol, 1.00 eq.) using 6,7-dibromonaphthalene-2,3-dicarbonitrile (65 mg, 192 μ mol, 1.00 eq.), Pd(PPh₃)₄ (23 mg, 19.2 μ mol, 0.10 eq.) dppf (11 mg, 19.2 μ mol, 0.10 eq.) and cesium carbonate (370 mg, 1.15 mmol, 6.00 eq.). The crude product was purified by flash column chromatography (silica gel, petroleum ether/ethyl acetate 80:20 to 75:25) to yield **5b-H₂** as a yellow solid (78 mg, 113 μ mol, 59%). M.p. 305 °C; ¹H NMR (500 MHz, CDCl₃, 25°C): δ = 7.82 (dd, J = 6.2, 3.3 Hz, 2H), 7.68 (s, 2H), 7.31 (dd, J = 6.2, 3.2 Hz, 2H), 6.88 (s, 2H), 6.42 (s, 2H), 1.28 – 1.20 (m, 42H); ¹³C NMR (126 MHz, CDCl₃, 25°C): δ = 134.75, 132.39, 132.31, 131.79, 129.51, 126.18, 125.07, 116.54, 108.17, 106.86, 105.31, 101.05, 99.46, 19.04, 11.45; IR (neat): ν (cm⁻¹) = 3384, 2941, 2863, 2227, 2125, 2125, 1528, 1467, 1437, 880; UV-vis (CH₂Cl₂): λ_{max} = 774 nm; HR-MS (ESI): *m/z* calcd. for C₄₄H₅₃N₄Si₂: [M+H]⁺ 693.38033, found: 693.38172, correct isotope distribution.

5b-H₂ (80.0 mg, 115 μ mol, 1.00 eq.) was subjected to **GP3**. After purification by flash column chromatography (silica gel, petroleum ether/dichloromethane 80:20 to 75:35), **5b** could be obtained as a dark green solid (63.6 mg, 92 μ mol, 80%). M.p. 310°C; ¹H NMR (301 MHz, CDCl₃, 25°C): δ = 8.82 (s, 2H), 8.69 (dd, J = 6.9, 3.2 Hz, 2H), 8.46 (s, 2H), 7.70 (dd, J = 6.9, 3.2 Hz, 2H), 1.43 – 1.35 (m, 42H). ¹³C NMR (76 MHz, CDCl₃, 25°C): δ = 142.56, 141.51, 138.31, 136.94, 131.68, 131.28, 129.66, 127.99, 121.31, 115.51, 110.61, 109.22, 102.51, 19.17, 11.80; IR (neat): ν (cm⁻¹) = 2937, 2862, 2888, 2233, 1522, 1462, 1387, 1080, 1044, 906; UV-vis (CH₂Cl₂): λ_{max} = 712 nm; HR-MS (ESI): *m/z* calcd. for C₄₄H₅₁N₄Si₂: [M+H]⁺ 691.36468, found: 691.36742, correct isotope distribution; elemental analysis: calcd. for C₄₄H₅₀N₄Si₂: C 76.47, H 7.29, N 8.11, found: C 76.47, H 7.47, N 7.63.

7,14-Bis((tri-*iso*-propylsilyl)ethynyl)benzo[*b*]naphtho[2,3-*i*]phenazine-2,3-dicarbonitrile (5c)

GP2 was applied to the *ortho*-diamine **1c** (104 mg, 182 μ mol, 1.10 eq.) using 6,7-dibromonaphthalene-2,3-dicarbonitrile (55.5 mg, 165 μ mol, 1.00 eq.), cesium carbonate (215 mg, 660 μ mol, 4.00 eq.) and PdRuPhos (6.7 mg, 8.25 μ mol, 0.05 eq.) in dry 1,4-dioxane (4 mL). Flash column chromatography (silica gel, petroleum ether/dichloromethane 60:40) yielded **5c-H₂** as a green solid (74 mg, 99.5 μ mol, 55%). M.p. 308-309 °C (decomp.); ¹H NMR (500 MHz, CDCl₃, 25°C): δ = 8.35 (s, 2H), 7.83 (dd, J = 6.3, 3.3 Hz, 2H), 7.80 (s, 2H), 7.39 (dd, J = 6.4, 3.2 Hz, 2H), 7.18 (s, 2H), 6.60 (s, 2H), 1.33 – 1.24 (m, 42H); ¹³C NMR (126 MHz, CDCl₃, 25°C): δ = 133.99, 132.78, 132.67, 131.98, 131.51, 128.04, 128.00, 125.79, 123.54, 116.59, 108.25, 107.40, 105.83, 99.81, 99.58, 19.09, 11.53; IR (neat): ν (cm⁻¹) = 3384, 2946, 2867, 2228, 2199, 2133, 1479, 1453, 1470, 875; UV-vis (CH₂Cl₂): λ_{max} = 490 nm; HR-MS (DART): *m/z* calcd. for C₄₈H₅₄N₄Si₂: [M]⁺ 742.3887, found: 742.3874, correct isotope distribution; elemental analysis: calcd. for C₄₈H₅₄N₄Si₂: C 77.58; H 7.32; N 7.54, found: C 77.31, H 7.39, N 7.19.

5c-H₂ (57 mg, 76.7 µmol, 1.00 eq.) was dissolved in CH₂Cl₂ (5 mL) and PbO₂ (365 mg, 1.53 mmol, 20.0 eq.) was added. After sonication for 1 h at RT the mixture was rapidly filtered through celite and the solvent was evaporated under reduced pressure. The crude product was purified by flash column chromatography (silica gel, petroleum ether/ethyl acetate 95:5), yielding **5c** as a quickly decomposing, black solid (5 mg, 6.74 µmol, 9%). ¹H NMR (500 MHz, CDCl₃, 25°C): δ = 9.34 (s, 2H), 8.92 (s, 2H), 8.55 (s, 2H), 7.98 (dd, J = 6.6, 3.3 Hz, 2H), 7.48 (dd, J = 6.7, 3.1 Hz, 2H), 1.47 – 1.38 (m, 42H); ¹³C NMR (126 MHz, CDCl₃, 25°C): δ = 142.37, 142.08, 138.68, 134.09, 134.03, 132.04, 131.81, 128.99, 127.90, 127.41, 121.41, 115.60, 112.38, 109.34, 103.79, 19.19, 11.85; IR (neat): IR: ν (cm⁻¹) = 3053, 2928, 2856, 2228, 2129, 1715, 1456, 1365, 1080, 901; UV-vis (CH₂Cl₂): λ_{max} = 890 nm; HR-MS (MALDI, DCTB): *m/z* calcd. for C₄₈H₅₂N₄Si₂: [M]⁺ 740.3731, found: 740.3725, correct isotope distribution.

CHAPTER 9

Supplementary Information

9.1. Chapter 3

NMR spectra

^1H , ^{13}C and ^{19}F NMR spectra were recorded with a Varian Mercury 400 spectrometer with a 5 mm probe. All chemical shifts have been quoted relative to deuterated solvent signals, δ in ppm, J in Hz.

Figure S1. ^1H NMR spectrum of **2**

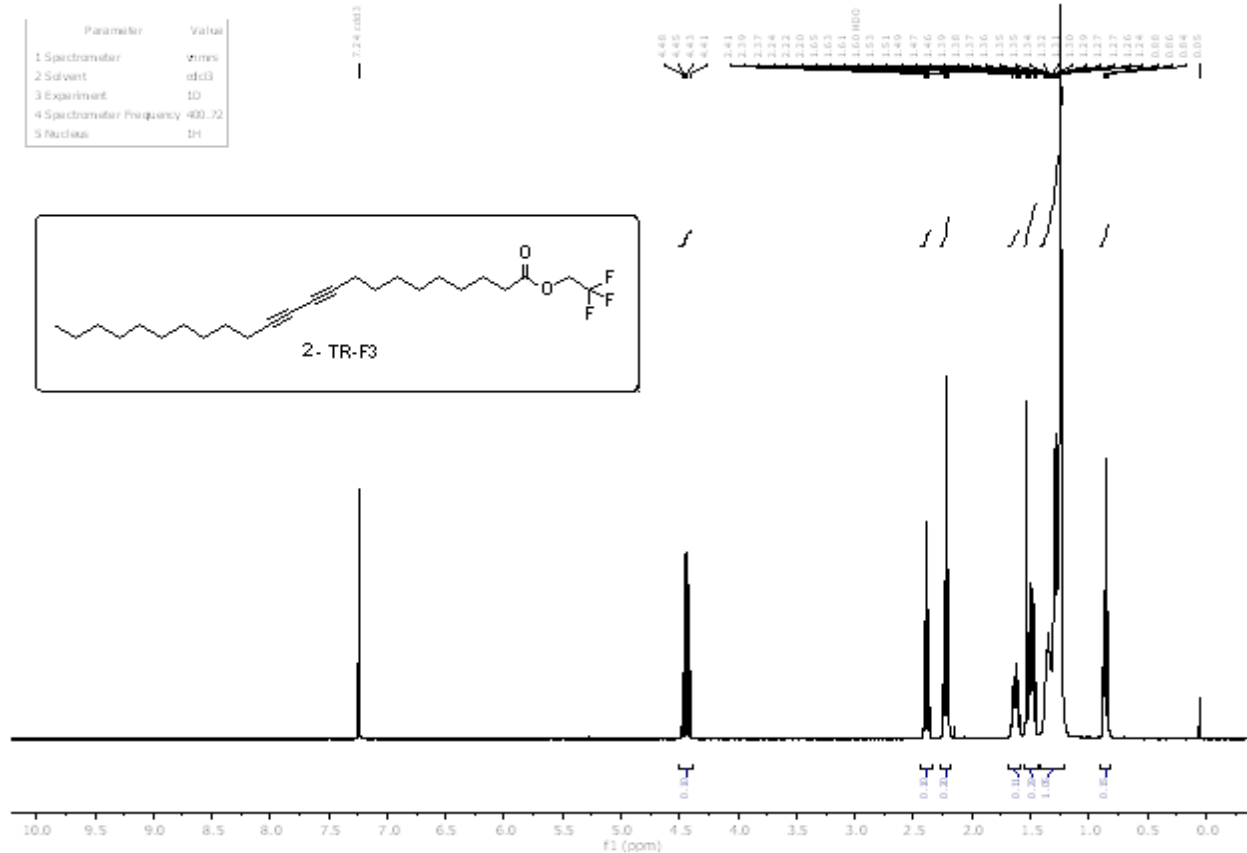


Figure S2. ^{13}C NMR spectrum of **2**

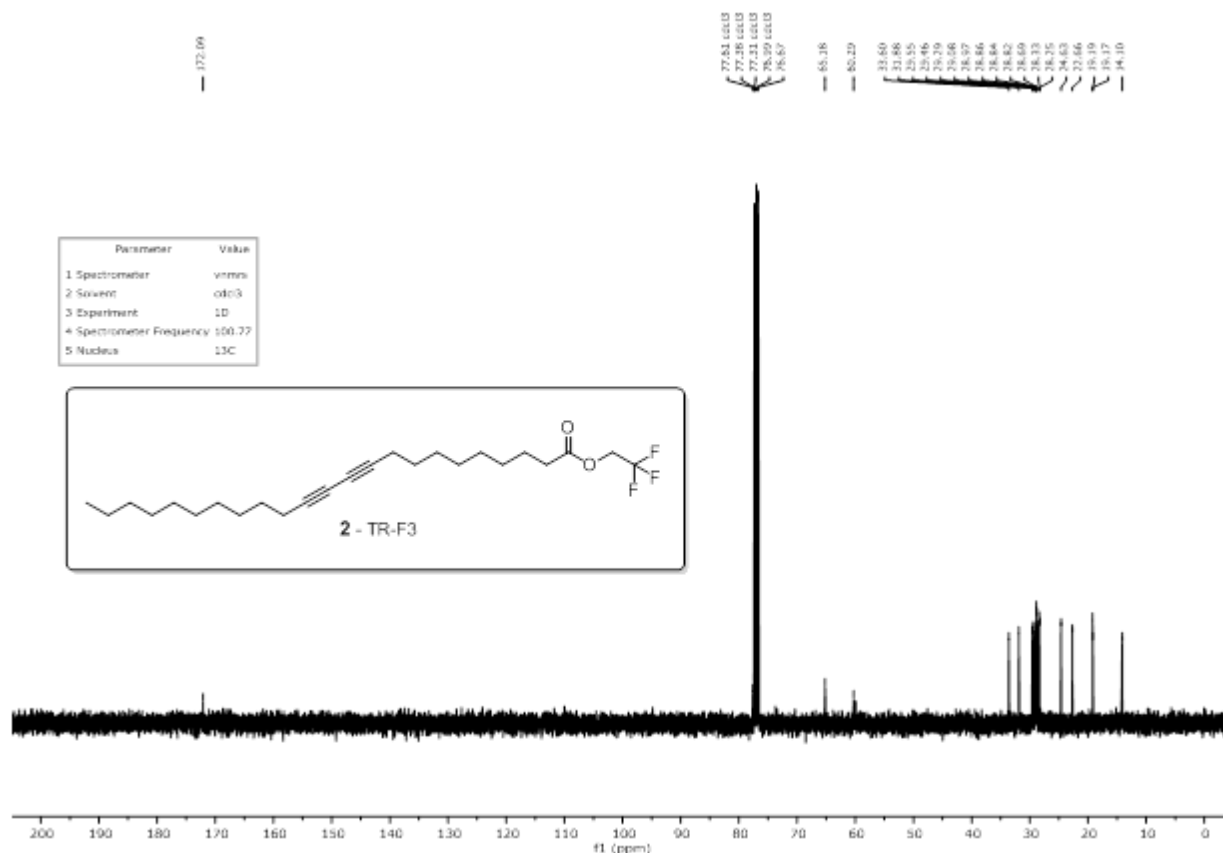


Figure S3. ^{19}F NMR spectrum of **2**

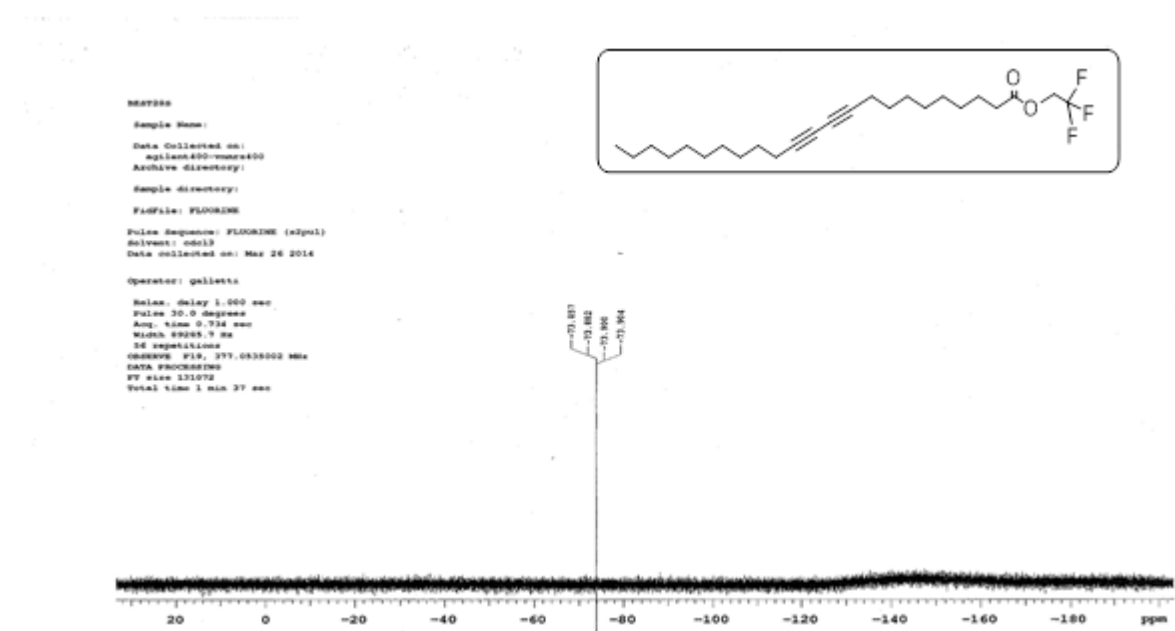


Figure S4. ^1H NMR spectrum of **3**

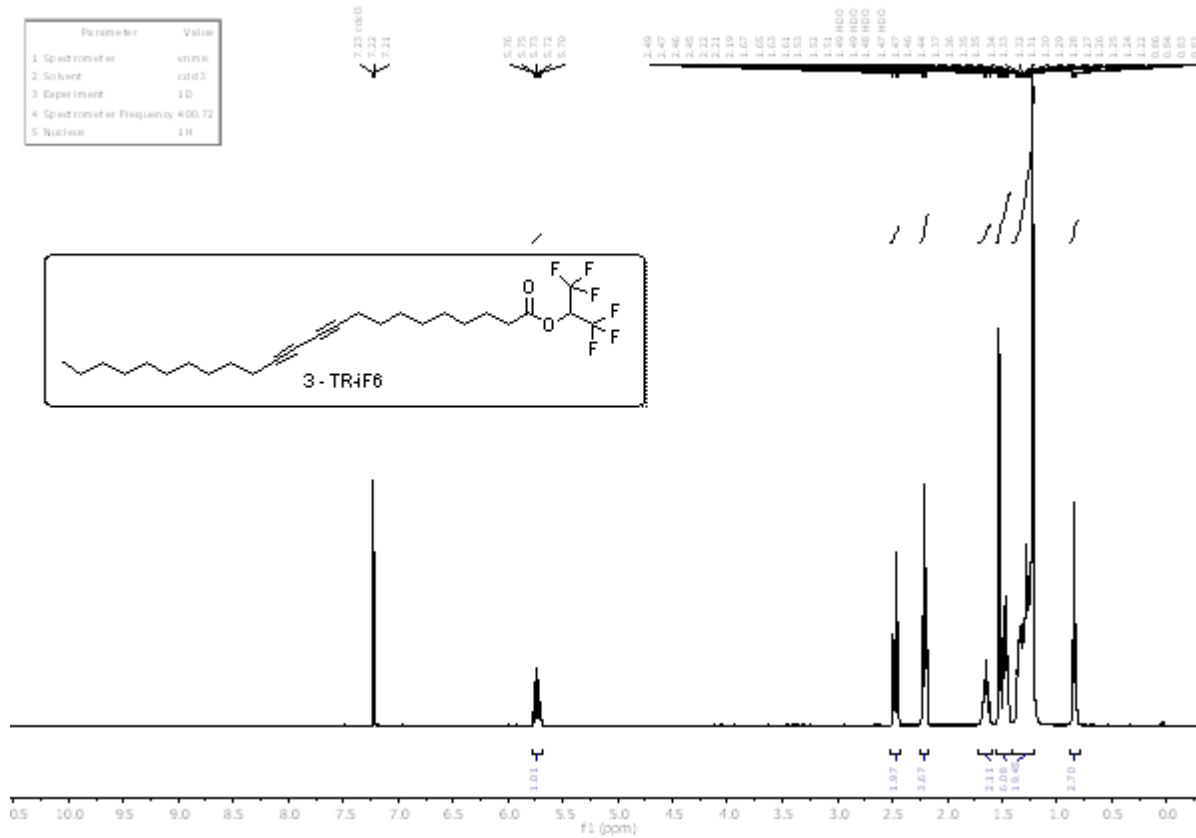


Figure S5. ^{13}C NMR spectrum of **3**

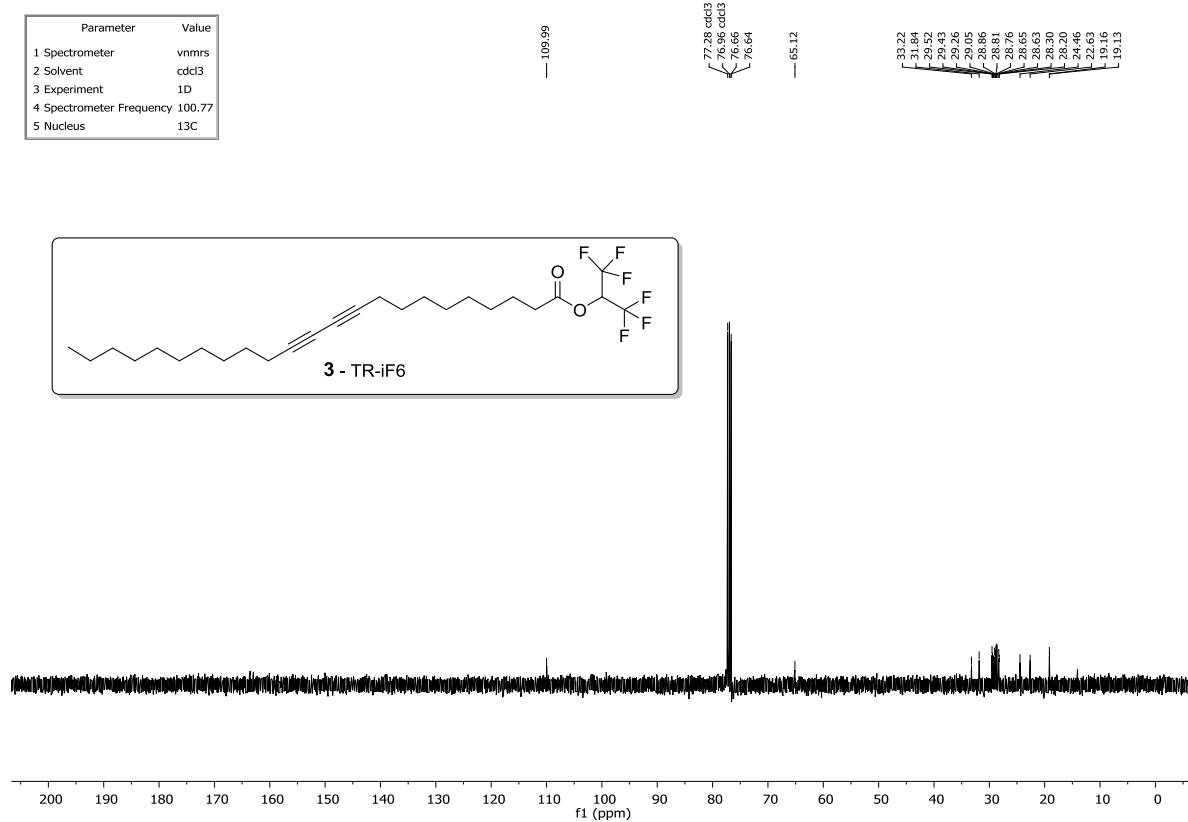


Figure S6. ^{19}F NMR spectrum of **3**

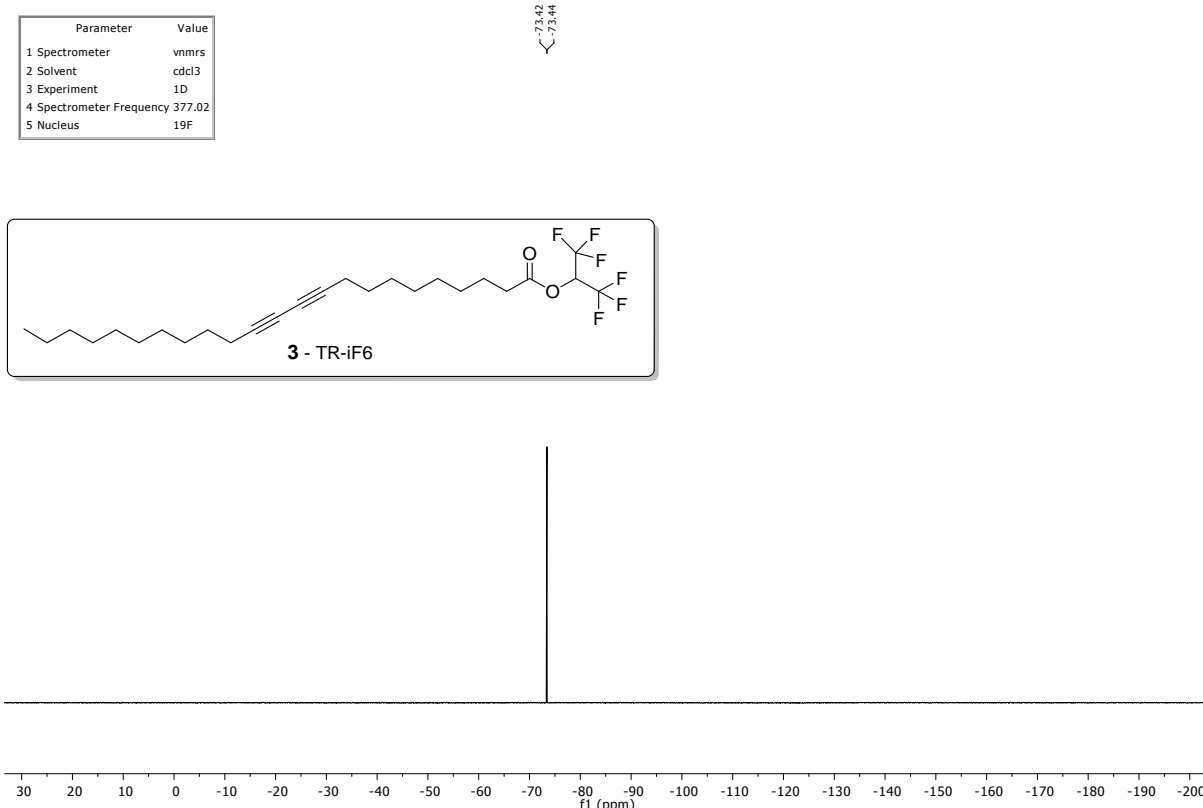


Figure S7. ^1H NMR spectrum of **4**

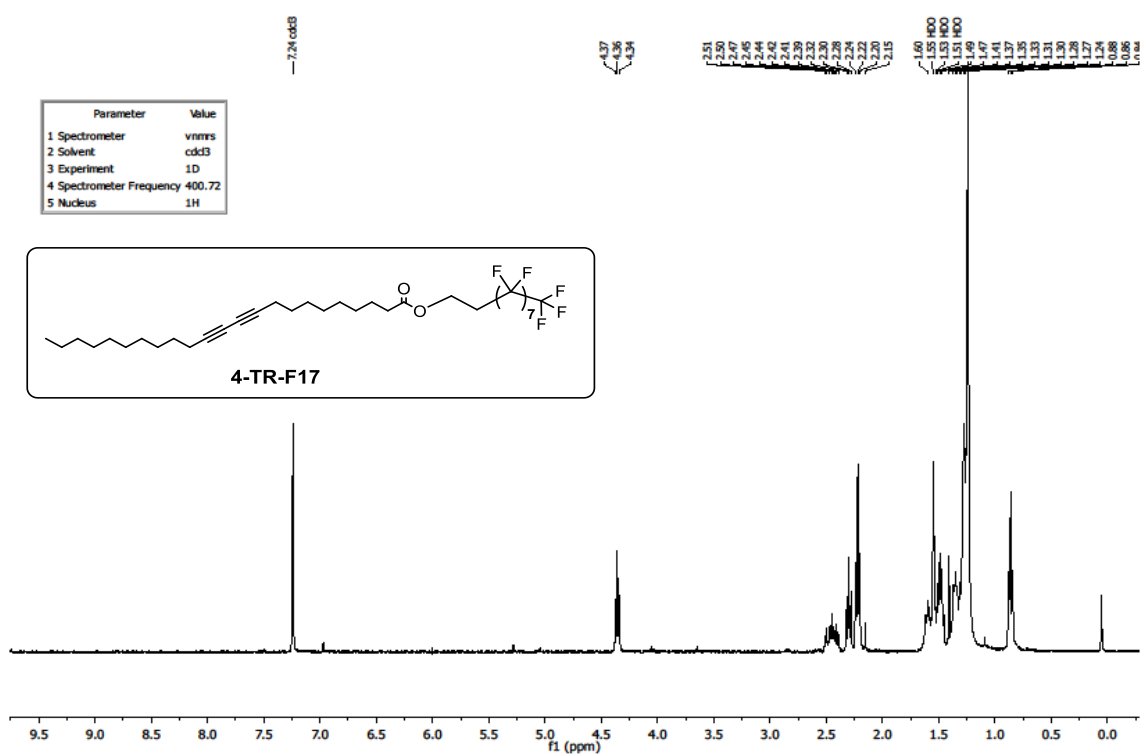


Figure S8. ^{13}C NMR spectrum of 4

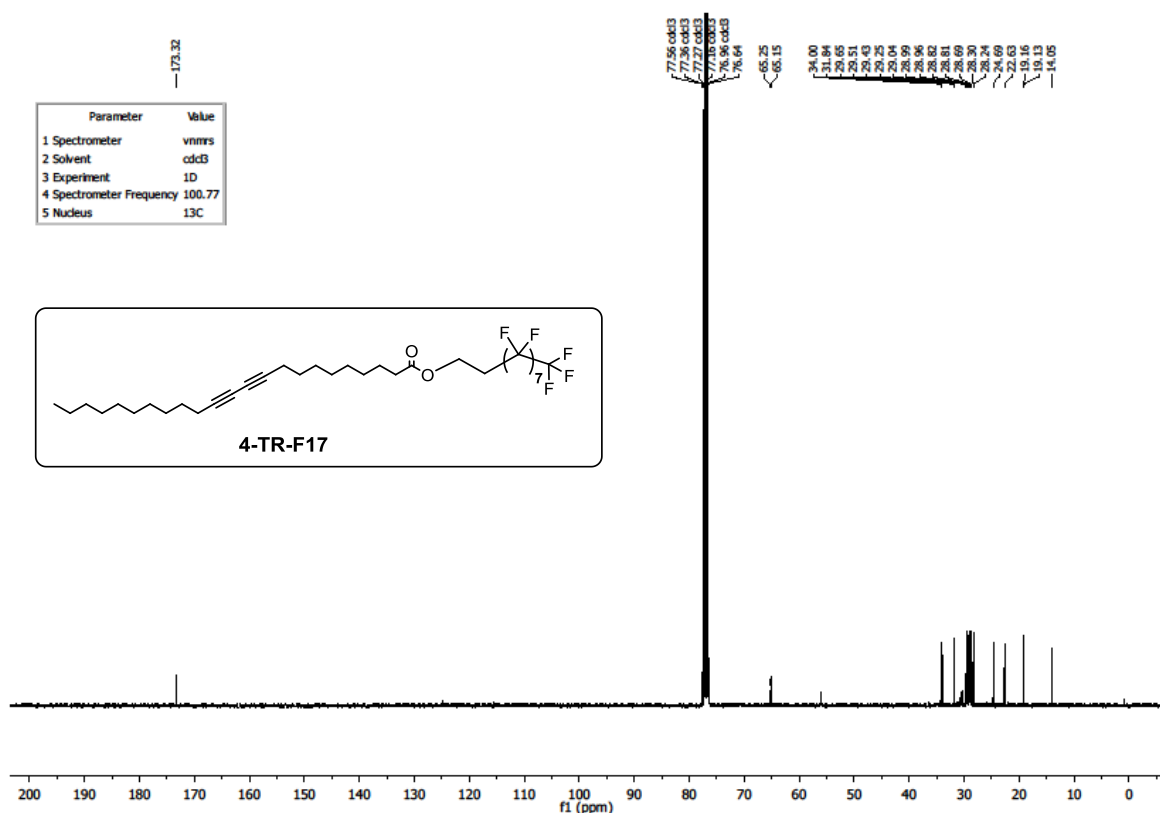


Figure S9. ^{19}F NMR spectrum of 4

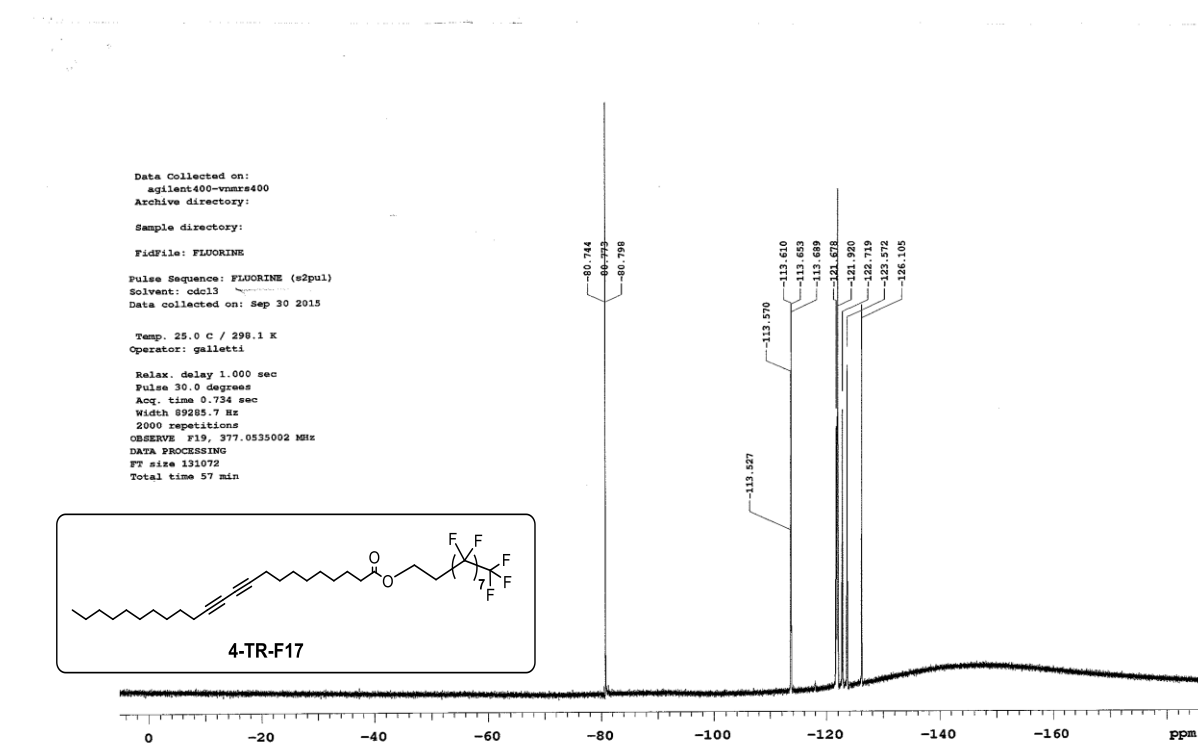


Figure S10. ^1H NMR spectrum of **5**

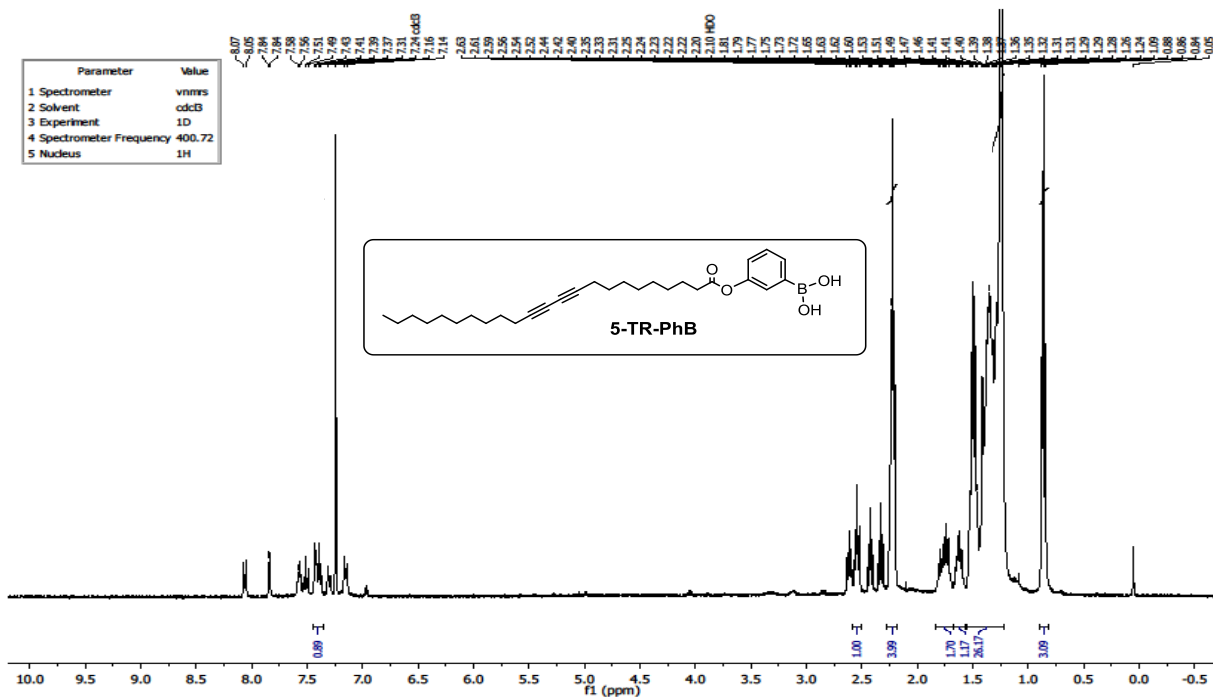


Figure S11. ^{13}C NMR spectrum of **5**

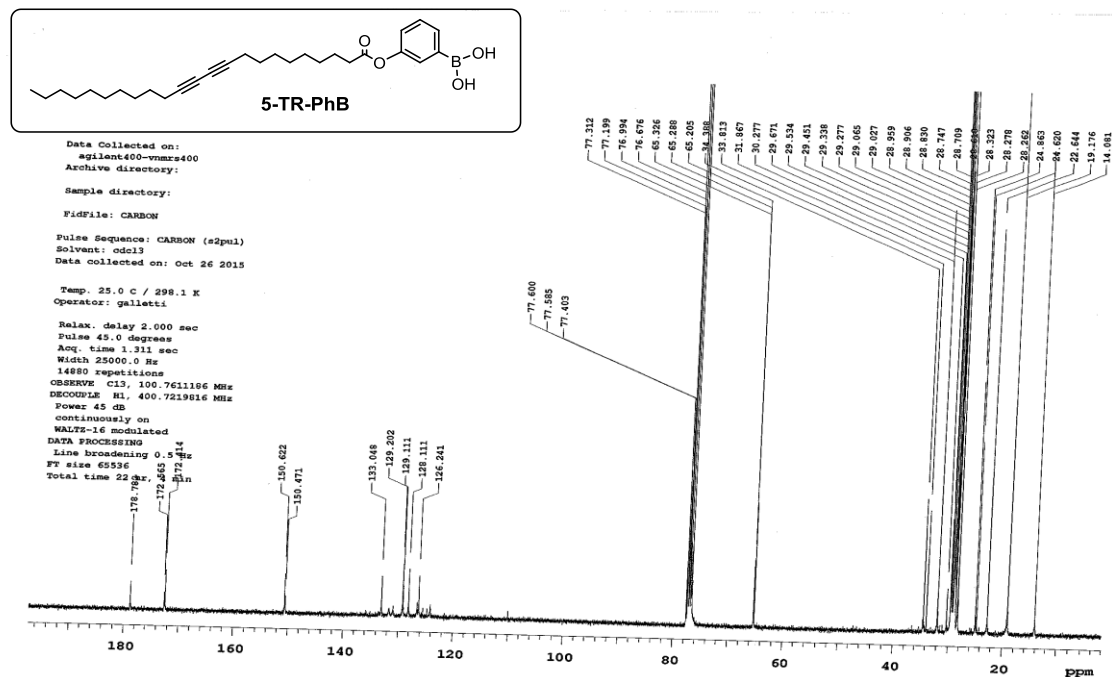


Figure S12. ^1H NMR spectrum of **6**

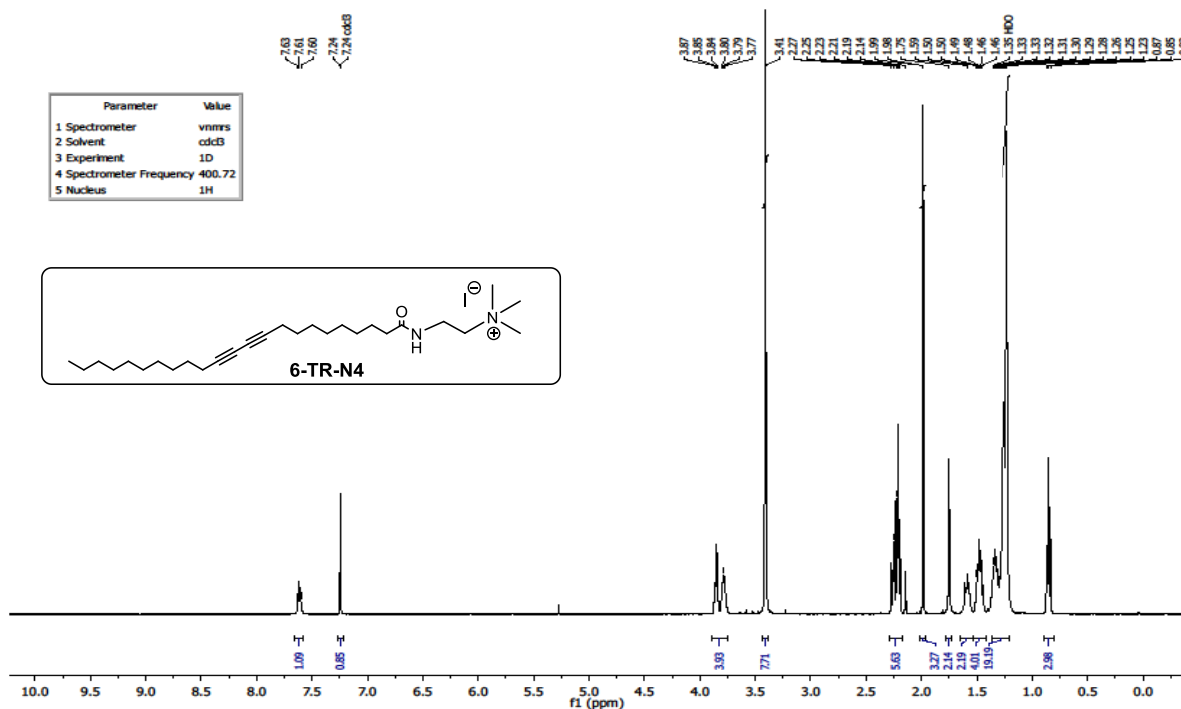


Figure S13. ^{13}C NMR spectrum of **6**

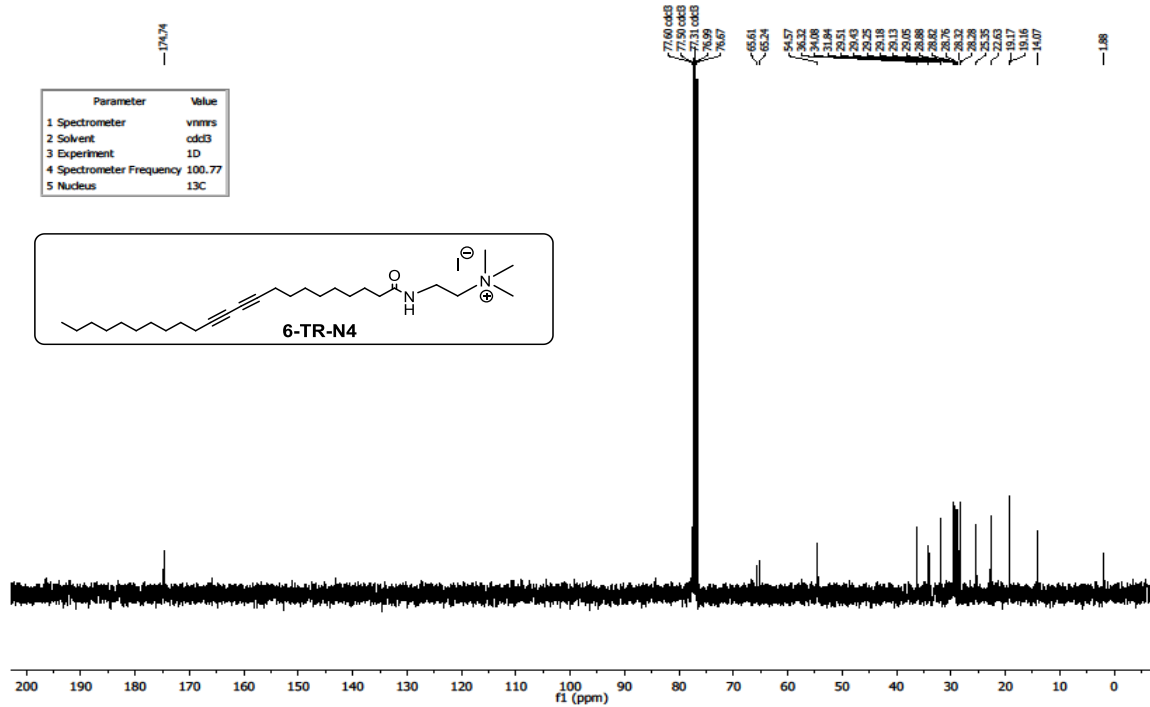


Figure S14. ^1H NMR spectrum of **7**

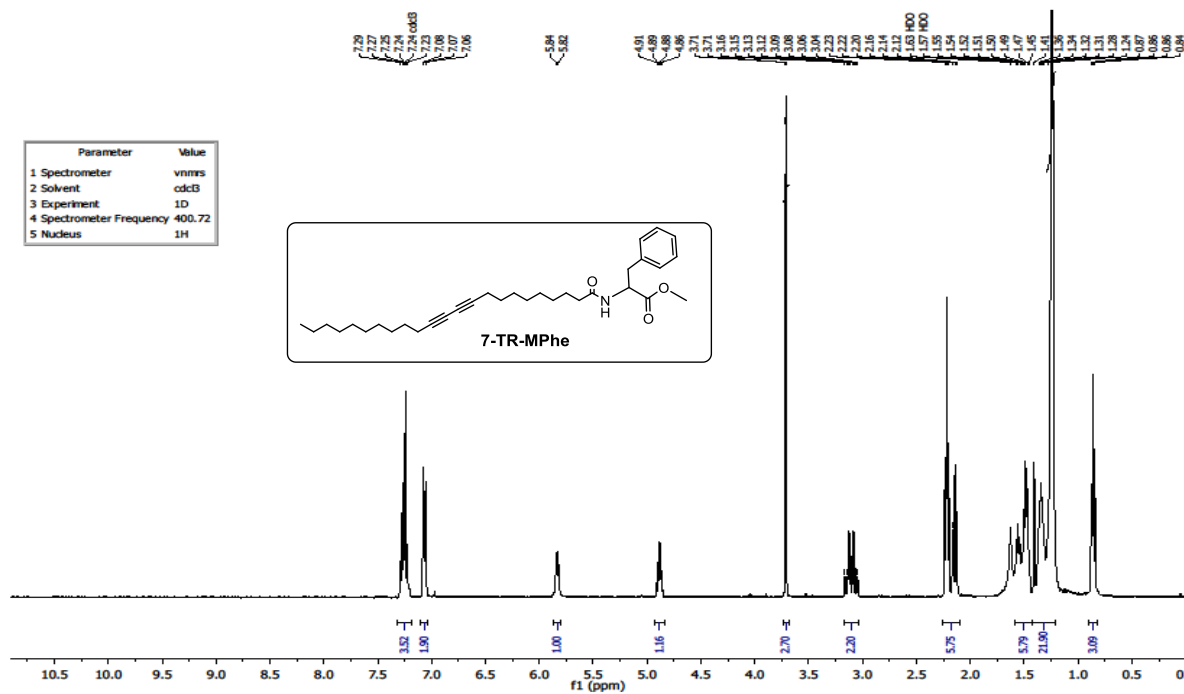


Figure S15. ^{13}C NMR spectrum of 7

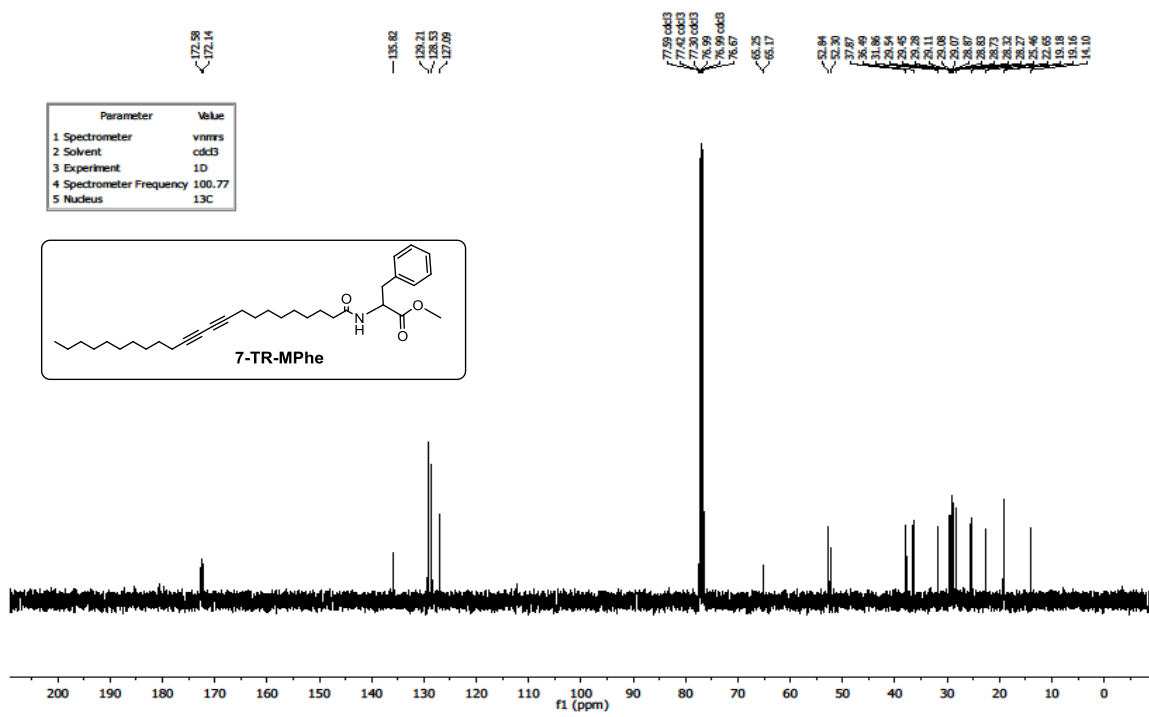


Figure S16. ^1H NMR spectrum of **8**

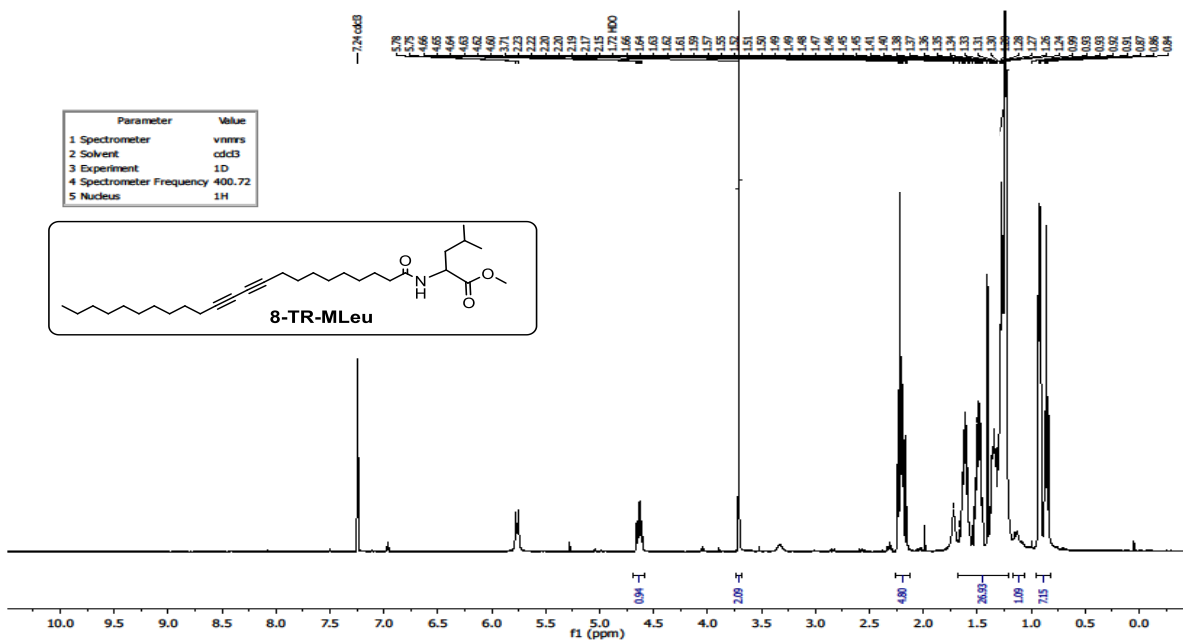


Figure S17. ^{13}C NMR spectrum of **8**

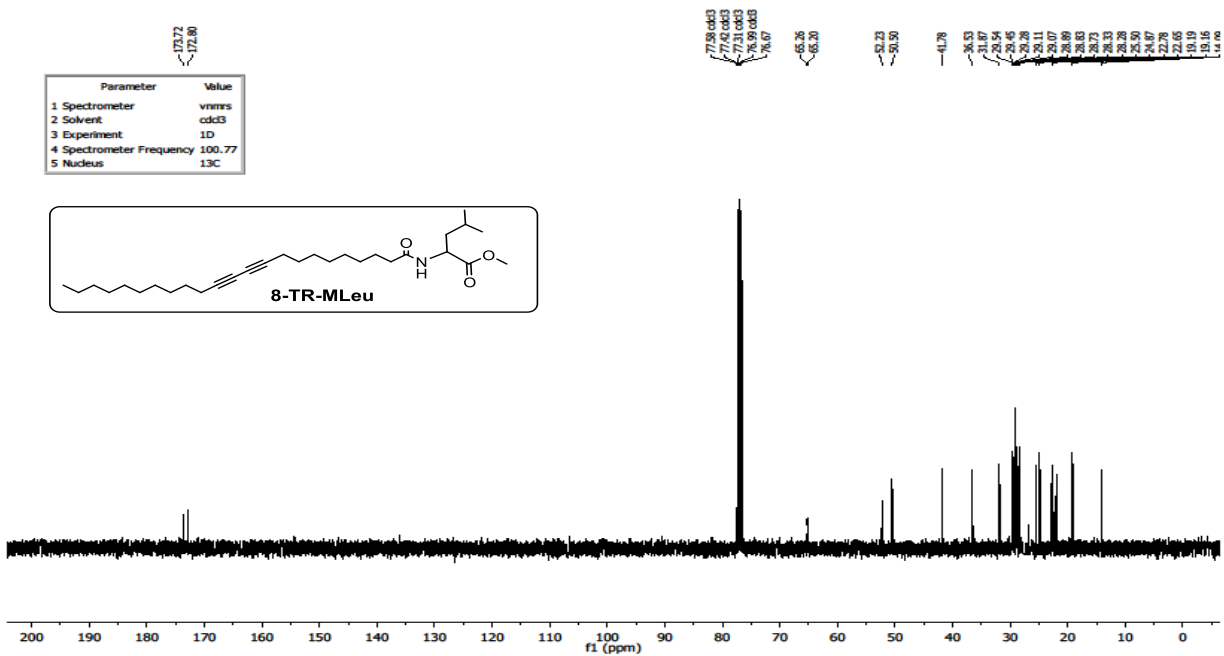


Figure S18. ^1H NMR spectrum of **9**

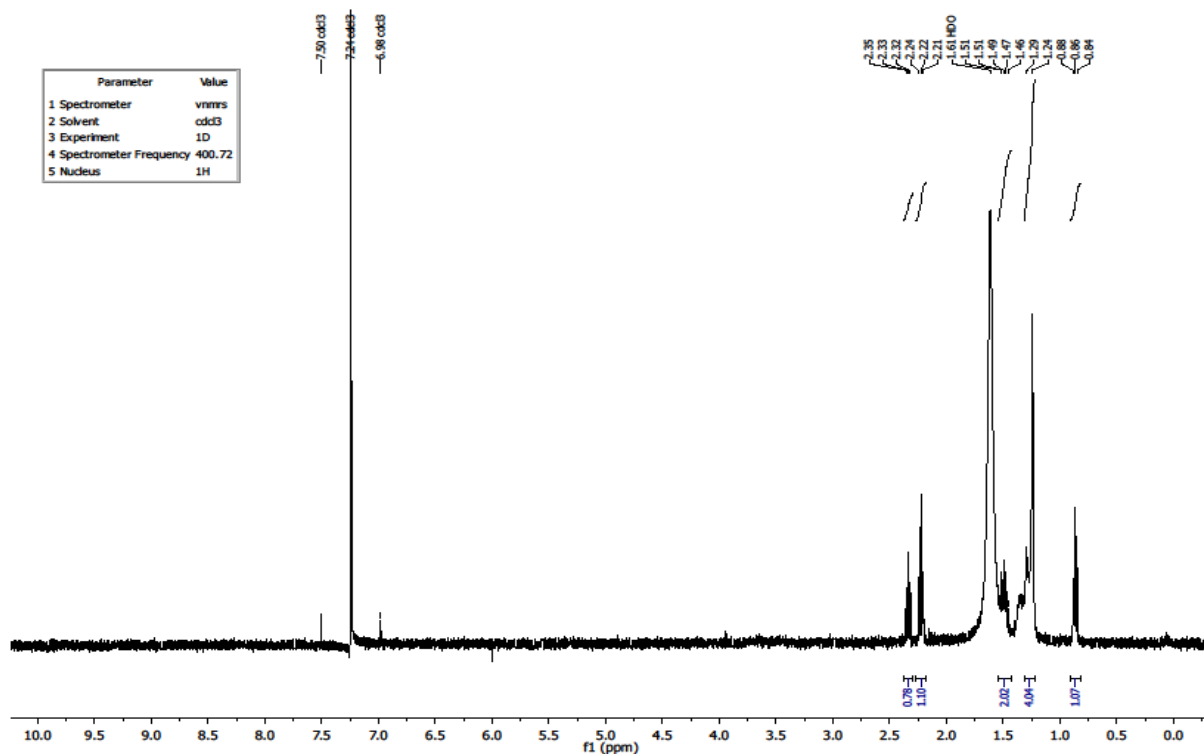


Figure S19. ^{13}C NMR spectrum of **9**

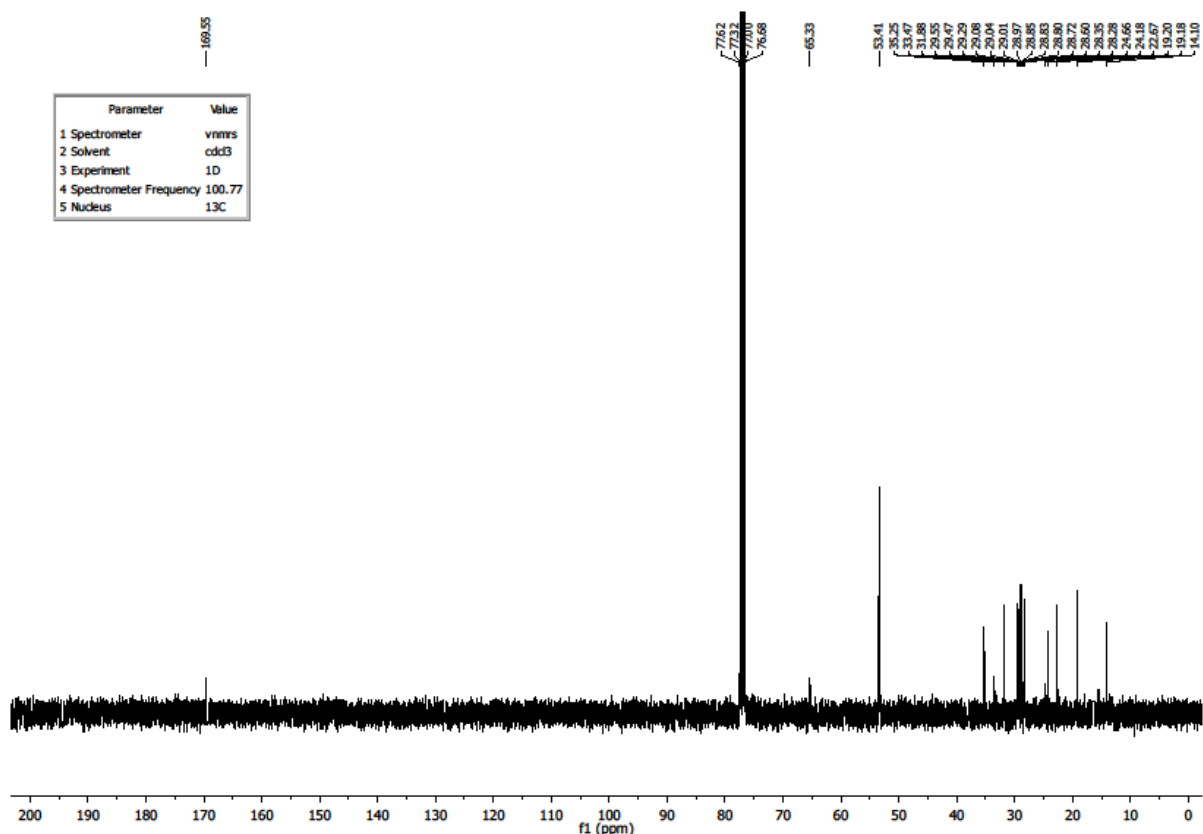


Figure S20. ^1H NMR spectrum of **10**

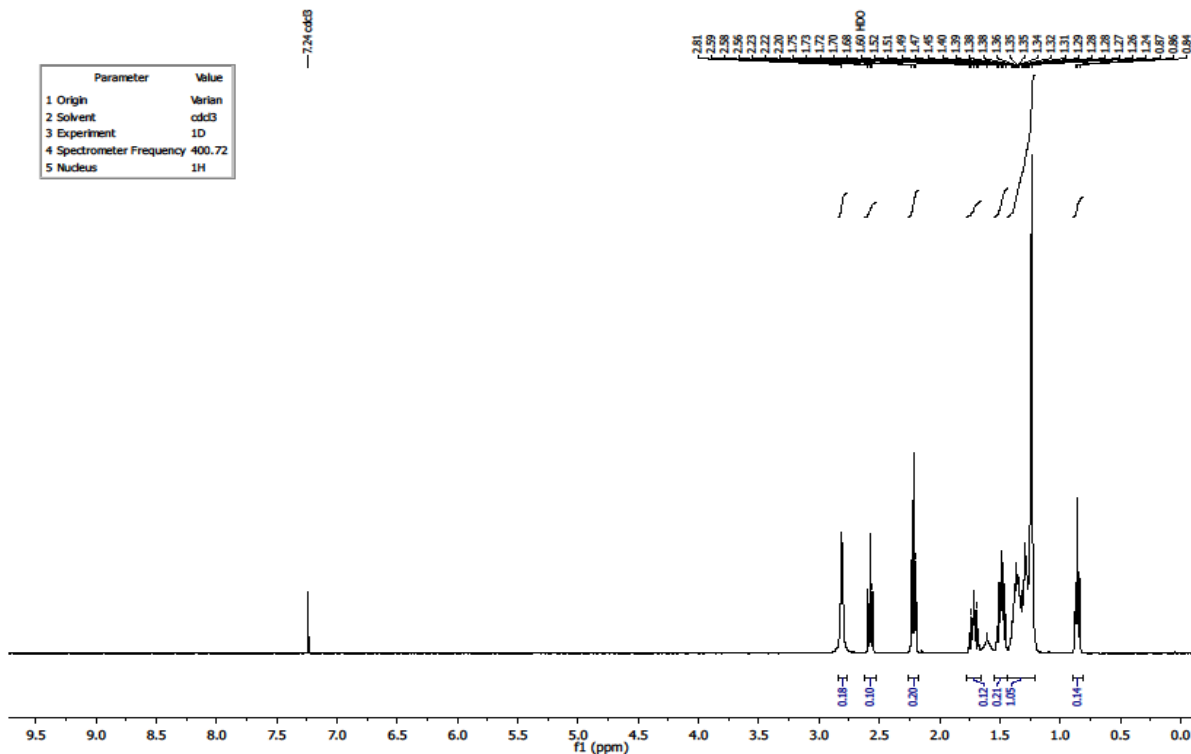


Figure S21. ^{13}C NMR spectrum of **10**

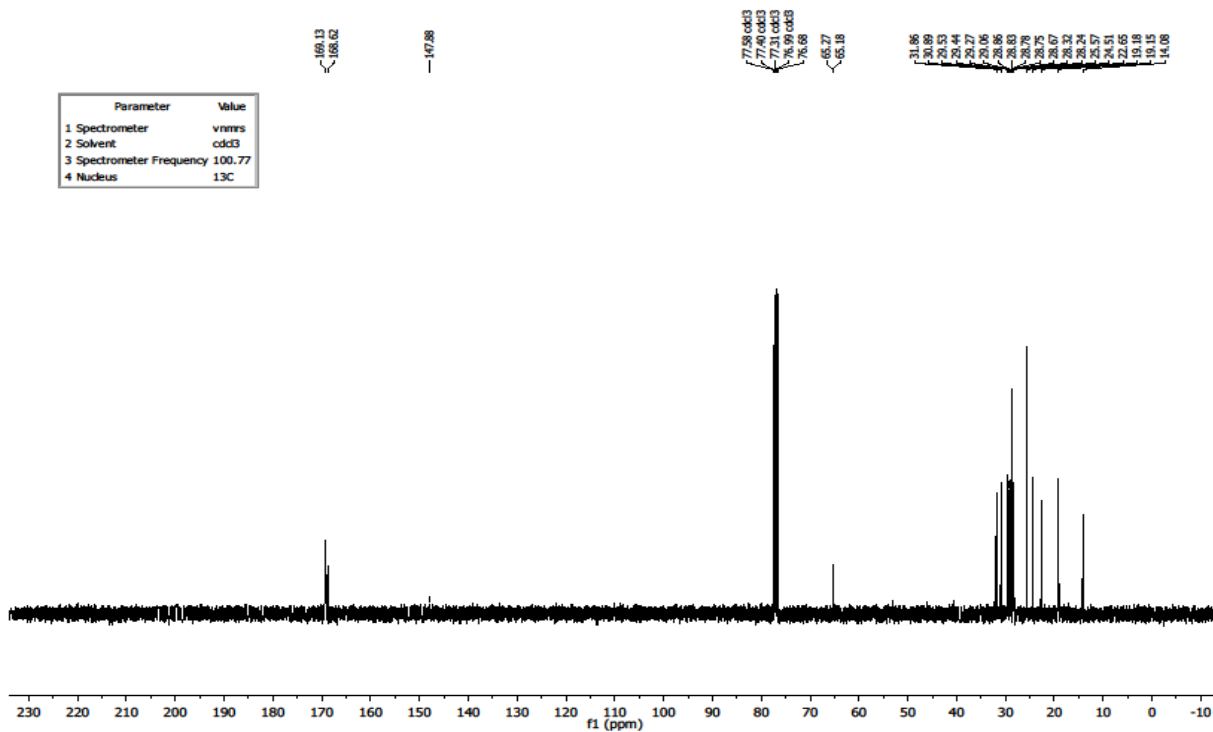


Figure S22. ^1H NMR spectrum of **11**

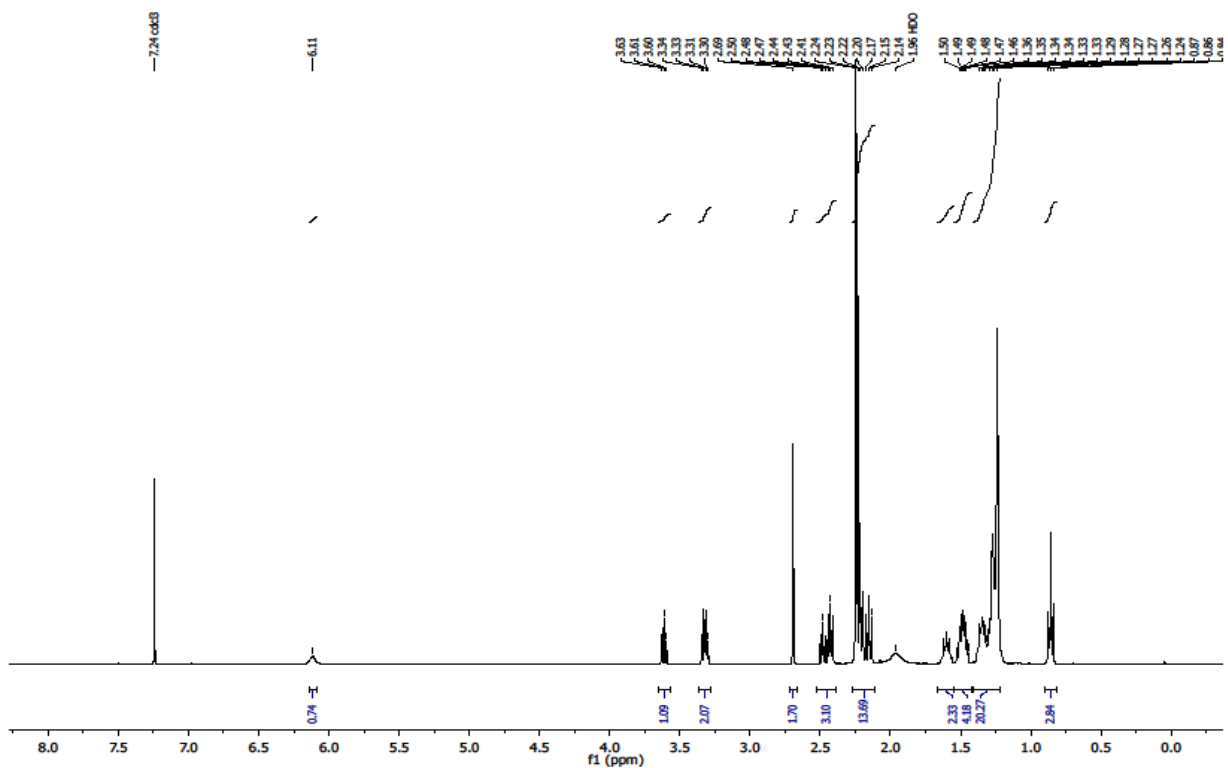


Figure S23. ^1H NMR spectrum of **12**

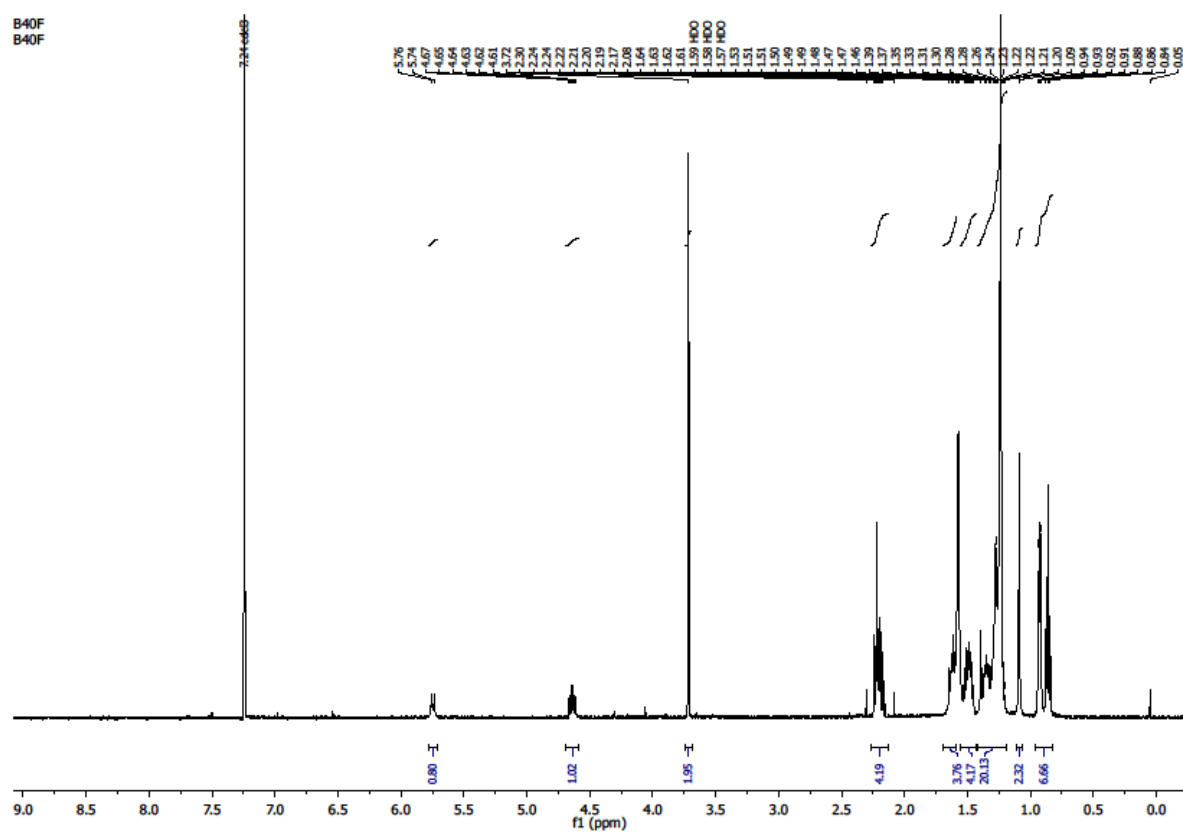


Figure S24. ^1H NMR spectrum of **13**

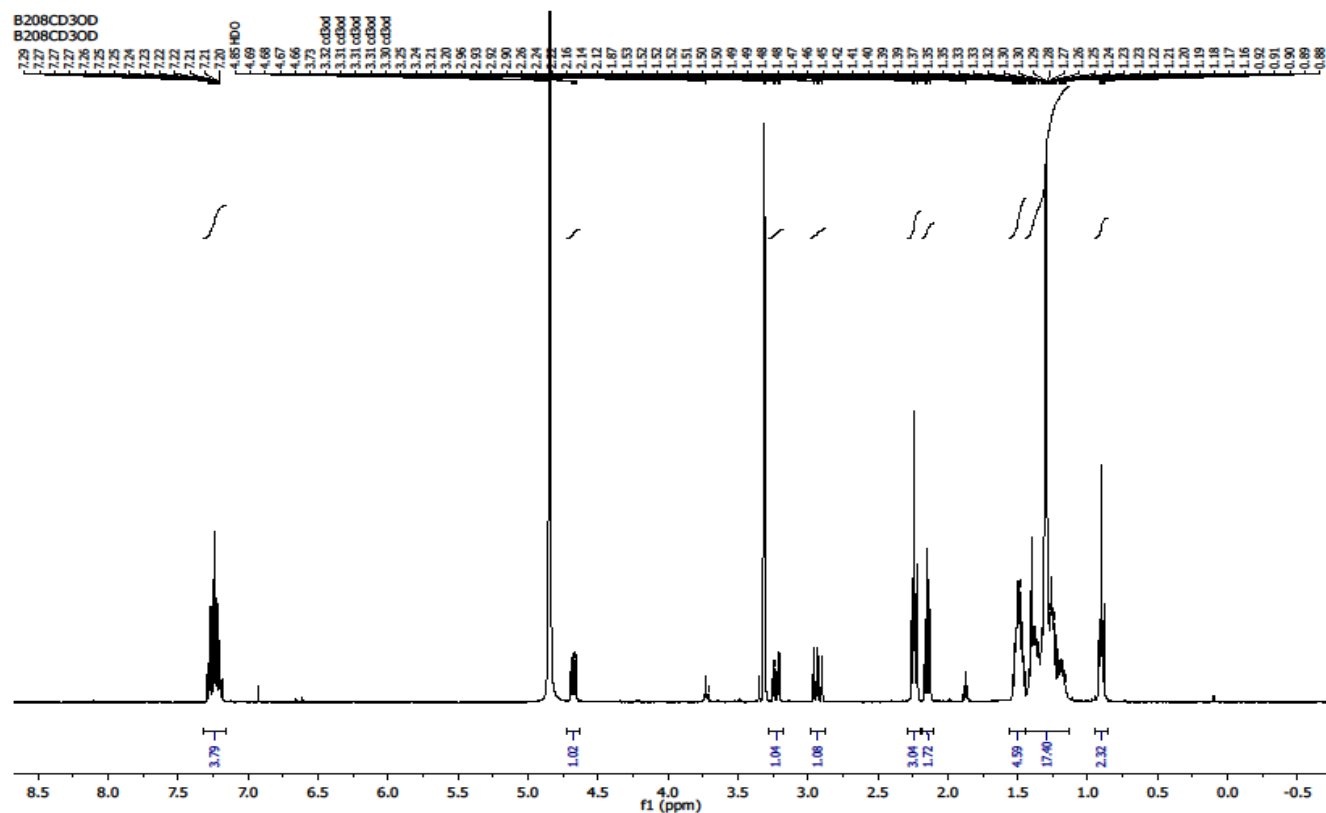


Figure S25. ^1H NMR spectrum of **14**

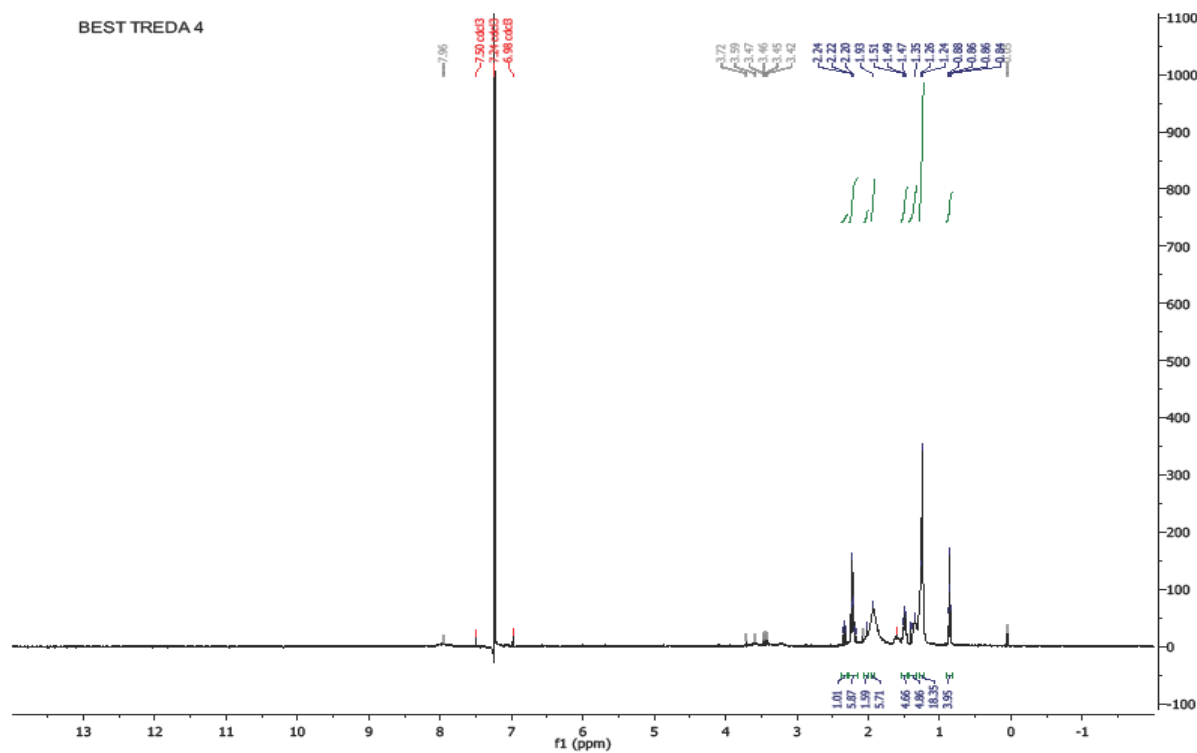


Figure S26. ^1H NMR spectrum of **15**

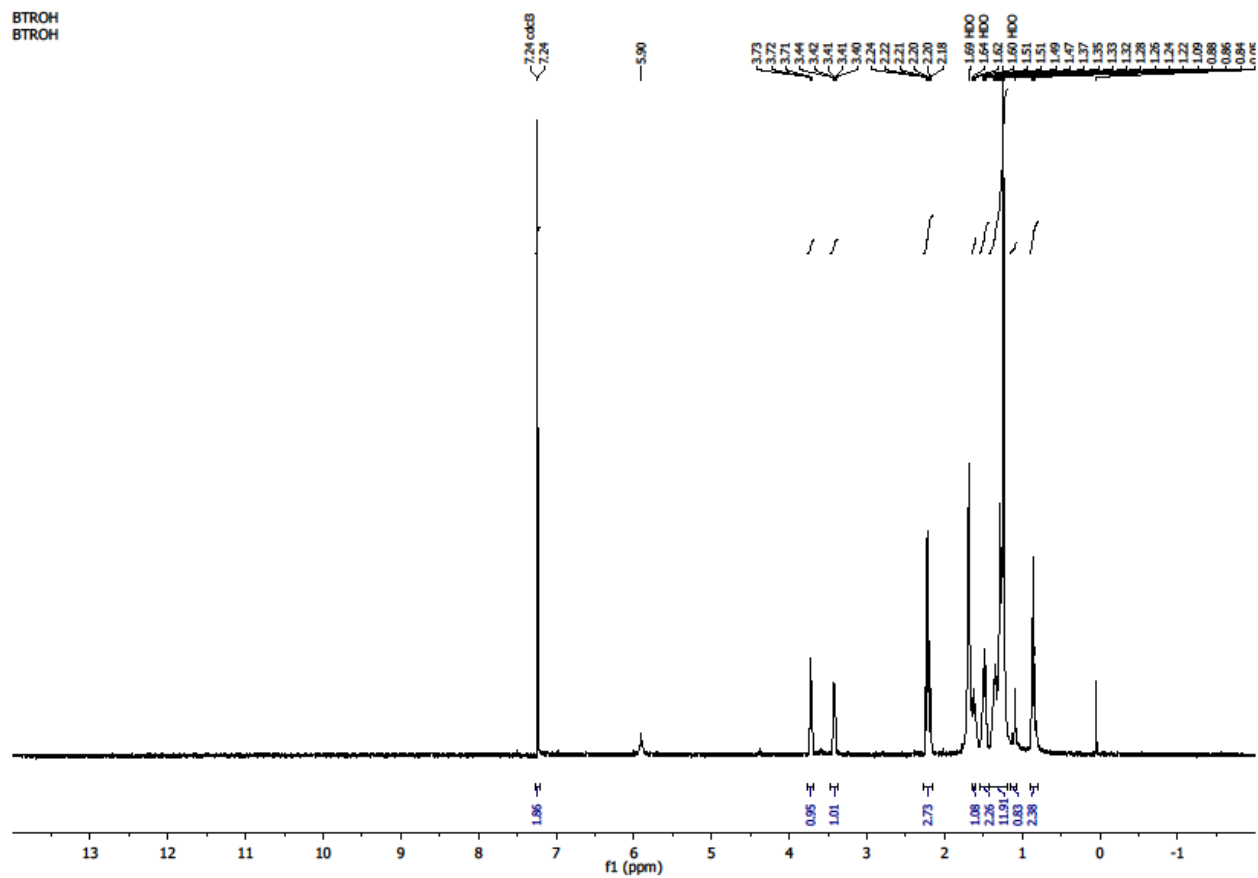


Figure S27. ^1H NMR spectrum of **16**

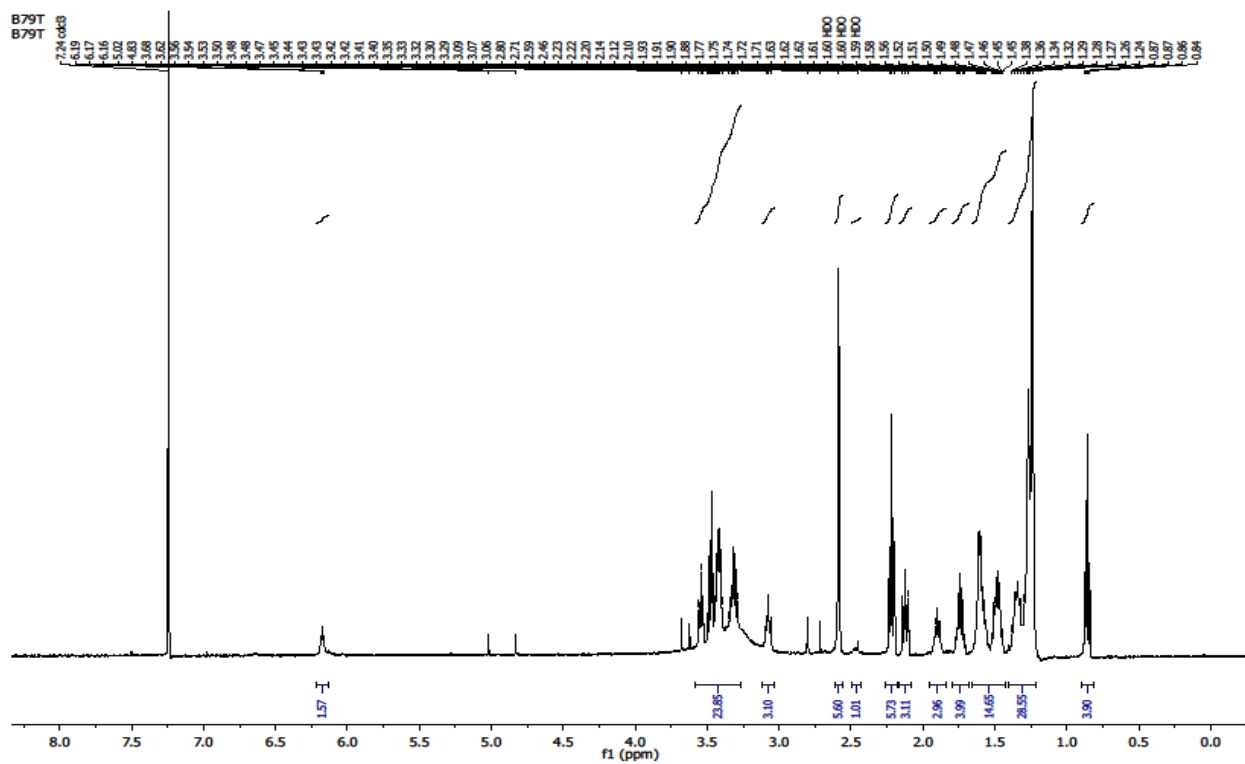


Figure S28. ^1H NMR spectrum of 17

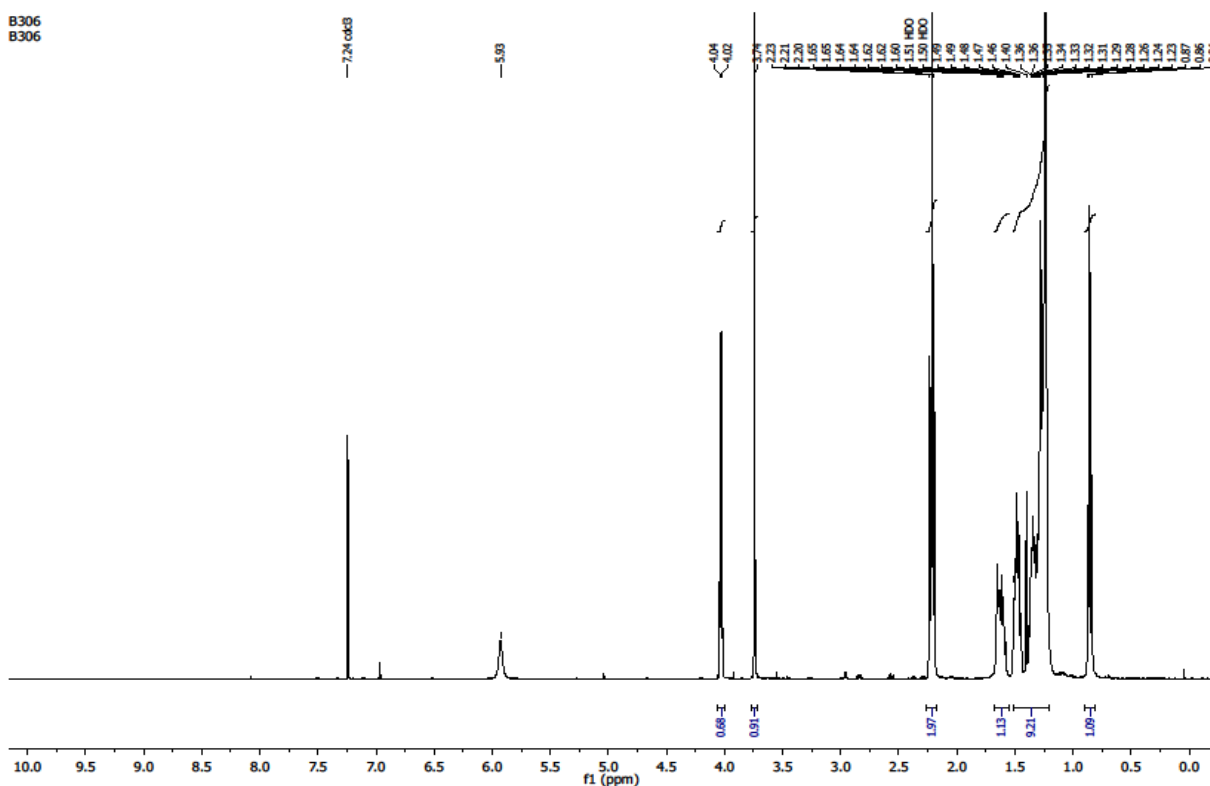


Figure S29. ^{13}C NMR spectrum of **17**

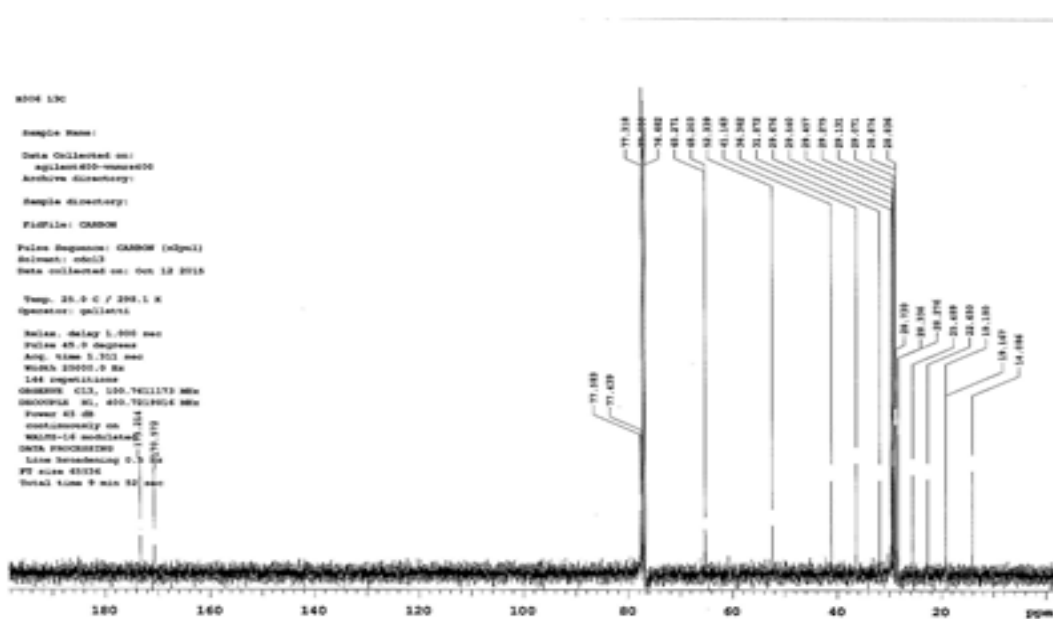


Figure S30. ^1H NMR spectrum of **18**

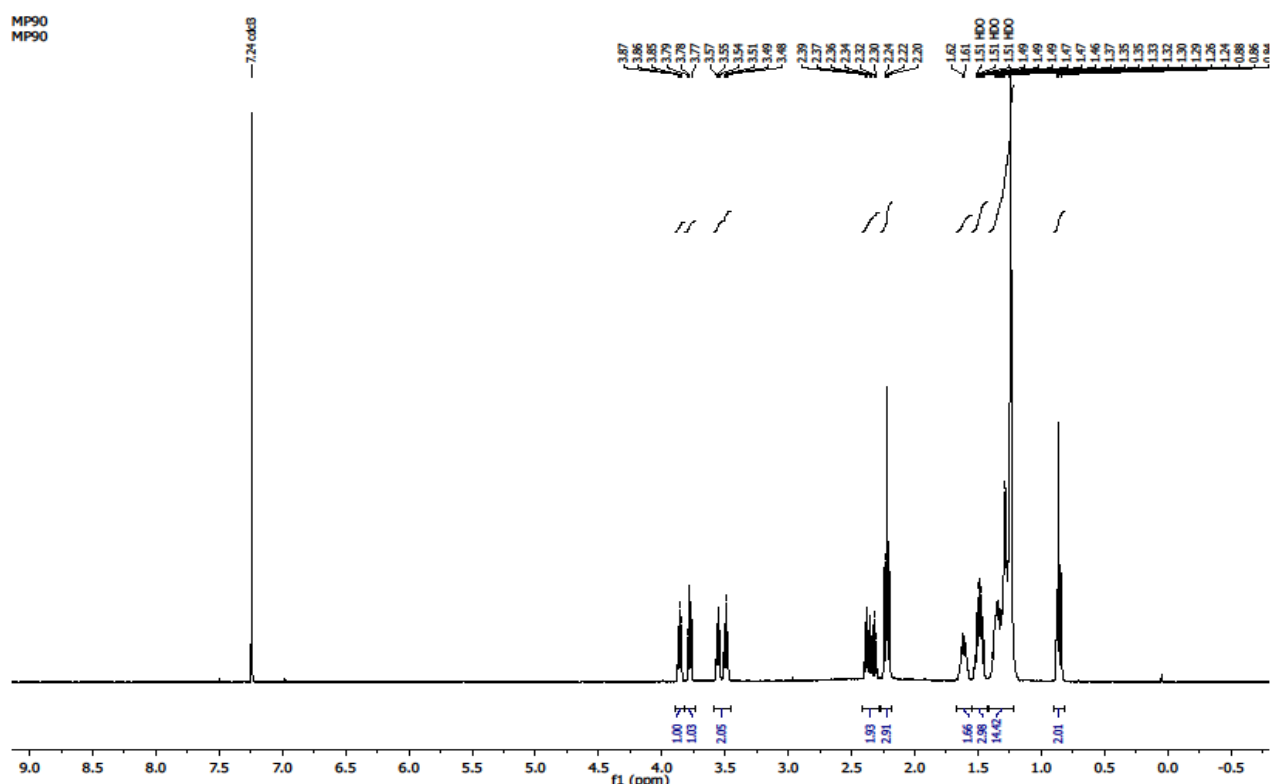


Figure S31. ^1H NMR spectrum of **19**

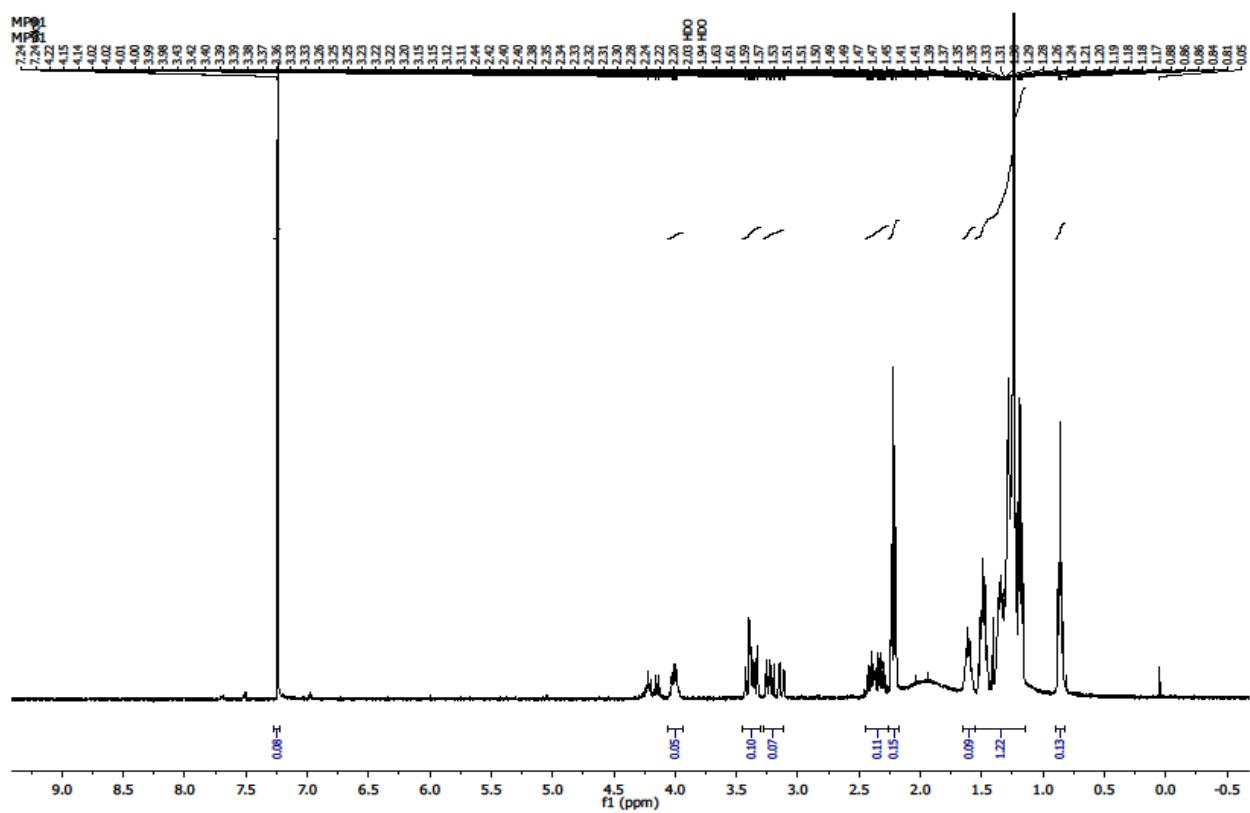


Figure S32. ^1H NMR spectrum of **20**

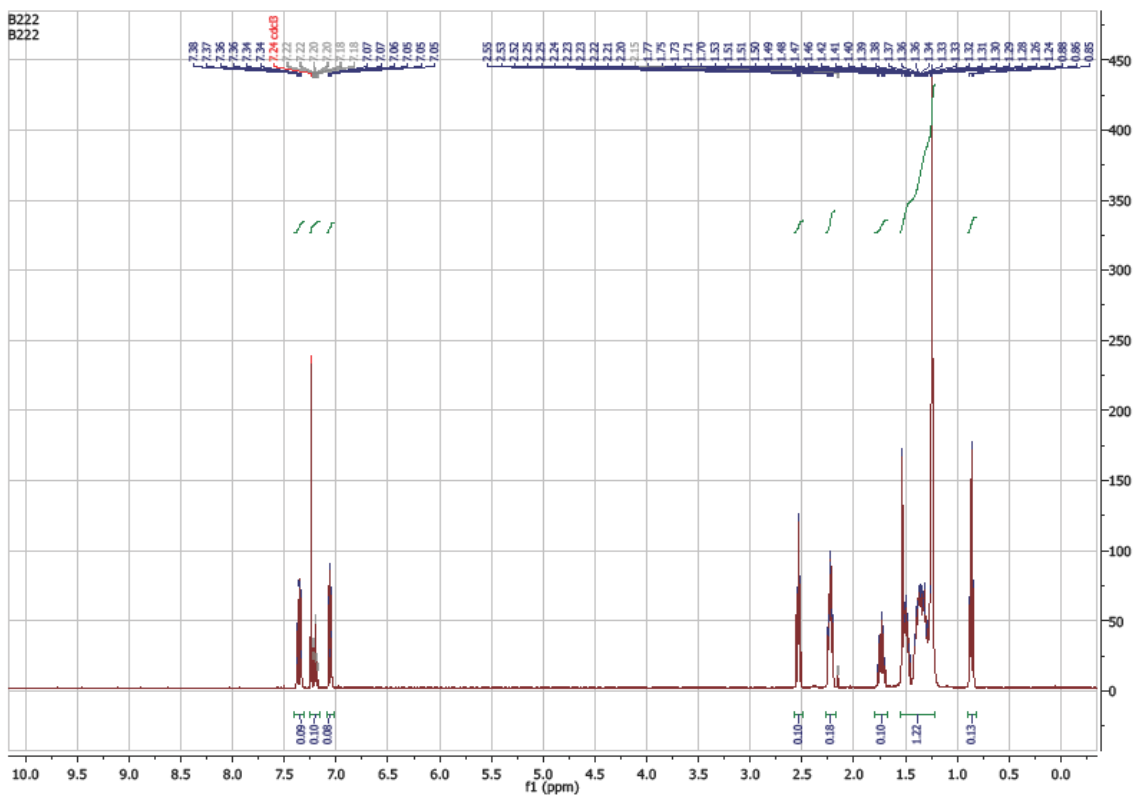


Figure S33. ^1H NMR spectrum of **24**

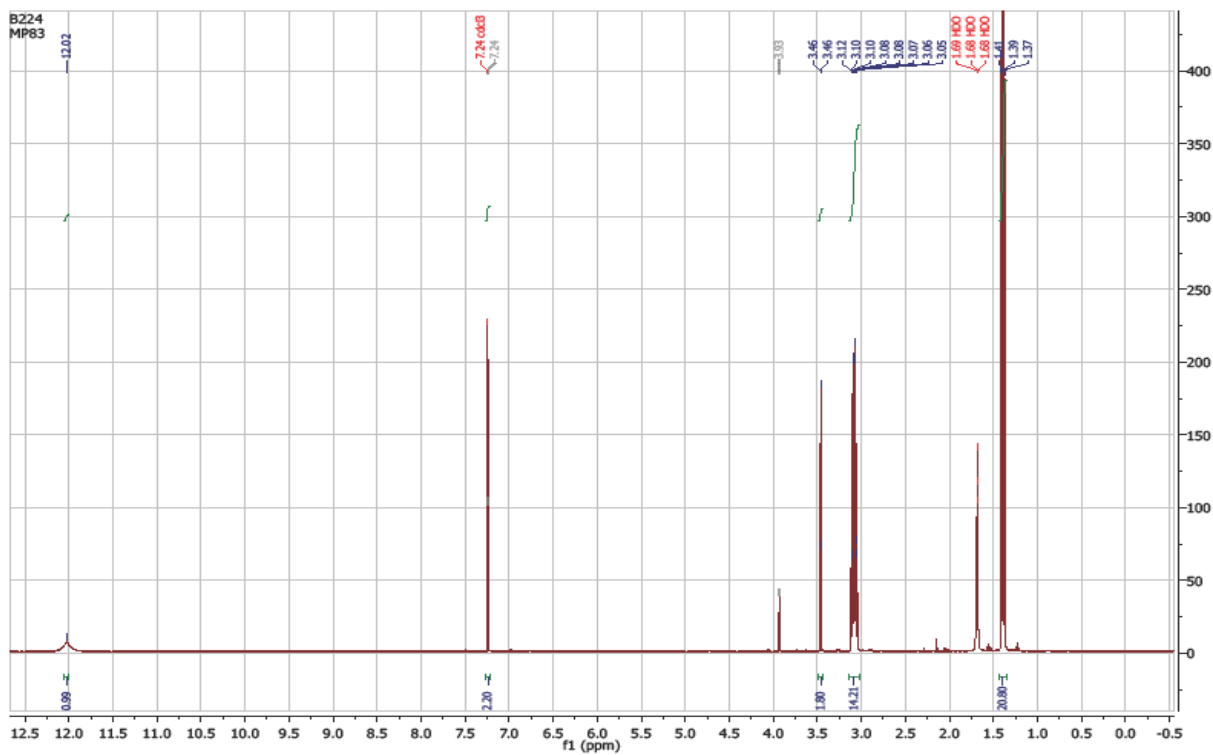


Figure S34. ^1H NMR spectrum of **25**

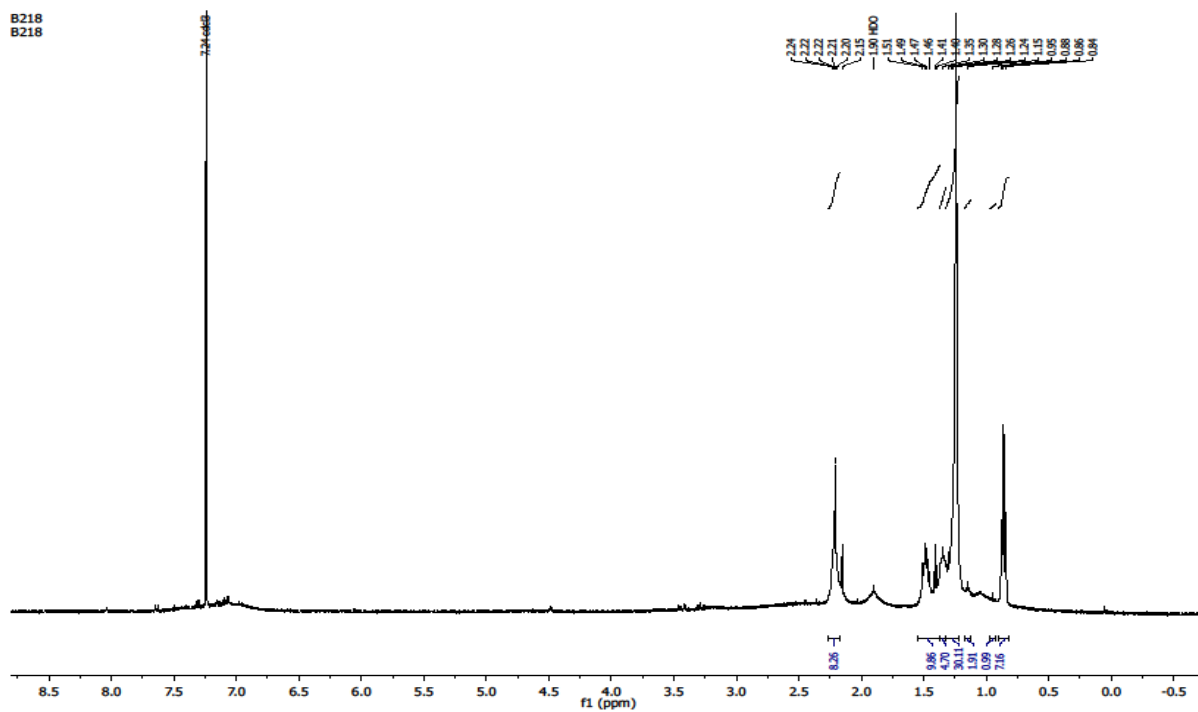


Figure S35. ^{13}C NMR spectrum of **31**

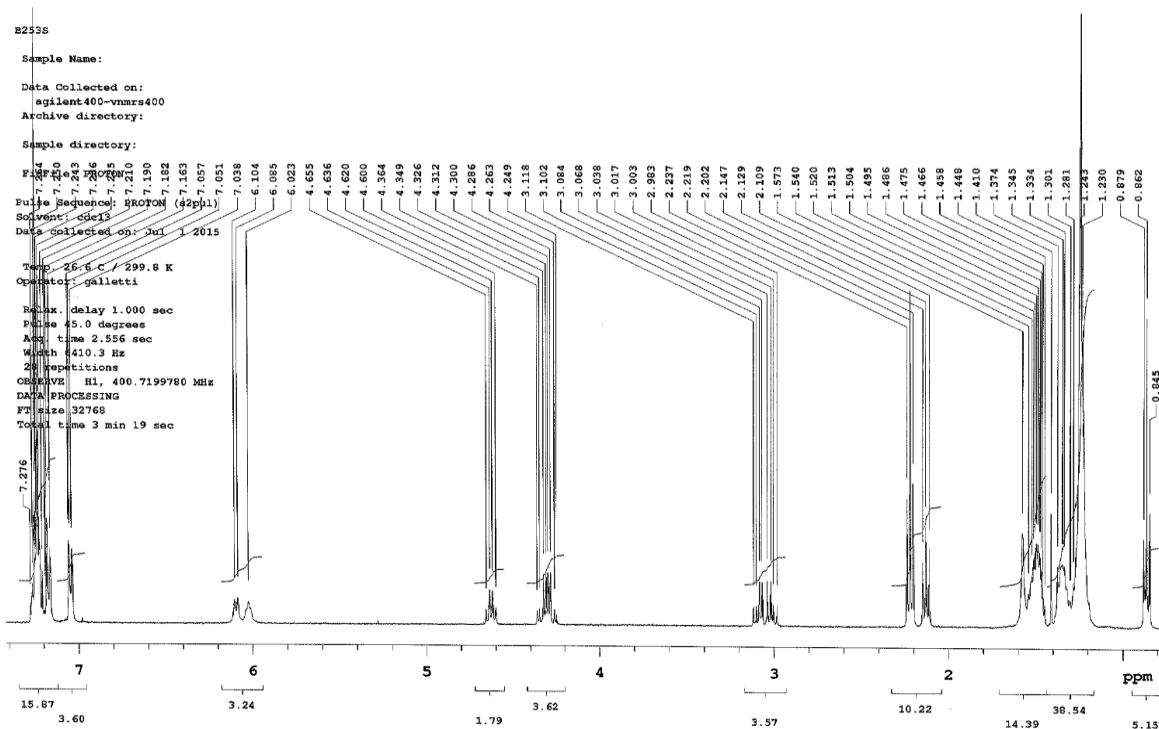


Figure S36. ^1H NMR spectrum of **33**

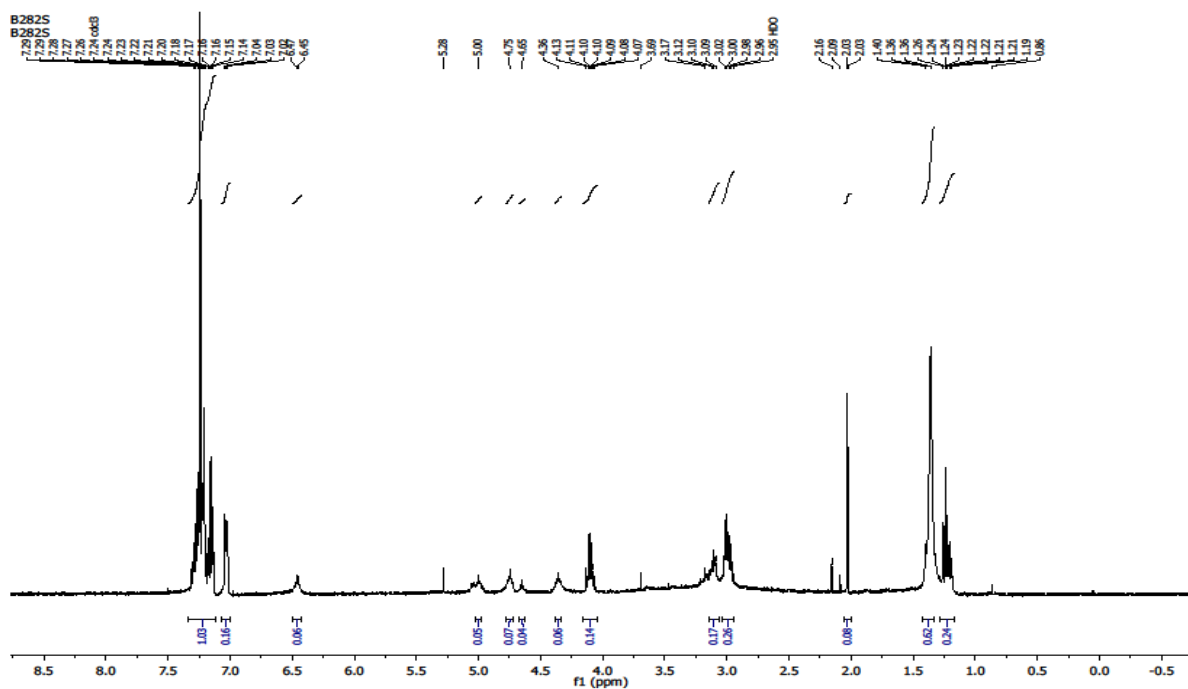


Figure S37. ^1H NMR spectrum of **38**

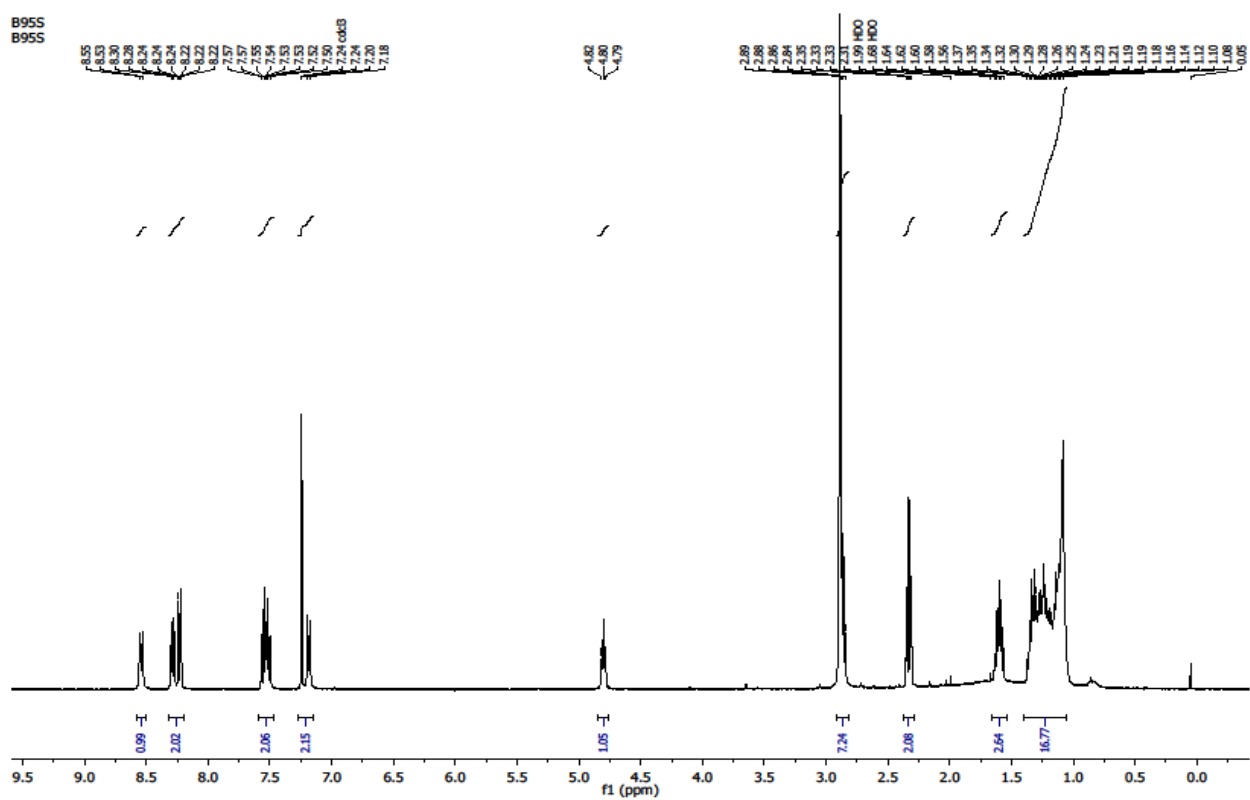


Figure S38. ^1H NMR spectrum of **39**

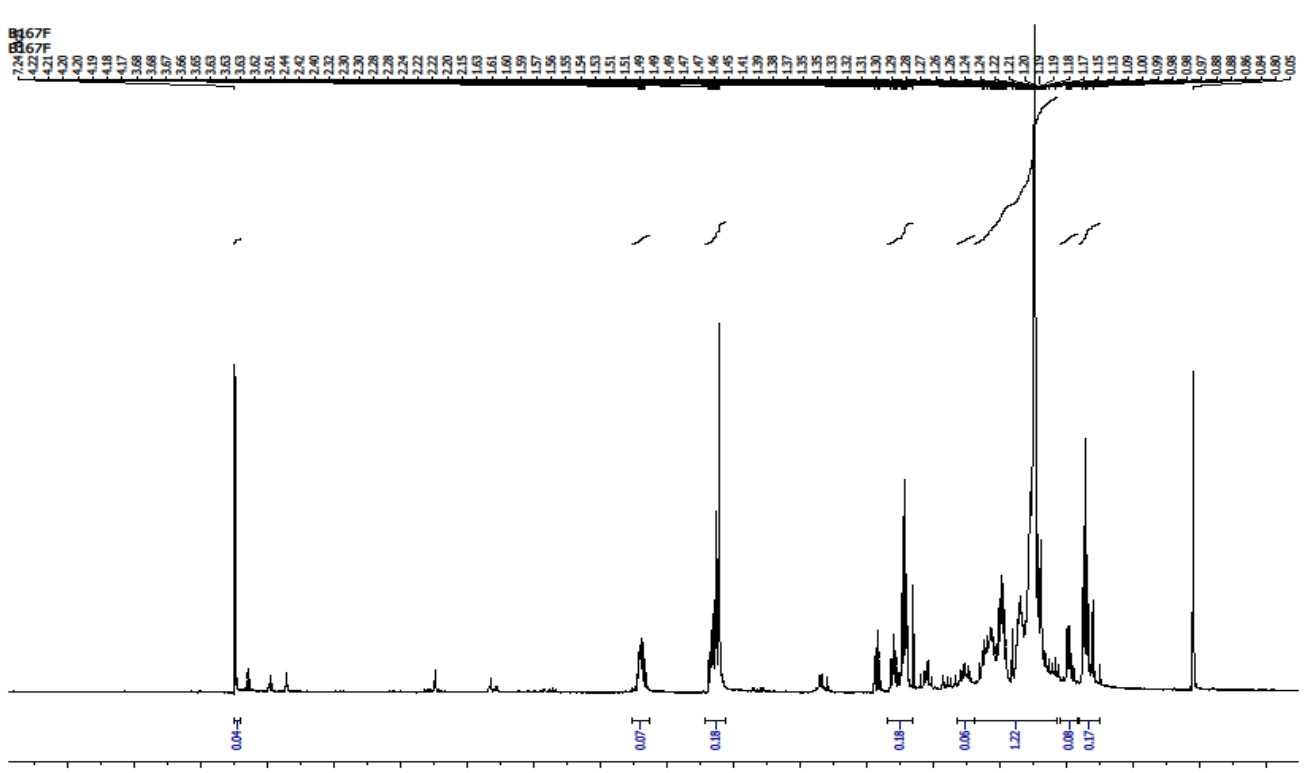
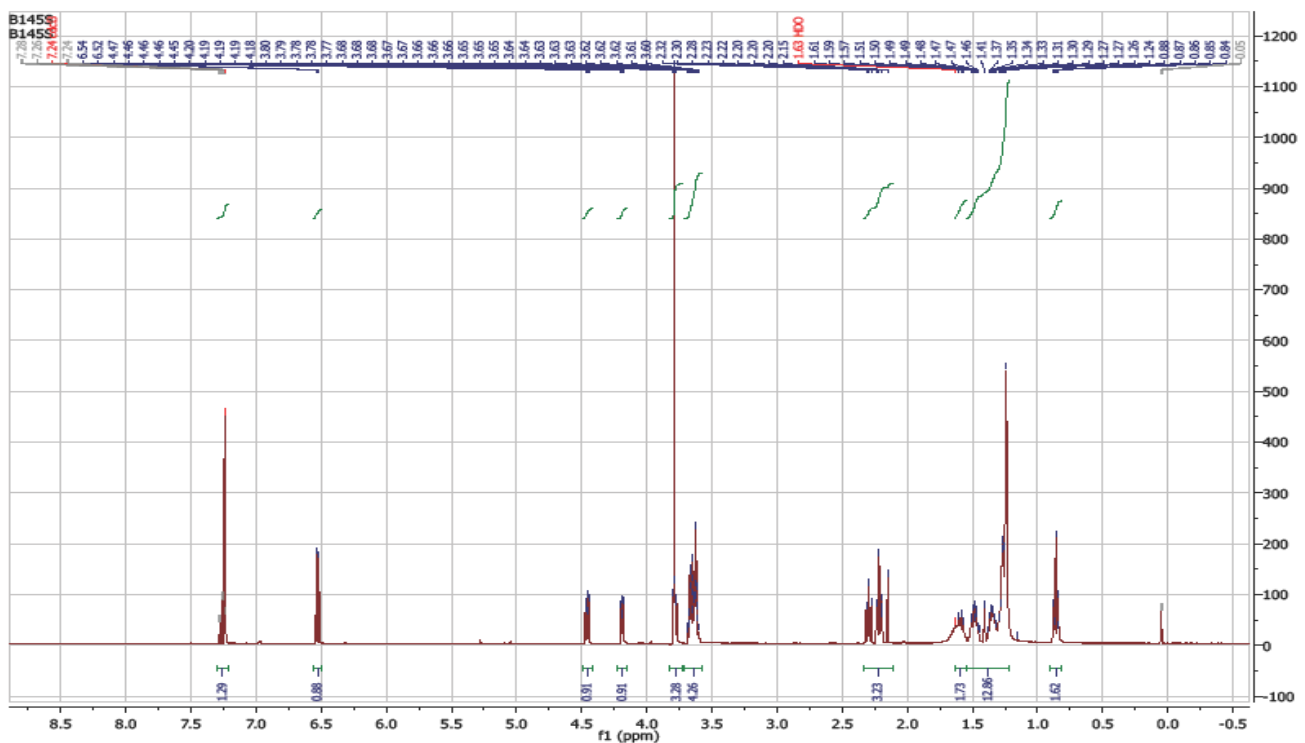


Figure S40. ^1H NMR spectrum of **41**

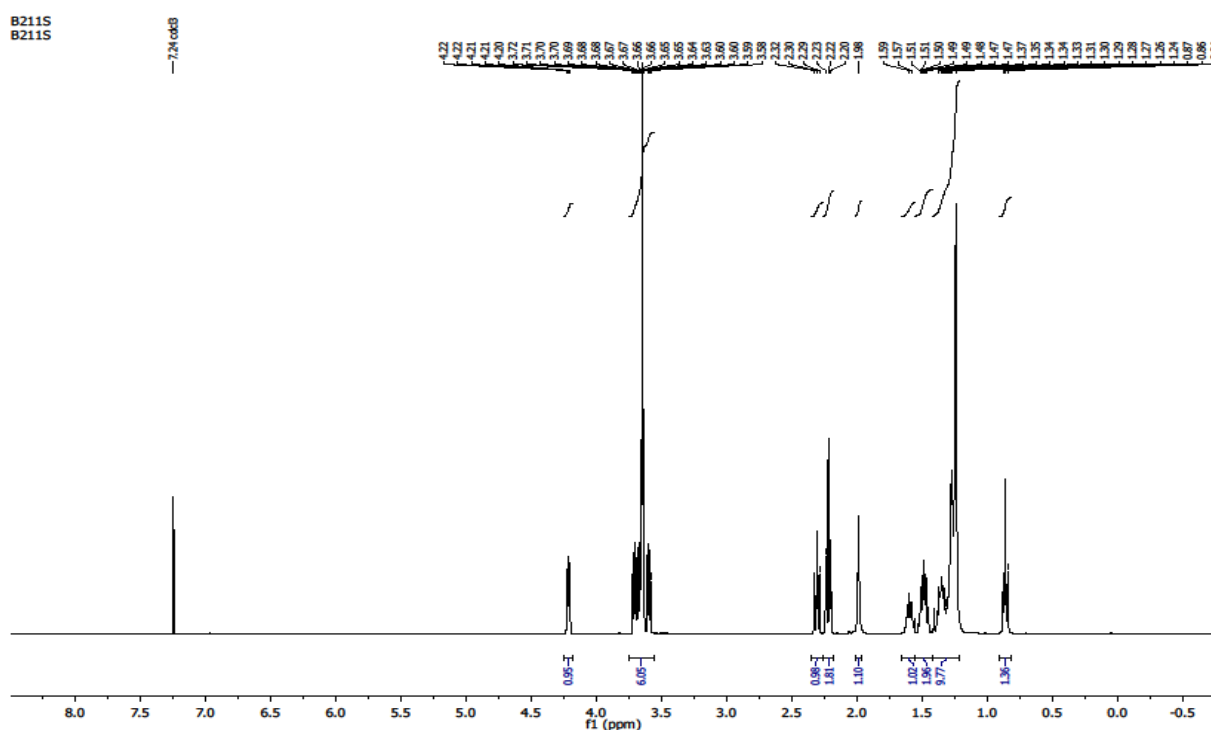


Figure S41. ^1H NMR spectrum of **42**

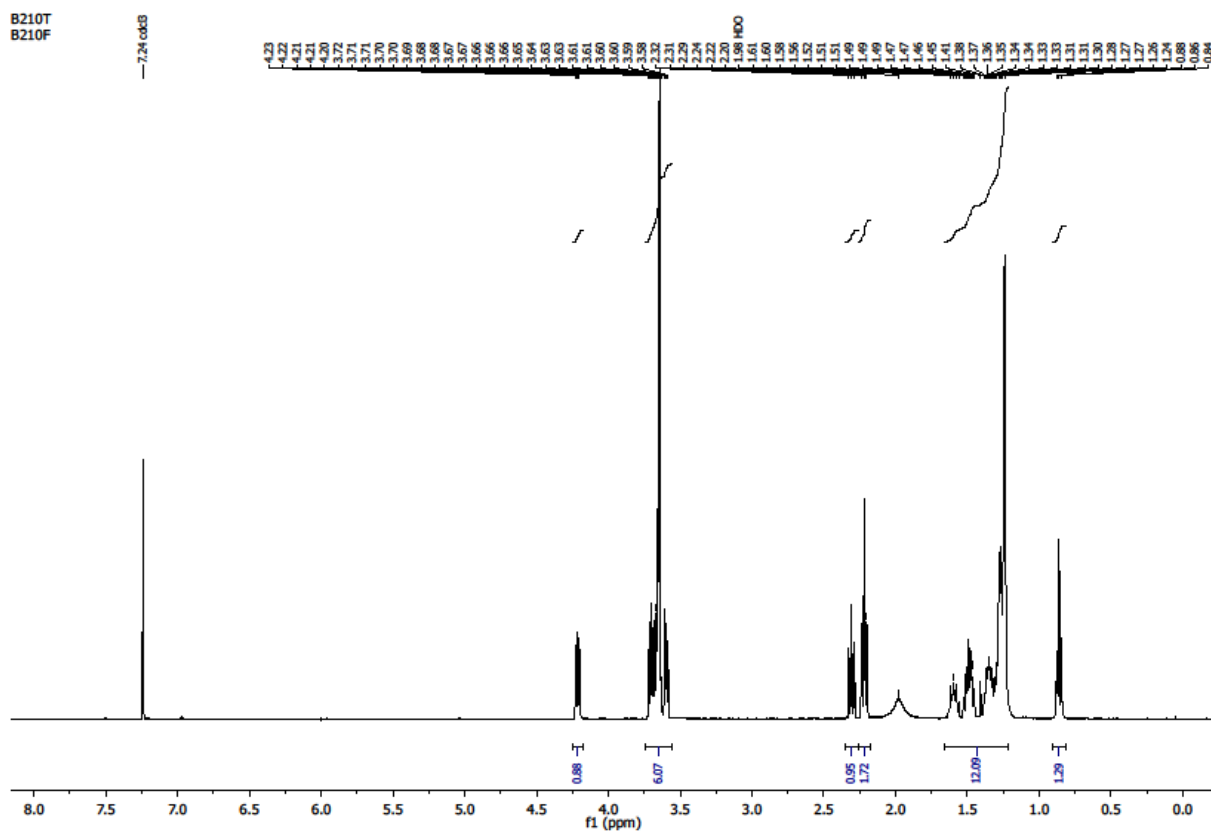
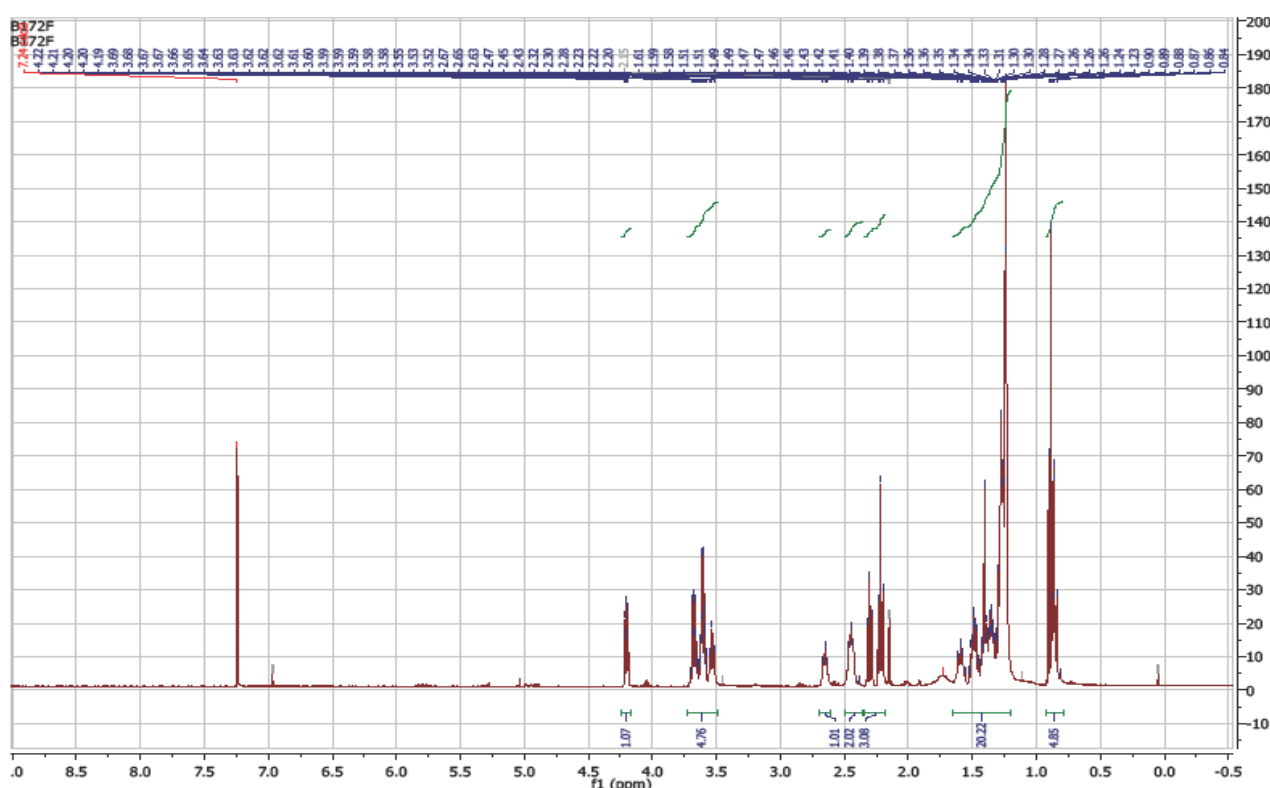


Figure S42. ^1H NMR spectrum of **43**



9.2. Chapter 4

Table S1. Monosaccharides (%) Composition of natural gums tested in the present study⁵⁰.

	Arabinose	Xylose	Rhamnose	Fucose	Glucuronic acid	Galacturonic acid	Glucose	Galactose	Mannose	Other
Arabic	37	-	11	-	7	-	-	45	-	-
Ghatti	47	-	3	-	11	-	-	36	2	1
Guar	35	15	3	7	4	14	11	10	-	1
Karaya	2	-	-	-	-	-	-	34	63	1
Tragacanth	-	-	25	-	4	7	-	64	-	-

Figure S43. Representative chemical structures of painting materials components used in the present study.

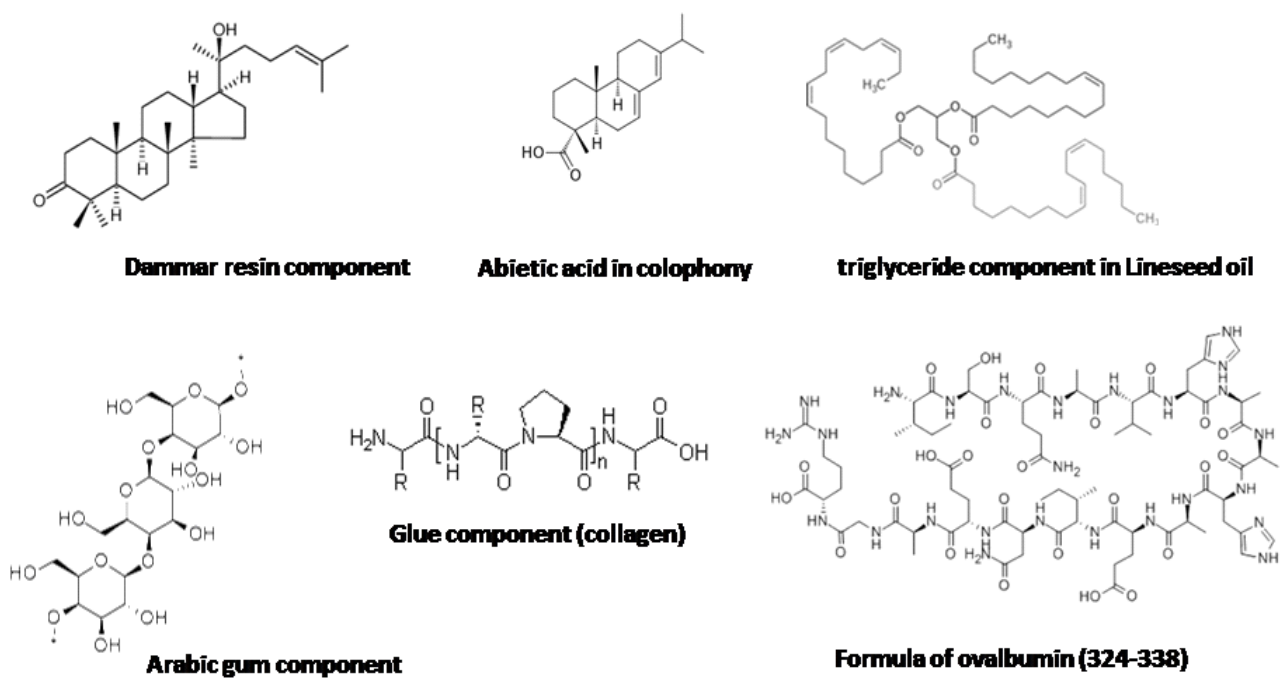


Figure S43a. Color transformations(scanned images after 90 min) of some TR derivatives upon interaction with model compounds of protective layers of paintings.

10 μ L of compounds + 300 μ L of Tris buffer (20mM PH-8)

9.3. Chapter 5

Figure S44: Synthesis scheme for the preparation of TR-NH₂. Procedure adapted from⁶¹.

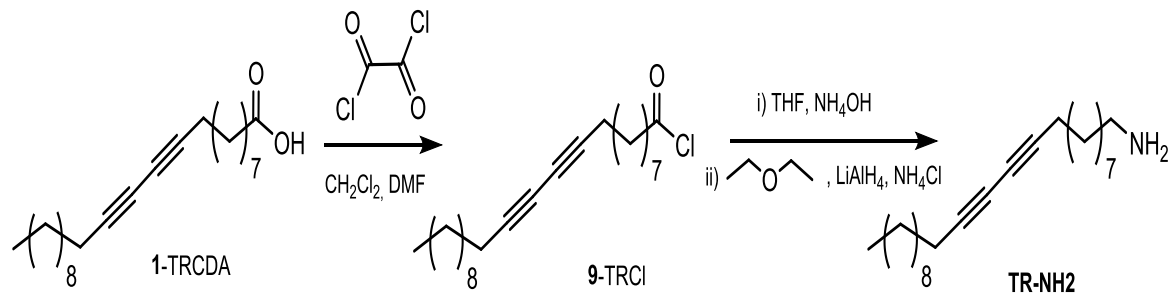


Figure S45: Synthesis scheme for the preparation of TR-MPhe 7(Chapter 8.1.8.).

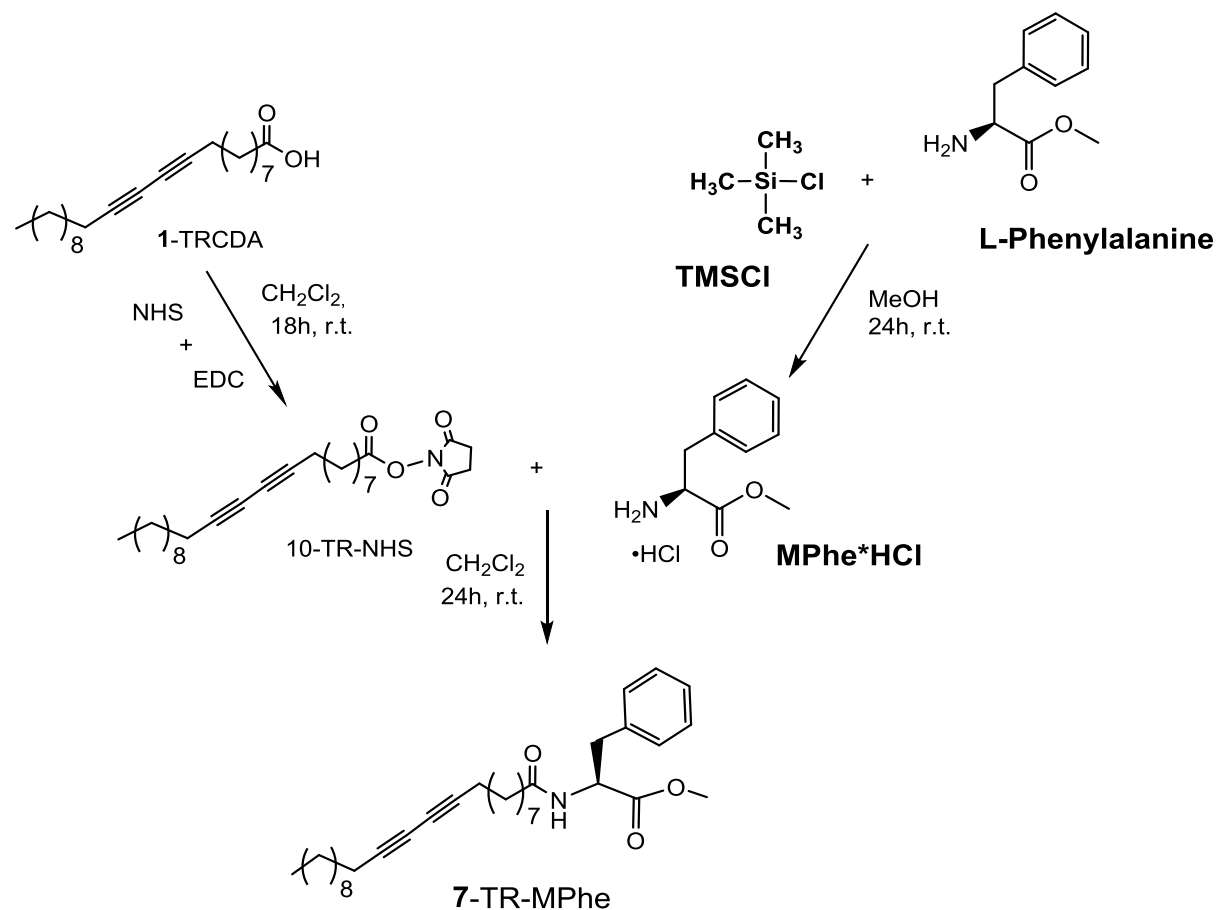


Figure S46: Schematic diagram of the experimental setup for VOC sensing.

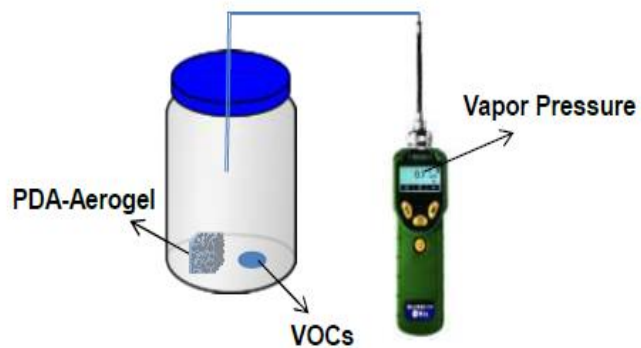


Figure S47: Color transformation titrations of PDA-aerogel (using monomer **1**) in the presence of different concentrations of different VOCs.

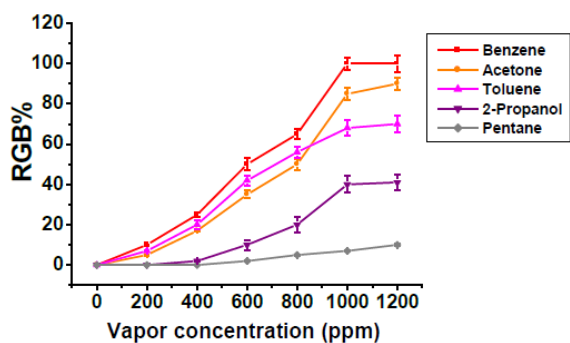
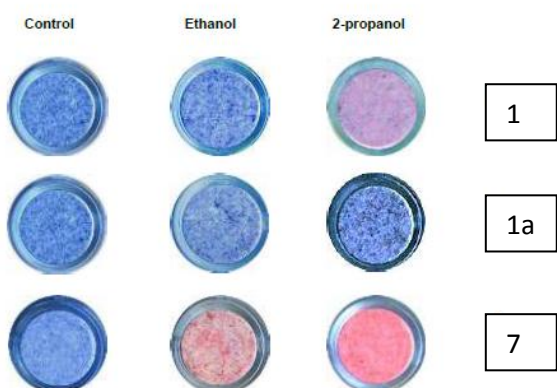


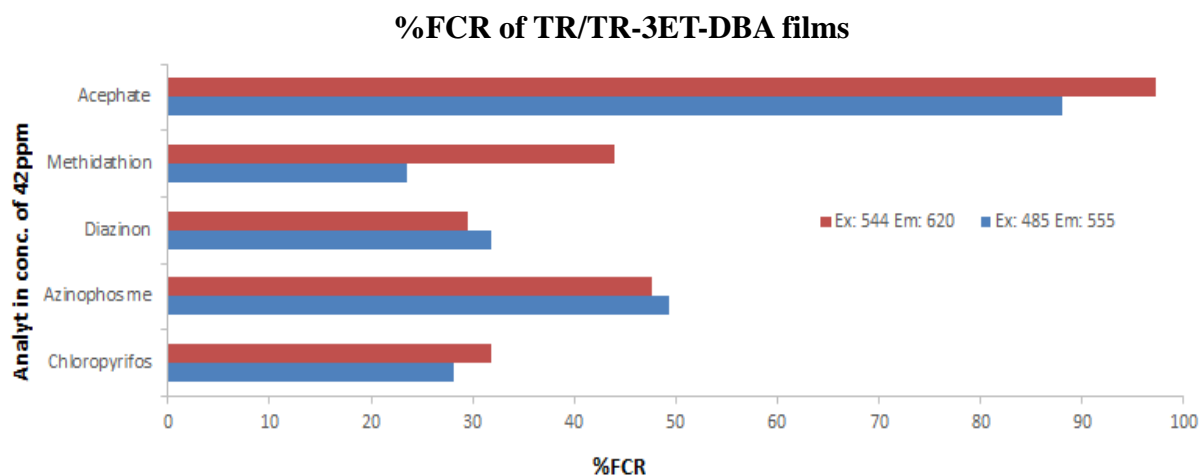
Figure S48: Color transformations of PDA-aerogel induced by ethanol and 2-propanol.



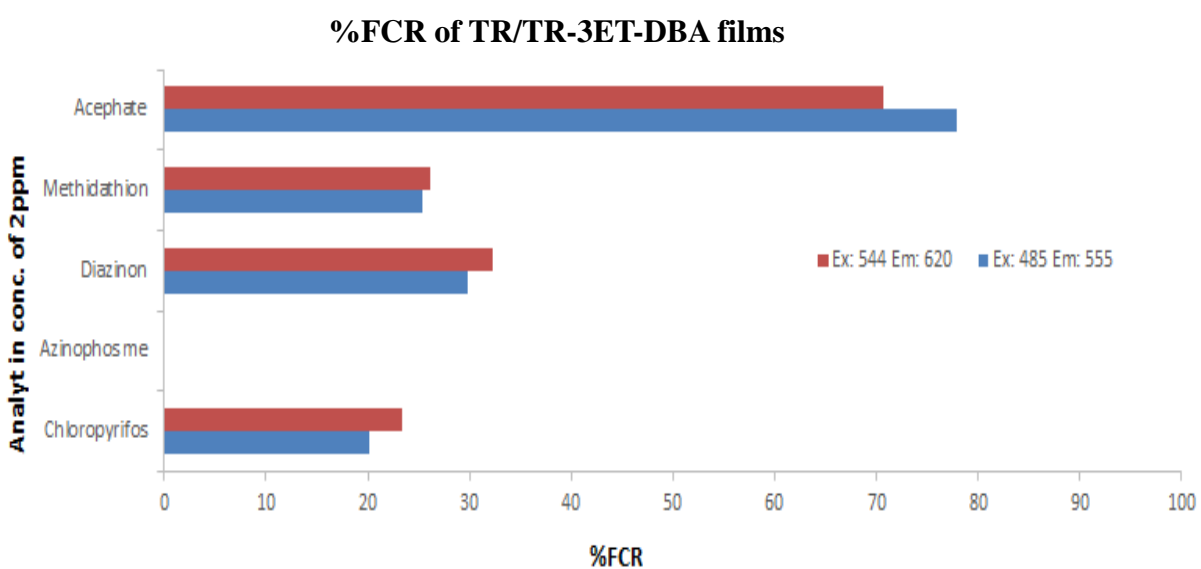
9.4. Chapter 6

Figure S49. Detection of OPs using TR/TR-3ET-DBA **43** sensor.

a) 40ppm



b) 1ppm

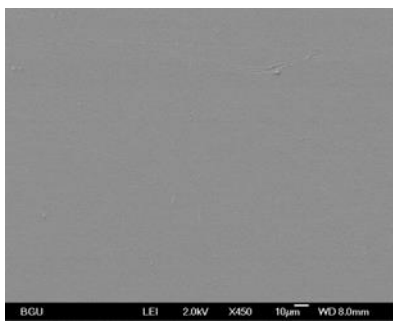


Scanning electron microscopy (SEM) images (Figure S50) of the PMMA substrate used prior to spin-coating & PDA film spin-coated over PMMA. It can be seen that the structure of each PDA is different. They arrange in different manner depending on their headgroup. The TR-DEA film has a porous like surface structure and high roughness. This can support the %FCR results that show the best OP detection with this TR.

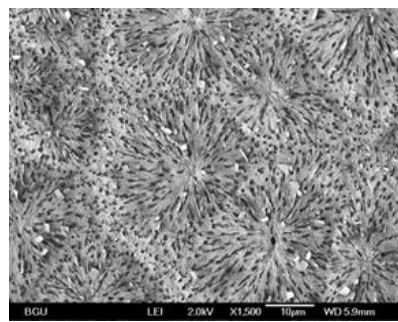
Figure S50. Films SEM images

PMMA

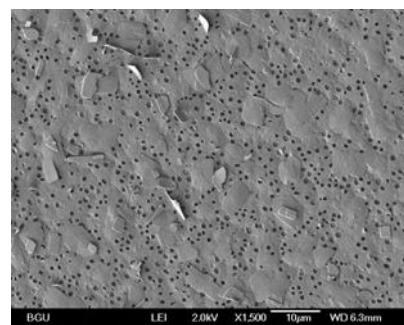
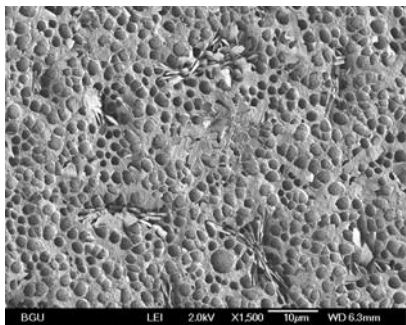
TRCDA



TR-DEA/TRCDA 1:1

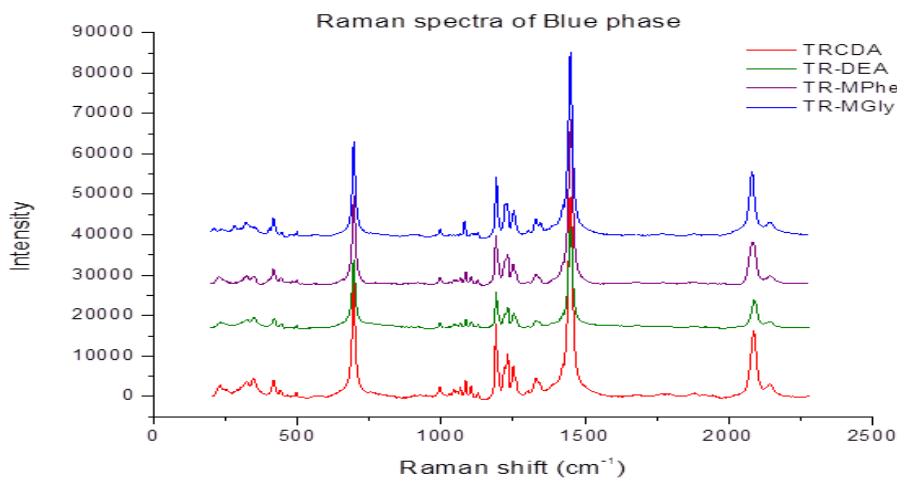


TR-MPhe/TRCDA 1:1



The Blue films' Raman spectra show no significant changes in the Blue phase.

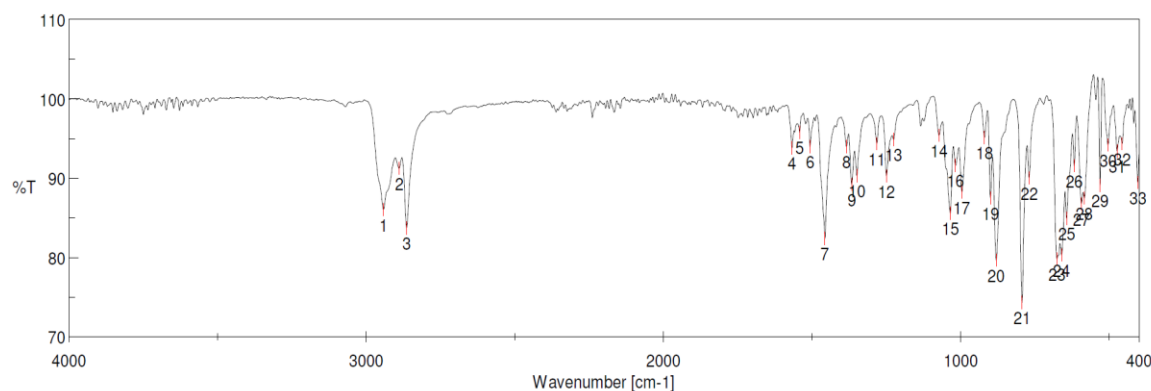
Figure S51. Raman spectra



9.5. Chapter 7

1) Infrared Spectroscopy

Peak Find - Memory-6

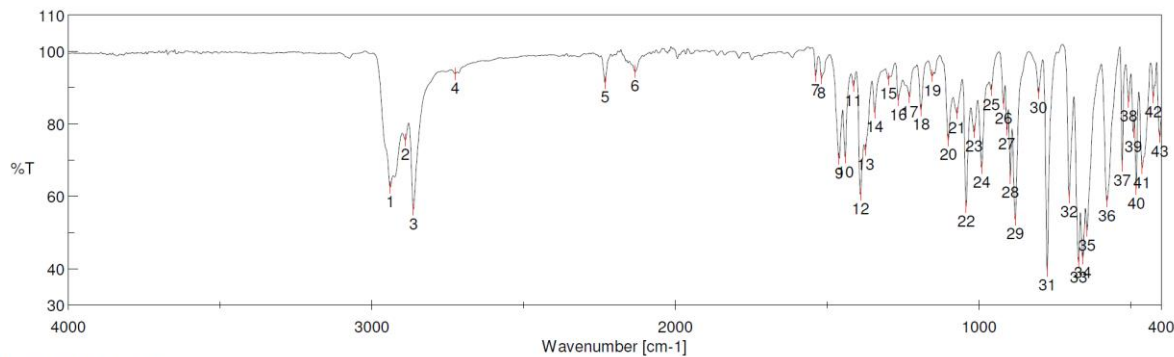


[Result of Peak Picking]

No.	Position	Intensity									
1	2941.88	86.0325	2	2888.84	91.2183	3	2863.77	83.7191	4	1567.84	93.7862
5	1541.81	95.7492	6	1506.13	93.9615	7	1456.96	82.4012	8	1384.64	93.9822
9	1366.32	89.2087	10	1348.96	90.3114	11	1282.43	94.3633	12	1249.65	90.2909
13	1225.54	94.8562	14	1072.23	95.3977	15	1034.62	85.597	16	1017.27	91.6019
17	996.053	88.2357	18	919.879	95.1109	19	899.63	87.4723	20	880.345	79.6675
21	793.564	74.3063	22	769.458	90.0504	23	675.928	79.8087	24	660.5	80.3078
25	643.144	84.9325	26	618.074	91.5487	27	593.968	86.7543	28	584.325	87.4782
29	531.293	89.0772	30	504.294	94.1923	31	473.439	93.4117	32	457.047	94.3437
33	404.014	89.4556									

Figure S52: IR spectrum of **3a** (neat).

Peak Find - OT398Aox.jws

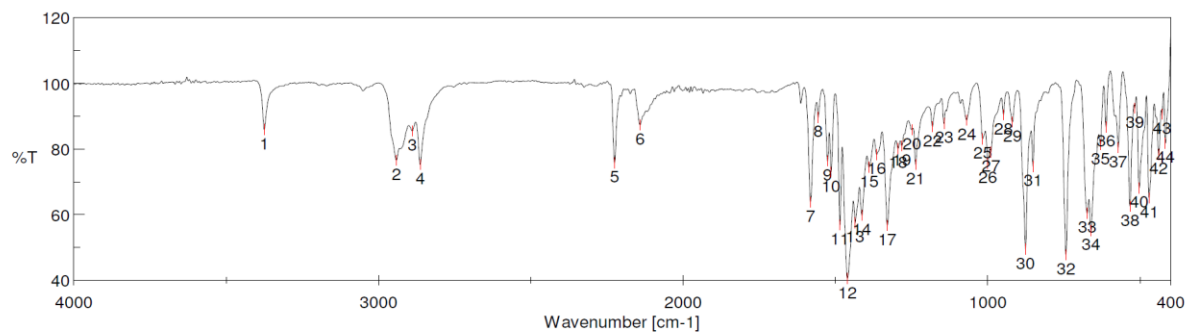


[Result of Peak Picking]

No.	Position	Intensity									
1	2938.98	62.4502	2	2889.81	75.5315	3	2862.81	56.3352	4	2725.89	93.8181
5	2232.2	91.2965	6	2132.88	94.3702	7	1537.95	93.278	8	1518.67	92.5515
9	1460.81	70.3623	10	1440.56	70.7155	11	1413.57	90.3847	12	1390.42	60.5185
13	1374.03	72.7673	14	1343.18	83.1548	15	1298.82	92.3191	16	1266.04	86.5555
17	1229.4	87.3364	18	1190.83	83.8606	19	1154.19	93.1637	20	1101.15	75.4776
21	1072.23	82.8986	22	1042.34	57.1031	23	1016.3	77.7676	24	991.232	67.8612
25	959.412	89.3082	26	918.914	85.518	27	908.308	78.4361	28	896.737	65.0684
29	880.345	53.6455	30	804.171	88.5071	31	775.244	39.4842	32	702.926	59.6872
33	672.071	41.7025	34	658.571	42.9007	35	644.108	50.474	36	578.54	58.6642
37	528.4	68.459	38	507.187	86.0553	39	491.759	77.7278	40	482.117	62.0529
41	462.832	67.762	42	426.191	87.3097	43	404.978	76.4215			

Figure S53: IR spectrum of **3b** (neat).

Peak Find - MM-85-2.jws

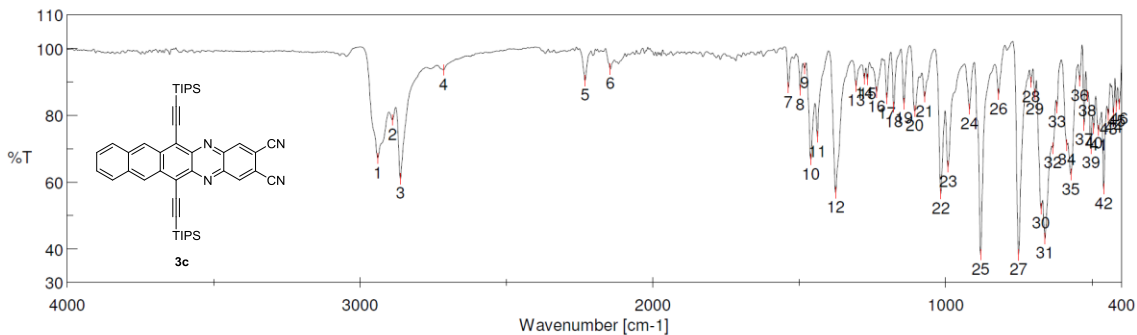


[Result of Peak Picking]

No.	Position	Intensity	No.	Position	Intensity	No.	Position	Intensity
1	3374.82	85.8814	2	2940.91	76.5603	3	2888.84	85.4645
4	2862.81	75.2402	5	2225.45	75.6782	6	2141.56	87.2999
7	1582.31	63.7572	8	1557.24	89.5425	9	1526.38	76.3289
10	1514.81	72.911	11	1485.88	56.8364	12	1460.81	40.4976
13	1435.74	57.4492	14	1413.57	59.7386	15	1389.46	74.3774
16	1365.35	78.2757	17	1329.68	56.6836	18	1294.97	80.1098
19	1282.43	80.8921	20	1249.65	85.8564	21	1237.11	75.23
22	1182.15	86.7937	23	1143.58	87.7138	24	1069.33	88.7734
25	1017.27	83.0584	26	999.91	75.5242	27	990.268	79.0354
28	948.806	90.411	29	918.914	88.1857	30	876.488	49.4447
31	851.418	74.6415	32	743.424	47.671	33	673.999	60.3805
34	661.464	55.085	35	630.609	81.2723	36	612.288	86.6793
37	571.79	80.381	38	533.221	62.5041	39	517.793	92.4331
40	503.33	68.0461	41	470.546	65.0403	42	439.69	78.3198
43	428.12	90.5662	44	417.513	81.752			

Figure S54: IR spectrum of **3c-H₂** (neat).

Peak Find - Memory-5



[Result of Peak Picking]

No.	Position	Intensity	No.	Position	Intensity	No.	Position	Intensity
1	2938.98	67.1071	2	2888.84	78.6037	3	2861.84	60.9536
4	2715.28	93.5121	5	2231.24	90.3603	6	2145.42	93.805
7	1537.95	88.2306	8	1497.45	87.5744	9	1482.03	94.0393
10	1460.81	66.777	11	1438.64	73.5008	12	1375.96	56.758
13	1306.54	88.7482	14	1278.57	90.9412	15	1267.97	90.6717
16	1236.15	86.9085	17	1201.43	84.9866	18	1177.33	82.3784
19	1142.62	83.4154	20	1105.98	81.2153	21	1072.23	85.4683
22	1017.27	56.5229	23	992.196	64.6003	24	918.914	81.8719
25	881.309	38.2874	26	819.598	86.247	27	751.138	38.1984
28	708.712	89.895	29	696.177	86.2579	30	674.963	52.0158
31	661.464	43.0724	32	634.466	70.1059	33	620.002	82.3666
34	586.254	71.0605	35	572.755	62.1985	36	542.863	90.2212
37	527.436	76.9972	38	516.829	85.6716	39	504.294	70.0962
40	494.652	75.9818	41	478.26	75.4899	42	460.904	57.9567
43	444.512	80.0963	44	427.155	80.7439	45	417.513	82.6419
46	407.871	83.3225						

Figure S55: IR spectrum of **3c** (neat).

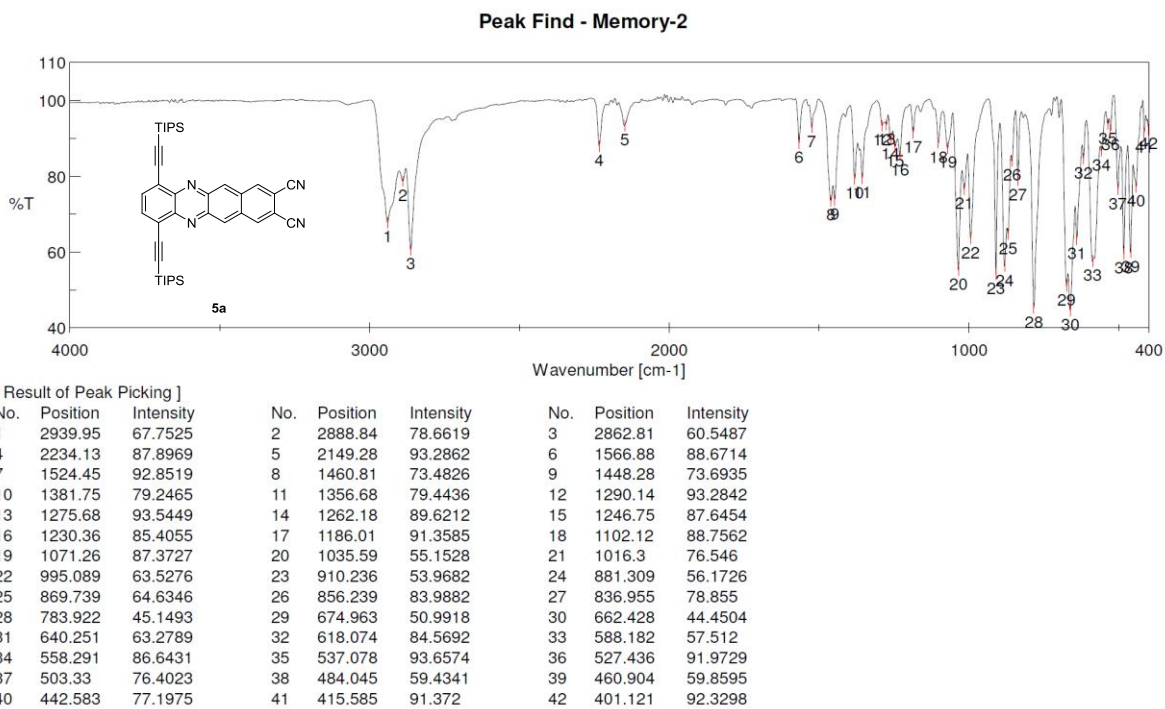


Figure S16: IR spectrum of **5a** (neat).

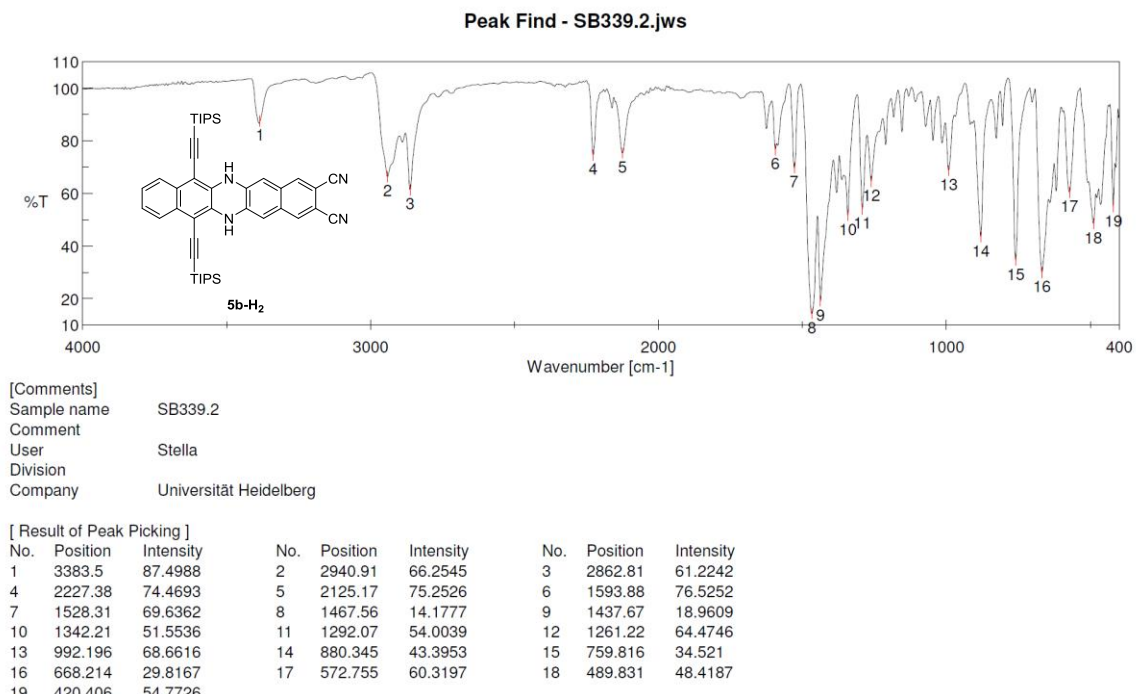


Figure S57: IR spectrum of **5b-H₂** (neat).

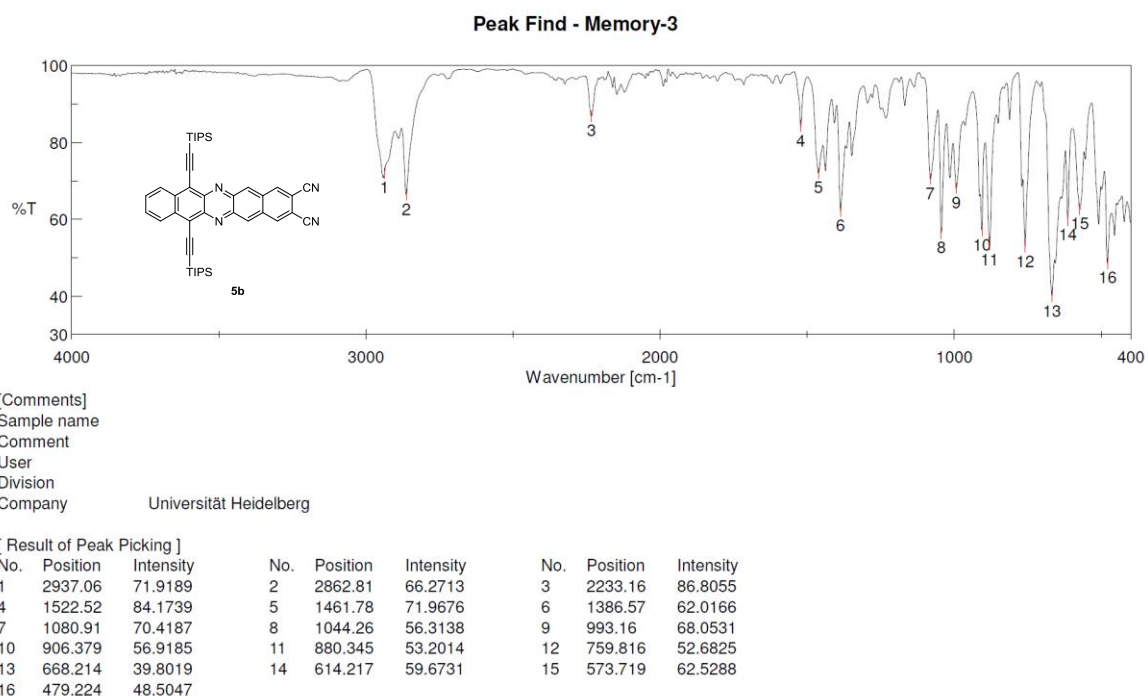


Figure S58: IR spectrum of **5b** (neat).

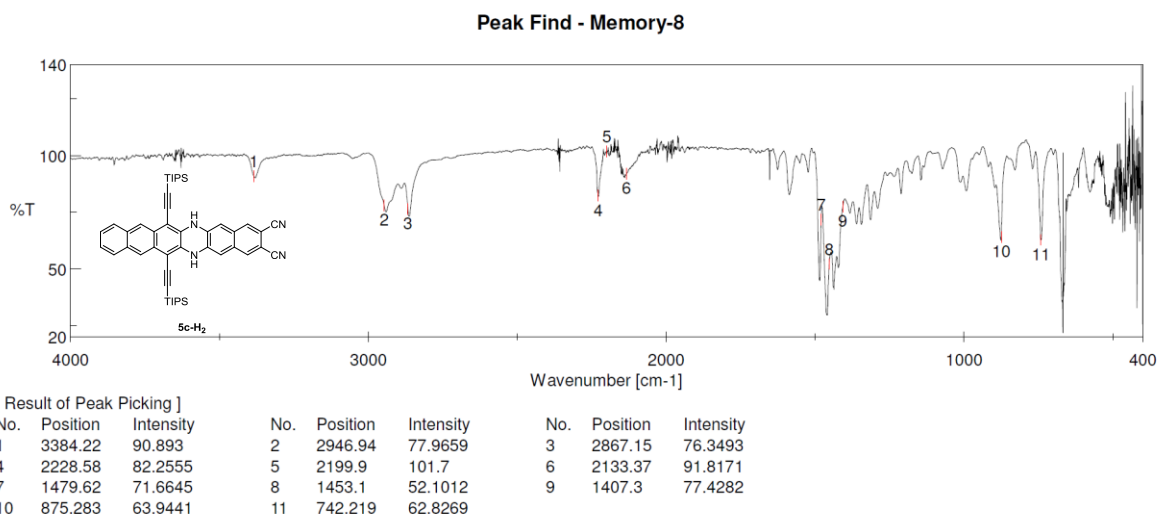


Figure S59: IR spectrum of **5c-H₂** (neat).

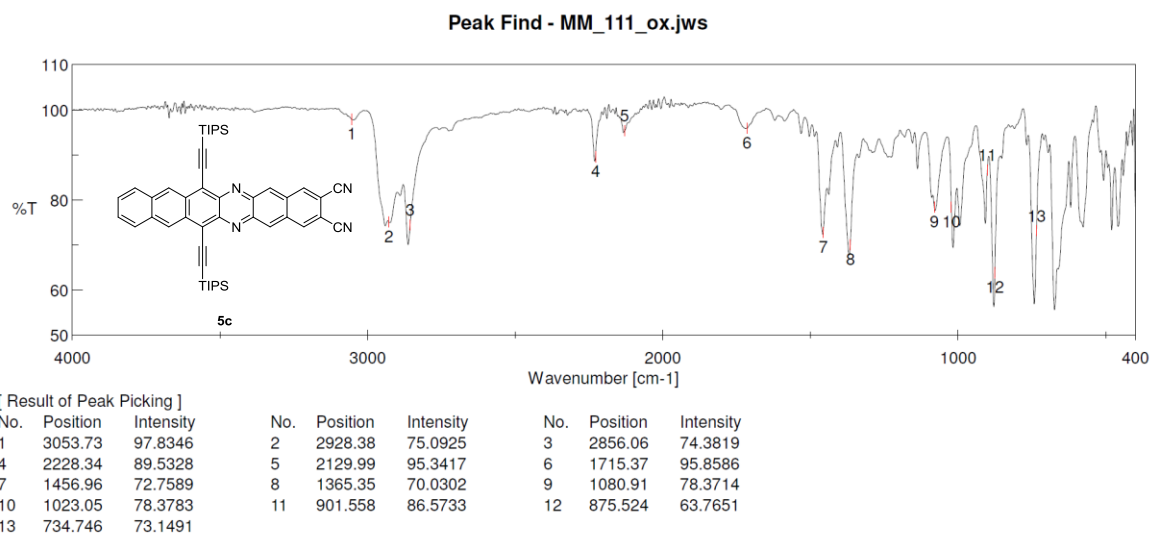


Figure S60: IR spectrum of **5c** (neat).

2) Cyclic Voltammetry

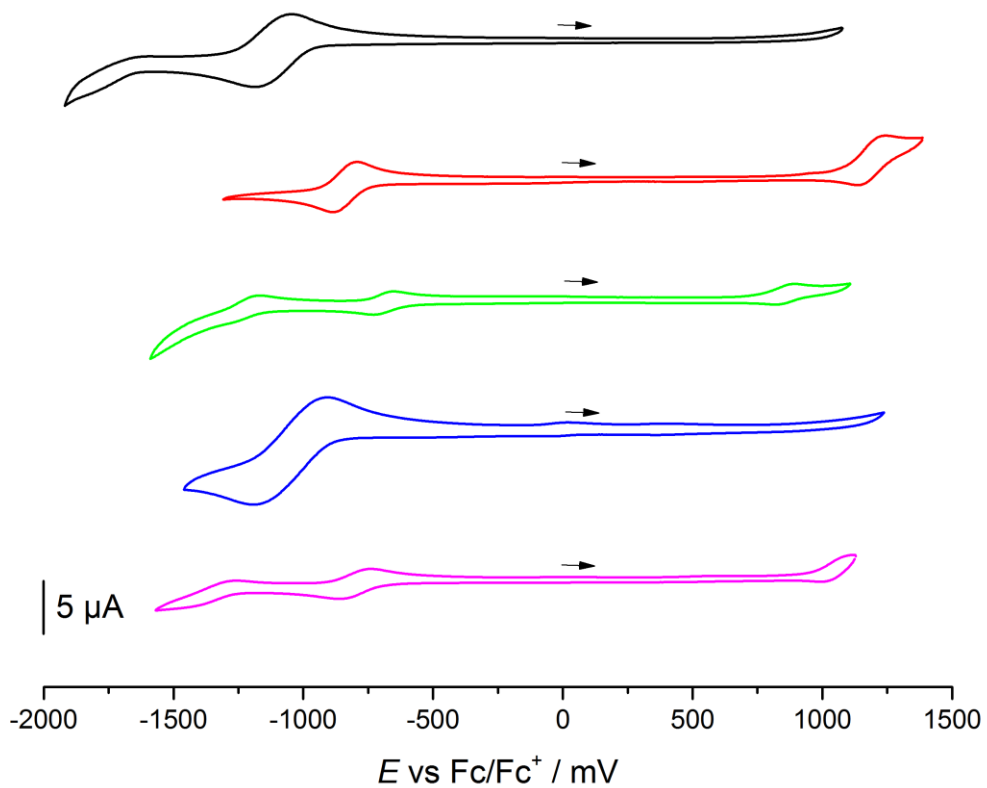


Figure S61: Cyclic voltammograms of **3a-c** and **5a-b** (from top to bottom, respectively).

All cyclic voltammetry experiments were carried out using a silver wire reference electrode, a platinum working electrode, a platinum/titanium wire auxiliary electrode, a 0.1 M NBu_4PF_6 solution in degassed, dry CH_2Cl_2 , a scan speed of 0.1 V s^{-1} and ferrocene/ferrocenium as reference redox system and internal standard (-5.1 eV)¹²².

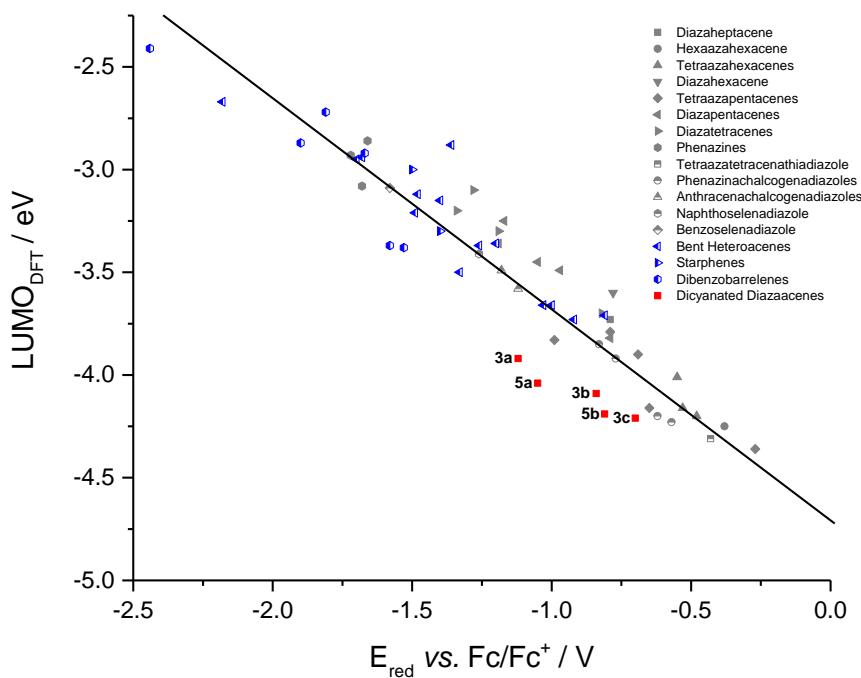


Figure S62: Correlation of the first reduction potentials as determined by CV and calculated DFT-LUMOs of linear heteroacenes (grey), non-linear heteroacenes (blue) and dicyanated, linear heteroacenes (red)¹²³.

3) NMR Spectroscopy

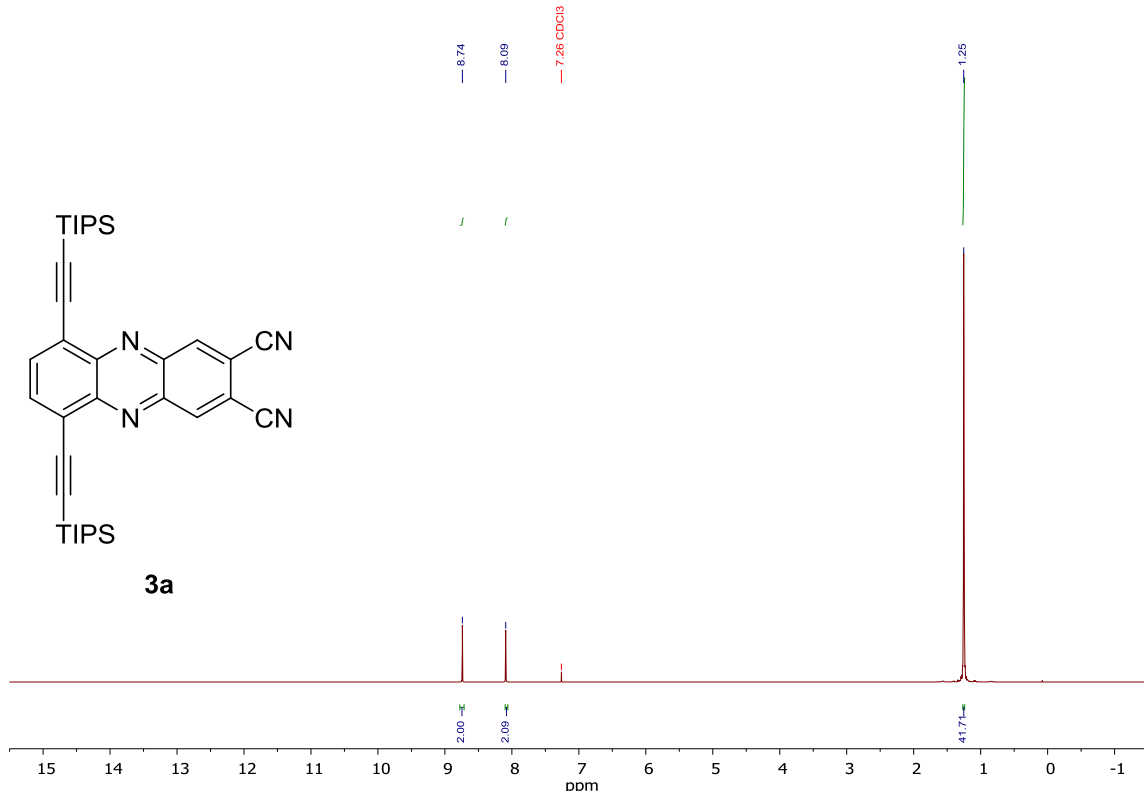


Figure S63: ^1H NMR (300 MHz, CDCl_3 , 25°C) of **3a**.

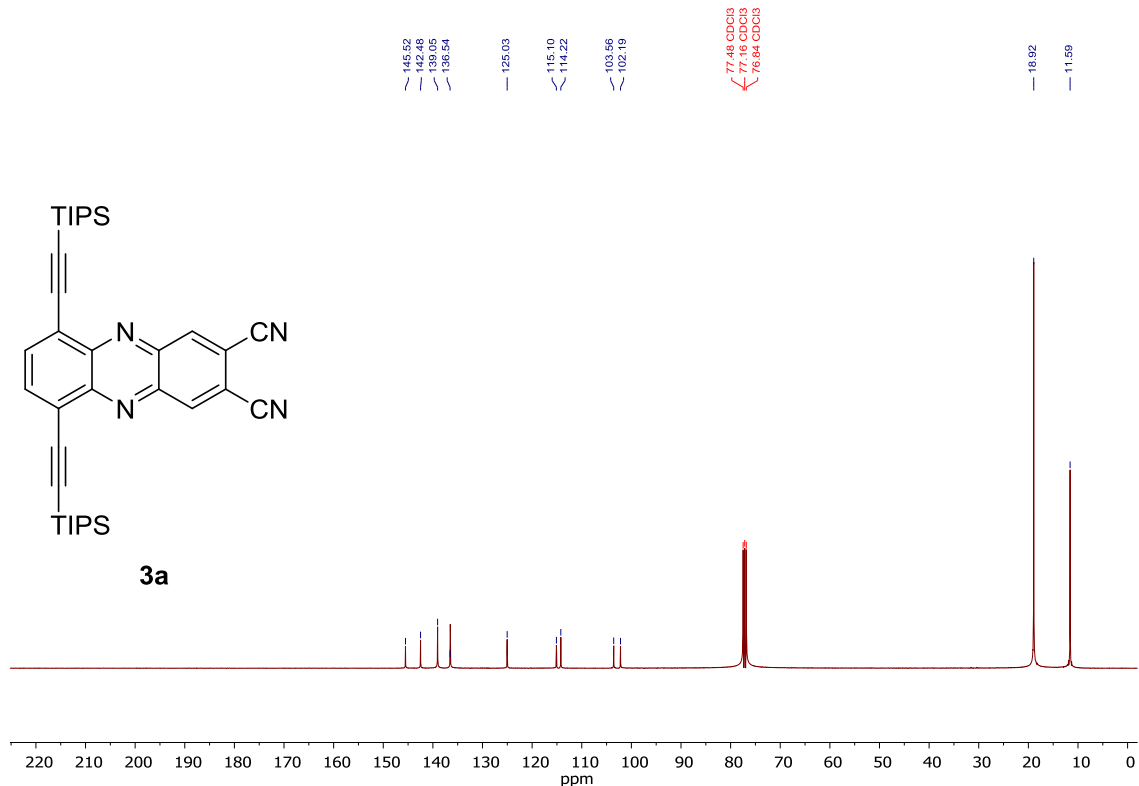


Figure S64: ¹³C NMR (101 MHz, CDCl₃, 25 °C) of **3a**.

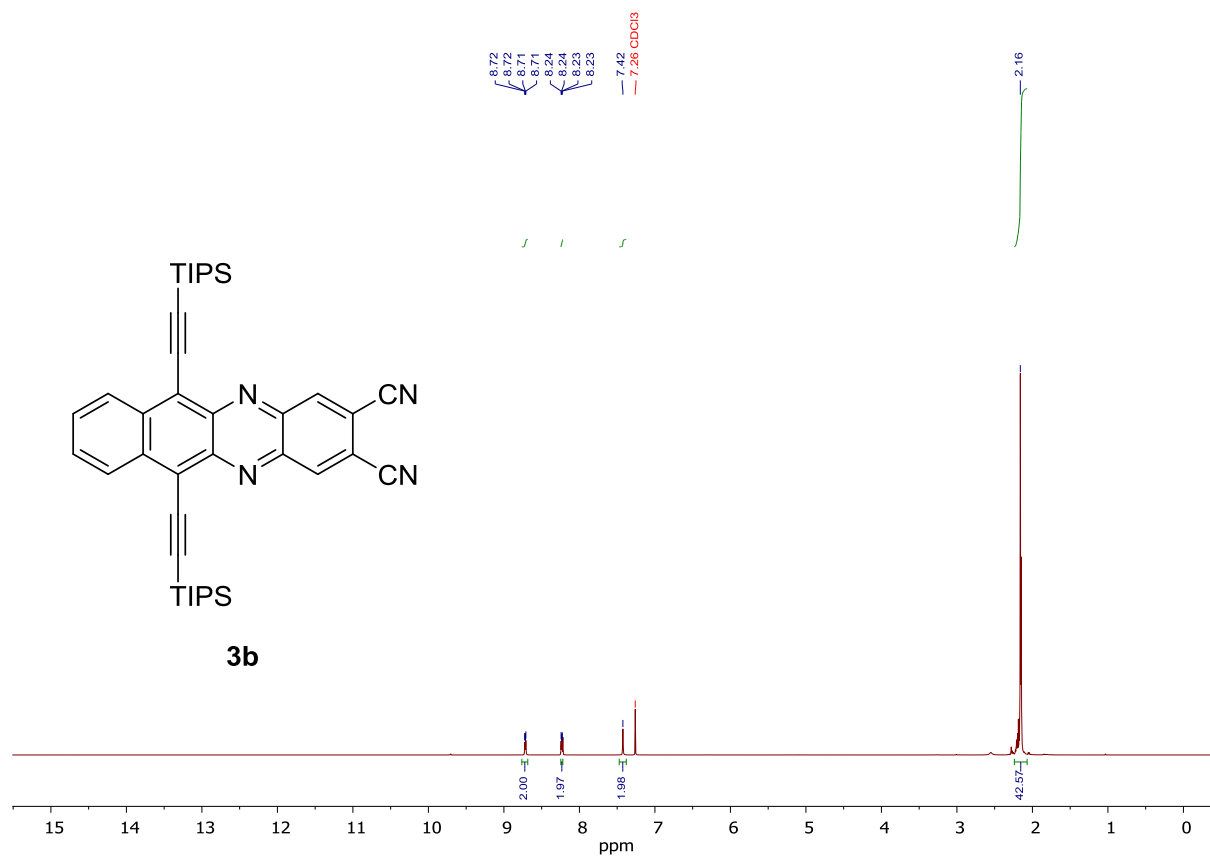


Figure S65: ¹H NMR (600 MHz, CDCl₃, 25°C) of **3b**.

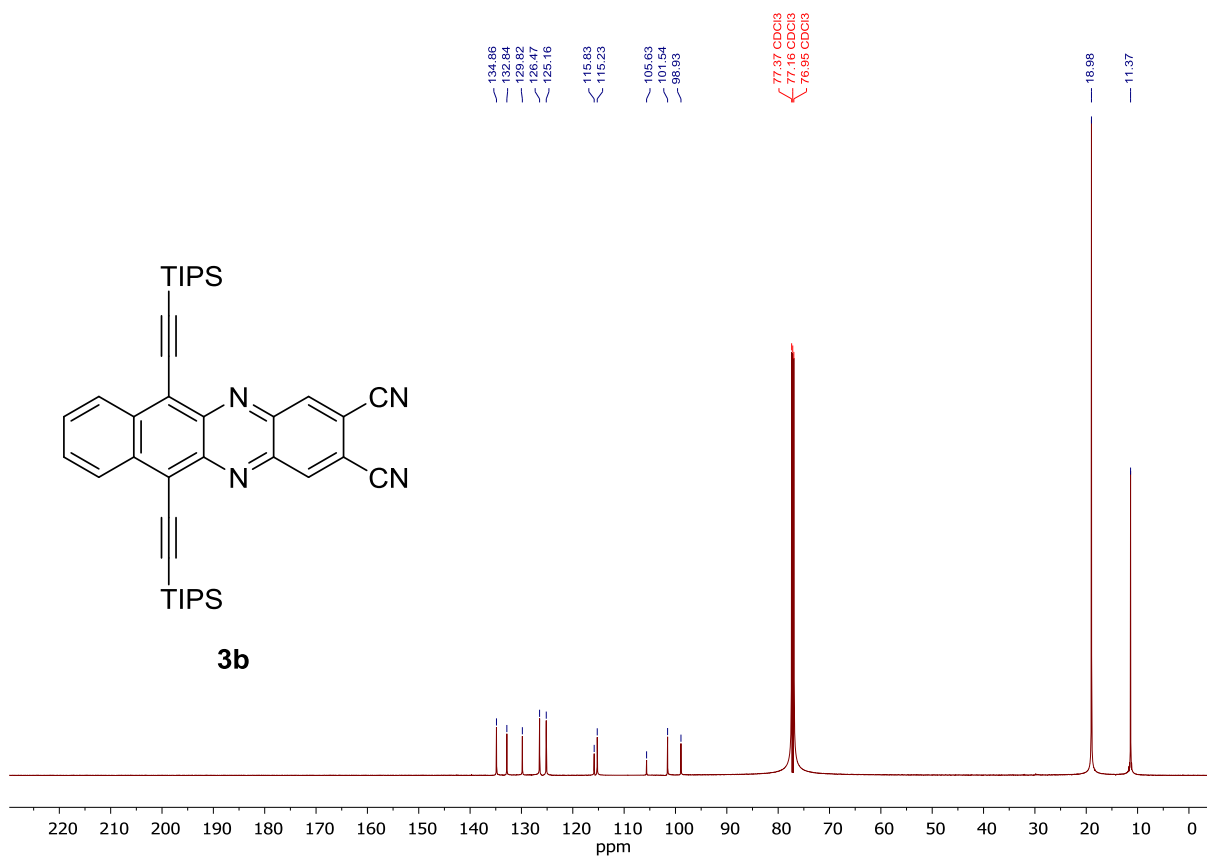


Figure S66: ^{13}C NMR (151 MHz, CDCl_3 , 25 °C) of **3b**.

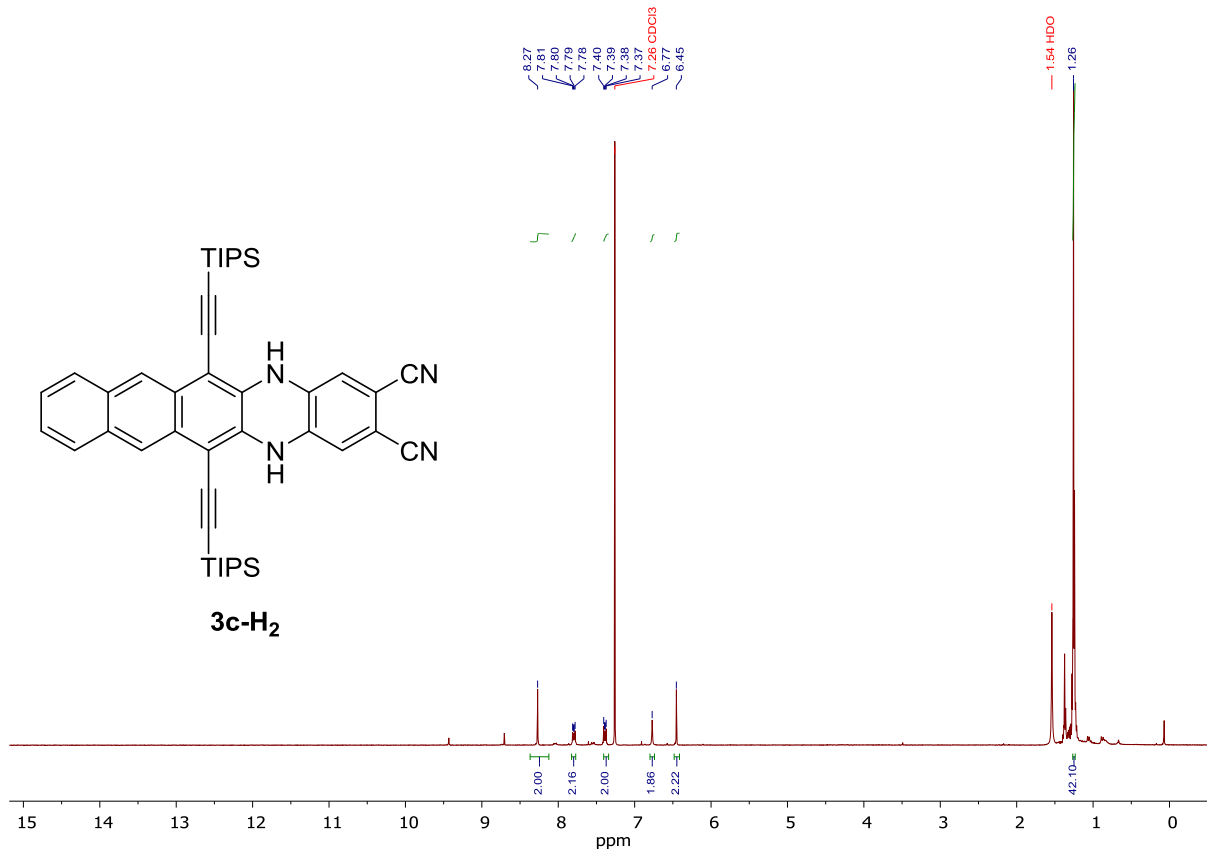


Figure S67: ^1H NMR (500 MHz, CDCl_3 , 25°C) of **3c-H₂**.

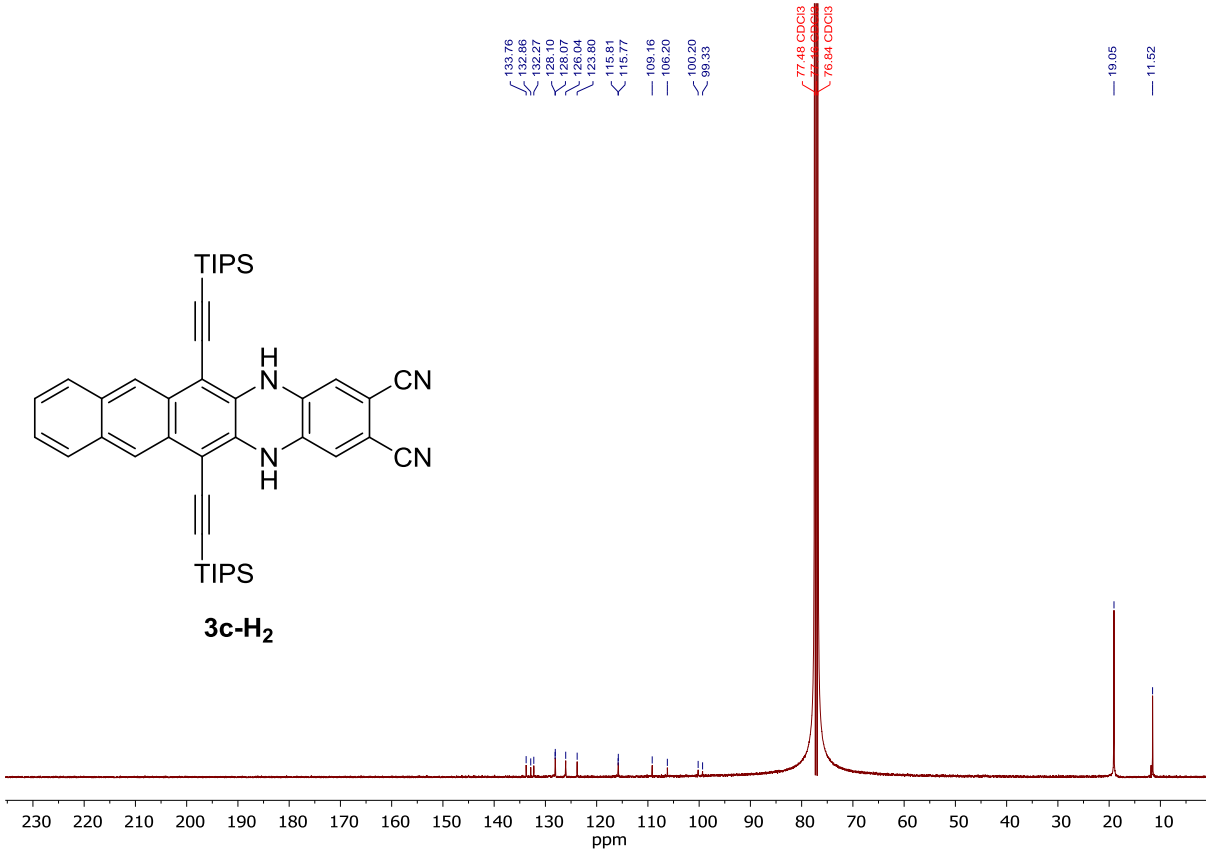


Figure S68: ^{13}C NMR (101 MHz, CDCl_3 , 25 °C) of **3c-H₂**.

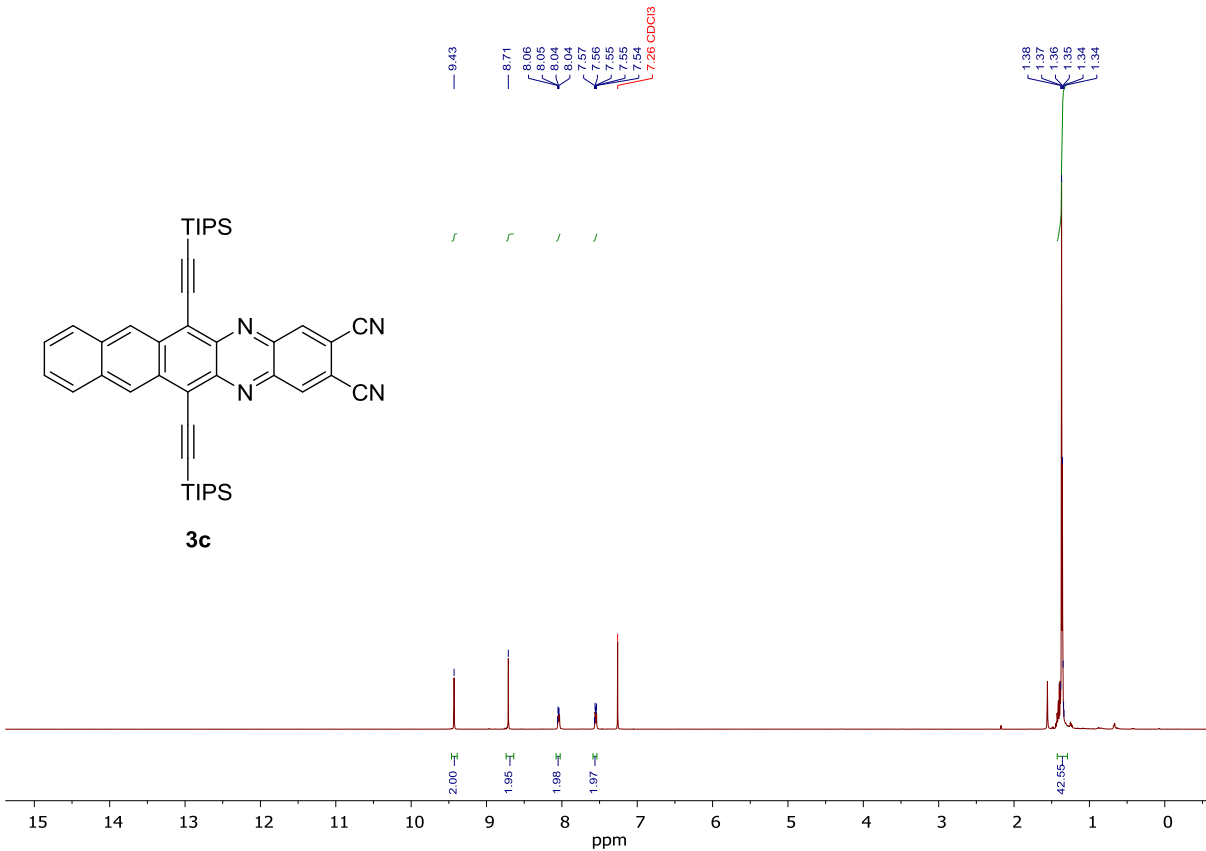


Figure S69: ^1H NMR (500 MHz, CDCl_3 , 25°C) of **3c**.

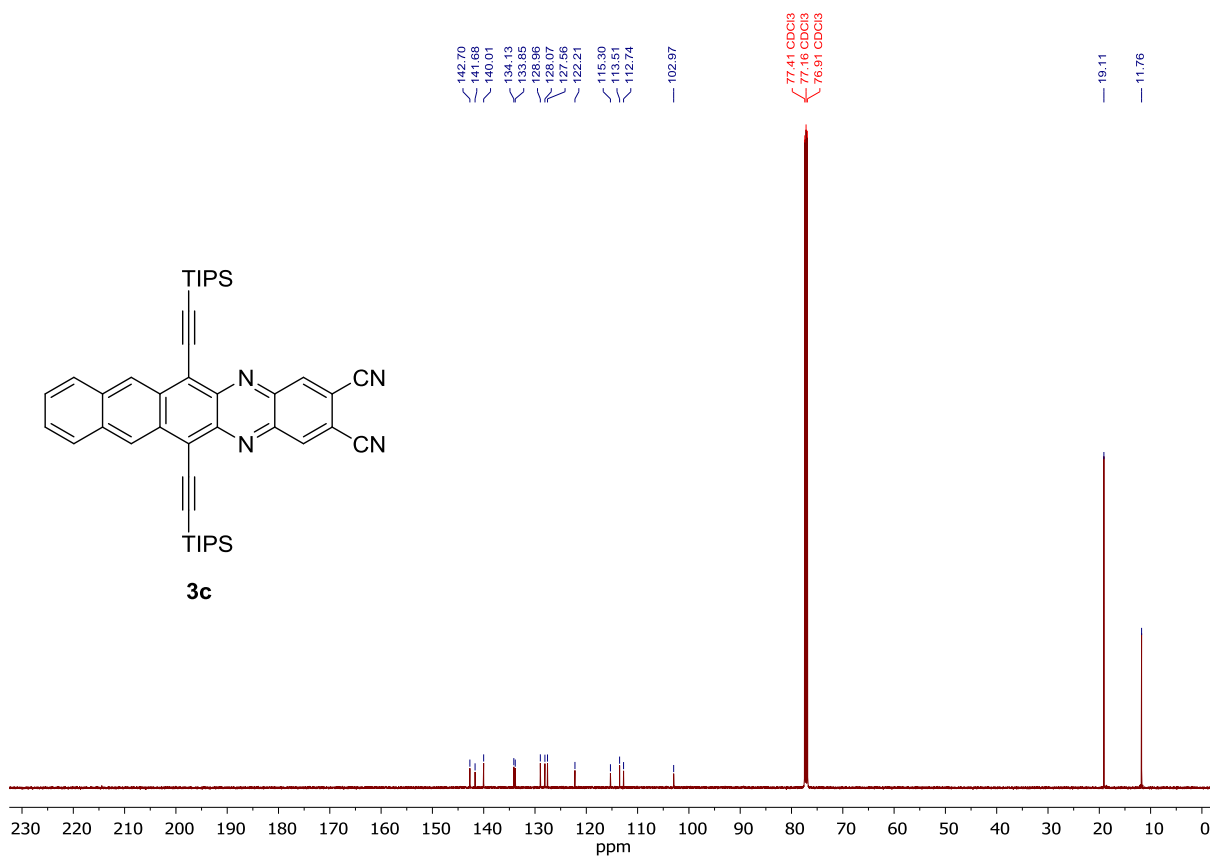


Figure S70: ^{13}C NMR (126 MHz, CDCl₃, 25 °C) of **3c**.

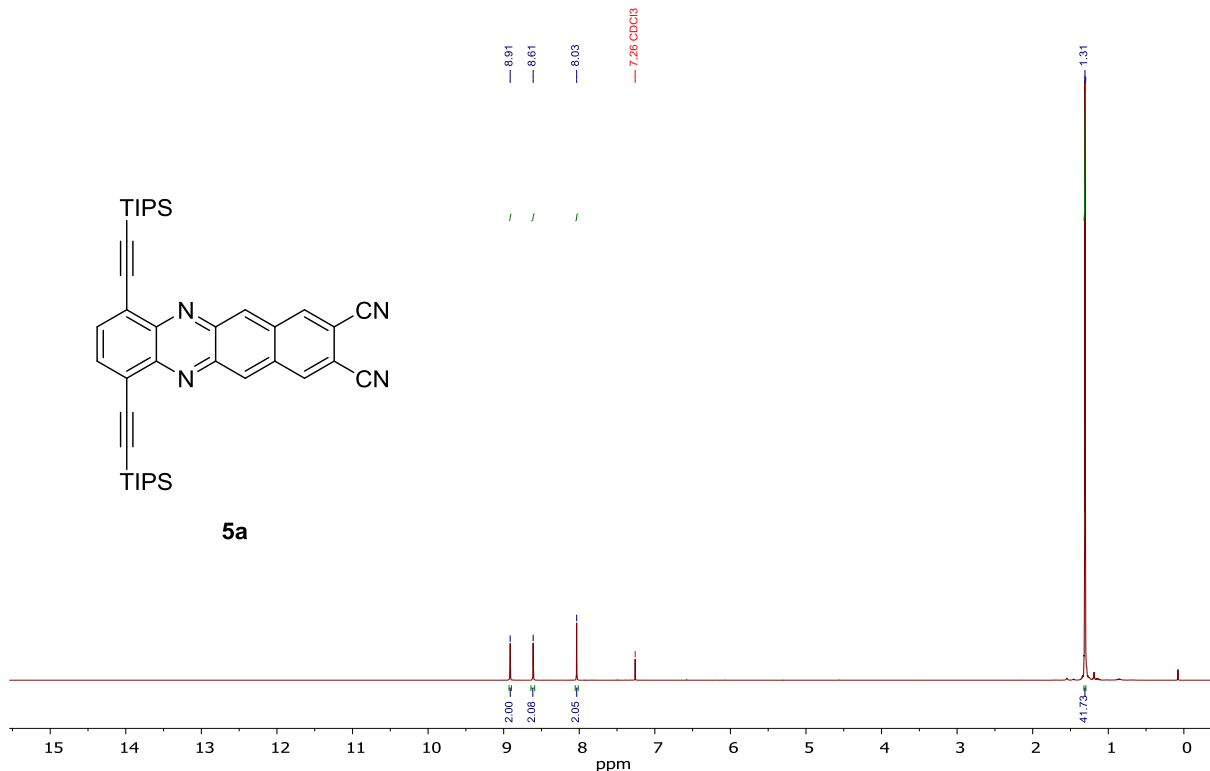


Figure S71: ^1H NMR (400 MHz, CDCl₃, 25°C) of **5a**.

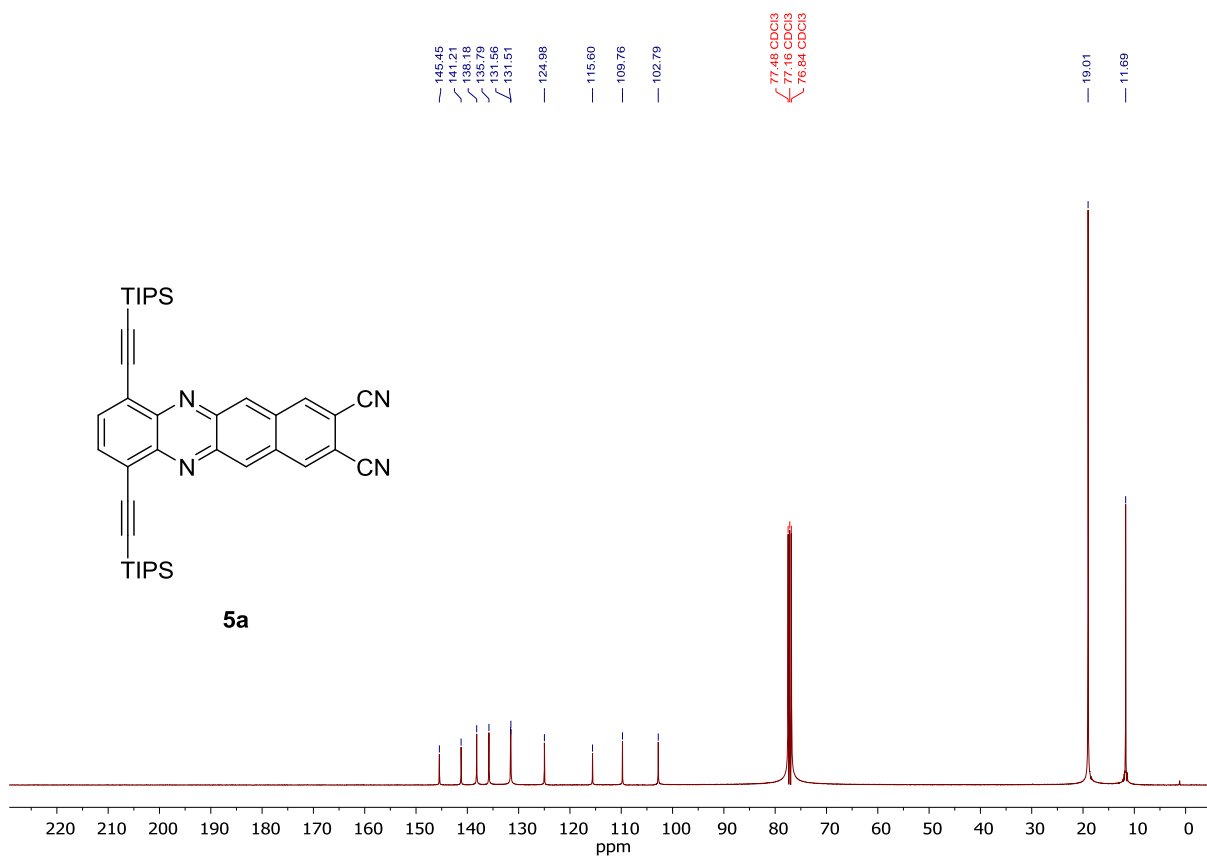


Figure S72: ¹³C NMR (101 MHz, CDCl₃, 25 °C) of **5a**.

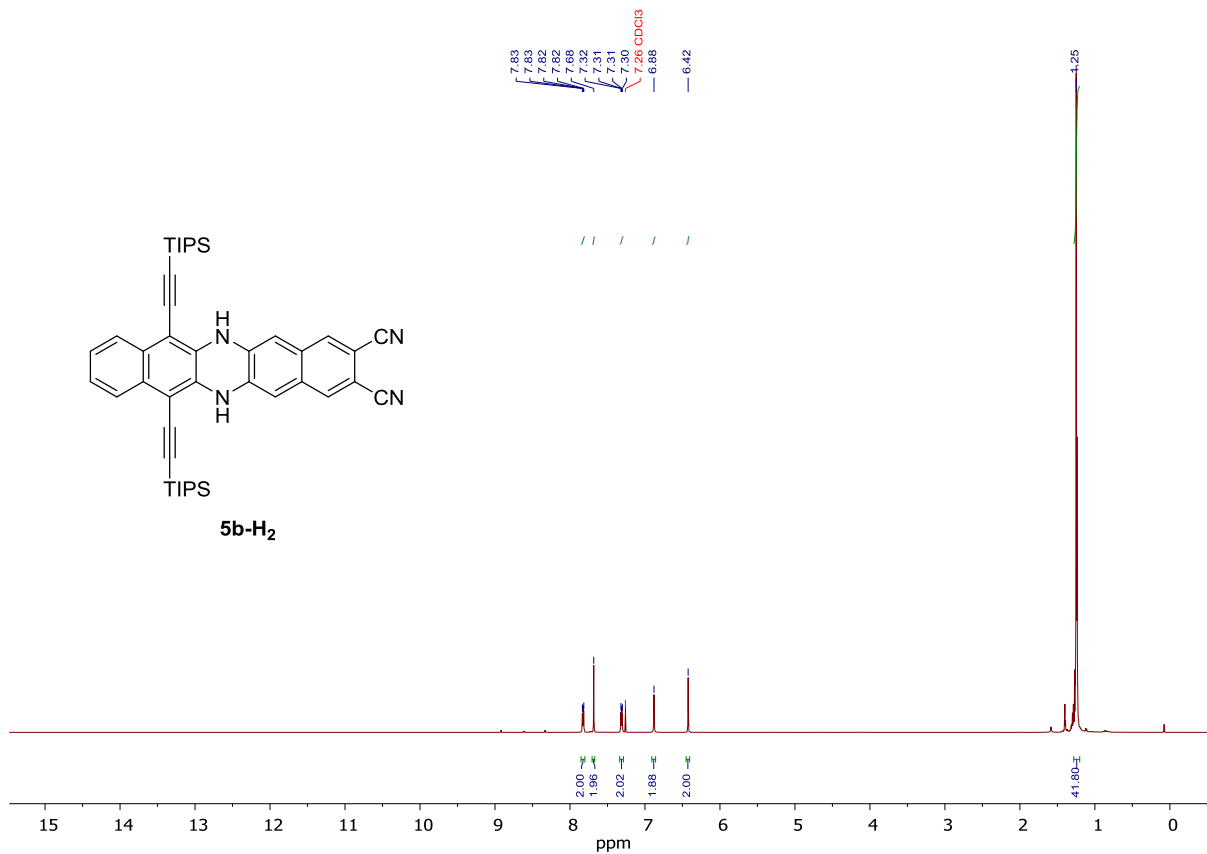


Figure S73: ¹H NMR (500 MHz, CDCl₃, 25°C) of **5b-H₂**.

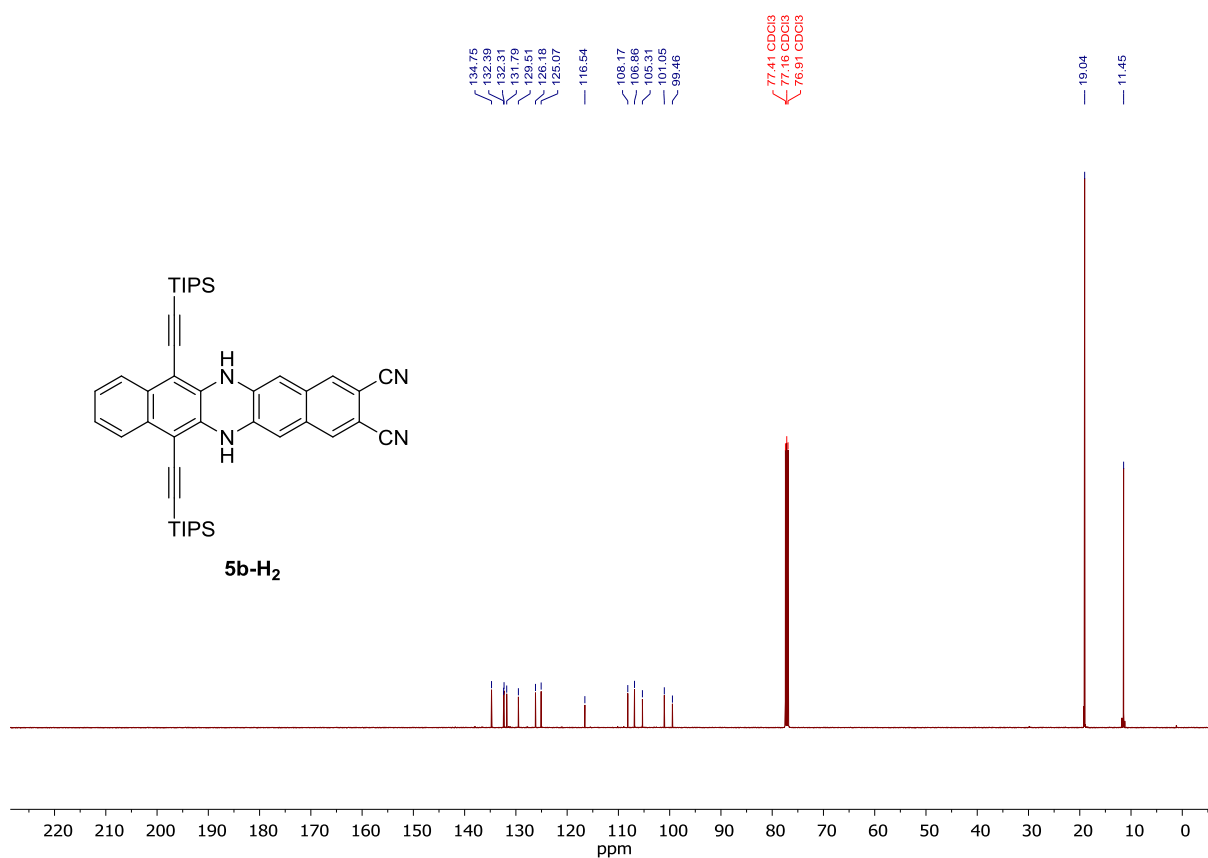


Figure S74: ¹³C NMR (126 MHz, CDCl₃, 25 °C) of **5b**-H₂.

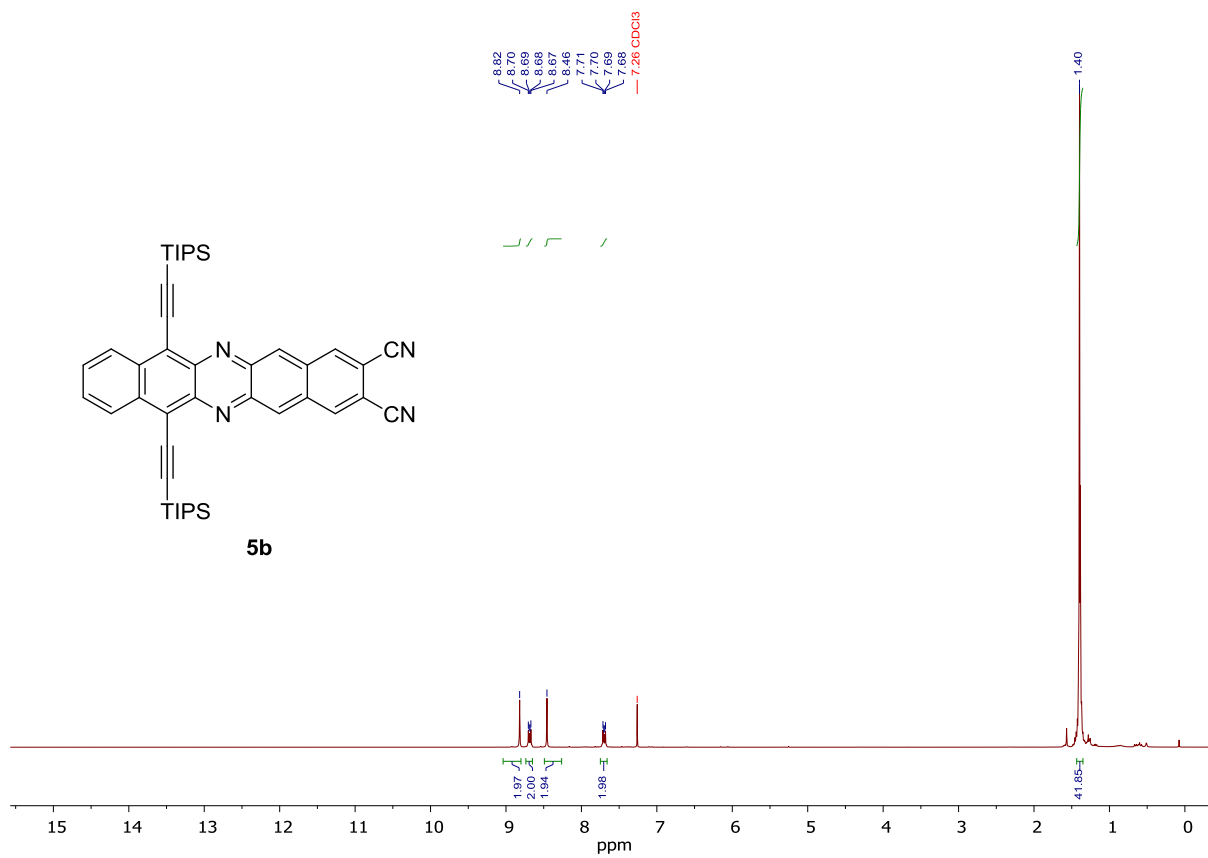


Figure S75: ¹H NMR (500 MHz, CDCl₃, 25 °C) of **5b**.

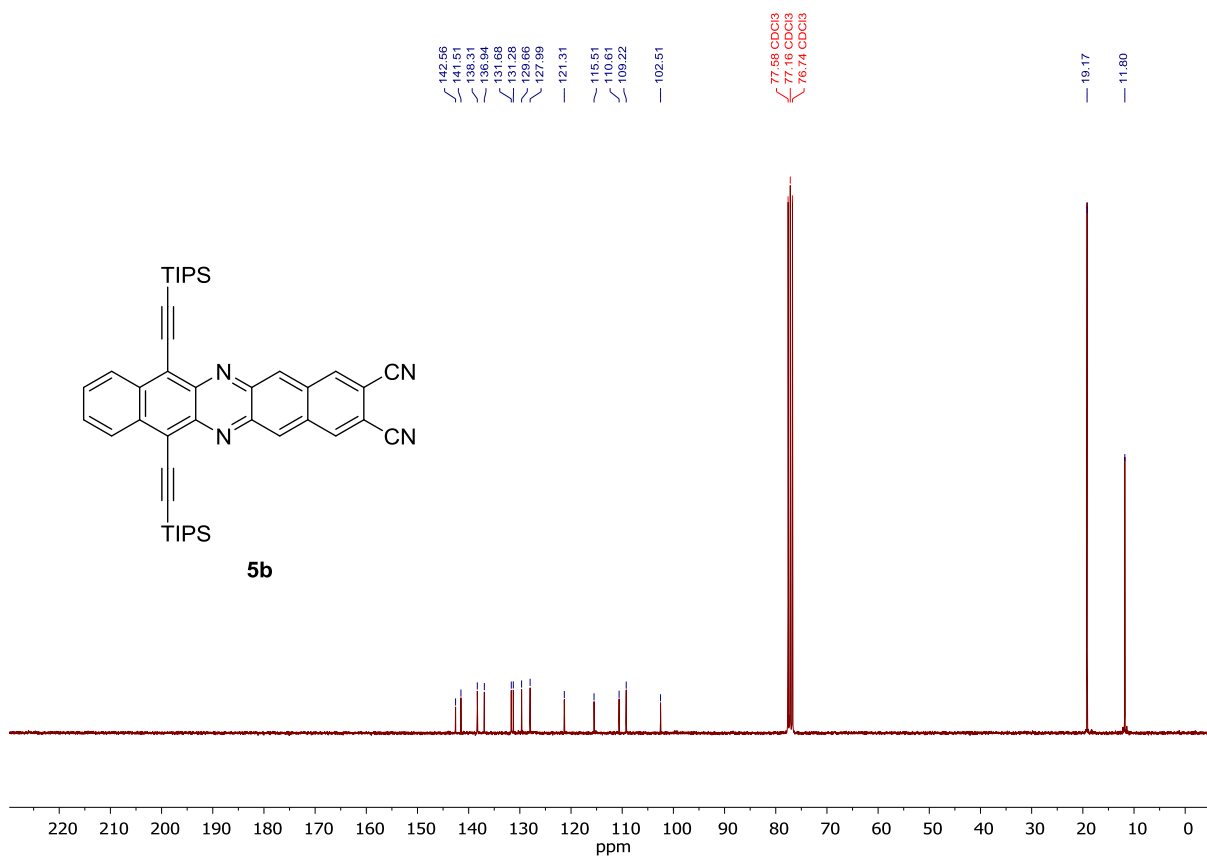


Figure S76: ^{13}C NMR (126 MHz, CDCl_3 , 25 °C) of **5b**.

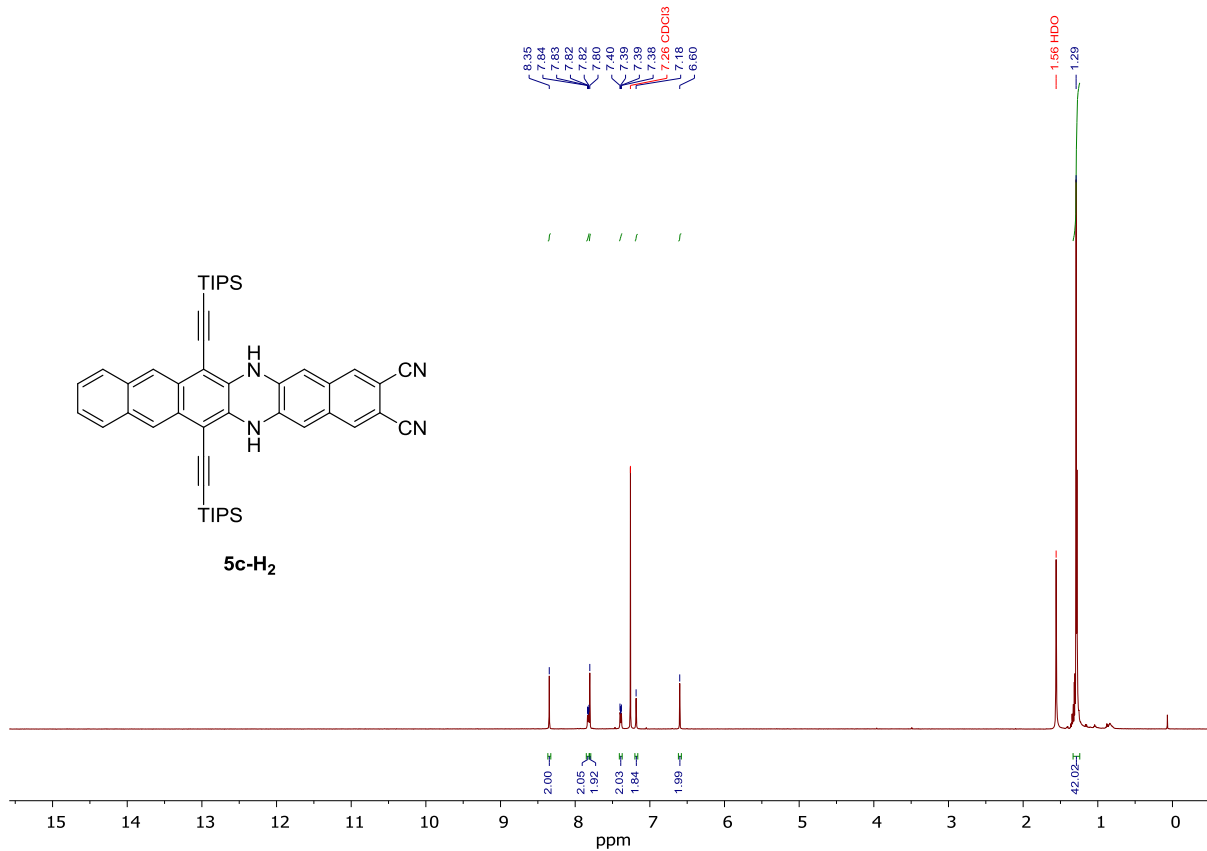


Figure S77: ^1H NMR (500 MHz, CDCl_3 , 25°C) of **5c-H₂**.

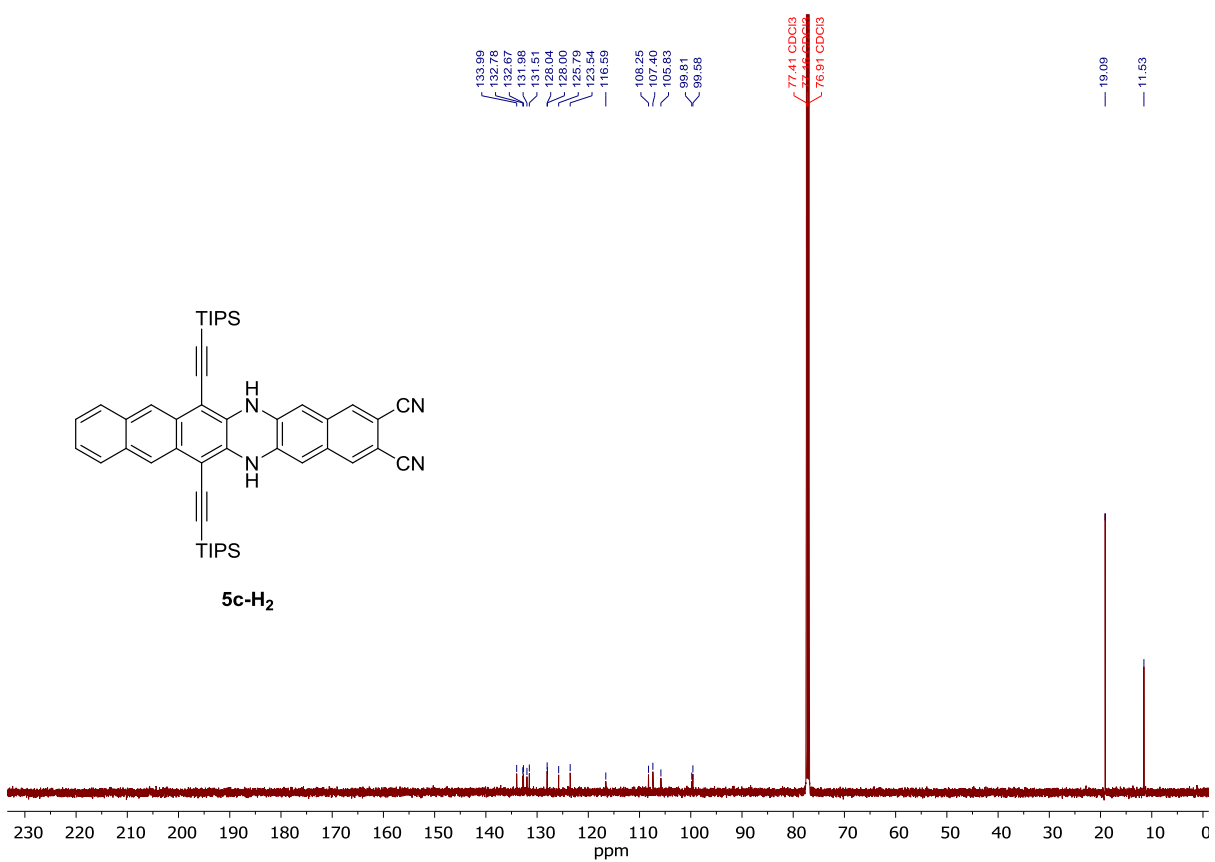


Figure S78: ¹³C NMR (126 MHz, CDCl₃, 25 °C) of **5c-H₂**.

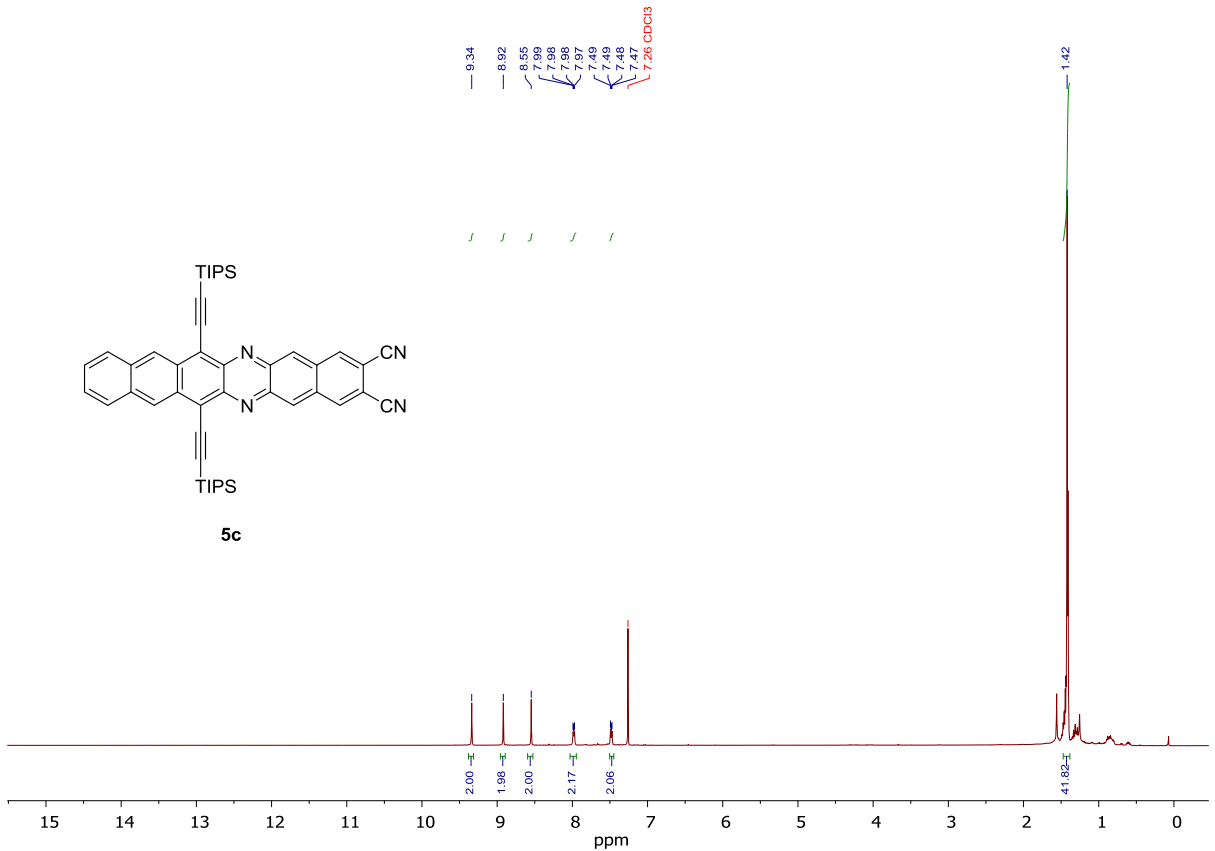


Figure S79: ¹H NMR (500 MHz, CDCl₃, 25°C) of **5c**.

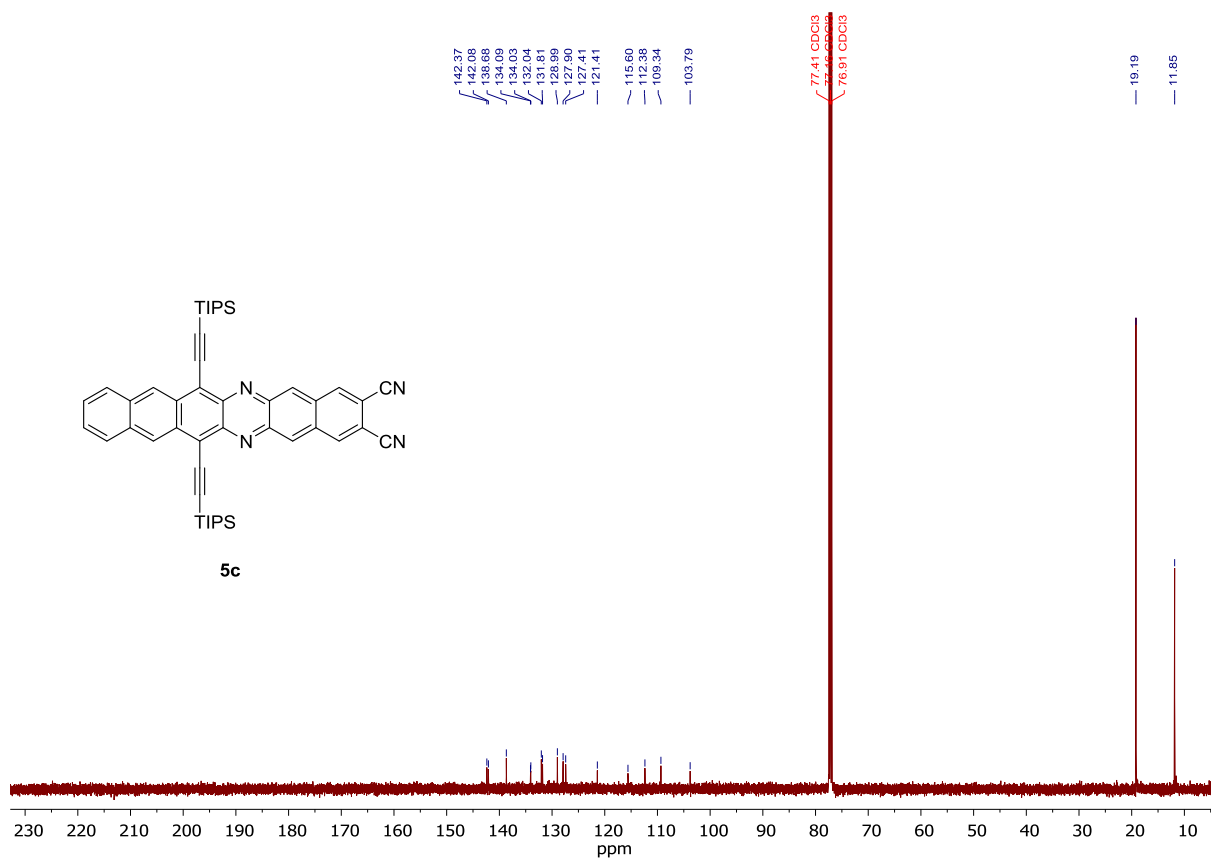
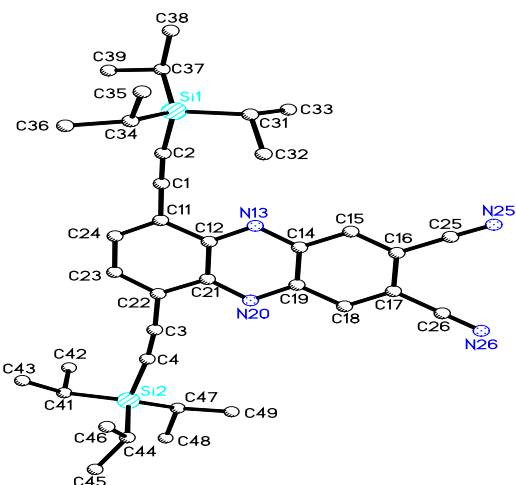


Figure S80: ^{13}C NMR (126 MHz, CDCl_3 , 25 °C) of **5c**.

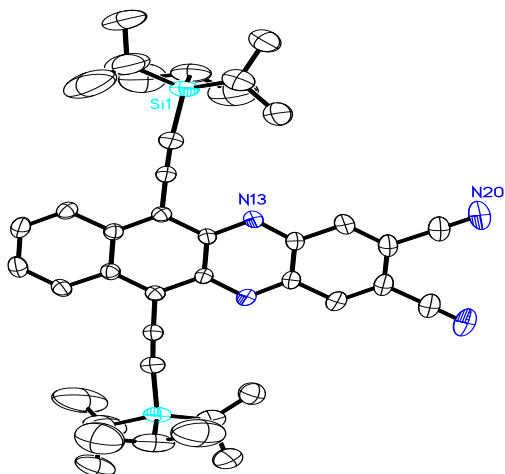
4) Crystallographic Data



Identification code	bu21
Empirical formula	$\text{C}_{36}\text{H}_{46}\text{N}_4\text{Si}_2$
Formula weight	590.95
Temperature	200(2) K
Wavelength	0.71073 Å
Crystal system	monoclinic

Space group	P2 ₁ /c
Z	4
Unit cell dimensions	a = 17.2725(7) Å α = 90 deg. b = 8.2047(3) Å β = 108.9219(10) deg. c = 26.2098(11) Å γ = 90 deg.
Volume	3513.6(2) Å ³
Density (calculated)	1.12 g/cm ³
Absorption coefficient	0.13 mm ⁻¹
Crystal shape	needle
Crystal size	0.180 x 0.130 x 0.110 mm ³
Crystal colour	orange
Theta range for data collection	1.2 to 24.9 deg.
Index ranges	-20 ≤ h ≤ 20, -9 ≤ k ≤ 9, -31 ≤ l ≤ 30
Reflections collected	21402
Independent reflections	6136 (R(int) = 0.0410)
Observed reflections	3934 ($I > 2\sigma(I)$)
Absorption correction	Semi-empirical from equivalents
Max. and min. transmission	0.96 and 0.87
Refinement method	Full-matrix least-squares on F ²
Data/restraints/parameters	6136 / 386 / 408
Goodness-of-fit on F ²	1.04
Final R indices ($I > 2\sigma(I)$)	R1 = 0.052, wR2 = 0.125
Largest diff. peak and hole	0.45 and -0.35 eÅ ⁻³

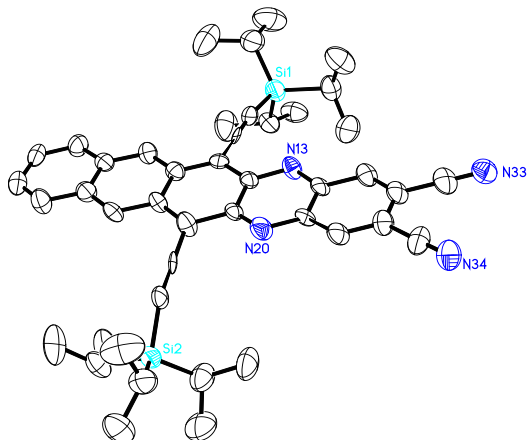
Figure S81: Crystal data and structure of **3a** (CCDC 1529783).



Identification code	bu18
Empirical formula	C ₄₀ H ₄₈ N ₄ Si ₂
Formula weight	641.00
Temperature	200(2) K
Wavelength	0.71073 Å
Crystal system	monoclinic
Space group	C2/c
Z	4
Unit cell dimensions	a = 7.6210(18) Å α = 90 deg. b = 15.040(4) Å β = 96.206(6) deg. c = 33.972(8) Å γ = 90 deg.
Volume	3871.1(16) Å ³
Density (calculated)	1.10 g/cm ³
Absorption coefficient	0.12 mm ⁻¹

Crystal shape	rod
Crystal size	0.290 x 0.130 x 0.080 mm ³
Crystal colour	red
Theta range for data collection	2.4 to 25.0 deg.
Index ranges	?≤h≤?, ?≤k≤?, ?≤l≤?
Reflections collected	6600
Independent reflections	2578 (R(int) = 0.0408)
Observed reflections	1891 (I > 2σ(I))
Absorption correction	Semi-empirical from equivalents
Max. and min. transmission	0.96 and 0.73
Refinement method	Full-matrix least-squares on F ²
Data/restraints/parameters	2578 / 221 / 236
Goodness-of-fit on F ²	1.11
Final R indices (I>2sigma(I))	R1 = 0.094, wR2 = 0.248
Largest diff. peak and hole	0.34 and -0.35 eÅ ⁻³

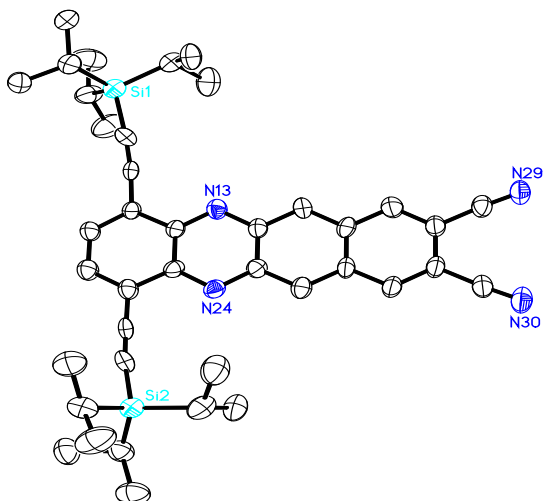
Figure S82: Crystal data and structure of **3b** (CCDC 1529784).



Identification code	mam2
Empirical formula	C ₄₄ H ₅₀ N ₄ Si ₂
Formula weight	691.06
Temperature	200(2) K
Wavelength	0.71073 Å
Crystal system	triclinic
Space group	P1
Z	2
Unit cell dimensions	a = 7.919(2) Å α = 74.640(5) deg. b = 15.072(5) Å β = 86.738(6) deg. c = 17.235(5) Å γ = 85.146(6) deg.
Volume	1975.2(10) Å ³
Density (calculated)	1.16 g/cm ³
Absorption coefficient	0.12 mm ⁻¹
Crystal shape	plate
Crystal size	0.160 x 0.110 x 0.020 mm ³
Crystal colour	green
Theta range for data collection	1.2 to 21.0 deg.
Index ranges	-7≤h≤7, -15≤k≤15, -17≤l≤17
Reflections collected	12987
Independent reflections	7747 (R(int) = 0.0788)
Observed reflections	3590 (I > 2σ(I))

Absorption correction	Semi-empirical from equivalents
Max. and min. transmission	0.96 and 0.83
Refinement method	Full-matrix least-squares on F^2
Data/restraints/parameters	7747 / 2535 / 902
Goodness-of-fit on F^2	1.00
Final R indices ($I > 2\sigma(I)$)	$R_1 = 0.083$, $wR_2 = 0.187$
Absolute structure parameter	0.0(5)
Largest diff. peak and hole	0.32 and -0.30 e \AA^{-3}

Figure S83: Crystal data and structure of **3c** (CCDC 1529785).

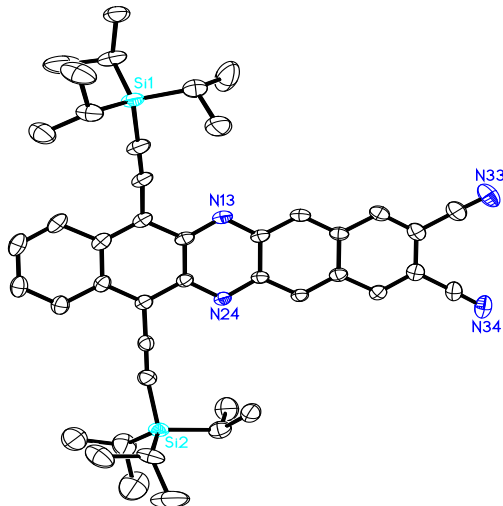


Identification code	bu20
Empirical formula	$C_{40}H_{48}N_4Si_2$
Formula weight	641.00
Temperature	100(2) K
Wavelength	1.54178 Å
Crystal system	triclinic
Space group	$P \bar{1}$
Z	2
Unit cell dimensions	$a = 8.6928(10)$ Å $\alpha = 92.488(11)$ deg. $b = 13.3928(16)$ Å $\beta = 94.648(10)$ deg. $c = 16.055(2)$ Å $\gamma = 96.30(1)$ deg.
Volume	$1849.2(4)$ Å 3
Density (calculated)	1.15 g/cm 3
Absorption coefficient	1.11 mm $^{-1}$
Crystal shape	building block
Crystal size	0.070 x 0.040 x 0.020 mm 3
Crystal colour	dark red
Theta range for data collection	3.3 to 47.8 deg.
Index ranges	-5 ≤ h ≤ 8, -12 ≤ k ≤ 12, -15 ≤ l ≤ 15
Reflections collected	8686
Independent reflections	3394 ($R(\text{int}) = 0.1192$)
Observed reflections	1815 ($I > 2\sigma(I)$)
Absorption correction	Semi-empirical from equivalents
Max. and min. transmission	1.62 and 0.62
Refinement method	Full-matrix least-squares on F^2
Data/restraints/parameters	3394 / 596 / 415
Goodness-of-fit on F^2	1.04

Final R indices ($I > 2\sigma(I)$)
Largest diff. peak and hole

$R_1 = 0.086, wR_2 = 0.190$
 $0.54 \text{ and } -0.26 \text{ e}\text{\AA}^{-3}$

Figure S84: Crystal data and structure of **5a** (CCDC 1529786).



Identification code	sbe2
Empirical formula	$C_{44}H_{50}N_4Si_2$
Formula weight	691.06
Temperature	100(2) K
Wavelength	1.54178 Å
Crystal system	monoclinic
Space group	P2 ₁ /n
Z	8
Unit cell dimensions	$a = 31.6841(12) \text{ \AA}$ $\alpha = 90 \text{ deg.}$ $b = 7.3987(2) \text{ \AA}$ $\beta = 110.344(3) \text{ deg.}$ $c = 35.9762(12) \text{ \AA}$ $\gamma = 90 \text{ deg.}$
Volume	7907.5(5) \AA^3
Density (calculated)	1.16 g/cm ³
Absorption coefficient	1.07 mm ⁻¹
Crystal shape	needle
Crystal size	1.000 x 0.040 x 0.030 mm ³
Crystal colour	black
Theta range for data collection	1.6 to 68.6 deg.
Index ranges	$-35 \leq h \leq 38, -4 \leq k \leq 8, -43 \leq l \leq 41$
Reflections collected	43608
Independent reflections	14140 ($R(\text{int}) = 0.0548$)
Observed reflections	10467 ($I > 2\sigma(I)$)
Absorption correction	Semi-empirical from equivalents
Max. and min. transmission	1.58 and 0.64
Refinement method	Full-matrix least-squares on F^2
Data/restraints/parameters	14140 / 3542 / 1083
Goodness-of-fit on F^2	1.02
Final R indices ($I > 2\sigma(I)$)	$R_1 = 0.064, wR_2 = 0.169$
Largest diff. peak and hole	0.62 and -0.41 e \AA^{-3}

Figure S85: Crystal data and structure of **5b** (CCDC 1529787).

Conclusions of the thesis

We have developed a new TR-based chemosensory system bearing different headgroups for the detection of various chemical substances of concern for the science of artworks, for environmental air and water pollution. We have shown that the adequate steric interactions between PDA headgroups can induce selective colorimetric change with tested compounds. TR derivatives described in Chapters 3 were successfully employed in the colorimetric and/or fluorescent detection of organic compounds present in binding materials of paintings, VOCs and organophosphate pesticides.

- 1) In conclusion of **Chapter 4**, this study shows that poly(methyl methacrylate)-supported polydiacetylene films comprising different TR derivatives could distinguish among paint constituents. The film assembly might be employed as a simple, on-site platform for monitoring degradation processes and planning restoration intervention. Importantly, the colour transformations can be readily quantified using simple spectrophotometer instrumentation. This study shows that the polydiacetylene technology might open new analytical avenues in molecular analysis, in general, painting restoration and conservation science, in particular.
- 2) In **Chapter 5**, we constructed a VOC sensor comprising TR and its derivatives within the porous framework of a silica aerogel. The structural and physical properties of both the aerogel matrix and embedded PDAs were retained following the fabrication procedure. The PDA-aerogel hybrid was used as a sensor for different VOCs, exploiting the porosity and high surface area for adsorption of the volatile compounds and their effects upon both the PDA color and fluorescence. Importantly, the observed chromatic modulation was dependent upon the electronic, structural features, and particularly the polarity of the VOCs. Accordingly, the PDA-aerogel vapor sensor could distinguish among different VOCs. The PDA-aerogel sensor exhibits notable practical advantages. Preparation of the hybrid material is straightforward, using inexpensive and readily available reagents. The actual sensing experiments are easy to perform and carried out through visible color transformations that could be also quantified using spectrophotometry.
- 3) Experiments reported in **Chapter 6** demonstrated the possible application of the TR/TR-derivatives systems for the detection of various organophosphate pesticides. Emphasis was given to the preparation of sensing systems with improved sensitivity and selectivity, by changing the chemical structure of the sensor and detecting a right target. New derivatives could be further tested on wider range of OPs, in metal ion recognition tests, bacteria, drug-delivery and other studies. By taking an advantage of the ease of functionalizing their potential use as colorimetric and fluorescent sensors, or targeted delivery should be further investigated.
- 4) In **Chapter 7**, I reported a research that was conducted in Prof. Uwe Bunz's laboratory at Organic Chemistry Institute, Heidelberg University, Germany, in the frame of Marco Polo fellowship. I have synthesized a series of dicyano-substituted diazaacenes, containing three to six rings. The targets were prepared by Pd-catalyzed coupling of suitable diamino-substituted arenes with either 4,5-dibromophthalonitrile or 6,7-dibromonaphthalene-2,3-dicarbonitrile. The resulting coupling products were oxidized by MnO_2 or by PbO_2 to give the desired diazaacenes, which were investigated by optical spectroscopy, cyclic voltammetry and single crystal X-ray analysis. An interesting observation is that the position of the cyano groups (either one or two benzene rings separated from the azaacene unit) influences both the reduction potential and thus the LUMO position. Some of these compounds could be processed into a thin film transistor with the high electron mobilities.

Acknowledgements

I would like to express my special gratitude to my supervisors Prof. Emilio Tagliavini and Prof. Paola Galletti, for giving me this opportunity to study for my PhD at University of Bologna, for scientific discussions and general help and support.

Special thanks to Prof. Raz Jelinek and his group for the fruitful cooperation, in particular, for the testing my TR derivatives upon detection of various analytes.

I would like to thank Prof. Uwe Bunz for the wonderful experience I gained during my internship in his group at the Organic Chemistry Institute, University of Heidelberg (Germany) in the frame of Marco Polo program and especially, I would like to thank Olena Tverskoy, Yury Kozhemyakin, Philipp Bieger, Matthias Müller and all students and staff for their kind attitude and general support.

I would like to thank all researchers and the staff of Ravenna Campus, University of Bologna, for beneficial working environment they created around me.

A final special thanks to Dr. Danilo Malferrari for his great scientific contribution to my thesis, precious advices and general help.

I hope I didn't forget anyone.....

References

-
- ¹ G. Wegner, *Z. Naturforsch. B*, **1969**, 24, 824–832.
 - ² G. Wegner, *Makromol. Chem.*, **1971**, 145, 85–94.
 - ³ B. Tieke et al., *Angew. Chem., Int. Ed.*, **1976**, 15, 764–765.
 - ⁴ B. Tieke et al., *Colloid Polym. Sci.*, **1977**, 255, 521–531.
 - ⁵ G. Odian, *Principles of Polymerization*, John Wiley & Sons, Inc., New York, 3rd edn, **1991**
 - ⁶ S. R. Sheth and D. E. Leckband, *Langmuir*, **1997**, 13, 5652–5662.
 - ⁷ G. N. Patel and G. G. Miller, *J. Macromol. Sci., Part B: Phys.*, **1981**, 20, 111–131.
 - ⁸ R. R. Chance, *Macromolecules*, **1980**, 13, 396–398.
 - ⁹ R. H. Baughman and R. R. Chance, *J. Polym. Sci., Polym. Phys. Ed.*, **1976**, 14, 2037–2045.
 - ¹⁰ J. Olmsted and M. Strand, *J. Phys. Chem.*, **1983**, 87, 4790–4792.
 - ¹¹ C. Bubeck et al., *Ber. Bunsenges. Phys. Chem.*, **1982**, 86, 495–498.
 - ¹² B. Tieke, *Adv. Polym. Sci.*, **1985**, 17, 79–151.
 - ¹³ H. Peng et al., *J. Am. Chem. Soc.*, **2006**, 128, 5304–5305.
 - ¹⁴ L. Tong et al., *Sens. Actuators, B*, **2011**, 155, 584–591.
 - ¹⁵ S. Kolusheva et al., *Anal. Chem.*, **2012**, 84, 5925–5931.
 - ¹⁶ S. K. Chae et al., *Adv. Mater.*, **2007**, 19, 521–524.
 - ¹⁷ J.-M. Kim et al., *Adv. Funct. Mater.*, **2006**, 16, 2103–2109.
 - ¹⁸ Z. Orynbayeva et al., *Angew. Chem., Int. Ed.*, **2005**, 44, 1092–1096.
 - ¹⁹ M.A. Reppy and B. A. Pindzola, *Chem. Commun.*, **2007**, 4317–4338
 - ²⁰ R. W. Carpick et al., *J. Phys.: Condens. Matter*, **2004**, 16, 679–697.
 - ²¹ R. R. Chance et al., *J. Chem. Phys.*, **1977**, 67, 3616–3618.
 - ²² H. Eckhardt et al., *J. Chem. Phys.*, **1986**, 85, 4116–4119.
 - ²³ D. J. Ahn et al., *J. Am. Chem. Soc.*, **2003**, 125, 8976–8977.
 - ²⁴ U. Jonas et al., *J. Am. Chem. Soc.*, **1999**, 121, 4580–4588
 - ²⁵ G. Eglington and W. McRae, *Adv. Org. Chem.*, **1963**, 4, 252–281.

-
- ²⁶ B. Tieke and G. Lieser, *J. Colloid Interface Sci.*, **1982**, 88, 471–486.
- ²⁷ H. Tachibana et al., *Macromolecules*, **1999**, 32, 8306–8309.
- ²⁸ H. Menzel et al., *Polymer*, **2000**, 41, 8113–8119.
- ²⁹ D. Day and H. Ringsdorf, *J. Polym. Sci., Polym. Lett. Ed.*, **1978**, 16, 205–210.
- ³⁰ N. Charoenthai et al., *J. Colloid Interface Sci.*, **2011**, 360, 565–573.
- ³¹ Y. Su, J. Li and L. Jiang, *Colloids Surf., B*, **2004**, 39, 113–118.
- ³² Y.-S. Cho and K. H. Ahn, *J. Mater. Chem. B*, **2013**, 1, 1182–1189.
- ³³ S. Seo et al., *Macromol. Rapid Commun.*, **2013**, 34, 743–748.
- ³⁴ R. Jelinek and M. Ritenberg, *RSC Adv.*, **2013**, 3, 21192–21201
- ³⁵ T. Eaidkong et al., *J. Mater. Chem.*, **2012**, 22, 5970–5977.
- ³⁶ T. A. Dickinson et al., *Trends Biotechnol.*, **1998**, 16, 250–258.
- ³⁷ X. Chen et al., *Angew. Chem., Int. Ed.*, **2010**, 49, 1422–1425.
- ³⁸ I. K. Kwon et al., *Biosens. Bioelectron.*, **2010**, 26, 1548–1553.
- ³⁹ B. Yoon et al., *Adv. Mater.*, **2011**, 23, 5492–5497.
- ⁴⁰ M. Ritenberg et al., *ChemPlusChem*, **2012**, 77, 752–757.
- ⁴¹ C. J. Brinker et al., *Thin Solid Films*, **1991**, 201, 97–108.
- ⁴² E. Morin et al., *Bioconjugate Chem.*, **2011**, 22, 1916–1923.
- ⁴³ B. Ma et al., *J. Controlled Release*, **2007**, 123, 184–194.
- ⁴⁴ U. Jonas et al., *J. Am. Chem. Soc.*, **1999**, 121 (19), pp 4580–4588
- ⁴⁵ Y. K. Jung et al., *Adv. Funct. Mater.*, **2008**, 18, 701–708
- ⁴⁶ Cheng et al., *Langmuir*, **2000**, 16, 5333–5342
- ⁴⁷ H. Jeon et al., *J. Mater. Chem.*, **2012**, 22, 3795–3799
- ⁴⁸ J. Lee et al., *Adv. Funct. Mater.*, **2011**, 21, 1032–1039
- ⁴⁹ S. Lee et al., *Adv. Funct. Mater.*, **2014**, 24(24), 3699–3705
- ⁵⁰ C. Torri et al., *Microchemical Journal*, **2013**, 110, 719–725.
- ⁵¹ A. Trachtenberg et al., *New J. Chem.*, **2016**, 40, 9054
- ⁵² S. Dolai et al., *ACS Appl. Mater. Interfaces*, **2017**, 9(3), 2891–2898
- ⁵³ Shukla, J. et al., *Chem. Sinica*, **2011**, vol. 2, no. 3, p. 4; Agbandjet, M. et al., *J. Med. Chem.*, **1992**, vol. 35, p. 1418; Júnior, C.O.R. et al., *Mem. Inst. Oswaldo Cruz*, **2009**, vol. 104, no. 5, p. 703; Petrovic, Z.D. et al., *Bioorg. Chem.*, **2009**, vol. 37, p. 162.
- ⁵⁴ Schwartz, A.M. and Perry, J.W., *Surface Active Agents, Their Chemistry and Technology*, New York, Interscience, **1949**, vol. 1, p. 212.
- ⁵⁵ POLY (METHYL METHACRYLATE)-SUPPORTED POLYDIACETYLENE FILMS AS COLORIMETRIC AND/OR FLUORESCENT DETECTORS(WO 2016/005987 A1).
- ⁵⁶ Amber M. King et al., *J. Med. Chem.*, **2011**, 54, 4815–4830.
- ⁵⁷ P. Narkwiboonwong et al., *Talanta*, **83 (2011)** 872–878.
- ⁵⁸ Bailey, F. E.; Callard, R. W., *J. Appl. Polym. Sci.* **1959**, 1, 56–62.
- ⁵⁹ Scientific Examination for the Investigation of Paintings: *A Handbook for Conservators and Restorers*, ed. D. Pinna; M. Galeotti and R. Mazzeo, Centro Di, Firenze, **2010**, ISBN: 88703845.
- ⁶⁰ T. D. James et al., *Angew. Chem.*, **1996**, 35, 1910–1922; G. Springsteen and B. Wang, *Tetrahedron*, **2002**, 58, 5291–5300.
- ⁶¹ K. P. Kootery et al., *ACS Appl. Mater. Interfaces*, **2014**, 6, 8613–8620.
- ⁶² B. Yoon et al., *Chem. Soc. Rev.*, **2009**, 38, 1958–1968; H. Jiang et al., *J. Phys. Chem. Lett.*, **2016**, 7, 1628–1631.
- ⁶³ X. Q. Chen et al., *Chem. Soc. Rev.*, **2012**, 41, 4610–4630.
- ⁶⁴ X. Chen et al., *Angew. Chem., Int. Ed.*, **2010**, 49, 1422.
- ⁶⁵ Y. Demikhovsky et al., *J. Colloid Interface Sci.*, **2011**, 364, 428–434.
- ⁶⁶ S. Okada et al., *Acc. Chem. Res.*, **1998**, 31, 229–239.

-
- ⁶⁷ The Organic Chemistry of Museum Objects, ed. J. S. Mills and R. White, *Butterworths*, London, **1987**.
- ⁶⁸ P. Vanloot et al., *Food Chem.*, **2012**, 135, 2554.
- ⁶⁹ P. Bosch-Roig and G. Ranalli, *Front. Microbiol.*, **2014**, 5, 155.
- ⁷⁰ Konvalina, G. and Haick, H., *Acc. Chem. Res.* **2014**, 47, 66-76.
- ⁷¹ Kim, J. S. et al., *Nano Lett.* **2014**, 14, 5941-5947.
- ⁷² Wang, R. X. et al., *Anal. Chem.* **2013**, 85, 8065-8069.
- ⁷³ Dolai, S. et al., *Sens. Actuators, B* **2017**, 241, 607-613.
- ⁷⁴ Buszewski, B. et al., *Biomed. Chromatogr.* **2009**, 23, 551-556.
- ⁷⁵ Grate, J. W. Et al., *Anal. Chem.* **1993**, 65, 1868-1881.
- ⁷⁶ Di Natale et al., *Biosens. Bioelectron.* **2003**, 18, 1209-1218.
- ⁷⁷ Turner, C. et al., *Rapid Commun. Mass Spectrom.* **2006**, 20, 61-68.
- ⁷⁸ Wang, D. et al., *Ind. Eng. Chem. Res.* **2011**, 50, 12177-12185.
- ⁷⁹ Zuo, L. Z. et al., *Materials* **2015**, 8, 6806-6848; Qi, H. S. et al., *Sens. Actuators, B* **2015**, 213, 20-26; Thubsuang, U. et al., *Mater. Sci. Eng., B* **2015**, 200, 67-77.
- ⁸⁰ Li, L. C. et al., *ACS Appl. Mater. Interfaces* **2009**, 1, 2491-2501;
- ⁸¹ Zou, J. H. et al., *ACS Nano*, 4, 7293-7302.
- ⁸² Kristiansen, T. et al., *J. Phys. Chem. C* **2011**, 115, 19260-19268.
- ⁸³ Chervin, C. N. et al., *Chem. Mater.* **2005**, 17, 3345-3351.
- ⁸⁴ Boday, D. J. et al., *ACS Appl. Mater. Interfaces* **2009**, 1, 1364-1369.
- ⁸⁵ Randall, J. P. et al., *ACS Appl. Mater. Interfaces* **2011**, 3, 613-626.
- ⁸⁶ Eaidkong, T. et al., *J. Mater. Chem.* **2012**, 22, 5970-5977.
- ⁸⁷ Potisatityuenyong, A. et al., *Langmuir* **2008**, 24, 4461-4463; Wu, J. C. et al., *J. Am. Chem. Soc.* **2011**, 133, 9720-9723; Charych, D. H. et al., *Science* **1993**, 261, 585-588; Koevoets, R. A. et al., *Macromolecules* **2009**, 42, 2609-2617; Pires, A. C. S. et al., *J. Phys. Chem. B* **2010**, 114, 13365-13371.
- ⁸⁸ Kang, D. H. et al., *Chem. Commun.* **2012**, 48, 5313-5315; Seo, S. et al., *ACS Appl. Mater. Interfaces* **2015**, 7, 20342-20348; Lee, J. et al., *Adv. Funct. Mater.* **2012**, 22, 1632-1638; Lee, S. et al., *Chem. Commun.* **2016**, 52, 9178-9196; Davis, B. W. et al., *Langmuir* **2014**, 30, 9616-9622; Kauffman, J. S. et al., *ACS Appl. Mater. Interfaces* **2009**, 1, 1287-1291; Park, M. K. et al., *Biosens. Bioelectron.* **2012**, 35, 44-49.
- ⁸⁹ Xu, Q. et al., *J. Am. Chem. Soc.* **2013**, 135, 17751-17754; Jeon, H. et al., *Macromol. Rapid Commun.* **2012**, 33, 972-976.
- ⁹⁰ Bheekhun, N. et al., *Adv. Mater. Sci. Eng.* **2013**, 2013, 406065.
- ⁹¹ Ribeiro do Carmo, D.; Paim, L. L., *Mater. Res.* **2013**, 16, 164-172.
- ⁹² Volinsky, R. et al., *Biosens. Bioelectron.* **2007**, 22, 3247-3251.
- ⁹³ Jiang, H. et al., *Langmuir* **2015**, 31, 5843-5850.
- ⁹⁴ Sun, X. M. et al., *Chem. Soc. Rev.* **2010**, 39, 4244-4257.
- ⁹⁵ Friedman, S. et al., *Anal. Chem.* **2008**, 80, 7804-7811; Lifshitz, Y. et al., *Soft Matter* **2011**, 7, 9069-9077; Wu, A. D. et al., *J. Phys. Chem. C* **2013**, 117, 19593-1960; Lim, C. et al., *Macromolecules* **2008**, 41, 675-681.

-
- ⁹⁶ Zhong, L. et al., *J. Phys. Chem. B* **2010**, 114, 8871-8878.
- ⁹⁷ Yoon, J. et al., *J. Am. Chem. Soc.* **2007**, 129, 3038-3039.
- ⁹⁸ Jiang, H. et al., *Sens. Actuators, B* **2010**, 143, 789-794.
- ⁹⁹ Hernandez, L. F. et al., *Quim. Nova* **2008**, 31, 1410-1416.
- ¹⁰⁰ Pattanatornchai, T. et al., *J. Colloid Interface Sci.* **2013**, 391, 45-53.
- ¹⁰¹ Wu, A. D. et al., *Colloid Polym. Sci.* **2014**, 292, 3137-3146.
- ¹⁰² Rakow, N. A.; Suslick, K. S., *Nature* **2000**, 406, 710-713.
- ¹⁰³ Ariese, F. et al., *Environ. Toxicol. Pharmacol.* **2001**, 10, 65-80.
- ¹⁰⁴ Karr, J.R.; Dudley, D.R., *Environ. Manage.* **1981**, 5, 55-68.
- ¹⁰⁵ U.S. EPA. Pesticides and food: Why children may be especially sensitive to pesticides. Available online: <http://www.epa.gov/pesticides/food/pest> (accessed on February 26, 2010)
- ¹⁰⁶ Survey, U.S.G. Organophosphorus pesticides occurrence and distribution in surface and ground water of the United States. Available online: <http://ga.water.usgs.gov/publications/ofr00-187.pdf> (accessed on 26 February 2010).
- ¹⁰⁷ Martínez-Máñez, R.; Sancenón, F., *Chem. Rev.* **2003**, 103, 4419-4476.
- ¹⁰⁸ A. Caballero et al., *J. Am. Chem. Soc.*, **2005**, 127, 15666-15667; I. Eryazici et al., *Rev.*, **2008**, 108, 1834-189; T. Sakamoto et al., *Chem. Commun.*, **2009**, 141-152; M. Kruppa and B. König, *Chem. Rev.*, **2006**, 106, 3520-3560.
- ¹⁰⁹ S. Lee et al., *Chem. Commun.*, **2016**, 52, 9178-9196
- ¹¹⁰ a) K. Zhou et al., *Phys. Chem. Chem. Phys.* **2014**, 16, 22448-22457; b) J. E. Anthony et al., *Adv. Mater.*, **2010**, 22, 3876-3892. c) S. C. Martens et al., *Chem. Eur. J.* **2012**, 18, 3498-3509.
- ¹¹¹ a) U. H. F. Bunz, *Chem. Eur. J.* **2009**, 15, 6780-6789; b) U. H. F. Bunz, *Pure Appl. Chem.* **2010**, 82, 953-968; c) U. H. F. Bunz et al., *Angew. Chem. Int. Ed.* **2013**, 52, 3810-3821; d) U. H. F. Bunz, *Acc. Chem. Res.* **2015**, 48, 1676-1686; e) U. H. F. Bunz, J. U. Engelhart, *Chem. Eur. J.* **2016**, 22, 4680-4689; e) S. Miao et al., *Chem. Eur. J.* **2009**, 15, 4990-4993; f) Z. Liang et al., *Adv. Mater.* **2011**, 23, 1535-1539.
- ¹¹² a) K. E. Maly, *Cryst. Growth Des.* **2011**, 11, 5628-5633; b) J. E. Anthony, *Chem. Rev.* **2006**, 106, 5028-5048.
- ¹¹³ a) S. Miao et al., *Chem. Eur. J.* **2009**, 15, 4990-4993; b) Z. Liang et al., *Adv. Mater.* **2011**, 23, 1535-1539.
- ¹¹⁴ a) C.-L. Song et al., *Org. Lett.* **2011**, 13, 2880-2883; b) Y.-Y. Liu et al., *J. Am. Chem. Soc.* **2010**, 132, 16349-16351.
- ¹¹⁵ J. Schwaben et al., *Chem. Eur. J.* **2015**, 21, 13758-13771.
- ¹¹⁶ M.-Y. Kuo et al., *Chem. Eur. J.* **2007**, 13, 4750-4758.
- ¹¹⁷ M. Winkler, K. N. Houk, *J. Am. Chem. Soc.* **2007**, 129, 1805-1815.
- ¹¹⁸ S. Miao, S. M. Brombosz, P. v. R. Schleyer, J. I. Wu, S. Barlow, S. R. Marder, K. I. Hardcastle, U. H. F. Bunz, *J. Am. Chem. Soc.* **2008**, 130, 7339-7344;
- ¹¹⁹ a) K. E. Maly et al., *Eur. J. Org. Chem.* **2015**, 1456-1463; b) D. Dini et al., *J. Phys. Chem. B*, Vol. 110, No. 25, **2006**
- ¹²⁰ J. U. Engelhart et al., *Chem. Eur. J.* **2013**, 19, 15089-15092.
- ¹²¹ P. Biegger et al., *J. Org. Chem.* **2015**, 80, 582-589.
- ¹²² C. M. Cardona et al., *Adv. Mater.* **2011**, 23, 2367-2371

-
- ¹²³ a) S. Hahn et al., *Chem. Eur. J.* **2016**, 22, 869-873; b) S. Hahn et al., *J. Org. Chem.* **2016**, 81, 8485-8494; c) E. C. Rüdiger et al., *Chem. Eur. J.* **2014**, 20, 12725-12728; d) B. D. Lindner et al., *J. Mater. Chem. C* **2014**, 2, 9609-9612; e) A. L. Appleton et al., *Org. Lett.* **2009**, 11, 5222-5225; f) B. D. Lindner et al., *Org. Lett.* **2013**, 15, 666-669; g) J. U. Engelhart et al., *J. Am. Chem. Soc.* **2014**, 136, 15166-15169; h) J. U. Engelhart et al., *J. Org. Chem.* **2016**, 81, 1198-1205; i) O. Tverskoy et al., *Angew. Chem. Int. Ed.* **2011**, 50, 3557-3560; j) A. L. B. Appleton et al., U. H. F., *Nature Comm.* **2010**, 91; k) M. Märkten et al., *Pure Appl. Chem.* **2014**, 86, 483-488.
- ¹²⁴ Jiabo Li and Yaowu Sha, *Molecules* **2008**, 13, 1111-1119
- ¹²⁵ Li et al., *J. Phys. Chem. B*, Vol. 112, No. 42, **2008**; T. Eaidkong et al., *J. Mater. Chem.*, **2012**, 22, 5970-5977
- ¹²⁶ Jie Song et al., *J. AM. CHEM. SOC.* **2004**, 126, 8459-8465
- ¹²⁷ D. Amilan Jose and B. König *Org. Biomol. Chem.*, **2010**, 8, 655-662
- ¹²⁸ J.A. Monti et al., *Life Sci.*, 21 (**1977**) 345-356.
- ¹²⁹ a) *J. Chem. Pharm. Res.*, **2015**, 7(10):677-692; b) *Org. Biomol. Chem.*, **2010**, 8, 655-662; *Chem. Soc. Rev.*, **2012**, 41, 4610-4630
- ¹³⁰ *Chemistry and Physics of Lipids*, 36 (**1985**) 197—207; *J. Phys. Chem. B*, Vol. 112, No. 42, **2008**
- ¹³¹ M. Juríček et al., *J. Org. Chem.* **2009**, 74, 21-25.
- ¹³² K. M. Psutka et al., *Eur. J. Org. Chem.* **2015**, 2015, 1456-1463.
- ¹³³ H. E. Gottlieb et al., *J. Org. Chem.* **1997**, 62, 7512-7515.
- ¹³⁴ G. W. T. M. J. Frisch et al., in *Gaussian 09*, Wallingford, **2009**.